Fullerenes for organic electronics

Kooistra, Floris Berend

Fullerenes for Organic Electronics

Floris Berend Kooistra

PhD thesis Groningen University
ISBN: 978-90-367-3256-7 (printed version)
ISBN: 978-90-367-3257-4 (electronic version)

Printed by: PrintPartners Ipskamp B.V., Enschede, The Netherlands.

Cover design: Floris Kooistra and Frank Brouwer
Cover picture: Michael Coleman (www.flickr.com)

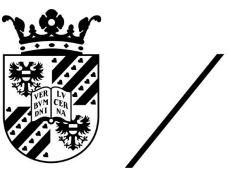

rijksuniversiteit
groningen

The work carried out in this thesis was performed within the Stratingh Institute of Chemistry of the University of Groningen

Part of the work described in this thesis was financially supported by the European Space Agency under project number: AO 99-121

University of Groningen
Zernike Institute
for Advanced Materials

Part of the work described in this thesis was financially supported by the Zernike Institute for Advanced Materials.

Zernike Institute PhD thesis series 2007-17

ISSN: 1570-1530

RIJKSUNIVERSITEIT GRONINGEN

Fullerenes for Organic Electronics

Proefschrift

ter verkrijging van het doctoraat in de
Wiskunde en Natuurwetenschappen
aan de Rijksuniversiteit Groningen
op gezag van de
Rector Magnificus, dr. F. Zwarts,
in het openbaar te verdedigen op
vrijdag 30 november 2007
om 13.15 uur

door

Floris Berend Kooistra

geboren op 28 april 1979
te Amersfoort

Promotor:	Prof. dr. J.C. Hummelen
Beoordelingscommissie:	Prof. dr. P.W.M. Blom
	Prof. dr. K. Meerholz
	Prof. dr. N. Martín León

ISBN: 978-90-367-3257-4 (electronic version)
ISBN: 978-90-367-3256-7 (printed version)

Contents

Chapter 1	**Introduction**	**5**
1.1	Fullerenes	6
1.2	PCBM	7
1.3	Fullerenes in Organic Electronics	8
1.4	Outline and Aim of this Thesis	21
1.5	List of Publications	22
1.6	References	23
Chapter 2	**[84]PCBM and its Application in a Bulk Heterojunction Solar Cell**	**31**
2.1	Introduction	32
2.2	Synthesis	36
2.3	Characterization	36
2.4	Photovoltaic Devices	41
2.5	Discussion	45
2.6	Conclusions	47
2.7	Experimental	48
2.8	References	50
Chapter 3	**Increasing the V_{oc} of Bulk Heterojunction Solar Cells by raising the LUMO level of the Acceptor**	**53**
3.1	Introduction	54
3.2	Synthesis	57
3.3	Characterization	60
3.4	Solar Cell Devices	64
3.5	Conclusions	65
3.6	Experimental	66
3.7	References	82

Chapter 4	**Air Stable Organic Field Effect Transistors**	**85**
4.1	Introduction	86
4.2	Synthesis	90
4.3	[84]PCBM Organic Field Effect Transistors	94
4.4	Field Effect Transistors of fluorine containing fullerene derivatives	101
4.5	Conclusions	106
4.6	Experimental	106
4.7	References	116
Chapter 5	**Fullerenes for Time-Gated Holographic Imaging**	**119**
5.1	Introduction	120
5.2	Fullerene Sensitizers for TGHI	125
5.3	Low T_g Fullerenes for inverted photorefractive materials	131
5.4	Conclusions	136
5.5	Experimental	136
5.6	References	154
Chapter 6	**π-Conjugated Fullerene Adducts**	**157**
6.1	Introduction	158
6.2	Synthesis	164
6.3	[6,6]Bridged Fullerenes	168
6.4	[5,6]Bridged Fulleroids	174
6.5	Conclusions	177
6.6	Experimental	178
6.7	References	181
Chapter 7	**Giant Pearl-Necklace Fullerene Macrocycles**	**185**
7.1	Introduction	186
7.2	Synthesis	191

7.3	MALDI-TOF Spectroscopy	193
7.4	Conclusions	197
7.5	Experimental	197
7.6	References	200
Appendix I	**MALDI-TOF Spectra Chapter 7**	**203**
Samenvatting		**213**
Summary		**219**
Dankwoord		**225**

Chapter 1

Introduction

Since the discovery of C_{60} as the third carbon allotrope, fullerenes have attracted much interest in the scientific world. Their unique properties have rendered them useful for many applications, ranging from medicine to electronics. In this chapter the structure and properties of fullerenes will be discussed, as well as their applicability in molecular electronics. The chapter will be concluded with a brief outline and aim of this thesis.

1.1 Fullerenes

The discovery of C_{60} by Kroto, Smalley and Curl in 1985 initiated a vastly expanding research field.[1] They gave C_{60} its more popular name of buckminsterfullerene or in short 'buckyball' after the architect Buckminster Fuller whose designs resemble the structure of the fullerenes. The definite breakthrough, that started off fullerene chemistry, was accomplished by Krätschmer and Huffman when they isolated solid C_{60}.[2,3] The unique electronic properties of fulllerenes make them highly interesting candidates for several applications in molecular electronics, some of which will be discussed in this chapter.

1.1.1 Fullerene design rules

Fullerenes are spherical, all carbon structures consisting of pentagons and hexagons. The Euler Theorem states that in order to close a sphere of *n* hexagons, 12 pentagons are required. Consequently all fullerenes, independent of their size, contain 12 pentagons. These pentagons, furthermore, have to be completely surrounded by hexagons (for energetic reasons), thus fulfilling the Isolated Pentagon Rule (IPR).[4,5] The definition of a fullerene therefore is: *"a spherical, all carbon, structure consisting of 12 pentagons which are completely surrounded by n hexagons"*. C_{60} is the smallest, stable, fullerene obeying this rule. Fullerenes consisting of more carbon atoms (higher fullerenes) are also possible[6] and are becoming increasingly popular in scientific research.

1.1.2 Buckminsterfullerene: C_{60}

The most famous and most abundant of all fullerenes is Buckminsterfullerene C_{60}. Consisting of 12 pentagons and 20 hexagons, it has I_h symmetry.[7-9] All 30 double bonds in the molecule are situated in the hexagons and are not delocalized like in benzene, although they do delocalize to some extent.[10] C_{60} is not an aromatic structure according to common rules for aromaticity. It is not planar and the double bonds are not fully delocalized. The 'aromaticity' of fullerenes has been extensively reviewed by Bühl and Hirsch in 2001.[11] Furthermore, aromatic substitution reactions are not possible since the π-conjugated system will not be retained upon addition reactions, obviously, there are also no substituents to be substituted.[12] This immedeately implies that common reactions on aromatic systems are not applicable to C_{60}. The chemistry of C_{60} in some respects resembles that of benzoquinone as was first mentioned by Wudl.[13] The oxidizing powers are similar, as well as the C=C bonds being electrophilic, dipolarophilic and dienophilic.

The reactivity of C_{60} is mainly explained by its cage structure. All carbon atoms are $sp^{2,3}$ hybridized. Since they can not be planar in a cage structure there is a certain degree of pyrimidalization, which causes strain. Relief of this strain is the main driving force for reactions on fullerenes.[12] The chemistry on C_{60} will not be discussed here, but is exellently summarized by Hirsch and Brettreich.[14a] New challenges in this field have been adequately described recently by Martín.[14b]

1.1.3 Higher Fullerenes

Fullerenes containing more than 60 carbon atoms are called 'higher fullerenes'. The next possible fullerenes, that fulfill the IPR rule, after C_{60} are C_{70}, C_{72}, C_{74}, C_{76}, C_{78}, C_{80}, C_{82}, C_{84}.[15-22] Of all these fullerenes at least one example of isolation and characterization is known, except for C_{72}.[19,21-30] Even higher fullerenes are theoretically possible and some have been detected.[17] In this thesis, however, no fullerenes higher than C_{84} will be discussed.

With the increasing number of carbon atoms the complexity of the possible fullerene structures increases as well. While the fullerenes up to C_{76} only have one possible IPR isomer, the number of isomers increases rapidly for higher fullerenes. There are 5 possible isomers for C_{78}, 24 for C_{84} and 46 for C_{90}.[20,31] Obviously this increases the complexity of derivatization. Furthermore, not all double bonds are the same in the higher fullerenes (which is the case for C_{60}), which causes formation of even more isomers upon derivatization.

In chapter 2 a more extensive introduction will be given with respect to the reactivity and properties of C_{84}.

1.2 PCBM

Within the field of molecular electronics and the role of fullerenes therein, PCBM (**1.1**) (phenyl-C_{61}-butyric acid methyl ester) plays a special role. In the search for a soluble fullerene for anti HIV treatment, PCBM was developed in the labs of Wudl by Hummelen.[32a] Although its use as an intermediate in the preparation of a medicine for anti HIV treatment never fully materialized,[32b] PCBM would later become the most widely used fullerene compound in molecular electronics.

In 1992 the groups of Heeger and Wudl showed, for the first time, ultrafast electron transfer from a polymer to buckminsterfullerene.[33] The application of C_{60} in, for example, solar cells, was however severely hampered by its poor solubility. The development of PCBM, as a highly soluble C_{60} derivative, offered the solution to this problem.[34] In the same paper, where PCBM was introduced as the electron acceptor in solar cells, the concept of mixing the donor and the acceptor, thus

forming a bulk heterojunction in the active layer, was introduced. This same concept was also shown for mixing two polymers by the groups of Friend and Holmes in the same year.[35] This initial discovery of using C_{60} as an electron acceptor, combined with the high solubility and processability of PCBM boosted a large increase in the field of organic solar cell research. Until today PCBM is used as the electron acceptor in every record breaking donor/acceptor bulk heterojunction solar cell.[36-39] Besides in plastic solar cells, PCBM has been successfully applied in OFETs[40-42], holographic imaging[43-45], and photodetectors.[46] Derivatization of higher fullerenes C_{70} and C_{84} with the same addend as in PCBM, thus creating [70]PCBM (**1.2**) and [84]PCBM (**1.3**) (as mixtures of isomers), has also led to successful applications in solar cells[47,48] and FETs.[49,50] The basic structure of PCBM has been the inspiration of many of the fullerenes that are presented in this thesis.

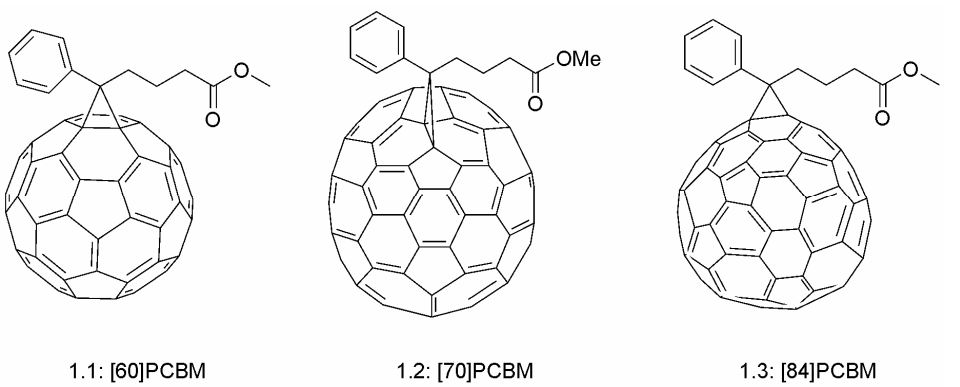

1.1: [60]PCBM 1.2: [70]PCBM 1.3: [84]PCBM

Fig. 1.1: Chemical structures of [60], [70] and [84]PCBM. Major isomers of [70] and [84]PCBM are shown.

1.3 Fullerenes in Organic Electronics

Fullerenes and their derivatives have been extensively used in molecular electronics. Their unique electron accepting capabilities,[51,52] combined with solubility in organic solvents, and easy functionalization have been applied in many different applications. In this section the three applications that are investigated in this thesis will be introduced.

1.3.1 Organic Solar Cells

Although a large variety of solar cells are being investigated, only organic solar cells will be discussed in this thesis.

The most famous application of fullerenes to date is probably found in organic photovoltaics. Not only are fullerenes excellent electron acceptors they also show exceptionally high mobility of electrons. The first significant organic solar cell was developed in 1986 by Tang.[53] The cell by Tang consists of a bilayer device, one layer with a hole conducting material (copper phthalocyanine) and a second layer with an electron conducting material (a perylenetetracarboxylic acid diimide derivative), resulting in an overal efficiency of 1%. A next big step forward was not made until 1992 with the discovery of charge transfer from a polymer to C_{60}.[33] This discovery initiated vast research into fullerene/polymer based solar cells.[54-56] The next paragraphs comprise a short introduction into the working principle, important parameters, and the bulk heterojunction concept.

1.3.1.1 General working principle

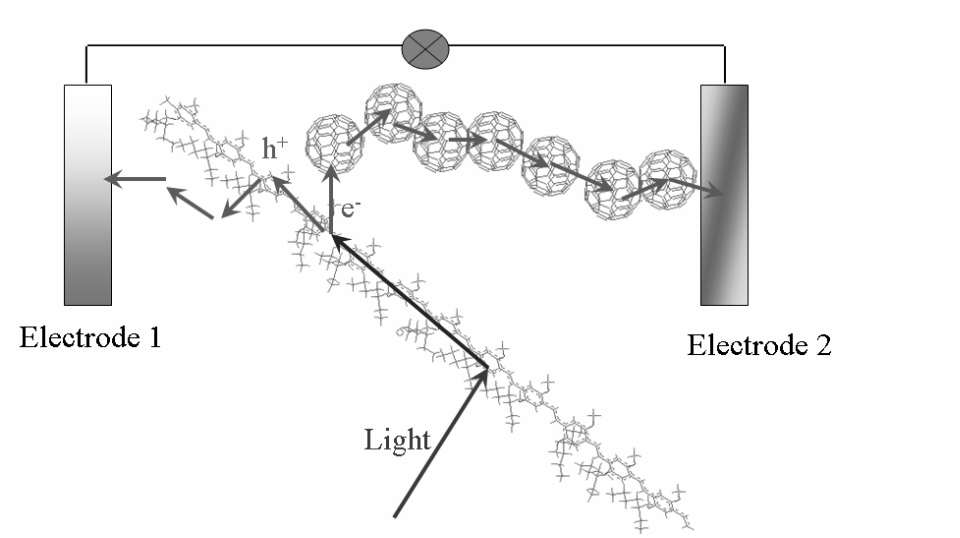

Fig. 1.2: Basic operation of a solar cell. Light absorption followed by charge separation and transport to the respective electrodes.

The general concept consists of the following: light is absorbed by the polymer creating an exciton (bound hole electron pair) in the polymer. This exciton can travel through the polymer until it decays, either by fluoresence or recombination, or until it is dissociated into a hole and an electron.[57] This dissociation occurs at the interface between polymer and fullerene phase. Once the exciton is dissociated, the charges are still coulombically bound and need to be separated after which the holes travel through the polymer to the anode while the electrons travel through the fullerenes to the cathode, thus creating a current (see Fig 1.2).

This mechanism is also applicable to a system consisting of a polymer donor and a polymer acceptor. Using two polymers offers the advantage that both components can be tuned to absorb different parts of the solar spectrum. However, the poor electron mobility in polymers caused these cells to show very low efficiencies, in the order of 10^{-2}%.[58-60] Although some improvements were reported,[61] problems remained abundant, like phase separation and poor electron mobilities. The development of new polymers has resulted in great improvements. Jenekhe et al. showed efficiencies around 1%[I] employing poly(benzimidazobenzophenanthroline ladder) (BBL) as the n-type polymer.[62,63] Efficiencies of 0.8% were reported by Veenstra et al.[64] while even higher efficiencies of 1.5% have been reported recently, by Koetse et al. using yet another n-type polymer: poly{9,9-dioctylfluorene-2,7-diyl-alt-1,4-bis[2-(5-thienyl)-1-cyanovinyl]-2-methoxy-5-(3,7-dimethyl-octyloxy)benzene} (PF1CVTP).[65] The main problem in these systems however, remains the electron mobility, which continues to be low.[66,67a] Even when good electron mobility is reached problems occur due to difficult separation of hole-electron pairs caused by low dielectric constants and strong intermixing of the polymers.[67b]

1.3.1.2 Solar Cell Parameters

When discussing the efficiency of a solar cell, several parameters are of importance. All of these parameters can be deduced from a J/V curve, where J is the current density (A/m^2) and V is the voltage (V) (see Fig. 1.3). The two parameters that are immedeately clear from the graph are the Jsc (short circuit current density), which is the current density at zero voltage and the Voc (open circuit voltage), which is the voltage at zero current. The point at which the cell operates most efficient is where V x J is at its maximum. This point is called the maximum power point (MPP).

[I] Depending on the light intensity used during measurements, efficiencies between 0.7% and 1.5% were reported.

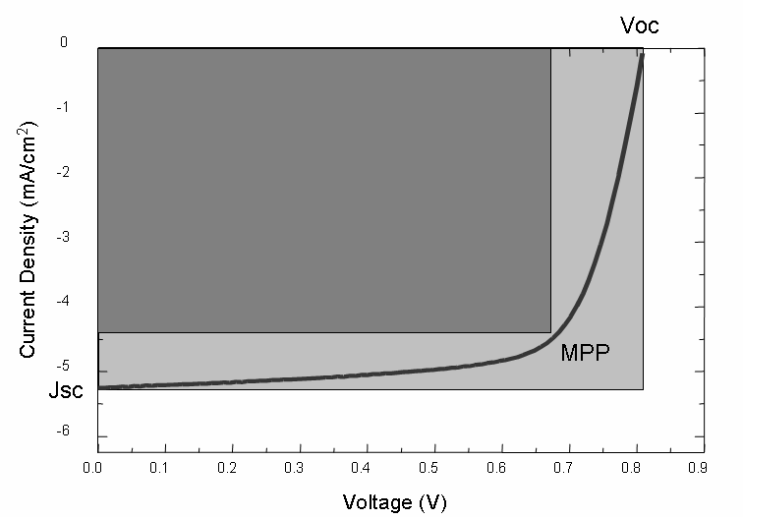

Fig. 1.3: Typical J/V curve, with MPP (maximum power point), Voc (open circuit voltage) and Jsc (short circuit current).

A last parameter of interest is the Fill Factor (FF). If we look at figure 1.3, the FF is the dark rectangle divided by the light rectangle. The FF is a measure giving information regarding a number of internal physical parameters and processes, like charge recombination, and (un)balanced charge carrier mobilities. The FF can be calculated by equation 1:

$$FF = \frac{J_{MPP} * V_{MPP}}{J_{SC} * V_{OC}} \tag{1}$$

When all these values are obtained from the J/V curve the efficiency can be calculated by the following formula:

$$\eta = \frac{V_{OC} * J_{SC} * FF}{P_{IN}}, \tag{2}$$

where η is the power conversion efficiency and P_{IN} is the incident light power density. The power conversion efficiency should furthermore be corrected with a mismatch factor, which describes the deviation of the equipment used, from the standard AM 1.5 conditions.

The AM 1.5 conditions are set as follows: a light intensity of 1000 W/m^2 with a standardized spectral density matching that of the sun when incident at an angle of 48.2^o.

1.3.1.3 Bulk Heterojunction Concept and Active Layer Morphology

Since charges can only be separated at the interface of the donor and the acceptor molecule, it is of the utmost importance to maximize this interface area. The traditional bilayer system is therefore highly inefficient in this type of solar cells. A large improvement was made with the introduction of the bulk heterojunction.[34,35] In a bulk heterojunction the two components are dissolved in one matrix and spincoated as such as the active layer, thus obtaining an interpenetrating network of donor and acceptor materials.

On the other hand charges must be able to move through the donor or acceptor phase to reach an electrode. An optimum must therefore be found between effective interface area and continuous conduction pathways within the active layer. This morphology of the active layer has been the interest of extensive research, leading to many improvements in the fabrication technique of organic solar cells. One striking example is the difference between spincoating PCBM/MDMO-PPV solar cells from toluene or from chlorobenzene. A three-fold increase in efficiency was obtained when spincoating from chlorobenzene due to a decrease in domain sizes and thus increase in interface area between the polymer and the fullerene.[36]

When using poly(3-hexyl) thiophene (P3HT) as the donor polymer, not only the spincoating solvent is of importance. Thermally annealing the active layer after spincoating causes the P3HT to partially crystallize, thus increasing the hole mobility in the P3HT phase as well as increasing its absorption properties.[37,38,68-81] Optimilization of the morphology of the active layer is therefore critical in the fabrication of organic solar cells.

1.3.1.4 Record Solar Cells

Almost every record breaking solar cell since 2005 has been based on the P3HT:PCBM combination, where morphology improving annealing steps are optimized. Efficiencies of 4.4% were reported by the group of Yang, in 2005, using morphology improving annealing steps in a 1:0.8 wt% mixture of P3HT and PCBM.[38] However, when their devices were subjected to standard test conditions (STC) at NREL an efficiency of only 3.6% was found, which was attributed to a spectral mismatch. The group of Carroll reported values of 4.9% in the same year, also using a P3HT:PCBM wt% of 1:0.8.[78]

Their values however, were measured at a different light intensity of 80 mW/cm^2 instead of the commonly used 100 mW/cm^2.

No spectral mismatch factors were taken into account and no measurements were performed at STC. In the same year Heeger et al. presented efficiencies approaching 5% using the same active layer as the above mentioned groups.[82] Here the spectral mismatch was taken into account and the measurements were performed at STC. It must be noted however, that the active area of all these solar cells vary. Heeger used 14.8 mm^2, while Carroll used 19 mm^2 and Yang 11 mm^2. It is commonly known that smaller areas yield higher efficiencies. Soon after the publication by Yang, which claimed record efficiencies at the time, a publication (in the same journal) appeared by Kim et al., in 2006, claiming 4.4% efficiencies as well.[83] A bulk heterojunction consisting of 1:1 wt% P3HT:PCBM was used. Just as all previous groups a morphology improving annealing step was applied. New in this publication was the study of different degrees of regio regularity in the P3HT. However, no active areas are reported and no STC measurement were performed. A final record was claimed in 2007 by the group of Carroll, reporting efficiencies of 6%.[39] The composition of the active layer was adjusted to 1:0.6 P3HT:PCBM wt% and again annealing steps were performed to enhance device performance. The active areas of these devices are however, very small (between 5 and 10 mm^2) also no STC measurements were reported.

Besides thermal annealing of the P3HT:PCBM active layer, some other improvements were reported. Heeger introduced a titanium oxide optical spacer, which improved the absorption properties of the cells.[77] An efficiency of 5% was claimed, using the same conditions as described above. Interestingly, it was claimed in this paper that the optical spacer caused an increase of the efficiency from 2.3% to 5%, while 5% solar cells without the use of an optical spacer were already claimed by the authors, applying excactly the same conditions. These values however, were not verified. A third way of improving morphology that is worth mentioning is 'slow drying'. This was introduced by the group of Yang in 2005.[38] Somewhat later the group of Blom reported efficiencies of 3.7% measured under STC applying slow drying methods.[84]

Most recently, an entire new donor acceptor combination yielded 5.5% efficiencies under STC conditions (without mentioning the active area though).[85] In this work, by the groups of Bazan and Heeger, a combination of [70]PCBM and poly[2,6-(4,4-bis-(2-ethylhexyl)-4*H*-cyclopenta[2,1-b;3,4-b']-dithiophene)-*alt*-4,7-(2,1,3-benzothiadiazole)] (PCPDTBT) was used as the active layer. 1,8-Octanedithiol was added to the active layer mixture. This improved the morphology of the active layer, thus explaining the high efficiencies that were obtained.

The latest record was set at ~6.5% efficiency (under illumination of 200 mW/cm^2) by the Heeger group in July of 2007, employing a solution processed tandem polymer solar cell.[86] A solution processed tandem solar cell consists of two bulk heterojunction solar cells on top of each other which are connected in series.[87]

In this example the bottom cell consisted of a bulk heterojunction made from P3HT and [70]PCBM while the top cell consisted of a bulk heterojunction made from a lower bandgap polymer (PCPDTBT) and [60]PCBM. Since both cells are connected in series the overall voltage is the sum of both cells. The current is determined by that of the worst cell. A great advantage of this structure is the use of two different polymers, thus absorbing a greater portion of the solar spectrum. However, these values were not verified.

1.3.1.5 Outlook

The field of organic photovoltaics is progressing rapidly in recent years with power conversion efficiencies of over 5% being reported on a more regular basis.[39,77,78,82,85,86] Although one could raise some concerns at times, regarding these values, it is clear that efficiencies are increasing rapidly.

Challenges however, remain. The percentage of light that is absorbed is still fairly low. The solution to this problem seems to be low bandgap polymers. Although many efforts have been reported that are promising, none show record efficiencies as of yet.[88-102] Most of these polymers are block copolymers consisting of donor and acceptor like blocks. It can be expected that this will cause serious problems with regard to hole conductivity. The low currents characteristically observed, might be caused by this transport problem. A positive exception of a low bandgap polymer (1.4 eV), that does show very high efficiencies, is PCPDTBT.

Another parameter that shows room for improvement is the open circuit voltage. Improvement of the open circuit voltage is discussed in detail in Chapter 3.

Taking everything into account, the future of organic solar cells looks bright. Power conversion effeciencies of around 5% make commercialization feasible.[103] There is still a lot of room for improvement and efficiencies of around 10% seem attainable in the near future.[104-106]

1.3.2 Field Effect Transistors

In recent years fullerenes have shown high potential in Organic Field Effect Transistors (OFETs).[40,41,49] In the next paragraphs the working principle of a FET will briefly be explained. The organic materials used for FET fabrication will be discussed shortly.[107]

1.3.2.1 General working principle

A FET is built up as follows: A gate electrode is separated from a semiconducting layer by an insulating gate dielectric. The semiconducting layer is in contact with two electrodes, a source and a drain electrode of width *W* (channel width), which are separated from each other by a distance *L* (channel length) (*W* >> *L*) (see Fig. 1.4)

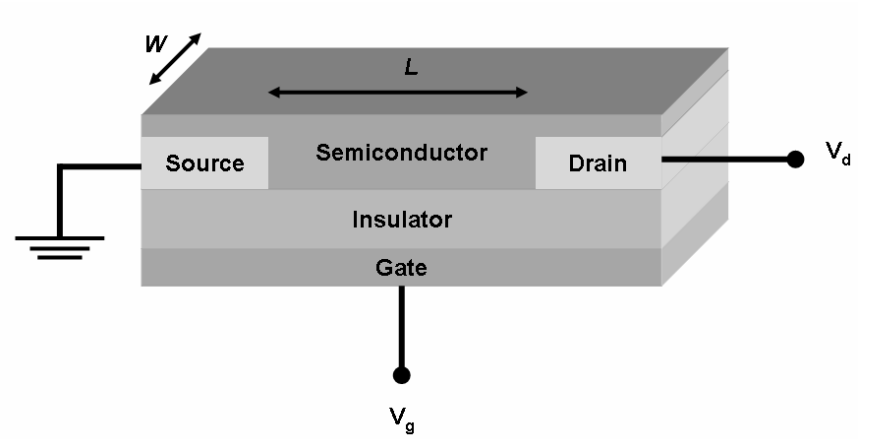

Fig. 1.4: Schematic FET layout

In the case of an organic field effect transistor the semiconducting layer is usually vacuum sublimed, spin-coated or drop-cast. The gate electrode is usually highly doped silicon which can simultaneously serve as the substrate. As gate dielectrics inorganic insulators are used (SiO_2, Al_2O_3, Si_3N_4), but polymeric insulators can be used effectively as well (PMMA, PVP).[108-110] As the source and drain electrodes, high workfunction metals are most commonly used (Au, Pd[111], Pt[112] and Ag[113,114]) although printable conducting polymers can be used as well (PEDOT:PSS[115-117], PANI[118-120]).

When operating, a voltage is applied to the gate and the drain while the source is grounded. The potential difference between the gate and the drain is called the gate voltage (V_G), the potential difference between the drain and the source is called the source-drain voltage (V_{ds}). When a potential is applied at the gate, opposite charges accumulate in the insulator/semiconductor layer, thus opening a channel for conduction of these charges. Since not all charges are mobile i.e. there are usually traps present and because there can be charges already present in the

insulator, a certain voltage has to be applied before a current is measured, this can be both positive and negative. This voltage is called the threshold voltage (V_{TH}). The effective gate voltage is therefore $V_G - V_{TH}$.

1.3.2.2 Materials

Materials for FETs can be divided in two main classes: p-type and n-type materials, where p-type depends on dominant hole transport, n-type depends on electron transport.

1.3.2.2.1 p-type organic FET materials

Charge carrier mobility is one of the most important FET parameters, since it determines the operation speed of the transistor. To date the highest mobilities for thin layer organic p-type FETs are obtained with vacuum sublimed pentacene (>1 cm^2/Vs).[121] Pentacene (**1.4**) is however, not solution processable, which would be more practical than vacuum sublimation. In recent years many efforts have been made to synthesize soluble pentacene derivatives, but they generally show much lower mobilities.[122,123] Functionalized anthradithiophenes (**1.7a**,**b**), however, do show mobilities close to 1 cm^2/Vs.[124-127]. Solution processable polymers offer a wide range of interesting materials for FET application. The polymer with the highest mobility is regio regular poly(3-hexyl)thiophene (RR-P3HT) (**1.8**), showing values of up to 0.1 cm^2/Vs, depending on the processing conditions.[124,128,129]. The highest mobilities however, are obtained from single crystal FETs.[130] The best examples of high mobility single crystals are vacuum sublimed pentacene[131], tetracene (**1.5**)[132] and rubrene (**1.6**).[133] Mobilities of up to 20 cm^2/Vs have been obtained with single crystal rubrene FETs.[134]

1.3.2.2.2 n-type organic FET materials

Whereas p-type FET materials are abundant, n-type FET materials are much rarer (see Fig. 1.6). Recently, however, more n-type materials are becoming available. The most successful class of compounds exibiting high n-type mobility in FETs is that of the fullerenes C_{60}, C_{70}, and their derivatives.[40,42,49,135-137] Mobilities close to 1 cm^2/Vs have been obtained. Other n-type materials are usually fluorinated p-type materials, like perfluorinated pentacene (**1.9**) [138] and thiophenes with fluorinated side chains (**1.10**, **1.11**, **1.12**).[139,140] One of the scarce (non fluorinated) polymers showing n-type conduction is poly(benzobisimidazobenzophenanthroline) (BBL, **1.13**). Good n-type conduction is furthermore obtained with TCNQ (**1.14**).[141]

The biggest challenge for n-type materials these days is air-stability. This particular aspect of n-type FET materials will be discussed in detail in Chapter 4.

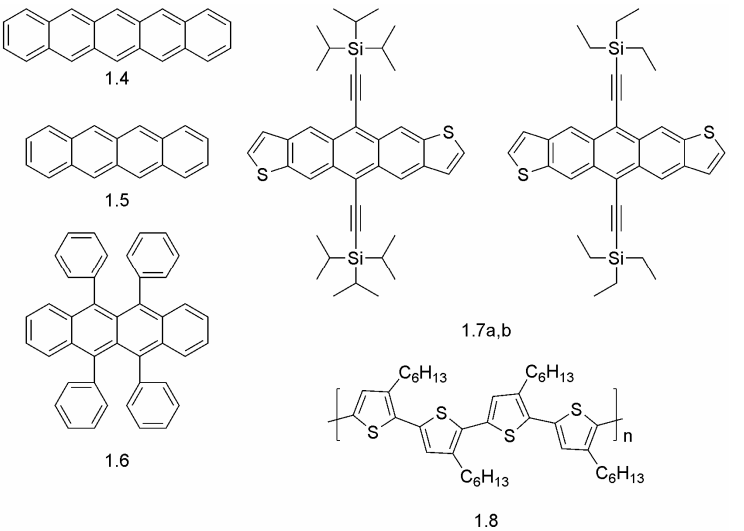

Fig. 1.5: organic materials for p-type FET applications.

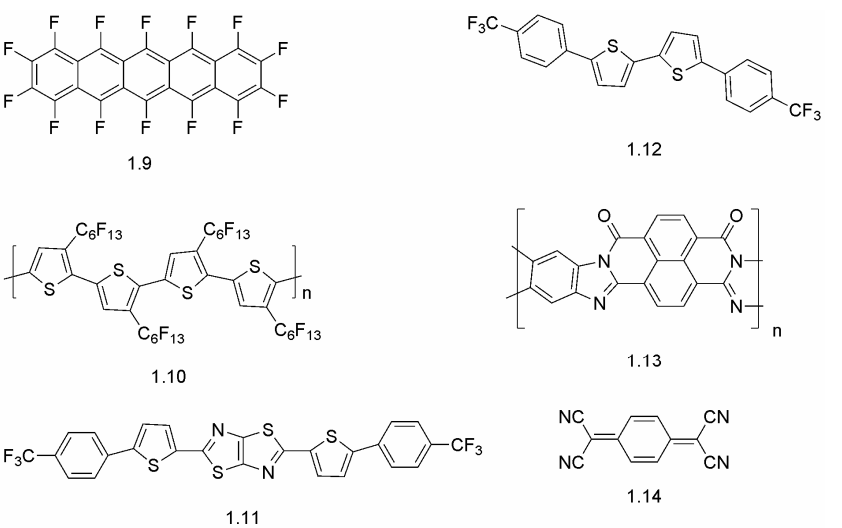

Fig. 1.6: n-type organic FET materials.

1.3.2.3 Outlook

The field of organic field effect transistors is expanding rapidly as increasing mobilities are obtained. The increasing availability of n-type FET materials will furthermore stimulate the development of organic FETs for commercially interesting applications as complementary circuit design is within reach. The development of good ambipolar materials would further simplify this.[142-146] The biggest challenge remaining in the field is the development of air-stable materials which can be solution processed under ambient conditions. Promising developments, which will be discussed in chapter 4, have been reported, stimulating further research.

1.3.3 Time Gated Holographic Imaging

One particularly interesting application of reversible holographic storage media is time-gated holographic imaging (TGHI).[147-151] TGHI has the potential to be used as a non-invasive medical diagnostic tool, somewhat related to a holographic variant of optical coherence tomography (OCT).[152,153] However, TGHI provides, in contrast to OCT, whole field depth-resolved images without further computations. In practise this would mean that one could make *in vivo* real-time images and even fly through movies of biological tissue. The transparency of biological tissue for near infra red (NIR 700-900 nm) light can be used for application in medical diagnosis.

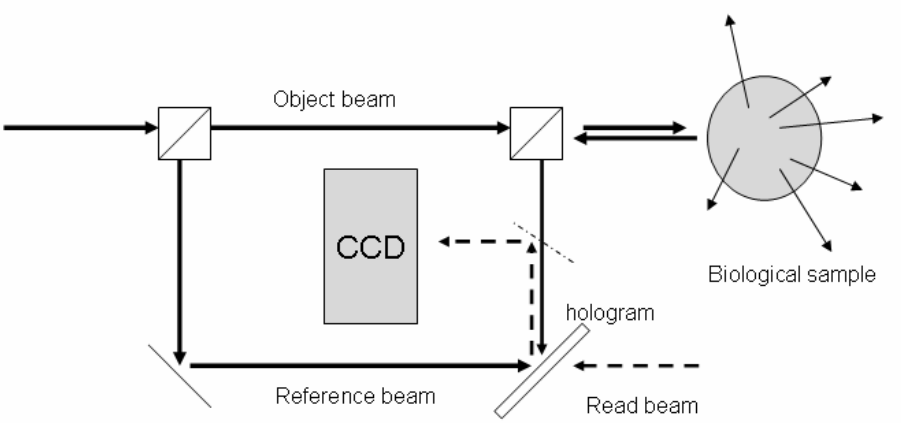

Fig. 1.7: Basic principle of holographic imaging. Small arrows are scattered light, thick arrow is single reflected light (ballistic photons)

The information about the tissue that is irradiated by a NIR laser can be detected by a holographic technique that can distuingish singly reflected photons (ballistic photons) from a certain depth from multiply scattered photons. (see Fig. 1.7) Important to note is that the depth resolution is inversely proportional to the coherence length of the laser source (smaller coherence length gives better resolution).

1.3.3.1 General working principle

The basic principle is as follows. The holographic material consists of three main components: 1) a photoconducting amorphous material[II] 2) non linear optical (NLO) chromophores 3) a sensitizer, typically in low content (1-10wt %). This material is used as a composite mixture. Before illumination the holographic storage material is pre-poled by an external electric field (E_0, see figure 1.8) causing the NLO chromophores to align. For orientation of the chromophore species, the glass transition temperature of the composite has to be below room temperature. Next the ballistic photons that are reflected from the biological sample interfere with a coherent reference laser beam. This reference beam can be delayed, thus tuning the depth of the features that are detected. The interference pattern that is formed, causes exciton formation (by direct excition of, in some cases, the sensitizer) in the bright regions of the interference pattern. Field assisted charge separation can then take place between the conducting amorphous material and the sensitizer. One of the charges is now trapped while the other is mobile. Due to the low content of sensitizer in the composite, electrons are trapped while holes can move through the hole-conducting polymer. The mobile charges drift (field induced) through the hole conducting matrix until they get trapped in the dark regions of the interference pattern. Since one charge is trapped and the other is mobile an internal space charge field (E_{sc}, see figure 1.8) is generated in the material upon this field induced drift. The NLO chromophores will now realign according to the sum of the external field and the internal field ($E=E_0+E_{sc}$, see Fig. 1.8). Due to this rearrangement, the refractive index of the holographic material is locally changed. This change can be probed by a read beam which in turn is translated to a video image. Crucial is the speed in which the hologram can be written, erased and written again. A higher time resolution will be obtained as the speed is increased. A speed of 50 cycles per second is necessary for good quality video rate.

[II] Conventional organic photorefractive materials are based on hole-transporting molecules/polymers. Within this work, inverse photorefractive materials with electron transport through fullerene moieties are introduced.

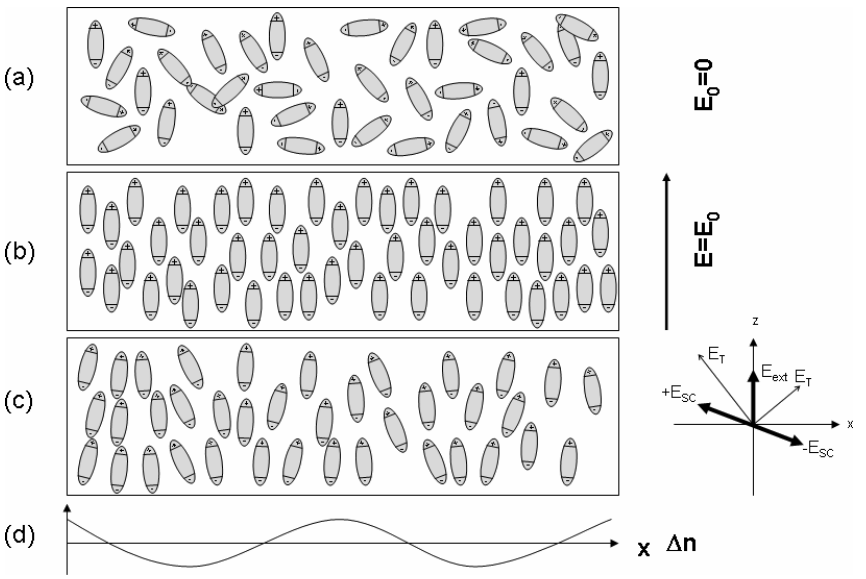

Fig. 1.8: Illustration of chromophore alignment a) no electric field, NLO chromophores are oriented randomly. b) external field applied and NLO chromophores orient accordingly. c)vectorial sum (E_T) of internal (E_{sc}) and external field (E_{ext}) and NLO chromophores re-orientation. d)refractive index modulation Δn.[148]

A substantial increase in speed can be achieved by 'gating' the material, which means that the material is pre-illuminated at 633 nm, causing the generation of charges prior to writing the hologram. The speed increase upon gating depends on material properties (for example: NIR charge generation efficiency, absorption coefficient) A 40 fold increase in speed can be achieved this way.[44]

1.3.3.2 Fullerenes in TGHI

Sensitizers play an important role in the total composite. The most successful sensitizers are fullerenes, in particular PCBM.[43-45] They offer the great advantage of fast charge transfer from polymer to fullerene and high stability of the thus created anion. The role of sensitizers in the composite, as well as all other materials, is explained in more detail in Chapter 5.

1.3.3.3 Outlook

With the achievement of video rate writing-reading-erasing of the holograms, the actual application of the technique is within reach. Further improvement in resolution (faster write speeds, better lasers) as well as a good understanding of the resulting images is still necessary.

However, first tests as components in photorefractive materials for an actual device application seems attainable in the near future.

1.4 Outline and Aim of this thesis

The aim of this thesis is to develop a broader understanding of the role of fullerenes in different applications in the field of organic electronics, as well as chemically improving fullerenes to better fit the desired application. One of the most important aspects in respect to this is the LUMO level of the fullerene. Central theme in this thesis therefore, is the chemical modification of fullerenes in such a way as to influence its LUMO level.

In *Chapter two* the derivatization, and application in solar cells, of the higher fullerene C_{84} is discussed. A soluble C_{84} derivative ([84]PCBM) was developed, and tested in organic solar cell devices as the electron acceptor in combination with MDMO-PPV as an electron donor.

In *Chapter three* the influence of the fullerene LUMO level with respect to the V_{OC} of organic solar cells is described. A series of fullerene derivatives was synthesized with different LUMO levels. The fullerenes were tested in solar cells as the electron acceptor.

In *Chapter four* the development of air-stable n-type field effect transistors is discussed. Two different strategies of obtaining such air stable FETs are presented. Correspondingly, two types of fullerenes were synthesized. First [84]PCBM was used as a semiconductor in FETs. Second a series of fullerenes with fluorinated side chains was investigated for air-stability in FETs.

In *Chapter five* the application of fullerenes in time gated holographic imaging (TGHI) is presented. Two different roles of fullerenes in TGHI are discussed. The influence of the fullerene LUMO level on its performance as a sensitizer is discussed as well as the application of fullerenes as the charge transporting matrix.

The final two chapters focus on more fundamental fullerene research where no direct applications are shown.

One of the greatest challenges remaining in fullerene chemistry is the synthesis of fullerene derivatives where the addend is in direct conjugation with the fullerene sphere, via an alternating single, double bond pathway. In *Chapter six* a methodology is devoloped for the synthesis of such 'conjugated' fullerene adducts.

We serendipitiously discovered a synthetic methodology for the synthesis of fullerene containing pearl-necklace macrocycles. This methodology, and the obtained structures are discussed in *Chapter seven.*

1.5 List of publications

1 Floris B. Kooistra, Valentin D. Mihailetchi, Lacramioara M. Popescu, David Kronholm, Paul W. M. Blom and Jan C. Hummelen. *Chemistry of Materials*, **2006**, *18*, 3068-3073

2 Thomas D. Anthopoulos, Floris B. Kooistra, Harry J. Wondergem, David Kronholm, Jan C. Hummelen, Dago M.de Leeuw. *Advanced Materials*, **2006**, *18*, 1679-1684

3 Afshin Hadipour, Bert de Boer, Jurjen Wildeman, Floris Kooistra, Jan C. Hummelen, Mathieu G. R. Turbiez, Martijn M. Wienk, Rene A. Janssen, and Paul W. M. Blom. *Advanced Functional Materials*, **2006**, *16*, 1897-1903

4 Afshin Hadipour, Bert de Boer, Jurjen Wildeman, Floris Kooistra, Jan C. Hummelen, Mathieu G. R. Turbiez, Martijn M. Wienk, Rene A. Janssen, and Paul W. M. Blom., *Proc. SPIE 6192*, 61920D (**2006**)

5 Floris B. Kooistra, Joop Knol, Fredrik Kastenberg, Lacramioara M. Popescu, Wiljan J.H. Verhees, Jan M. Kroon and Jan C. Hummelen. *Organic Letters*, **2007**, *9*, 551-554

6 Sebastian Köber, Floris B. Kooistra, Francisco Gallego-Gomez, Michael Salvador, Felix Mielke, Oscar Nuyken, Jan C. Hummelen and Klaus Meerholz. *Submitted for publication.*

7 Sebastian. Köber, Floris B. Kooistra, Francisco Gallego-Gomez, Michael Salvador, Felix Mielke, Oscar Nuyken, Jan C. Hummelen and Klaus Meerholz. *OSA proceedings, **2007**, accepted.*

8 Martijn Lenes, Gert-Jan A. H. Wetzelaer, Floris B. Kooistra, Jan C. Hummelen and Paul W. M. Blom, *submitted for publication.*

9 Magda M. Mandoc, Floris B. Kooistra, Jan C. Hummelen, Bert de Boer, and Paul W. M. Blom, *submitted for publication.*

10 Floris B. Kooistra, Frank Brouwer, and Jan C. Hummelen, *submitted for publication.*

11 Floris B. Kooistra, Tessa M. Leuning, Enrique Maroto Martinez, and Jan C. Hummelen, *submitted for publication.*

12 Paul Wöbkenberg, Donal D. C. Bradley, David F. Kronholm, Floris B. Kooistra, Jan C. Hummelen, Michael Cölle, Dago M. de Leeuw, and Thomas D. Anthopoulos, *submitted for publication*

13 Martijn Lenes, Floris B. Kooistra, Jan C. Hummelen and Paul W. M. Blom, *submitted for publication.*

14 Sebastian Köber, Floris B. Kooistra, Johannes Beerlink, Francisco Gallego-Gomez, Michael Salvador, Felix Mielke, Oscar Nuyken, Jan C. Hummelen and Klaus Meerholz. *Inverted photorefractive materials, to be published*

15 Sebstian Köber, Floris B. Kooistra, Michael Salvador, Jan C. Hummelen and Klaus Meerholz. *1064 nm sensitized photorefractive polymers, to be published*

1.6 References

1. H. W. Kroto, J. R. Heath, S. C. O'Brien, R. F. Curl, and R. E. Smalley, *Nature*, 1985**, 318**, 162.
2. W. Krätschmer, K. Fostiropoulos, and D. R. Huffman, *Chem.Phys.Lett.*, 1990**, 170**, 167.
3. W. Krätschmer, L. D. Lamb, K. Fostiropoulos, and D. R. Huffman, *Nature*, 1990**, 347**, 354.
4. T. G. Schmalz, W. A. Seitz, D. J. Klein, and G. E. Hite, *Chem.Phys.Lett.*, 1986**, 130**, 203.
5. H. W. Kroto, *Nature*, 1987**, 329**, 529.
6. P. W. Fowler and D. E. Manolopoulos, in *An Atlas of Fullerenes*, Oxford University Press, Oxford, 1 ed., 1995.
7. S. Liu, Y. Lu, M. M. Kappes, and J. A. Ibers, *Science*, 1991**, 254**, 408.
8. K. Hedberg, I. Hedberg, D. S. Bethune, C. A. Brown, H. C. Dorn, R. D. Johnson, and M. De Vries, *Science*, 1991**, 254**, 410.
9. W. I. F. David, R. M. Ibberson, J. C. Matthewman, K. Prassides, T. J. S. Dennis, J. P. Hare, H. W. Kroto, R. Taylor, and D. R. M. Walton, *Nature*, 1991**, 353**, 147.
10. C. S. Yannoni, P. P. Bernier, D. S. Bethune, G. Meijer, and J. R. Salem, *J.Amer.Chem.Soc.*, 1991**, 113**, 3190.
11. M. Buhl and A. Hirsch, *Chem.Rev.*, 2001**, 101**, 1153.
12. R. C. Haddon, *Science*, 1993**, 261**, 1545.
13. C. Bellavia-Lund, M. Keshavarz-K, R. González, J. C. Hummelen, R. Hicks, and F. Wudl, *Phosphorus, Sulfur, and Silicon*, 1997**, 120 & 121**, 107.

14. a) A. Hirsch and M. Brettreich, in *Fullerenes Chemistry and Reactions*, Wiley-VCH Verlag GmbH & Co. KgaA, Weinheim, 2005. b) N. Martín, *Chem.Commun.,* 2006, 2093.
15. P. W. Fowler, *J.Chem.Soc.Faraday.Trans.*, 1991**, 87**, 1945.
16. M. D. Diener and J. M. Alford, *Nature*, 1998**, 393**, 668.
17. K. Kikuchi, N. Nakahara, T. Wakabayashi, M. Honda, H. Matsumiya, T. Moriwaki, S. Suzuki, H. Shiromaru, K. Saito, I. Yamauchi, I. Ikemoto, and Y. Achiba, *Chem.Phys.Lett.*, 1992**, 188**, 177.
18. F. Diederich and R. L. Whetten, *Acc.Chem.Res.*, 1992**, 25**, 119.
19. F. H. Hennrich, R. H. Michel, A. Fischer, S. Richard-Schneider, S. Gilb, M. M. Kappes, D. Fuchs, M. Bürk, K. Kobayashi, and S. Nagase, *Angew.Chem.Int.Ed.*, 1996**, 35**, 1732.
20. P. W. Fowler, R. C. Batten, and D. E. Manolopoulos, *J.Chem.Soc.Faraday.Trans.*, 1991**, 87**, 3103.
21. R. Ettl, I. Chao, F. Diederich, and R. L. Whetten, *Nature*, 1991**, 353**, 149.
22. F. Diederich, R. Ettl, Y. Rubin, R. L. Whetten, R. Beck, M. Alvarez, S. Anz, D. Sensharma, F. Wudl, K. C. Khemani, and A. Koch, *Science*, 1991**, 252**, 548.
23. K. Kikuchi, N. Nakahara, T. Wakabayashi, S. Suzuki, H. Shiromaru, Y. Miyake, K. Saito, I. Ikemoto, M. Kainosho, and Y. Achiba, *Nature*, 1992**, 357**, 142.
24. R. Taylor, G. J. Langley, A. G. Avent, T. J. S. Dennis, H. W. Kroto, and D. R. M. Walton, *J.Chem.Soc.Perkin.Trans.2*, 1993, 1029.
25. A. L. Balch, A. S. Ginwalla, J. W. Lee, B. C. Noll, and M. M. Olmstead, *J.Amer.Chem.Soc.*, 1994**, 116**, 2227.
26. T. J. S. Dennis, T. Kai, T. Tomiyama, and H. Shinohara, *Chem.Commun.*, 1998, 619.
27. F. Diederich, R. L. Whetten, C. Thilgen, R. Ettl, I. Chao, and M. Alvarez, *Science*, 1991**, 254**, 1768.
28. R. Taylor, G. J. Langley, T. J. S. Dennis, H. W. Kroto, and D. R. M. Walton, *J.Chem.Soc.Chem.Commun.*, 19921043.
29. A. G. Avent, D. Dubois, A. Pénicaud, and R. Taylor, *J.Chem.Soc.Perkin.Trans.2*, 19971907.
30. R. H. Michel, M. M. Kappes, P. Adelmann, and G. Roth, *Angew.Chem.Int.Ed.*, 1994**, 33**, 1651.
31. K. Balasubramanian, *Chem.Phys.Lett.*, 1993**, 206**, 210.
32. a) J. C. Hummelen, B. W. Knight, F. Lepeq, F. Wudl, J. Yao, and C. L. Wilkins, *J.Org.Chem.*, 1995**, 60**, 532. b) Schinazi, A. McMillan, A.S. Juodawlkis, J. Pharr, R. Sijbesma, G. Srdanov, J.C. Hummelen, F.D. Boudinot, C.L. Hill, and F.Wudl, *Proc. Electrochem. Soc*. 1994, **94**-24, 689.
33. N. S. Sariciftci, L. Smilowitz, A. J. Heeger, and F. Wudl, *Science*, 1992**, 258**, 1474.
34. G. Yu, J. Gao, J. C. Hummelen, F. Wudl, and A. J. Heeger, *Science*, 1995**, 270**, 1789.

35. J. J. M. Halls, C. A. Walsch, N. C. Greenham, E. A. Marseglia, R. H. Friend, S. C. Moratti, and A. B. Holmes, *Nature*, 1995**, 376**, 498.
36. S. E. Shaheen, C. J. Brabec, N. S. Sariciftci, F. Padinger, T. Fromherz, and J. C. Hummelen, *Appl.Phys.Lett.*, 2001**, 78**, 841.
37. F. Padinger, R. S. Rittberger, and N. S. Sariciftci, *Adv.Funct.Mater.*, 2003**, 13**, 85.
38. G. Li, V. Shrotriya, J. Huang, Y. Yao, T. Moriarty, K. Emery, and Y. Yang, *Nat.Mater.*, 2005**, 4**, 864.
39. K. Kim, J. Liu, M. A. G. Namboothiry, and D. L. Carroll, *Appl.Phys.Lett.*, 2007**, 90**, 163511.
40. T. D. Anthopoulos, C. Tanase, S. Setayesh, E. Meijer, J. C. Hummelen, P. W. M. Blom, and D. M. de Leeuw, *Adv.Mater.*, 2004**, 16**, 2174.
41. T. D. Anthopoulos, D. M. de Leeuw, E. Cantatore, S. Setayesh, E. J. Meijer, C. Tanase, J. C. Hummelen, and P. W. M. Blom, *Appl.Phys.Lett.*, 2004**, 85**, 4205.
42. C. Waldauf, P. Schillinsky, M. Perisutti, J. Hauch, and C. J. Brabec, *Adv.Mater.*, 2003**, 15**, 2084.
43. E. Mecher, C. Bräuchle, H. H. Hörhold, J. C. Hummelen, and K. Meerholz, *Phys.Chem.Chem.Phys.*, 1999**, 1**, 1749.
44. E. Mecher, F. Gallego-Gómez, H. Tillman, H. H. Hörhold, J. C. Hummelen, and K. Meerholz, *Nature*, 2002**, 418**, 959.
45. E. Mecher, F. Gallego-Gómez, K. Meerholz, H. Tillman, H. H. Hörhold, and J. C. Hummelen, *CHEMPHYSCHEM*, 2004**, 5**, 277.
46. X. H. Wang, O. Hofmann, R. Das, E. M. Barrett, A. J. Demello, J. C. Demello, and D. D. C. Bradley, *Lab on A Chip*, 2007**, 7**, 58.
47. F. B. Kooistra, V. D. Mihailetchi, L. M. Popescu, D. Kronholm, P. W. M. Blom, and J. C. Hummelen, *Chem.Mater.*, 2006**, 18**, 3068.
48. M. M. Wienk, J. M. Kroon, W. J. H. Verhees, J. Knol, J. C. Hummelen, P. A. van Hal, and R. A. J. Janssen, *Angew.Chem.Int.Ed.*, 2003**, 42**, 3371.
49. T. D. Anthopoulos, D. M. de Leeuw, E. Cantatore, P. van 't Hof, J. Alma, and J. C. Hummelen, *J.Appl.Phys.*, 2005**, 98**, 054503.
50. T. D. Anthopoulos, F. B. Kooistra, H. J. Wondergem, D. Kronholm, J. C. Hummelen, and D. M. de Leeuw, *Adv.Mater.*, 2006**, 18**, 1679.
51. P. M. Allemand, A. Koch, F. Wudl, Y. Rubin, F. Diederich, M. M. Alvarez, S. J. Anz, and R. L. Whetten, *J.Amer.Chem.Soc.*, 1991**, 133**, 1050.
52. B. Miller, J. M. Rosamilia, G. Dabbagh, R. Tycko, R. C. Haddon, A. J. Muller, W. Wilson, D. W. Murphy, and A. F. Hebard, *J.Amer.Chem.Soc.*, 1991**, 113**, 6291.
53. C. W. Tang, *Appl.Phys.Lett.*, 1986**, 48**, 183.
54. S. Günes, H. Neugebauer, and N. S. Sariciftci, *Chem.Rev.*, 2007**, 107**, 1324.
55. H. Hoppe and N. S. Sariciftci, *J.Mater.Res.*, 2004**, 19**, 1924.
56. E. A. Katz, in *Encyclopedia of Nanaoscience and Nanotechnology*, ed.H. S. Nalwa, 2003, pp. 1-23.

57. J. M. Nunzi, *C.R.Physique*, 2002**, 3**, 532.
58. H. Antoniadis, B. R. Hsieh, M. A. Abkowitz, S. A. Jenekhe, and M. Stolka, *Synth.Met.*, 1994**, 62**, 265.
59. R. N. Marks, J. J. M. Halls, D. D. C. Bradley, R. H. Friend, and A. B. Holmes, *J.Phys.Cond.Matter.*, 1994**, 6**, 1379.
60. J. J. M. Halls, C. A. Walsh, N. C. Greenham, E. A. Marseglia, R. H. Friend, S. C. Moratti, and A. B. Holmes, *Nature*, 1995**, 376**, 498.
61. G. Yu and A. J. Heeger, *J.Appl.Phys.*, 1995**, 78**, 4510.
62. S. A. Jenekhe and S. Yi, *Appl.Phys.Lett.*, 2000**, 77**, 2635.
63. M. M. Alam and S. A. Jenekhe, *Chem.Mater.*, 2004**, 16**, 4647.
64. S. C. Veenstra, W. J. H. Verhees, J. M. Kroon, M. M. Koetse, J. Sweelsen, J. J. A. M. Bastiaansen, H. F. M. Schoo, X. Yang, A. Alexeev, J. Loos, U. S. Schubert, and M. M. Wienk, *Chem.Mater.*, 2004**, 16**, 2503.
65. M. M. Koetse, J. Sweelssen, K. T. Hoekerd, H. F. M. Schoo, S. C. Veenstra, J. M. Kroon, X. Yang, and J. Loos, *Appl.Phys.Lett.*, 2006**, 88**, 083504.
66. A. J. Breeze, Z. Schlesinger, S. A. Carter, H. Tillmann, and H. H. Hörhold, *Sol.En.Mater.Sol.Cells*, 2004**, 83**, 263.
67. a) P. A. C. Quist, T. J. Savenije, M. M. Koetse, S. C. Veenstra, J. M. Kroon, and L. D. A. Siebbeles, *Adv.Funct.Mater.*, 2005**, 15**, 469. b) M. M. Mandoc, W. Veurman, L. J. A. Koster, B. de Boer, P. W. M. Blom, *Adv.Funct.Mater.,* 2007, **17**, 2167.
68. D. Chirvase, Z. Chiguvare, M. Knipper, J. Parisi, V. Dyakonov, and J. C. Hummelen, *J.Appl.Phys.*, 2003**, 93**, 3376.
69. N. Camaioni, G. Ridolfi, G. Casalbore-Miceli, A. Possamai, and M. Maggini, *Adv.Mater.*, 2002**, 14**, 1735.
70. P. Schillinsky, C. Waldauf, and C. J. Brabec, *Appl.Phys.Lett.*, 2002**, 81**, 3885.
71. T. Erb, U. Zhokhavets, G. Gobsch, S. Raleva, B. Stühn, P. Schillinsky, C. Waldauf, and C. J. Brabec, *Adv.Funct.Mater.*, 2005**, 15**, 1193.
72. D. Chirvase, J. Parisi, J. C. Hummelen, and V. Dyakonov, *Nanotechnology*, 2004**, 15**, 1317.
73. T. Ahn, H. Lee, and S.-H. Han, *Appl.Phys.Lett.*, 2002**, 80**, 392.
74. F. Zhang, M. Svensson, M. R. Andersson, M. Maggini, S. Bucella, E. Menna, and O. Inganäs, *Adv.Mater.*, 2001**, 13**, 1871.
75. P. J. Brown, D. S. Thomas, A. Köhler, J. S. Wilson, and J.-S. Kim, *Phys.Rev.B*, 2003**, 67**, 064203.
76. T. J. Prosa, M. J. Winokur, J. Moulton, P. Smith, and A. J. Heeger, *Macromolecules*, 1992**, 25**, 4364.
77. J. Y. Kim, S. H. Kim, H.-H. Lee, K. Lee, W. Ma, W. Gong, and A. J. Heeger, *Adv.Mater.*, 2006**, 18**, 572.
78. M. Reyes-Reyes, K. Kim, and D. L. Carroll, *Appl.Phys.Lett.*, 2005**, 87**, 083506.
79. Y. Yao, C. Shi, G. Li, V. Shrotriya, Q. Pei, and Y. Yang, *Appl.Phys.Lett.*, 2006**, 89**, 153507.

80. V. D. Mihailetchi, H. Xie, B. de Boer, L. J. A. Koster, and P. W. M. Blom, *Adv.Funct.Mater.*, 2006**, 16**, 699.
81. R. C. Hiorns, R. de Bettignies, J. Leroy, S. Bailly, M. Firon, C. Sentein, A. Khoukh, H. Preud'homme, and C. Dagron-Lartigau, *Adv.Funct.Mater.*, 2006**, 16**, 2263.
82. W. Ma, C. Yang, X. Gong, K. Lee, and A. J. Heeger, *Adv.Funct.Mater.*, 2005**, 15**, 1617.
83. Y. Kim, S. Cook, S. M. Tuladhar, S. A. Choulis, J. Nelson, J. R. Durrant, D. D. C. Bradley, M. Giles, I. McCulloch, C.-S. Ha, and M. Ree, *Nat.Mater.*, 2006**, 5**, 197.
84. V. D. Mihailetchi, H. Xie, B. de Boer, L. M. Popescu, J. C. Hummelen, and P. W. M. Blom, *Appl.Phys.Lett.*, 2006**, 89**, 012107.
85. J. Peet, J. Y. Kim, N. E. Coates, W. L. Ma, D. Moses, A. J. Heeger, and G. C. Bazan, *Nat.Mater.*, 2007**, 6**, 497.
86. J. Y. Kim, K. Lee, N. E. Coates, D. Moses, T.-Q. Nguyen, M. Dante, and A. J. Heeger, *Science*, 2007**, 317**, 222.
87. A. Hadipour, B. de Boer, J. Wildeman, F. B. Kooistra, J. C. Hummelen, M. G. R. Turbiez, M. M. Wienk, R. A. J. Janssen, and P. W. M. Blom, *Adv.Funct.Mater.*, 2006**, 16**, 1897.
88. C. Winder, G. Matt, J. C. Hummelen, R. A. J. Janssen, N. S. Sariciftci, and C. J. Brabec, *Thin Solid Films*, 2002**, 403-404**, 373.
89. C. Winder and N. S. Sariciftci, *J.Mater.Chem.*, 2004**, 14**, 1077.
90. F. Zhang, E. Perzon, X. Wang, W. Mammo, M. R. Andersson, and O. Inganäs, *Adv.Funct.Mater.*, 2005**, 15**, 745.
91. X. Wang, E. Perzon, F. Oswald, F. Langa, S. Admassie, M. R. Andersson, and O. Inganäs, *Adv.Funct.Mater.*, 2005**, 15**, 1665.
92. D. Gupta, D. Kabra, N. Kolishetti, S. Ramakrishnan, and K. S. Narayan, *Adv.Funct.Mater.*, 2007**, 17**, 226.
93. L. H. Nguyen, S. Gunes, H. Neugebauer, N. S. Sariciftci, K. Colladet, S. Fourier, T. J. Cleij, L. Lutsen, J. Gelan, and D. Vanderzande, *Eur.Phys.J.-Appl.Phys.*, 2006**, 36**, 219.
94. L. H. Nguyen, S. Gunes, H. Neugebauer, N. S. Sariciftci, F. Banishoeib, A. Henckens, T. Cleij, L. Lutsen, and D. Vanderzande, *Sol.En.Mater.Sol.Cells*, 2006**, 90**, 2815.
95. F. L. Zhang, W. Mammo, L. M. Andersson, S. Admassie, M. R. Andersson, L. Inganäs, S. Admassie, M. R. Andersson, and O. Inganäs, *Adv.Mater.*, 2006**, 18**, 2169.
96. X. J. Wang, E. Perzon, W. Mammo, F. Oswald, S. Admassie, N. K. Persson, F. Langa, M. R. Andersson, and O. Inganäs, *Thin Solid Films*, 2006**, 511**, 576.
97. A. J. Mozer and N. S. Sariciftci, *Comptes Rendus Chimie*, 2006**, 9**, 568.
98. E. Perzon, X. J. Wang, F. L. Zhang, W. Mammo, J. L. Delgado, P. de la Cruz, O. Inganäs, F. Langa, and M. R. Andersson, *Synth.Met.*, 2005**, 154**, 53.

99. C. Soci, I.-W. Hwang, D. Moses, Z. Zhu, D. Waller, R. Gaudiana, C. J. Brabec, and A. J. Heeger, *Adv.Funct.Mater.*, 2007**, 17**, 632.
100. F. Zhang, W. Mammo, L. M. Andersson, S. Admassie, M. R. Andersson, and O. Inganäs, *Adv.Mater.*, 2006**, 18**, 2169.
101. C. Shi, Y. Yao, Y. Yang, and Q. Pei, *J.Amer.Chem.Soc.*, 2006**, 128**, 8980.
102. D. Mühlbacher, M. Scharber, M. Morana, Z. Zhu, D. Waller, R. Gaudiana, and C. J. Brabec, *Adv.Mater.*, 2006**, 18**, 2884.
103. C. J. Brabec, *Sol.En.Mater.Sol.Cells*, 2004**, 83**, 273.
104. M. C. Scharber, D. Mühlbacher, M. Koppe, P. Denk, C. Waldauf, A. J. Heeger, and C. J. Brabec, *Adv.Mater.*, 2006**, 18**, 789.
105. L. J. A. Koster, V. D. Mihailetchi, and P. W. M. Blom, *Appl.Phys.Lett.*, 2006**, 88**, 093511.
106. K. M. Coakley and M. D. McGehee, *Chem.Mater.*, 2004**, 16**, 4533.
107. J. Zaumseil and H. Sirringhaus, *Chem.Rev.*, 2007**, 107**, 1296.
108. C. D. Dimitrakopoulos and P. R. L. Malenfant, *Adv.Mater.*, 2002**, 14**, 99.
109. A. Facchetti, M.-H. Yoon, and T. J. Marks, *Adv.Mater.*, 2005**, 17**, 1705.
110. J. Veres, S. Ogier, and G. Lloyd, *Chem.Mater.*, 2004**, 16**, 4543.
111. H. Klauk, D. J. Gundlach, J. A. Nichols, and T. N. Jackson, *IEEE Trans.Electron Devices*, 1999**, 46**, 1258.
112. L. A. Majewski, R. Schroeder, and M. Grell, *Appl.Phys.Lett.*, 2004**, 85**, 3620.
113. J. Tate, J. A. Rogers, C. D. W. Jones, B. Vyas, D. W. Murphy, W. Li, Z. Bao, R. E. Slusher, A. Dodabalapur, and E. A. Katz, *Langmuir*, 2000**, 16**, 6054.
114. X. Cai, M. W. Burand, C. R. Newman, D. A. da Silva Filho, T. M. Pappenfus, M. M. Bader, J. L. Brédas, K. R. Mann, and C. D. Frisbie, *J.Phys.Chem.B*, 2006**, 110**, 14590.
115. C. W. Sele, T. von Werne, R. H. Friend, and H. Sirringhaus, *Adv.Mater.*, 2005**, 17**, 997.
116. H. Sirringhaus, T. Kawase, R. H. Friend, T. Shimoda, M. Inbasekaran, W. Wu, and E. P. Woo, *Science*, 2000**, 290**, 2123.
117. T. Kawase, T. Shimoda, C. Newsome, H. Sirringhaus, and R. H. Friend, *Thin Solid Films*, 2003**, 438-439**, 279.
118. T. Makela, S. Jussila, H. Kosonen, T. G. Backlund, H. G. O. Sandberg, and H. Stubb, *Synth.Met.*, 2005**, 153**, 285.
119. K. S. Lee, T. J. Smith, K. C. Dickey, J. E. Yoo, K. J. Stevenson, and Y.-L. Loo, *Adv.Funct.Mater.*, 2006**, 16**, 2409.
120. M. Lefenfeld, G. Blanchet, and J. A. Rogers, *Adv.Mater.*, 2003**, 15**, 1188.
121. C. D. Sheraw, L. Zhou, D. J. Huang, D. J. Gundlach, T. N. Jackson, M. G. Kane, M. S. Hill, J. Campi, B. K. Greening, J. Francl, and J. West, *Appl.Phys.Lett.*, 2002**, 80**, 1088.
122. A. Afzali, C. D. Dimitrakopoulos, and T. L. Breen, *J.Amer.Chem.Soc.*, 2002**, 124**, 8812.
123. A. Afzali, C. R. Kagan, and G. P. Traub, *Synth.Met.*, 2005**, 155**, 490.

124.H. Sirringhaus, P. J. Brown, R. H. Friend, M. M. Nielsen, K. Bechgaard, B. M. W. Langeveld-Voss, A. J. H. Spiering, R. A. J. Janssen, E. W. Meijer, P. Herwig, and D. M. de Leeuw, *Nature*, 1999**, 401**, 685.
125.K. C. Dickey, J. E. Anthony, and Y. L. Loo, *Adv.Mater.*, 2006**, 18**, 1726.
126.M. M. Payne, S. R. Parkin, J. E. Anthony, C.-C. Kuo, and T. N. Jackson, *J.Amer.Chem.Soc.*, 2005**, 127**, 4986.
127.J. E. Anthony, *Chem.Rev.*, 2006**, 106**, 5028.
128.J.-F. Chang, B. Sun, D. W. Breiby, M. M. Nielsen, T. I. Sölling, M. Giles, I. McCulloch, and H. Sirringhaus, *Chem.Mater.*, 2004**, 16**, 4772.
129.R. J. Kline, M. D. McGehee, E. N. Kadnikova, J. Liu, J. M. J. Fréchet, and M. F. Toney, *Macromolecules*, 2005**, 38**, 3312.
130.R. W. I. de Boer, M. E. Gershenson, A. F. Morpurgo, and V. Podzorov, *physica status solidi (a)*, 2004**, 20**, 1302.
131.V. Y. Butko, X. Chi, D. V. Lang, and A. P. Ramirez, *Appl.Phys.Lett.*, 2003**, 83**, 4773.
132.V. Y. Butko, X. Chi, and A. P. Ramirez, *Solid State Commun.*, 2003**, 128**, 431.
133.V. Podzorov, V. M. Pudalov, and M. E. Gershenson, *Appl.Phys.Lett.*, 2003**, 82**, 1739.
134.E. Menard, V. Podzorov, S.-H. Hur, A. Gaur, M. E. Gershenson, and J. A. Rogers, *Adv.Mater.*, 2004**, 16**, 2097.
135.M. Chikamatsu, S. Nagamatsu, Y. Yoshida, and K. Kikuchi, *Appl.Phys.Lett.*, 2005**, 87**, 203504.
136.Th. B. Singh, N. Marjanovic, G. J. Matt, S. Günes, N. S. Sariciftci, A. Montaigne Ramil, A. Andreev, H. Sitter, R. Schwödiauer, and S. Bauer, *Org.Electron.*, 2005**, 6**, 105.
137.S. Kobayashi, T. Takenobu, S. Mori, A. Fujiwara, and Y. Iwasa, *Appl.Phys.Lett.*, 2003**, 82**, 4581.
138.Y. Sakamoto, T. Suzuki, M. Kobayashi, Y. Gao, Y. Fukai, Y. Inoue, F. Sato, and S. Tokito, *J.Amer.Chem.Soc.*, 2004**, 126**, 8140.
139.S. Ando, J. Nishida, H. Tada, Y. Inoue, S. Tokito, and Y. Yamashita, *J.Amer.Chem.Soc.*, 2005**, 127**, 5336.
140.A. Facchetti, M. Mushrush, M.-H. Yoon, G. R. Hutchison, M. A. Ratner, and T. J. Marks, *J.Amer.Chem.Soc.*, 2004**, 126**, 13874.
141.H. Ohnuki, K. Ikegami, T. Ida, and M. Izumi, *Colloids Surf., A*, 2005**, 257-258**, 381.
142.T. D. Anthopoulos, S. Setayesh, E. Smits, M. Cölle, E. Cantatore, B. de Boer, P. W. M. Blom, and D. M. de Leeuw, *Adv.Mater.*, 2006**, 18**, 1900.
143.R. J. Chesterfield, C. R. Newman, T. M. Pappenfus, P. C. Ewbank, M. H. Haukaas, K. R. Mann, L. L. Miller, and C. D. Frisbie, *Adv.Mater.*, 2003**, 15**, 1278.
144.Y. Kunugi, K. Takimiya, N. O. Negishi, T. Otsubo, and Y. Aso, *J.Mater.Chem.*, 2004**, 14**, 2840.

145.E. J. Meijer, D. M. de Leeuw, S. Setayesh, E. van Veenendaal, B. H. Huisman, P. W. M. Blom, J. C. Hummelen, U. Scherf, J. Kadam, and T. M. Klapwijk, *Nat.Mater.*, 2005**, 2**, 678.
146.M. Funahashi, F. Zhang, and N. Tamaoki, *Adv.Mater.*, 2007**, 19**, 353.
147.S. C. W. Hyde, N. P. Barry, R. Jones, J. C. Dainty, and P. M. W. French, *Opt.Commun.*, 1996**, 122**, 111.
148.O. Ostroverkhova and W. E. Moerner, *Chem.Rev.*, 2004**, 104**, 3267.
149.S. C. W. Hyde, N. P. Barry, R. Jones, P. M. W. French, M. B. Klein, and B. A. Wechsler, *Opt.Lett.*, 1995**, 20**, 1331.
150.D. D. Steele, B. L. Volodin, O. Savina, B. Kippelen, N. Peyghambarian, H. Rckel, and S. R. Marder, *Opt.Lett.*, 1998**, 23**, 153.
151.R. Jones, S. C. W. Hyde, M. J. Lynn, N. P. Barry, J. C. Dainty, P. M. W. French, K. M. Kwolek, D. D. Nolte, and M. R. Melloch, *Appl.Phys.Lett.*, 1996**, 69**, 1837.
152.W. Drexler, U. Morgner, F. X. Krtner, S. A. Boppart, X. D. Li, E. P. Ippen, and J. G. Fujimoto, *Opt.Lett.*, 1999**, 24**, 1221.
153.D. Huang, E. A. Swanson, C. P. Lin, J. S. Schuman, W. G. Stinson, W. Chang, M. R. Hee, T. Flotte, K. Gregory, and C. A. Puliafito, *Science*, 1991**, 254**, 1178.

Chapter 2

[84]PCBM and its Application in a Bulk Heterojunction Solar Cell

In this Chapter the synthesis and characteristics of a new C_{84} adduct, realized via a diazomethane addition reaction, are described. [84]PCBM was obtained as a mixture of three major isomers. The thus obtained isomeric mixture was used as an acceptor molecule in a bulk heterojunction solar cell in combination with poly(2-methoxy-5-(3',7'-dimethyloctyloxy)-p-phenylene-vinylene) (MDMO-PPV) as the donor molecule. Spin coating the active layer blend from 1-chloronaphthalene (the very best fullerene solvent) instead of ortho-dichlorobenzene was necessary to obtain the more efficient photovoltaic device. The PV results indicate that the hole mobility of MDMO-PPV may not be increased upon blending with [84]PCBM. This explains the relatively low I_{SC} of the device as due to the build up of space charge. The V_{OC} of the device is ~500 mV lower than that of the one with [60]PCBM, while [84]PCBM has a 350 mV higher electron affinity than [60]PCBM. This loss surpasses the linear relation between the donor HOMO acceptor LUMO energy gap and the V_{OC} in this type of device. A maximum power conversion efficiency of 0.25% was reached for the MDMO-PPV:[84]PCBM cells.

*Part of this work was published:

Floris B. Kooistra, Valentin D. Mihailetchi, Lacramioara M. Popescu, David Kronholm, Paul W. M. Blom, and Jan C. Hummelen. *Chemistry of Materials.* **2006***,* 18*, 3068-3073.*

2.1 Introduction

In 1991 Diederich et al. succeeded for the first time in isolating C_{84}.[1] After C_{60} and C_{70}, C_{84} was found to be the third most abundant fullerene. Of all formed fullerenes in the graphite arc process[2] only 3 to 4 % per weight consists of fullerenes other than C_{60} or C_{70}.[1] Due to its scarcity and high cost, research has focused mainly on its structural properties rather than on functionalization or application.

The research presented in this chapter was a collaboration between our labs and Valentin D. Mihailetchi of the group of prof. P.W.M. Blom.

2.1.1 Structural Properties

Calculations predict a total of 24 posible isomers of C_{84} obeying the isolated pentagon rule.[3] MDMO calculations furthermore predict that the two isoenergetic D_2 (22) and D_{2d} (23) isomers (numbers in accordance with the isomer numbering of Manolopoulos and Fowler[3] (Fig. 2.2)) are the most stable isomers by about 23 kJ mol^{-1} compared to the next stable ones.[4-7] Analysis of ^{13}C NMR spectra of C_{84}, obtained with the standard graphite arc process, is consistent with a 2:1 thermodynamic mixture of the isoenergetic D_2 and D_{2d} isomers.[8] This can also be interpreted as a 1:1:1 mixture because the D_2 isomer is chiral, and thus two enantiomers are present in equal ammount. Interestingly these two isomers only differ by one Stone-Wales transformation.[9] (see Fig 2.1)

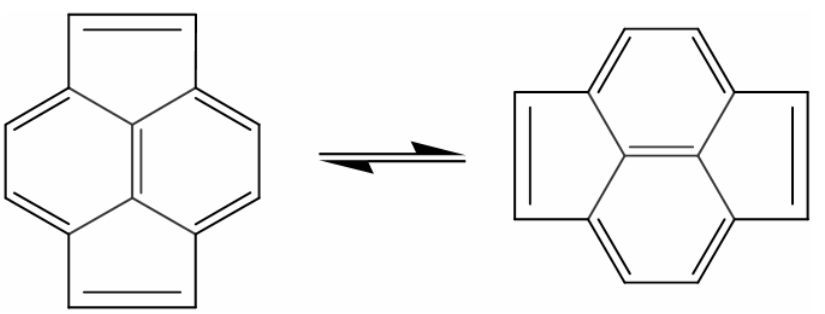

Fig. 2.1: Stone Wales transformation

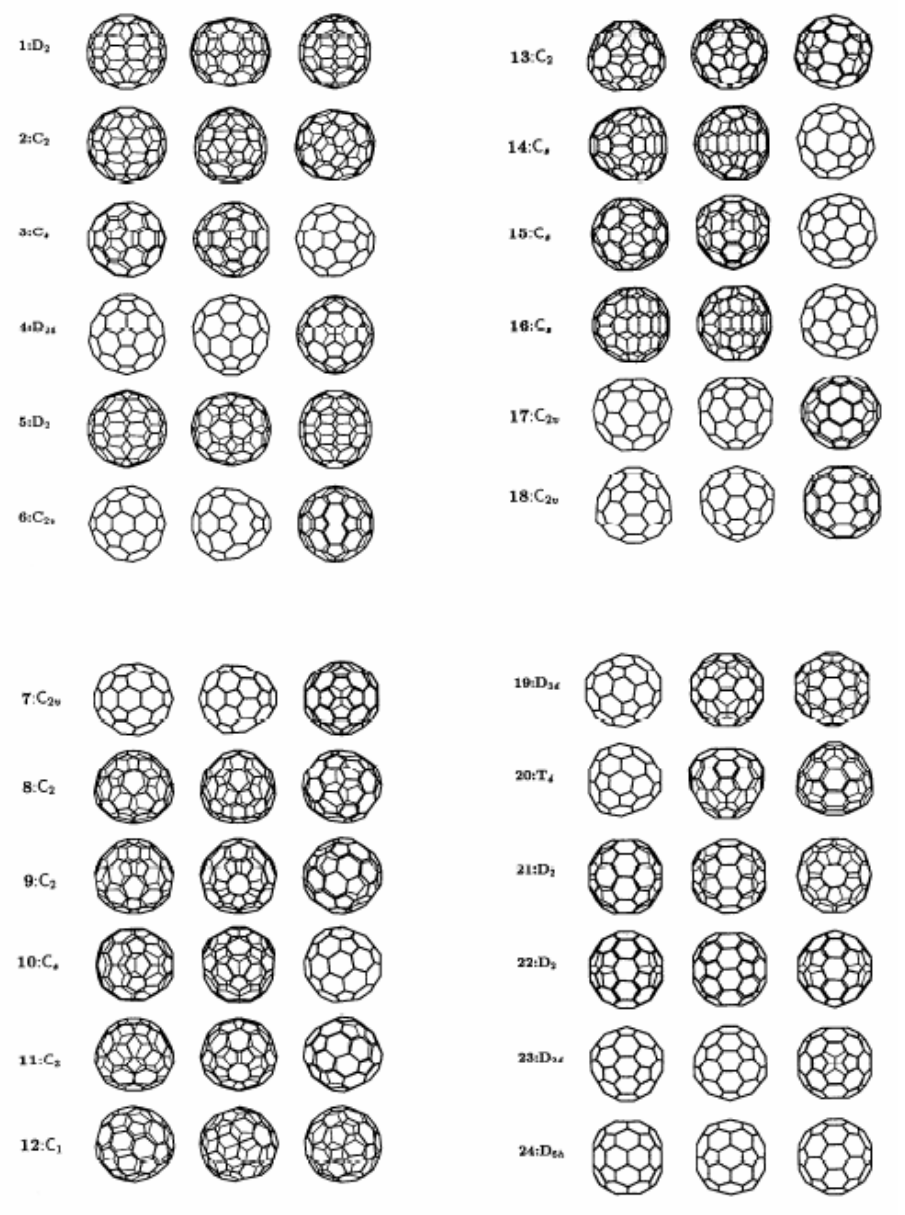

Fig. 2.2: All 24 possible structural isomers of C_{84} fullfilling the IPR rule.[3]

The group of Hawkins studied the possibilty of interconverting both isomers by Stone-Wales transformations. The enantiomers of the D_2 isomer can theoretically be interconverted by two Stone-Wales shifts. Enantiomerically enriched C_{84} was subjected to heat (700 °C) and UV radiation (193 nm), but no interconversion was observed.[10]

Since the isolation of C_{84} many efforts have been made to separate the isomeric mixture (D_2 and D_{2d}). Using an $Ir(CO)Cl(PPh_3)_2$ complex, Balch et al. succeeded in 1994 in separating the major isomers and revealed the structure of the D_{2d} isomer by X-ray chrystallography.[11] In the same year the kinetic resolution of the chiral D_2 isomer was published by the group of Hawkins.[10] Later, separation by HPLC methods was succesfully applied.[12] Another separation method using the Bingel-retro-Bingel strategy was applied by Crassous et al.[13]

Other isomers of C_{84} have been obtained by applying metal-doped graphite rods in the carbon arc procedure. So far 10 of the possible 24 isomers have been isolated, although not all can be conclusively assigned.[12,14-16]

2.1.2 Reactivity of C_{84}

As a result of the very limited availability of pure C_{84} only very few reactions have been carried out on this fullerene. So far most reactions were performed with the goal to separate the different isomers or to test the reactivity of C_{84}.[10,13,17-20] An Important factor in reactions with C_{84} is the difference in reactivity of the various C=C double bonds. Whereas all double bonds in C_{60} are equivalent, this is not the case in C_{84}. Both C_{84} isomers contain 42 C=C double bonds, of which six are inter-pentagonal. Calculations by Taylor predict the highest π-density for the D_2 isomer at the identical 9–10 and 17–18 inter-pentagonal double bonds. The highest π-density for the D_{2d} isomer was calculated to be at the identical 32–53 and 42–43 inter-pentagonal double bond.[21] (see Fig. 2.3). In case of the D_{2d} isomer this was experimentally proven by the selective formation of the $[(\eta^2\text{-}D_{2d}\text{-}C_{84})Ir(CO)Cl(PPh_3)_2$ complex at the 32–53 bond.[11]

2.1.3 Applications of C_{84}

The intrinsic properties of C_{84} have been studied quite extensively. Examples are the aforementioned NMR spectroscopy, electrochemistry[22], Infrared spectroscopy[23-26], ionization energy[27,28], and circular dichroism properties of the chiral isomers.[29,30] However, very little research has been done on actual applications of C_{84}. A C_{84} based field effect transistor was developed by Shibata et al.[31] and some pioneering work has been done in the field of superconductivity and nonlinear optics.[32,33]

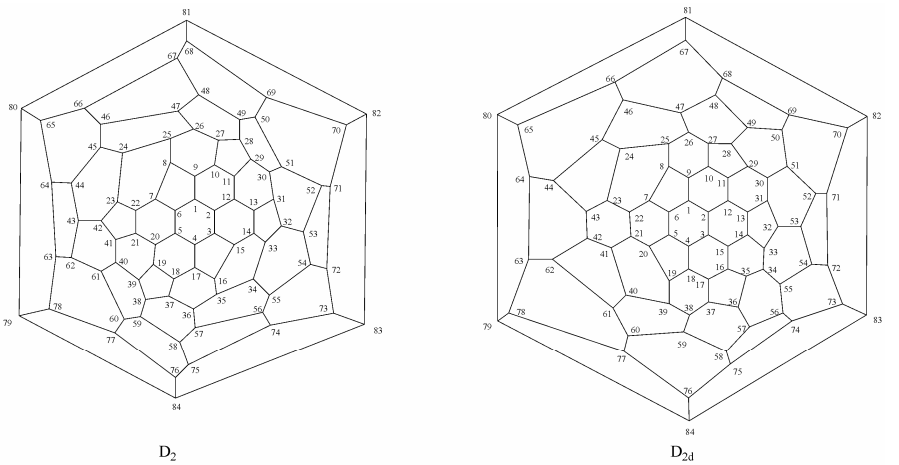

Fig. 2.3: Schlegel Diagram of the D_2 and D_{2d} isomers of C_{84}

2.1.4 Research Goal

In the past good results where obtained in our group by using a C_{70} derivative, [70]PCBM, as the alternative for [60]PCBM as the acceptor component in PCBM:MDMO-PPV bulk heterojunction solar cells. A power conversion efficiency of 3.0% was obtained. [34] The improved performance of this solar cell was atributed to the significantly increased and broader absorption of the solar spectrum by the acceptor, resulting in a higher current output. C_{84} has an even broader absorption than C_{70}, extending to the near infrared (NIR)[1,33-35], and, therefore, a possible further improvement of the current output was expected, especially when used in combination with a relatively wide bandgap donor material like MDMO-PPV. An additional potential advantage of C_{84} is its much larger photostability compared to C_{60} and C_{70}.[36]. This is considered to be highly advantageous for the lifetime of the solar cell device, because it is expected that the major degradation proces in organic solar cells is the formation of singlet oxygen by quenching of the triplet state of the fullerene (i.e., the fullerene acting as a sensitizer in relatively large fullerene domains, in which the initial singlet excited state is not effictively quenched by hole transfer to the donor but is allowed time for intersystem crossing to the triplet state).[37]

The goal of the research presented in this chapter was the synthesis and study of the properties of a functionalised C_{84} fullerene as an acceptor molecule in combination with MDMO-PPV as a donor molecule in a bulk heterojunction organic solar cell.

2.2 Synthesis

As a target molecule [84]PCBM was choosen. The synthesis of the C_{60} and C_{70} analogues are well known, thus providing a clear synthetic methodology.[34,38] Furthermore, processing [60]PCBM and [70]PCBM for organic solar cells is also intensively investigated. Since C_{84} is only available in extremely small quantaties it was deemed prudent to follow well-known methodologies as much as possible. In order to synthesize [84]PCBM a diazoalkane addition reaction, using C_{84} and 4-benzoyl-methylbutyrate *p*-tosylhydrazone (**2.1**), was performed. (Fig. 2.4)

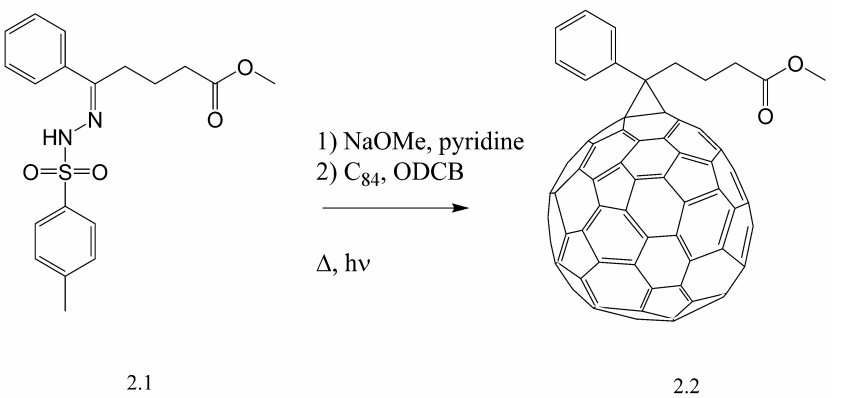

Fig. 2.4: Synthesis [84]PCBM

[84]PCBM was obtained as a mixture of three major isomers in a total yield of 23%. In the next paragraph the characterization of the mixture will be discussed in detail.

2.3 Characterization

The formation of a minimum of two [84]PCBM isomers was to be expected because the C_{84} itself consisted of two isomers. According to HPLC analysis, the combustion–produced C_{84} used throughout this thesis consisted of approximately 80% D_{2d} isomer and 20% D_2 isomer. The HPLC trace of the reaction product showed 3 major peaks, likely all [6,6] isomers. (Fig. 2.5)

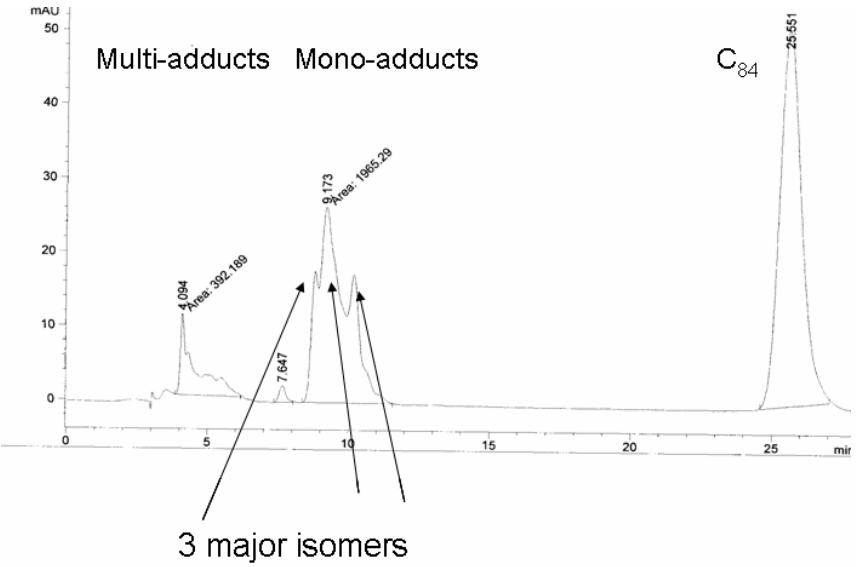

Fig. 2.5: HPLC trace of the reaction mixture. Experimental conditions: Eluted with toluene on a Cosmosil Buckyprep® column (4.6 x 250 mm) at 1 ml/min.

These isomers were not separated but used as a mixture since the mixture showed a clean first reduction potential (see paragraph 2.3.3). In the following section the characterization data will be discussed in more detail.

2.3.1 Nuclear Magnetic Resonance Spectroscopy

Proton NMR of the reaction mixture clearly showed the presence of three major isomers. At 3.46 ppm a triplet with a small secondary coupling was seen, next to an identical pattern of smaller itensity at 3.27 ppm, and a third such triplet is partly hidden underneath the methoxy signals at ~3.65 ppm. Such a patern is typical for the protons on the methylene group next to the cyclopropane moiety in PCBX type methanofullerenes. Two signals were observed at 3.65 and 3.63 ppm, respectivily, of which one was of higher intensity and one was of low intensity for the OCH_3 group. Three $–CH_2COOR$ triplets can be seen at 3.09 (minor), 2.54 (major), and 2.49 (minor) ppm. The middle CH_2 protons of the butyric acid moiety can be seen in the area of 2.2 ppm as usual.

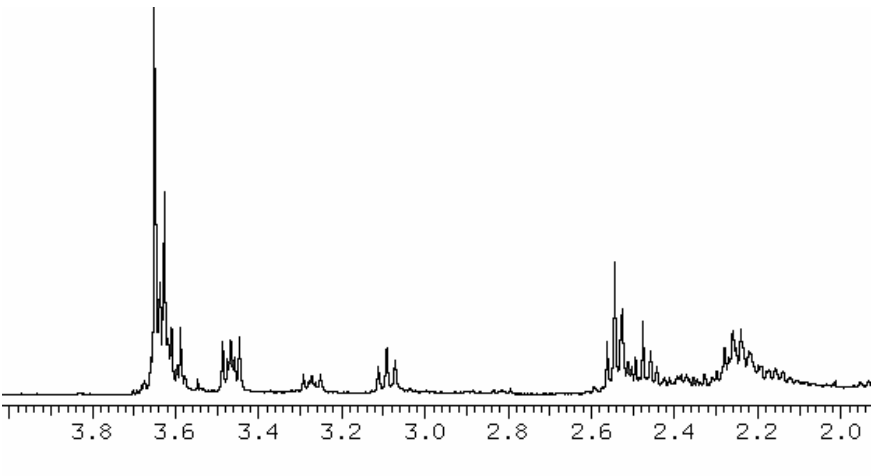

Fig. 2.6: ^{1}H NMR reaction product.

In carbon NMR only two carbonyl resonances were observed separately, namely, at 170.86 and 170.80 ppm. Furthermore three bridgehead carbon signals were observed at 64.75, 61.98, and 61.74 ppm, again indicating the presence of three isomers.

2.3.2 UV/Vis Spectroscopy

As mentioned in section 2.1.4 an increase in photocurrent was expected as C_{84} exibits a stronger and broader absorption than C_{60} and C_{70} in the visible region. In order to investigate the absorption properties of [84]PCBM a UV/Vis spectrum was taken and compared to those of [60]PCBM and [70]PCBM. (Fig. 2.7). It appears that the absorption of [70]PCBM and [84]PCBM is much stronger than that of [60]PCBM. Furthermore, in the area of 630–800 nm, where [60]PCBM and [70]PCBM are very close to transparant, [84]PCBM still absorps significantly. Hence, a better match with the AM 1.5 solar spectrum is observed for [84]PCBM, but the molar absorption in the 400–500 nm range is somewhat weaker than that of [70]PCBM. The optical bandgap of [84]PCBM could not be determined since our equipment did not allow for measurement in the NIR, but from the spectrum it appears to be smaller than 1.5 eV.

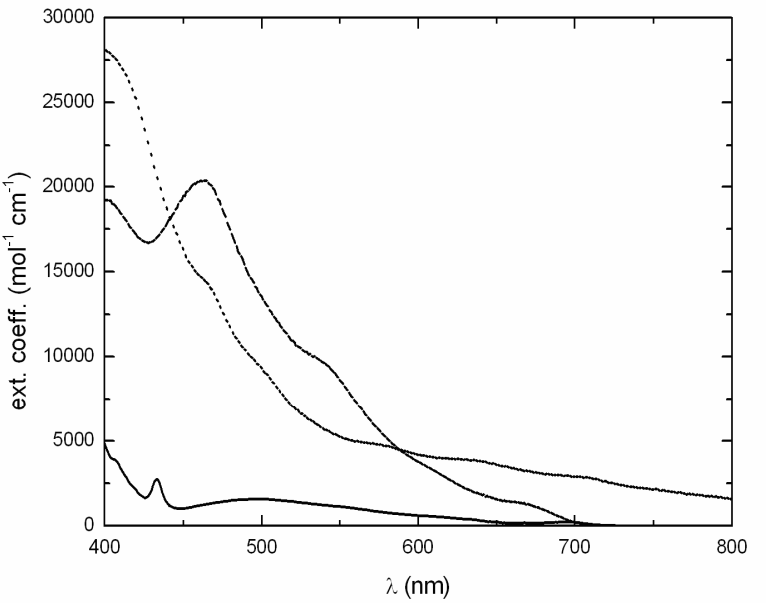

Fig. 2.7: UV/Vis spectra of [84]PCBM (dotted line), [70]PCBM (dashed line), and [60] PCBM (straight line), all in toluene (10^{-5} M).

2.3.3 Electrochemical Properties

In order to test the electron accepting properties of [84]PCBM both cyclic voltammetry (CV) and differential pulse voltammetry (DPV) measurements were performed. A comparison was made with [60]PCBM and [70]PCBM. From both the CV and DPV (see Fig. 2.8 and Fig. 2.9) data it can be concluded that [84]PCBM is a much better electron acceptor than [60]PCBM and [70]PCBM by about 350 mV (Table 2.1). Furthermore the CV data clearly show a nice reversible first reduction wave. This is of great importance because this means that the LUMO levels of the different isomers in the reaction mixture are at approximately the same energy. Hence this mixture can be effectively used as an acceptor molecule in solar cells (or other devices), since no electron traps are induced due to possible isomers with lower lying LUMO levels.

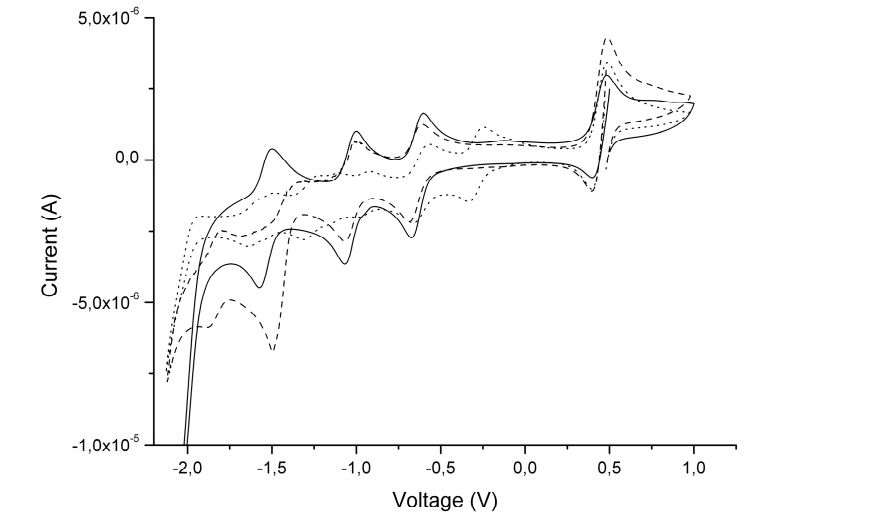

Fig. 2.8: Cyclic voltammetry data. [60]PCBM (straight), [70]PCBM (dashed) and [84]PCBM (dotted).

Table 2.1: CV/DPV Data

	CV		DPV	
Compound[a]	**$E^{1/2}$ 1, red (V)**	**$E^{1/2}$ 2, red (V)**	**$E^{1/2}$ 1, red (V)**	**$E^{1/2}$ 2, red (V)**
[60]PCBM	-1.078	-1.475	-1.084	-1.480
[70]PCBM[b]	-1.089	-1.479	-1.096	-1.479
[84]PCBM[b]	-0.730	-1.054	-0.736	-1.067

[a] Experimental conditions: V vs Fc/Fc^+, Bu_4NPF_6 (0.1M) as the supporting electrolyte, $ODCB/CH_3CN$ (4:1) as the solvent; scan rate, 10 mV/s. [b] Isomeric mixture

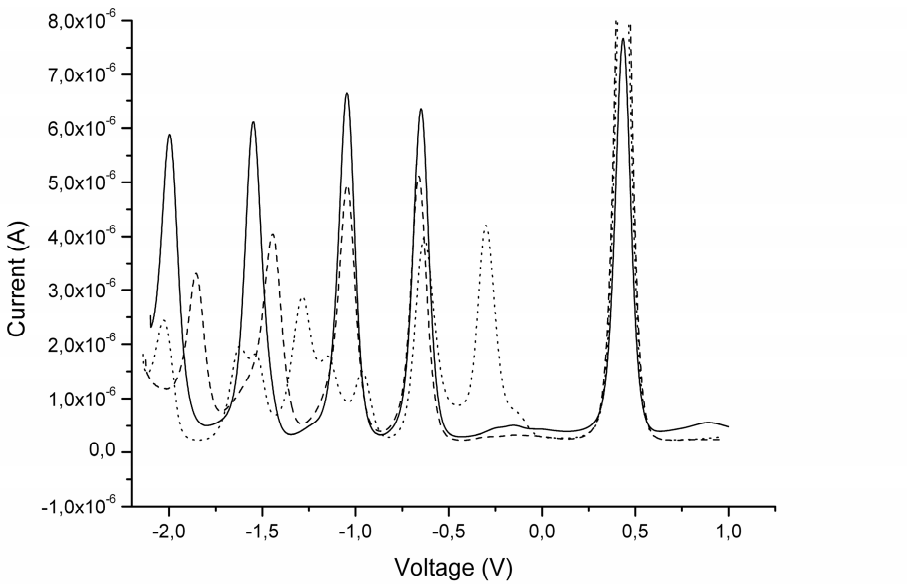

Fig. 2.9: Differential Pulse Voltammetry [60]PCBM (straight), [70]PCBM (dashed) and [84]PCBM (dotted). (The little bump visible around 0.2 V is a device artefact and is always observed with this equipment).

The much better electron accepting properties of [84]PCBM immediately imply that the open circuit voltage that can be obtained with solar cell devices using [84]PCBM as the acceptor and MDMO-PPV as the donor will be dramatically lower than those obtained with [60]PCBM and [70]PCBM, because the maximum open circuit voltage that can be obtained is directly correlated to the energy difference between the HOMO of the donor and the LUMO of the acceptor.[39-41]

2.4 Photovoltaic Devices

Despite the expected reduction in open-circuit voltage due to the low lying LUMO level of [84]PCBM we were still interested in researching its behavior in a bulk heterojunction organic solar cell, since its increased absorption should result in a high photocurrent.

2.4.1 Morphology

Next to the intrinsic properties of the donor and the acceptor molecule, the photovoltaic performance of a bulk heterojunction solar cell is also strongly dependent on the morphology of the composite active layer.[42] Charge generation and separation can only be efficient if the PCBM and PPV are evenly dispersed in the active layer. Since the solubility of fullerenes tends to decrease with their size, the processing of higher fullerenes becomes increasingly difficult. A clear-cut example of this tendency is the fact that for optimal processing conditions for [70]PCBM:MDMO-PPV active layers are spun from ortho-dichlorobenzene (ODCB) whereas [60]PCBM:MDMO-PPV active layers are spun from chlorobenzene.[34,42] The choice of solvent is therefore a critical parameter in obtaining the best photovoltaic performance. In order to investigate the structure of different [84]PCBM:MDMO-PPV (4:1, w/w) mixtures, tapping-mode atomic force microscopy was employed.

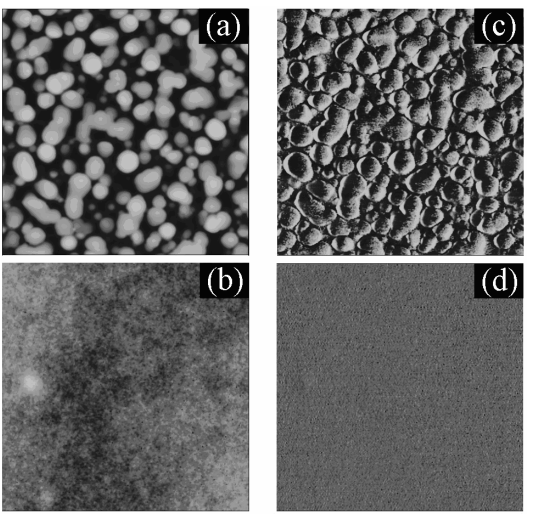

Fig. 2.10: AFM tapping-mode height (a,b) and simultaneously taken phase (c,d) images of [84]PCBM:MDMO-PPV (4:1, w/w) blends, with a size of 5.0 µm x 5.0 µm. The films are spun from ODCB (a, c; z range = 180 nm, RMS roughness = 12.16 nm) and 1-chloronaphthalene (b, d; z range = 10 nm, RMS roughness = 0.88 nm).

The “standard” weight ratio was used for two reasons, this results in a comparable volume ratio of donor and acceptor in all three blends ([60]PCBM, [70]PCBM and [84]PCBM in combination with MDMP-PPV) and because this ratio was used in optimized solar cells of [60]PCBM and [70]PCBM. Furthermore, it was expected that there is no significant difference between bulk and surface morphologies as was confirmed earlier by investigating the morphology at different depths of [60]PCBM:MDMO-PPV blends.[43]

Fig. 2.10 shows the height and corresponding phase images obtained by AFM for composite films of [84]PCBM:MDMO-PPV, spun from two different solvents: ODCB and 1-chloronaphthalene (the best fullerene solvent). In order to match the conditions used for the device preparation, the films were spun on ITO-substrates covered with an additional layer of PEDOT-PSS, which forms the bottom hole-injection electrode of the photovoltaic device. The height images spun from ODCB show an extremely uneven surface with a reproducible phase contrast, which clearly indicates that the “peaks” are of different chemical nature than the “valleys”. Domains of one phase in a matrix of another phase can easily be recognized. On the other hand, the samples fabricated from 1-chloronaphthalene show extremely smooth and even surfaces as well as little phase contrast. Where the layer spun from ODCB shows feature sizes of 200–400 nm and a root-mean-square (RMS) roughness of 12.16 nm, the layer from 1-chloronaphthalene shows sizes of 20–50 nm and a RMS of 0.88 nm. Such small domain sizes favor exciton separation and charge generation since the exciton diffusion length in organic materials is around 10 nm. Thus, spincoating from 1-chloronaphthalene results in morphologies similar to those of [60]PCBM:MDMO-PPV spun from chlorobenzene and [70]PCBM:MDMO-PPV spun from ODCB.

2.4.2 Device Performance

The difference in morphology between [84]PCBM:MDMO-PPV solar cells spun from ODCB and 1-chloronaphthalene is clearly reflected in the photovoltaic behavior of these cells. The cells were constructed in the following way: The [84]PCBM:MDMO-PPV active layer was sandwiched between two metal electrodes of different work function. As a hole collecting electrode a transparant ITO/PEDOT:PSS high-work function bottom electrode was employed. For the collection of electrons a low-work function electrode of LiF/Al was used. Moreover, it has been shown that both these electrodes favor Ohmic contact, LiF/Al with PCBM for electrons and ITO/PEDOT:PSS for holes.[44] Only under these circumstances is the open circuit voltage (V_{OC}) of the device maximized and limited by the energy difference of the acceptor LUMO and the donor HOMO level.[39,40,44] The solar cell devices were illuminated with a tungsten/halogen lamp, with a spectral range of 400–800 nm, calibrated to an intensity of approximately 0.82 suns (82 mW/cm^2). As a reference, [60]PCBM solar cell devices were also constructed. The only difference being the spincoating solvent, which was chlorobenzene for [60]PCBM devices.

The current density-voltage characteristics of the [84]PCBM device spun from 1-chloronaphthalene and ODCB can be seen in Fig.2.10. A number of devices were averaged giving the following properties.

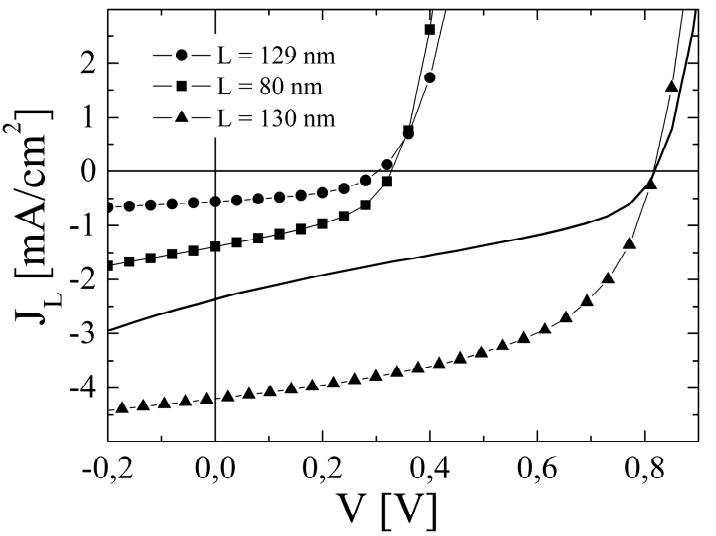

Fig. 2.11: Current density–voltage characteristics under illumination (J_L) of [84]PCBM:MDMO-PPV (4:1, w/w) devices, spun from ODCB (●) and 1-chloronaphthalene (■), together with a [60]PCBM:MDMO-PPV (4:1, w/w) device spun from chlorobenzene (▲), used as a reference. The device thicknesses (L) are provided in the figure. The solid line represents the experimental data of the [84]PCBM device in 1-chloronaphthalene (■), scaled for the same V_{OC} as the reference device. All devices were illuminated using a tungsten/halogen lamp with a spectral range of 400–800 nm, calibrated to an intensity of 82 mW/cm^2.

The V_{OC} of both [84]PCBM type devices were, as expected, very low. The device spun from ODCB gave a V_{OC} value of 317 ± 7.6 mV while the device spun from 1-chloronaphthalene gave a slightly better value of 335 ± 5.4 mV. The V_{OC} of these devices is a factor 2.5 lower than that of [60]PCBM:MDMO-PPV devices which give a V_{OC} value of 819 ± 8.2 mV. This is mostly, although not fully, accounted for by their difference in LUMO levels (Table 2.1). An additional cause might be the low photocurrent causing uncomplete splitting of the quasi-Fermi levels (see paragraph 3.1.1).

The short-circuit current density (J_{sc}) of the [84]PCBM devices is strongly dependent on the spincoating solvent. Spincoating from 1-chloronaphthalene instead of ODCB results in a more than two-fold increase of the short-circuit current density. Increasing from 0.59 ± 0.036 mA/cm^2 to 1.38 ± 0.004 mA/cm^2. This increase is attributed to an enhanced generation of charge carriers due to an increased donor/acceptor interface area, which facilitated exciton dissociation. These current densities however, are a factor three lower than that obtained with [60]PCBM, eventhough the optical density of the blend has increased considerably. Moreover, the fill factors (FF)[I] of the devices made with [84]PCBM are much lower than those made with [60]PCBM (44.6 ± 2.1% vs 56.4 ± 2.8%). Consequently the overall power conversion efficiency (η)[II] is only 0.25% being approximately 10 times lower than obtained with the reference [60]PCBM:MDMO-PPV devices.

2.5 Discussion

The most important factor limiting the device efficiency of the [84]PCBM:MDMO-PPV solar cells is the V_{OC}. All other solar cells parameters (J_{sc}, FF and η) are related in some way to the V_{OC}. For the case of [60]PCBM this was shown by Mihailetchi et al.[45] It was demonstrated that the photocurrent shows an universal behavior when scaled for the effective applied voltage on the device, given by V_{OC}–V. It is then possible to predict all other solar cells parameters. A drop in V_{OC} therefore triggers a concommitant drop in both J_{sc} and FF, which of course strongly reduces the effeciency (η). In order to compare the results obtained with the [84]PCBM and [60]PCBM one should therefore scale both for the same effective applied voltage (V_{OC}–V). The solid line in Fig. 2.11 represents the experimental data of the [84]PCBM:MDMO-PPV device from 1-chloronaphthalene, scaled for the same V_{OC} as the reference [60]PCBM device. It can be clearly seen that the difference in current density cannot be explained entirely by the low V_{OC}. Although the absorption of [84]PCBM in the visible region is much higher than that of [60]PCBM, the current density is still a factor of 1.7 lower after rescaling.

An important question of course is whether the [84]PCBM actually contributes efficiently to the charge generation in the device. The low current density could very well be explained if this was not the case. The action spectrum of a [60]PCBM:MDMO-PPV cell was therefore compared with that of a [84]PCBM:MDMO-PPV cell, the latter with the active layer spun from ODCB. Eventhough spincoating from this solvent proved to be far from optimal, the [84]PCBM cell shows a significant action up to and beyond 900 nm, parallel to the

[I] The FF is defined as FF[%] = (J_M x V_M x 100)/(J_{sc} x V_{oc}), where J_M and V_M are current density and voltage at the maximum power point respectively

[II] The power conversion efficiency is defined as η[%] = (J_{sc} x V_{oc} x FF)/P_{in}, where P_{in} represents the incident light power.

absorption spectrum of [84]PCBM (Fig.2.12). The low current density obtained with these devices can therefore not be explained by inactivity of the [84]PCBM.

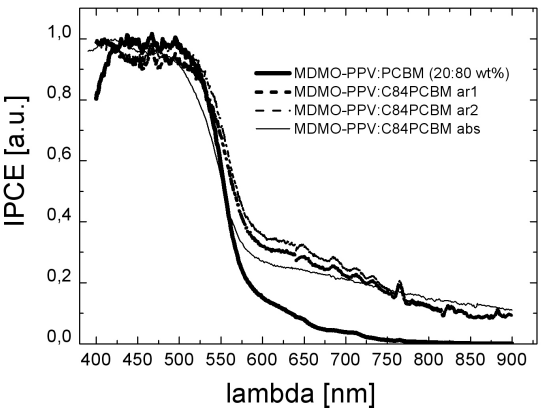

Fig. 2.12: Normalized action spectrum of [84]PCBM:MDMO-PPV and [60]PCBM:MDMO-PPV solar cells. (IPCE = incident photo to current efficiency)

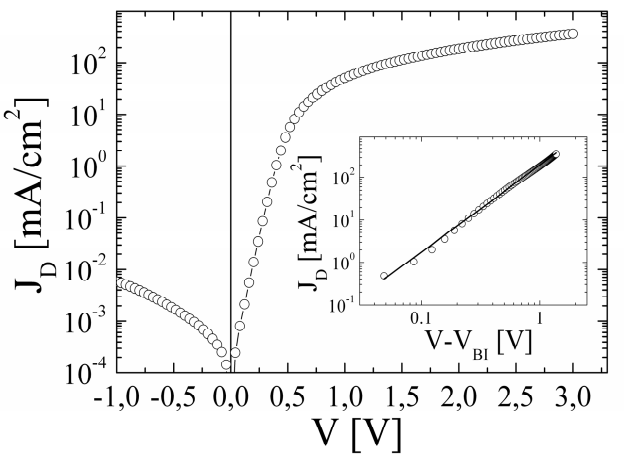

Fig. 2.13: Dark current density-voltage characteristics (J_D) of an ITO/PEDOT:PSS/[84]PCBM:MDMO-PPV (4:1, w/w)/LiF/Al diode with the thickness of 129 nm at a temperature of 295 K. The inset shows the log(J_D)–log(V) characteristic corrected for the built in voltage (V_{BI} = 0.31 V), together with the calculated SCLC (solid line).

Another important parameter that can limit the device performance is charge carrier mobility. The main reason [60]PCBM:MDMO-PPV solar cells show efficiencies up to 2.5% is the enhancement, by more than two orders of magnitude, of the hole mobililty of the MDMO-PPV upon blending with PCBM.[46] Additionally, despite such a strong enhancement of the hole mobility the dark current (J_D) of these devices is still dominated by the electron transport through the [60]PCBM phase.[47], being at least one order of magnitude higher. The electron mobility of the [84]PCBM phase was estimated accordingly. Fig. 2.13 shows the experimental J_D–V characteristics of an ITO/PEDOT:PSS/[84]PCBM:MDMO-PPV (4:1, w/w)/LiF/Al diode with an active layer thickness of 129 nm, at room temperature. The slope of the $\log(J_D)$–$\log(V\text{-}V_{BI})$ plot, shown in the inset of Fig. 2.13 indicates that J_D depends quadratically on the voltage, which is characteristic for the space-charge limited current (SCLC).[47,48] From this data the electron mobility of [84]PCBM can be extracted. A value of 1.0×10^{-3} $cm^2/(V\ s)$ is found coinciding with the mobility found in commercially available C_{84}.[31] It must be noted however, that the isomeric constitution of the C_{84} used in reference 31 is not revealed by the authors. The high electron mobility in the [84]PCBM phase, which is comparable to that of [60]PCBM[48], indicates clearly that this is not limiting the cell performance.

The most likely factor limiting the performance of the [84]PCBM:MDMO-PPV devices is unbalanced transport of holes and electrons. When the difference between the hole and electron mobility exceeds an order two of magnitude the photocurrent in PPV:PCBM devices can be limited by the development of space charge.[49] In this case the photocurrent is the maximum electrostatically allowed current that can be generated into the external circuit. This strongly impacts the FF and the J_{SC} of the solar cell. Typically the FF of these devices limited by SCLC is close to 42%.[49] The FF found for the [84]PCBM:MDMO-PPV devices of 44% is very close to this space-charge limited value, indicating that the performance of these cells is indeed limited by the formation of space charge. A possible reason for this would be that upon mixing with [84]PCBM, MDMO-PPV does not show a strong enhancement of the hole mobility like it does when mixed with [60]PCBM. Measurements of the hole mobility however would be necessary to confirm this.

2.6 Conclusions

A 1,3-dipolar addition reaction was succesfully performed on C_{84} (as a 4:1 mixture of the D_2 and D_{2d} isomers), obtaining a mixture of mainly three [84]PCBM isomers, as most clearly indicated by NMR and HPLC data. [84]PCBM is a better electron acceptor than [60]PCBM and [70]PCBM by ~350 mV, as determined electrochemically. This in combination with the known photostability of C_{84} makes [84]PCBM an interesting material for molecular electronics applications. In this chapter this new C_{84} derivative was applied as an acceptor molecule in a bulk heterojunction solar cell, using MDMO-PPV as the donor molecule. The reduced solubility of [84]PCBM resulted in undesirable morphologies of the active layer

when spun from ODCB. However spincoating from the best known fullerene solvent, 1-chloronaphthalene, resulted in smooth films and a concommitant 2-fold increase of the current output. In accordance with the NIR absorbance of [84]PCBM, the action spectrum of the photovoltaic device extended up to and beyond 900 nm. However, as a result of the low V_{OC} of the devices, in combination with a low J_{SC}, the overall efficiency was limited to 0.25%. The combination of the electron mobility of the [84]PCBM phase, being of the same order as the electron mobility of [60]PCBM, the FF of 44% and the relatively very low J_{SC} of the [84]PCBM devices point to the explanation that the hole mobility of the MDMO-PPV phase is not as greatly enhanced by mixing with [84]PCBM as it is when mixed with [60]PCBM. Nevertheless [84]PCBM is still an interesting candidate for solar cell applications especially when combined with a more miscible and weaker donor than MDMO-PPV.

2.7 Experimental

Device Preparation:

The solar cell devices were prepared using indium-tin-oxide (ITO) coated glass substrates. To supplement this bottom electrode, a hole transport layer of PEDOT:PSS (Bayer AG) was spun from an aqueous dispersion solution, under ambient conditions, before drying the substrates at 140 ^{o}C for 10 minutes. Next, the photoactive layer consisting of [84]PCBM:MDMO-PPV (4:1 w/w) was spin-coated from either *ortho*-dichlorobenzene or 1-chloronaphthalene solution on top of the PEDOT:PSS layer in the N_2 atmosphere. To complete the solar cell devices, 1 nm lithium fluoride (LiF), topped with aluminum (Al, 100 nm) electrodes were deposited by thermal evaporation under vacuum (<10^{-7} mbar).

Device Measurements:

The current density vs. voltage curves were measured in N_2 atmosphere (<1 ppm O_2 and <1 ppm H_2O) at room temperature with a computer-controlled Keithley 2400 Source Meter. In order to measure the photocurrent (J_L), the devices were illuminated at the transparent ITO electrode by a white light tungsten-halogen lamp, with a spectral range of 400-800 nm, calibrated against a calibrated Si diode to an intensity of 82 mW/cm^2 (0.82 Sun illumination). AFM images were recorded on ITO/PEDOT:PSS covered-glass substrate, with a DI NanoScope IV AFM operating under ambient conditions in tapping mode.

Materials:

All reagents and solvents were used as received or purified using standard procedures. [84]-Fullerene (98%) was supplied by Nano-C, Inc. and used without further purification. Flash chromatography was performed using silica gel (Kieselgel Merck Type 9385 (230-400 mesh)). ^{1}H NMR and ^{13}C NMR were performed on a Varian Unity Plus (400 MHz) instrument at 298 K. IR measurements were performed on a Nicolet Nexus FT-IR instrument. UV/VIS was performed on a Perkin-Elmer Instruments Lambda 900 spectrometer. HPLC analyses were performed on a Hewlett Packard HP LC-Chemstation 3D (HP 1100 Series) using an analytical Cosmosil Buckyprep® column (4.6 x 250 mm). Cyclic Voltammetry and Differential Pulse Voltammetry were performed using an Autolab PGStat 100.

Synthesis and characterization of [84]PCBM:

A flame dried 100 ml 3-necked flask, equipped with a stirring egg, thermometer, N_2-inlet and condensor was charged with 4-benzoyl-methylbutyrate p-tosylhydrazone (**2.1**) (55.2 mg, 0.147 mmol, 1.07 eq.), NaOMe (8.2 mg, 0.152 mmol, 1.1 eq.) and dry pyridine (2 ml). The resulting mixture was stirred for 1.5 h. To the mixture a solution of C_{84} (139 mg, 0.138 mmol) in ortho-dichlorobenzene (25 ml) was added. The resulting mixture was heated to 80 °C and irradiation was started with a 150 W Na-lamp. The irradiation was stopped after ~4h. All pyridine was evaporated in vacuo and the remaining mixture was purified by column chromatography. Elution with CS_2 yielded unreacted C_{84}. Subsequent elution with cyclohexane/toluene (1:1) yielded the mono-adduct fraction. Both fractions were evaporated to dryness, and the residues were redissolved in a minimal amount of ortho-dichlorobenzene and precipitated with MeOH. The resulting suspensions were centrifuged and the MeOH was decanted. The resulting brown pellets were washed twice with MeOH, centrifuged and decanted. The obtained brown pellets were dried at 50 ^{0}C in vacuo for 2 days. Isolated yields: Recovered C_{84}: 48.6 mg (4.8 10^{-2} mmol, 35%). Mono-adduct (isomeric mixture): 37.5 mg (3.12 10^{-2} mmol, 23%). Isomer assignment is based on varation among signals in different batches. The presented spectroscopic data is that of combined [84]PCBM batches. IR (KBr); ν (cm^{-1}): 2942 (m), 1737 (s), 1628 (m), 1600 (w), 1517 (w), 1493 (w), 1455 (s), 1434 (s), 1384 (m), 1330 (m), 1261 (m), 1155 (m), 1056 (w), 1034 (s), 795 (s), 749 (s), 727 (w), 702 (s), 643 (s), 576 (m), 527 (w), 515 (w), 499 (m), 455 (w), 432 (w), 426 (w), 415 (w), 405 (w). ^{1}H NMR (CS_2/ D_2O, 400 MHz); δ (ppm): 8.0 (d, J = 7.0 Hz), 7.89 (d, J = 6.6 Hz), 7.58–7.41 (m), 7.26–7.23 (m), 3.65 (s) (isomer A and C), 3.63 (s) (isomer B), 3.47 (m) (isomer A), 3.27 (m) (isomer C), 3.09 (t, J = 8.1 Hz) (isomer C), 2.54 (t, J = 7.3 Hz) (isomer A), 2.49 (t, J = 7.3 Hz) (isomer B), 2.28–2.22 (m). ^{13}C NMR (CS_2, 100 MHz); δ (ppm): 170.86, 170.80, 153.74, 151.57, 151.47, 151.29, 150.72, 149.95, 149.83, 143.57, 143.51, 143.09, 142.86, 142.56, 142.50, 142.16, 141.65, 141.45, 140.97, 140.90, 140.62, 140.57, 140.33, 140.31, 138.82, 138.78, 137.97, 137.93, 137.89, 137.47, 137.46, 137.33, 137.28, 137.23, 137.15, 137.01, 136.37, 135.77, 134.56, 134.50, 133.34, 133.07, 132.05, 131.94,

131.62, 130.02, 128.13, 128.08, 127.97, 127.84, 127.04, 64.75, 61.98, 61.74, 54.12, 50.83, 50.65, 50.62, 50.53, 37.23, 35.58, 35.05, 34.91, 34.78, 34.46, 33.88, 33.30, 33.26, 33.08, 33.03, 32.89, 29.75, 28.65, 26.37, 22.93, 22.84, 22.56, 21.86, 21.69, 21.37, 20.95, 20.69, 20.15. HPLC (toluene 1ml/min) retention times (min): 8.77, 9.15, 10.16.

2.8 References

1. F. Diederich, R. Ettl, Y. Rubin, R. L. Whetten, R. Beck, M. Alvarez, S. Anz, D. Sensharma, F. Wudl, K. C. Khemani, and A. Koch, *Science*, 1991, **252**, 548.
2. W. Krätschmer, L. D. Lamb, K. Fostiropoulos, and D. R. Huffman, *Nature*, 1990, **347**, 354.
3. D. E. Manolopoulos and P. W. Fowler, *J.Chem.Phys.*, 1992, **96**, 7603.
4. D. Bakowies, M. Kolb, W. Thiel, S. Richard, R. Ahlrichs, and M. M. Kappes, *Chem.Phys.Lett.*, 1992, **200**, 411.
5. D. E. Manolopoulos, P. W. Fowler, R. Taylor, H. W. Kroto, and D. R. M. Walton, *J.Chem.Soc.,Faraday Trans.,* 1992, **88**, 3117.
6. K. Raghavachari, *Chem.Phys.Lett.*, 1992, **190**, 397.
7. B. L. Zhang, C. Z. Wang, and K. M. Ho, *J.Chem.Phys.*, 1992, **96**, 7183.
8. K. Kikuchi, N. Nakahara, T. Wakabayashi, S. Suzuki, H. Shiromaru, Y. Miyake, K. Saito, I. Ikemoto, M. Kainosho, and Y. Achiba, *Nature*, 1992, **357**, 142.
9. A. J. Stone and D. J. Wales, *Chem.Phys.Lett.*, 1986, **128**, 501.
10. J. M. Hawkins, M. Nambu, and A. Meyer, *J.Amer.Chem.Soc.*, 1994, **116**, 7642.
11. A. L. Balch, A. S. Ginwalla, J. W. Lee, B. C. Noll, and M. M. Olmstead, *J.Amer.Chem.Soc.*, 1994, **116**, 2227.
12. T. J. S. Dennis, T. Kai, T. Tomiyama, and H. Shinohara, *Chem.Comm.*, 1998, 619.
13. J. Crassous, J. Rivera, N. S. Fender, L. H. Shu, L. Echegoyen, C. Thilgen, A. Herrmann, and F. Diederich, *Angew.Chem.Int.Ed.*, 1999, **38**, 1613.
14. T. J. S. Dennis, T. Kai, K. Asato, T. Tomiyama, H. Shinohara, T. Yoshida, Y. Kobayashi, H. Ishiwatari, Y. Miyake, K. Kikuchi, and Y. Achiba, *J.Chem.Phys.A*, 1999**, 103**, 8747.
15. N. Tagmatarchis, A. G. Avent, K. Prassides, T. J. S. Dennis, and H. Shinohara, *Chem.Comm.*, 1999, 1023.
16. N. Tagmatarchis, K. Okada, T. Yoshida, Y. Kobayashi, and H. Shinohara, *Chem.Comm.*, 2001, 1366.
17. A. D. Darwish, N. Martsinovich, and R. Taylor, *Org.Biom.Chem.*, 2004, **2**, 1364.
18. R. Nuffer, A. Bartl, L. Dunsch, and C. Mathis, *Synth.Met.*, 2001, **121**, 1151.

19. T. Wakahara, A. H. Han, Y. Niino, Y. Maeda, T. Akasaka, T. Suzuki, K. Yamamoto, M. Kako, Y. Nakadaira, K. Kobayashi, and S. Nagase, *J.Mater.Chem.*, 2002, **12**, 2061.
20. G. W. Wang, M. Saunders, A. Khong, and R. J. Cross, *J.Amer.Chem.Soc.*, 2000, **122**, 3216.
21. R. Taylor, *J.Chem.Soc.,Perkin Trans.2*, 1993813.
22. P. L. Boulas, M. T. Jones, R. S. Ruoff, D. C. Lorents, R. Malhotra, D. S. Tse, and K. M. Kadish, *J.Phys.Chem.*, 1996, **100**, 7573.
23. H. F. Bettinger and G. E. Scuseria, *Chem.Phys.Lett.*, 2000**, 332**, 35.
24. T. J. S. Dennis, M. Hulman, H. Kuzmany, and H. Shinohara, *J.Phys.Chem.B*, 2000, **104**, 5411.
25. T. Nishikawa, T. Kinoshita, S. Nanbu, and M. Aoyagi, *J.Mol.Struct.-Theochem*, 1999, **462**, 453.
26. G. von Helden, I. Holleman, M. Putter, A. J. A. van Roij, and G. Meijer, *Chem.Phys.Lett.*, 1999, **299**, 171.
27. O. V. Boltalina, I. N. Ioffe, L. N. Sidorov, G. Seifert, and K. Vietze, *J.Amer.Chem.Soc.*, 2000, **122**, 9745.
28. H. Steger, J. Holzapfel, A. Hielscher, W. Kamke, and I. V. Hertel, *Chem.Phys.Lett.*, 1995, **234**, 455.
29. M. Fanti, G. Orlandi, G. Poggi, and F. Zerbetto, *Chem.Phys.,* 1997, **223**, 159.
30. F. Furche and R. Ahlrichs, *J.Amer.Chem.Soc.*, 2002, **124**, 3804.
31. K. Shibata, Y. Kubozono, T. Kanbara, T. Hosokawa, A. Fujiwara, Y. Ito, and H. Shinohara, *Appl.Phys.Lett.*, 2004, **84**, 2572.
32. M. S. Denning, T. J. S. Dennis, M. J. Rosseinsky, and H. Shinohara, *Chem.Mater.*, 2001, **13**, 4753.
33. K. Harigaya, *J.Lumin.*, 1998**, 76-7**, 652.
34. M. M. Wienk, J. M. Kroon, W. J. H. Verhees, J. Knol, J. C. Hummelen, P. A. van Hal, and R. A. J. Janssen, *Angew.Chem.Int.Ed.*, 2003, **42**, 3371.
35. H. Ajie, M. M. Alvarez, S. J. Anz, R. D. Beck, F. Diederich, K. Fostiropoulos, D. R. Huffman, W. Krätschmer, Y. Rubin, K. E. Schriver, D. Sensharma, and R. L. Whetten, *J.Phys.Chem.,* 1990, **94**, 8630.
36. L. Juha, B. Ehrenberg, S. Couris, E. Koudoumas, S. Leach, V. Hamplova, Z. Pokorna, A. Mullerova, and P. Kubat, *Chem.Phys.Lett.,* 2001, **335**, 539.
37. J. C. Hummelen, J. Knol, and L. Sanchez, *Proceedings of SPIE-Int.Soc.Opt.Eng.*, 2001, **76**, 4108.
38. J. C. Hummelen, B. W. Knight, F. Lepeq, F. Wudl, J. Yao, and C. L. Wilkins, *J.Org.Chem.*, 1995, **60**, 532.
39. C. J. Brabec, A. Cravino, D. Meissner, N. S. Sariciftci, T. Fromherz, M. T. Rispens, L. Sanchez, and J. C. Hummelen, *Adv.Funct.Mater.*, 2001, **11**, 374.
40. C. J. Brabec, A. Cravino, D. Meissner, N. S. Sariciftci, M. T. Rispens, L. Sanchez, J. C. Hummelen, and T. Fromherz, *Thin Solid Films*, 2002, **403-404**, 368.
41. M. C. Scharber, D. Mühlbacher, M. Koppe, P. Denk, C. Waldauf, A. J. Heeger, and C. J. Brabec, *Adv.Mater.*, 2006, **18**, 789.

42. S. E. Shaheen, C. J. Brabec, N. S. Sariciftci, F. Padinger, T. Fromherz, and J. C. Hummelen, *Appl.Phys.Lett.,* 2001, **78**, 841.
43. J. K. J. van Duren, X. Yang, J. Loos, C. W. T. Bulle-Lieuwma, A. B. Sieval, J. C. Hummelen, and R. A. J. Janssen, *Adv.Funct.Mater.*, 2004, **14**, 425.
44. V. D. Mihailetchi, P. W. M. Blom, J. C. Hummelen, and M. T. Rispens, *J.Appl.Phys.*, 2003, **94**, 6849.
45. V. D. Mihailetchi, L. J. A. Koster, and P. W. M. Blom, *Appl.Phys.Lett.*, 2004, **85**, 970.
46. C. Melzer, E. J. Koop, V. D. Mihailetchi, and P. W. M. Blom, *Adv.Funct.Mater.*, 2004, **14**, 865.
47. J. K. J. van Duren, V. D. Mihailetchi, P. W. M. Blom, T. van Woudenbergh, J. C. Hummelen, M. T. Rispens, R. A. J. Janssen, and M. M. Wienk, *J.Appl.Phys.*, 2003, **94**, 4477.
48. V. D. Mihailetchi, J. K. J. van Duren, P. W. M. Blom, J. C. Hummelen, R. A. J. Janssen, J. M. Kroon, M. T. Rispens, W. J. H. Verhees, and M. M. Wienk, *Adv.Funct.Mater.*, 2003, **13**, 43.
49. V. D. Mihailetchi, J. Wildeman, and P. W. M. Blom, *Phys.Rev.Lett.,* 2005, **94**, 126602.

Chapter 3

Increasing the V_{oc} of Bulk Heterojunction Solar Cells by raising the LUMO level of the Acceptor

In this Chapter the synthesis, characterization and electrochemical properties of a large number of new fullerene derivatives for usage in organic solar cells are described. The phenyl ring of PCBM was substituted with electron-donating and electron withdrawing substituents to study their influence on the LUMO level of the parent fullerene. The LUMO level was varied over a range of 85 mV. A small but significant change in the open circuit voltage is observed upon application in MDMO-PPV:methanofullerene bulk heterojunction photovoltaic solar cells.

*Part of this chapter was published:

Floris B. Kooistra, Joop Knol, Frederik Kastenberg, Lacramioara M. Popescu, Wiljan J. H. Verhees, Jan M. Kroon, and Jan C. Hummelen. *Organic Letters*, **2007**, 9, 551–554

3.1 Introduction

In order to optimize the performance of organic photovoltaic devices a lot of parameters need further investigation. In the case of photovoltaic devices using poly-3-hexyl-thiophene:PCBM mixtures as the active layer, a lot of progress has been reported with respect to morphology improving procedures on the composite film.[1-5] On the other hand it is also possible to use different fullerenes. Our group has shown that substituting [60]PCBM by [70]PCBM in MDMO-PPV:fullerene type devices yields increased efficiencies from 2.5% to 3.0%.[6] We have also shown that using a fullerene derivative with a thienyl ring instead of a phenyl ring can give favorable improvement of photovoltaic devices when used in combination with P3HT as the donor polymer.[7] Furthermore optimizing processing conditions can be of critical importance. In the case of PCBM:MDMO-PPV solar cells, spincoating the active layer from chlorobenzene instead of from toluene led to a 3-fold increase of the device efficiency.[8] In Chapter 2 a similar effect was described, spincoating [84]PCBM:MDMO-PPV active layers from 1-chloronaphtalene instead of ortho-dichlorobenzene (ODCB) led to a more than 2-fold increase in current output. Despite the considerable effort put forth by many research groups there is still a lot of room for improvement. One parameter that has received much attention lately is the open circuit voltage.[9-12]

The research presented in this chapter has been a collaboration between our labs and those of ECN (Energy Research Centre of the Netherlands).

3.1.1 Origin of the Open Circuit Voltage

The open circuit voltage (V_{OC}) is defined as the voltage at zero current. This voltage is the maximum possible voltage that can be extracted from a single device. From semiconductor physics it is predicted that the V_{OC} should be equal to the difference in workfunction of both electrodes according to the Metal-Insulator-Metal (MIM) model.[13,14] Brabec et al. found only a small variation in the V_{OC} of 160 meV, while varying the negative electrode over a range of 2.2 eV.[15,16] Note however, that they included electrodes with workfunctions much higher than the acceptor LUMO level. They also found a direct correlation between the acceptor strength of the electron accepting material and the V_{OC}. A series of four different fullerene acceptors (Fig. 3.1) were tested in combination with MDMO-PPV as the donor material.

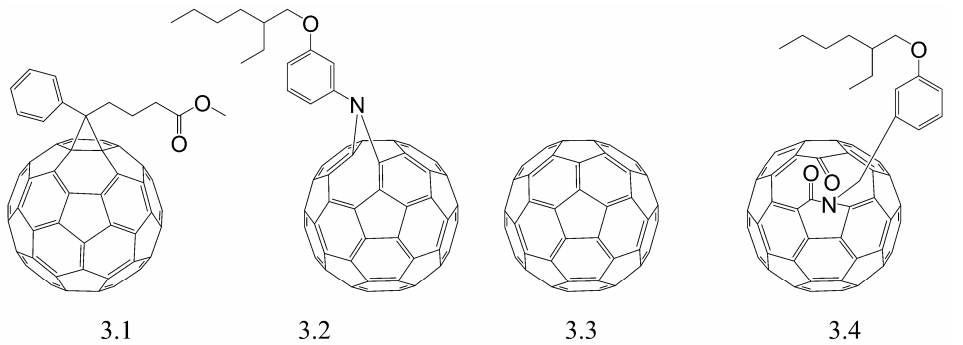

*Fig. 3.1: Series of fullerenes with decreasing LUMO levels (from left to right). PCBM (**3.1**), Azafulleroid (**3.2**), C_{60} (**3.3**) and Ketolactam (**3.4**)*

Lowering the LUMO level of the acceptor resulted in a decrease of the V_{OC} in a linear way. From this work it was concluded that the open circuit voltage is directly correlated to the energy difference of the donor HOMO level and the acceptor LUMO level. This observation was explained by Fermi level pinning, meaning that the workfunction of the metal is pinned to the workfunction of the semiconductor, in this case the fullerene. Therefore, independent of the metal used, the same V_{OC} will be found for one donor-acceptor combination.

A later study by Mihailetchi et al. however showed that this explanation does not fully describe the origin of the V_{OC}.[17] A difference has to be made between ohmic and non-ohmic contacts. The latter being the case when the workfunction of the metal is not at the same position as the semiconductor HOMO (for the donor) or LUMO (for the acceptor) level. When non-ohmic contacts are formed the V_{OC} is in agreement with the MIM model. However, in the case of ohmic contacts where the positive electrode matches the HOMO of the donor and the negative electrode that of the LUMO of the acceptor, the V_{OC} is governed by the HOMO-LUMO difference of the donor and the acceptor. Band bending at the contacts furthermore reduces the V_{OC} by ~0.2 eV at each electrode in this case according to the same study.[17]

Koster furthermore shows in his PhD thesis[18] that the p-n model does not correctly describe the origin of the V_{OC} for bulk heterojunction solar cells. He found a dependency of the V_{OC} on light intensity (in bulk heterojunctions), inconsistent with the p-n model. The main cause for this inconsistency is that the strong voltage dependence of the photocurrent is not taken into account in the p-n model.[19]

One more important condition that has to be met is that enough charges have to be created in the device. From semiconductor physics it is know that creating enough charges ensures that the quasi-Fermi levels are split up completely. When no charges are created the Fermi level will be in the middle in between the valence band and the conduction band. Once charges are formed this Fermi level will split up into two quasi-Fermi levels. One describing the Fermi distribution for holes and one describing the Fermi distribution for electrons. The more charges created, the

further the quasi-Fermi levels are split up, with a maximum splitting when the quasi-Fermi levels approach the valence band and the conduction band. Hence, when the V_{OC} of a device is experimentally determined it is of great importance that enough charges are created to give maximal splitting of the quasi-Fermi levels for the given light intensity.[20] (Fig. 3.2). We assume here that the same holds for bulk heterojunctions where we look at HOMO and LUMO levels instead of a valence and a conduction band. However, there is no literature available, which offers evidence that this is indeed the case.

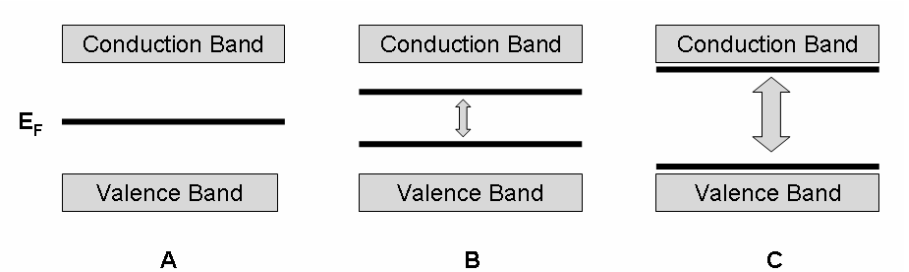

Fig. 3.2: Splitting of the Fermi level. No charges: E_F in the middle (A), few charges: incomplete splitting (B), many charges: complete splitting (C)

Considering all experimental and theoretical data discussed, it is clear that the maximum attainable V_{OC} is directly correlated to the distance between the HOMO level of the donor and the LUMO level of the acceptor *if* ohmic contacts are formed with both electrodes and *if* there is complete splitting of the quasi-Fermi levels. For the latter, an optimum morphology is essential as well.[17,21]

3.1.2 Research Goal

Now that the origin of the V_{OC} has been established we can deduct that it should be possible to increase the V_{OC} by increasing the HOMO-LUMO distance between donor and acceptor. Two possible ways of accomplishing this can be imagined, either lowering the HOMO level of the donor polymer or raising the LUMO level of the acceptor fullerene. Lowering the HOMO level of the polymer has been successfully accomplished by several groups.[9,12,22] These polymers were applied in photovoltaic devices and indeed a correlation between the HOMO level of the polymer and the obtained V_{OC} was seen.

In this chapter the other approach, namely raising the LUMO level of the acceptor, is described. It should be kept in mind, however, that a minimal energy difference between the LUMO level of the donor and the LUMO level of the acceptor is necessary for efficient charge separation. Since the LUMO levels in MDMO-PPV and [60]PCBM are estimated to be at 2.8 and 3.7 eV below the vacuum level,

respectively[23] (i.e. a 0.9 eV difference) it is expected that the LUMO level of the acceptor can still be raised to quite an extent before the driving force for charge separation is lost. State of the art MDMO-PPV:PCBM solar cells show V_{OC} values around 850 meV while the HOMO-LUMO gap is 1.3 eV. Since a loss of 0.2 eV at each electrode should be taken into account for ohmic contacts (which is the case for ITO/PEDOT:PSS and LiF/Al electrodes) this seems to be the maximum obtainable value for this donor acceptor pair. If the LUMO-LUMO gap (between donor and acceptor) could be diminished from 0.9 to 0.5 eV (still allowing efficient charge separation) an additional 0.4 eV could be won. In theory, it should therefore be possible to increase the V_{OC} to about 1.3 eV by raising the LUMO level of the acceptor. An increased V_{OC} would raise the overall efficiency even by a superlinear way by increasing the fill factor.[24,25] The goal of this research was therefore to design, synthesize and measure new fullerenes with higher lying LUMO levels in order to increase the V_{OC} in bulk heterojunction photovoltaic devices.

3.2 Synthesis

The main challenge is to alter a methanofullerene by substituent effects in such a way that its LUMO level is raised to an extent where it is still fully located on the fullerene moiety and without introducing *intra*molecular and/or *inter*molecular (in the solid state) photoinduced electron (or hole) transfer. The group of Verhoeven observed this for example in a 4-alkylaminophenyl-substituted fulleropyrolidine.[26] Wudl et al. have found that para substituents on the phenyl rings in diphenylmethano[60]fullerenes have a negligable effect on the reduction potential of the fullerene.[27] A better interaction in spiromethanofullerenes between the aromatic substituent and the fullerene was claimed through peri-conjugation. A maximum effect of ~70 meV was found. High V_{OC} values of 0.96 V have been reported by Riedel et al. employing a C_{60} adduct (DPM–12) and MDMO-PPV.[28] However the origin of this high value remained unclear, because the first reduction potential was identical to PCBM.

In contrast to the above mentioned two approaches, we aimed for a direct through space effect of a substituent with the parent fullerene. Such an effect has been previously observed with methylthio-groups on naphthalenes.[29] When taking PCBM as a scaffold we imagined that an electron donating substituent would be at closest proximity to the fullerene cage when introduced at the '2' position of the phenyl ring. Subsequent alkoxy or thioether substituents on the phenyl ring could then add to the effect of the ortho substituent by resonance contribution through the phenyl ring, provided that they are placed at the correct position on the ring i.e. ortho or para from the '2' position. In total a series of seven different methoxy substituted and two thioether substituted PCBM analogues were synthesized. Furthermore a pentafluoro[60]PCBM derivative was synthesized in order to investigate the influence of electron withdrawing groups on the LUMO level of the fullerene.

3.2.1 Synthesis of methoxy-substituted PCBM derivatives

In order to functionalize the parent fullerene, 1,3-dipolar addition reactions were employed. The active diazo species is generated *in situ* from a tosylhydrazone by addition of a base. Subsequent addition of a solution of C_{60} under the influence of heat and light allows for the formation of the desired fullerene adducts (see Scheme 3.1).[30] The necessary tosylhydrazones can be formed from a condensation reaction of p-tosylhyrazide with a ketone functionality. The necessary ketones were formed either by Friedel–Crafts acylation of the corresponding methoxy benzene with methyl-5-chloro-5-oxopentanoate or with glutaric anhydride, followed by esterification with methanol. In the case of 2-OMe-PCBM (**3.8d**) a cuprate addition of 5-chloro-5-oxopentanoate to the corresponding 2-bromoanisole was used. (Scheme 3.2)

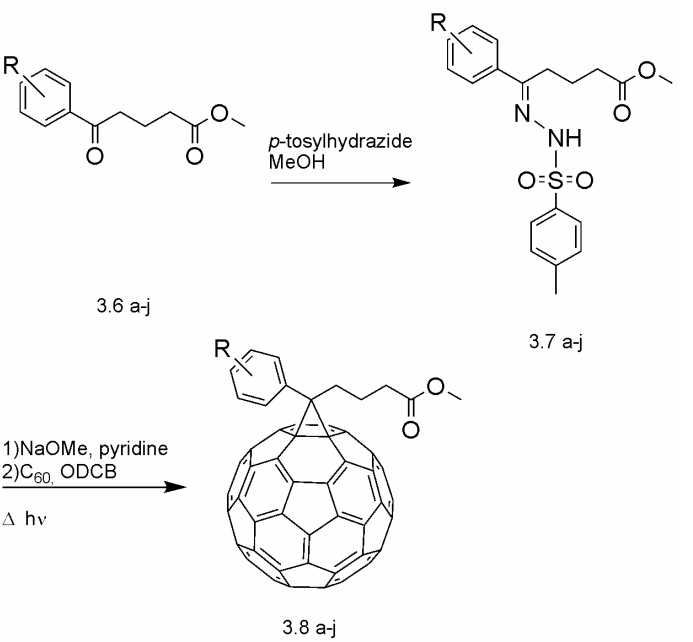

Scheme 3.1: Synthesis of new fullerene derivatives:. (a) R = 4-OMe (b) R = 3,4-OMe (c) R = 2,3,4-OMe (d) R = 2-OMe (e) R = 2,5-OMe (f) R = 2,4,6-OMe (g) R = methylenedioxy (h) R = 2-SMe (i) R = 4-SMe (j) R = pentafluoro

According to the above mentioned hypothesis the most effective methoxy-substituted PCBM derivative would be a 2,3,5-trismethoxy-PCBM. We have

extensively attempted to synthesize this molecule, but we have been unable to prepare the corresponding methyl benzoylbutyrate derivative.

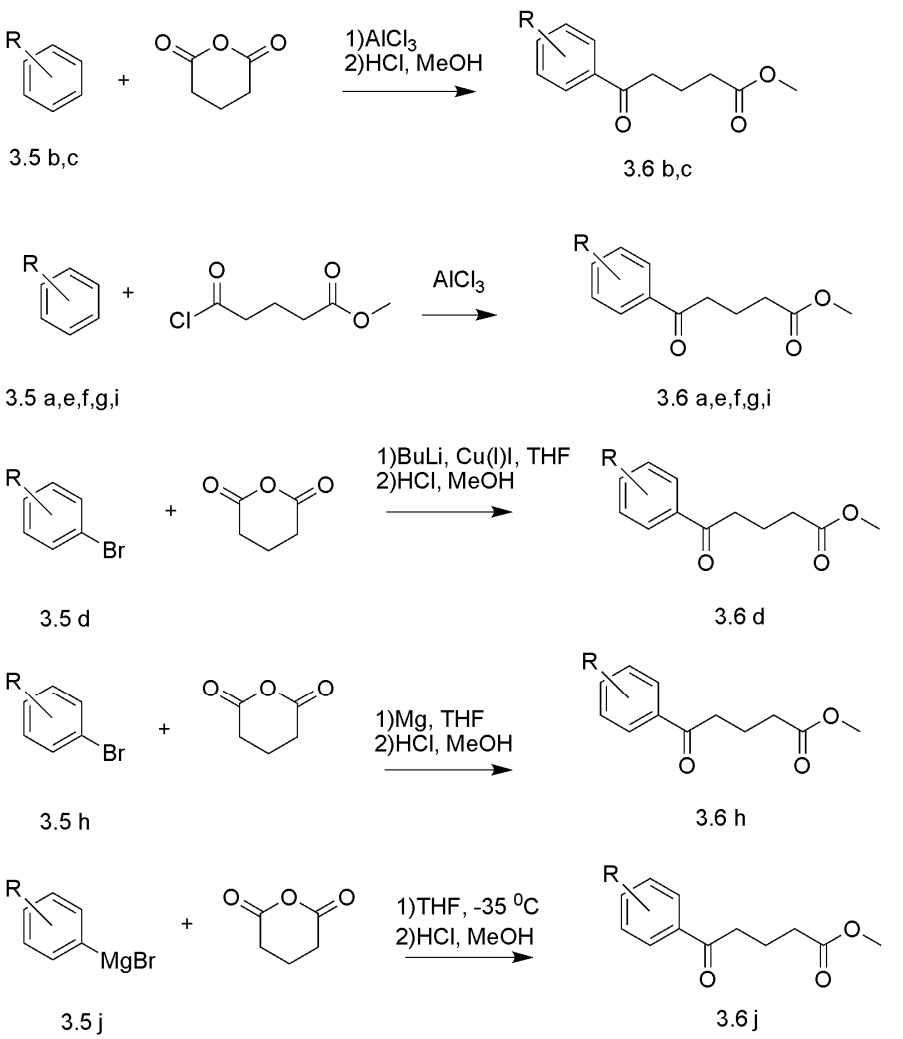

Scheme 3.2: Synthesis of keto-ester precursors. (a) R = 4-OMe (b) R = 3,4-OMe (c) R = 2,3,4-OMe (d) R = 2-OMe (e) R = 2,5-OMe (f) R = 2,4,6-OMe (g) R = methylenedioxy (h) R = 2-SMe (i) R = 4-SMe (j) R = pentafluoro

3.2.2 Synthesis of thioether substituted PCBM derivatives

Both thioether substituted derivatives were synthesized in almost the same manner as the methoxy substituted analogues. 4-SMe-PCBM was prepared starting with a Friedel-Crafts acylation of thioanisole with 5-chloro-5-oxopentanoate (Scheme 3.2). A subsequent condensation reaction with p-tosylhydrazide yielded the tosylhydrazone which was used to perform a 1,3-dipolar addition reaction on C_{60}. The synthesis of 2-SMe-PCBM proved to be somewhat more challenging. We eventually succesfully applied a Grignard reaction of 2-bromothioanisole with glutaric anydride followed by esterification of the acid functionality with methanol. Again a condensation reaction with p-tosylhydrazide gave the corresponding tosylhydrazone, which was used in the addition reaction to $C_{60.}$ (see Scheme 3.1)

3.2.3 Synthesis of pentafluoro-PCBM

A commercially available solution of pentafluorophenyl magnesium bromide in ether was used to perform a Grignard addition on glutaric anhydride followed by esterification with methanol (Scheme 3.2). The corresponding ketone functionality was transformed to the tosylhydrazone upon reaction with p-tosylhydrazide, which in turn was used for the addition reaction to C_{60}. (see Scheme 3.1)

3.3 Characterization

A good overlap between the oxygen or sulphur lone pairs and the fullerene π-system is only possible if the phenyl ring with its substituents cannot rotate freely. If it does, there will be no net interaction. ^{13}C–NMR should give a good indication whether the phenyl ring can rotate freely or not. The two sp^3 carbon atoms of the cyclopropyl ring on the fullerene are identical if the phenyl ring rotates freely. However, if the phenyl ring shows hindered rotation, or even stronger no rotation at all on the NMR time-scale at RT, the symmetry of the system is lost and two resonances will be observed.

Furthermore, the electron accepting capabilities of the fullerenes have been investigated with cyclic voltammetry and differential pulse voltammetry.

Lastly, we investigated whether intramolecular photoinduced electron transfer took place by performing fluorescence measurements.

3.3.1 Nuclear Magnetic Resonance Spectroscopy

The ^{13}C–NMR spectra of all ortho-methoxy and ortho-thioether substituted PCBM derivatives showed two resonances in the 80 ppm area. (Fig. 3.3) These peaks are typical for the two sp^3 carbon atoms of the cyclopropyl moiety of the fullerene cage.

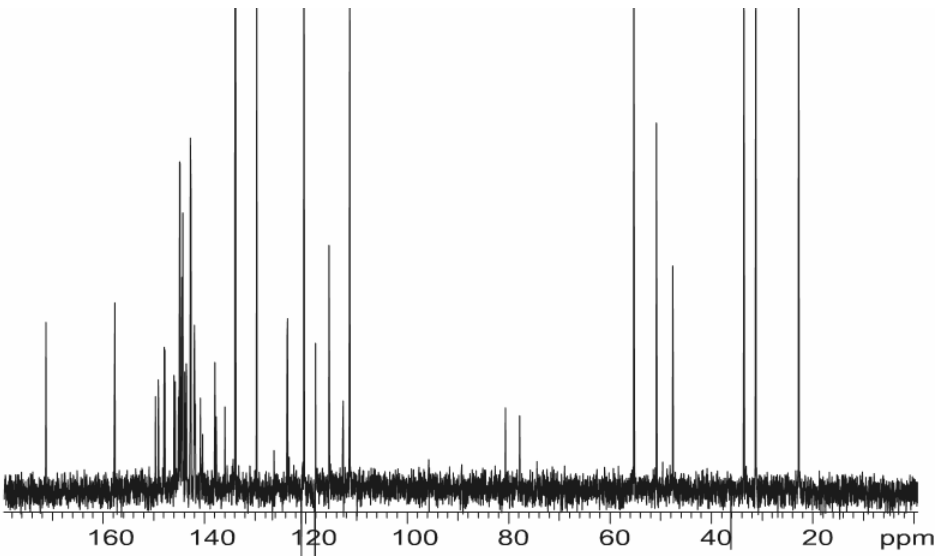

*Fig. 3.3: ^{13}C-NMR of 2-OMe-PCBM (**3.8d**). Illustrative ^{13}C-NMR of ortho-substituted PCBM derivatives showing two resonances in the 80 ppm region.*

Normally only one such signal is visible since both carbon atoms are equivalent. The appearance of two signals is highly indicative of severely hindered rotation of the phenyl ring. We therefore conclude that in the ortho-methoxy and ortho-methyl thioether substituted PCBM derivatives the phenyl rings are, with strong preference, in a conformation close to horizontal with respect to the fullerene surface. Which, in principle, might allow for effective overlap of the oxygen and sulphur lone pairs with the fullerene π-system.

3.3.2 Electrochemistry

In order to study whether this potential overlap between the oxygen and sulphur lone pairs with the fullerene π-system indeed occurs, cyclic voltammetry measurements were performed. A proof of such an overlap can be found if a lowering of the first reduction potentials (with respect to the Fc/Fc^+ redox couple) of the ortho-substituted PCBM derivatives, when compared to the PCBM derivatives

without ortho-substitution, is observed. Furthermore, a difference between the oxygen and sulphur versions was expected. Since sulphur has a larger atomic radius it can be expected that the overlap between its lone pair and the π-system of the fullerene is more effective. The obtained CV data are presented in Table 3.1. All reductions were reversible.

Table 3.1: Cyclic Voltammetry data.

Compound[a]	$E_{1/2}$,1,reduction (V)
2-OMe-PCBM (**3.8d**)	–1.104
4-OMe-PCBM (**3.8a**)	–1.096
2,5-OMe-PCBM (**3.8e**)	–1.106
3,4-OMe-PCBM (**3.8b**)	–1.099
3,4-methylenedioxy-PCBM (**3.8g**)	–1.071
2,3,4-OMe-PCBM (**3.8c**)	–1.118
2,4,6-OMe-PCBM (**3.8f**)	–1.128
2-SMe-PCBM (**3.8h**)	–1.086
4-SMe-PCBM (**3.8i**)	–1.085
F5-PCBM (**3.8j**)	–1.042
PCBM (**3.1**)	–1.084

[a]Experimental conditions: V vs Fc/Fc^+, Bu_4NPF_6 (0.1M) as the supporting electrolyte, ODCB/acetonitril (4:1) as the solvent, 10 mV/s scan rate.

Since the first reduction potentials of all but one of the methoxy-substituted PCBM derivatives are more negative than the first reduction potential of PCBM we can conclude that indeed we have been able to effectively, though slightly, raise the LUMO levels of the methoxy-substituted PCBM compounds with respect to the LUMO level of PCBM. However, we do not observe a clear difference between ortho-substituted derivatives and the derivatives without an ortho substituent. If we compare for example 2-OMe-PCBM with 4-OMe-PCBM we only see a difference of 8 mV. When we compare 2,5-OMe-PCBM and 3,4-OMe-PCBM a difference of only 7 mV is found. Therefore, although we see a small difference, we conclude that the ortho position of the phenyl substituent does *not* result in the expected direct through space electronic overlap between the oxygen lone pair and the fullerene π-system. A significant decrease in the first reduction potential is observed however, when going from two to three alkoxy substituents. Hence, it appears that the number of alkoxy substituents is of greater importance than the location of the

substituents on the phenyl ring. Furthermore, we can conclude that substituting the phenyl ring with methyl-thioether moieties has no effect on the LUMO level of the parent fullerene, indicating that their donating power is insufficient. The electron withdrawing effect of the fluorine atoms is clearly visible in the first reduction potential of F5-PCBM, resulting in a difference of 42 mV with PCBM.

3.3.3 Fluorescence Spectra

One problem that might be encountered when raising the LUMO level of PCBM is the possibility of intramolecular charge transfer. We therefore measured the fluorescence spectra of the compounds with the strongest electron donating groups in benzonitrile. Since the dielectric constant of benzonitril is much higher than that of the corresponding MDMO-PPV:PCBM blends in the thin film, lack of photoinduced charge transfer can be taken as a good indication that this process will not take place in the solid state in the PV device. All fluorescence spectra were quantitatively and qualitatively very similar. Hence, significant photoinduced intramolecular charge transfer does not take place in this polar solvent.

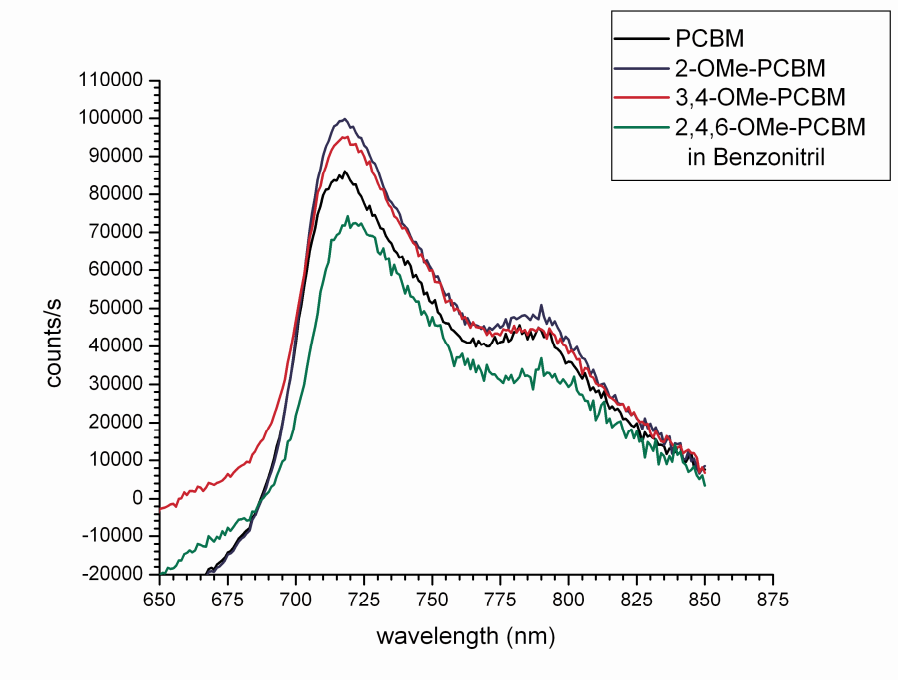

*Fig. 3.4: Fluorescence Spectroscopy of PCBM (**3.1**), 2-OMe-PCBM (**3.8d**), 3,4-OMe-PCBM (**3.8b**) and 2,4,6-OMe-PCBM (**3.8f**).*

The spectrum shows the characteristic singlet excitation and fluoresence of [60]fullerenes. The low intensity is due to the very efficient inter system crossing from the singlet S_1 to the triplet T_1 state.[31,32]

3.4 Solar Cell Devices

A series of ten photovoltaic devices was fabricated containing MDMO-PPV as the electron donor and the ten new fullerene derivatives as the electron acceptors. The devices were made with the following configuration: ITO/PEDOT:PSS/MDMO-PPV:methanofullerene/LiF/Al. In earlier work it was shown that for the specific combination of MDMO-PPV (from Covion) and PCBM, maximum power conversion efficiencies of 2.5% at standard test conditions (AM 1.5, 100 mW/cm^2) could be obtained by using a high content of PCBM (80 wt %) relative to MDMO-PPV and with chlorobenzene as the solvent for spincoating. However, it turned out that most of the new fullerene derivatives were only sparingly soluble in chlorobenzene, so that devices could not be made in a proper way from this solvent. Of all the derivatives only 3,4-OMe-PCBM and 2,3,4-OMe-PCBM were soluble enough in chlorobenzene for device fabrication. We therefore chose ODCB as a common solvent for all derivatives. In Fig. 3.5 the V_{OC} values (average values)[I] are plotted against the measured reduction potentials (Table 3.1) of the alkoxy-substituted PCBM derivatives. In a separate experiment, devices were constructed with both thioether substituted PCBMs and the F5-PCBM analogue. A slightly lower V_{OC} value of 4-SMe-PCBM (**3.8i**) to PCBM (20 mV lower) was found. F5-PCBM (**3.8j**) gave a value of 40 mV lower than that of PCBM, according to expectations. The insolubility of 2-SMe-PCBM (**3.8h**) in ODCB rendered it impossible to construct a respresentable device. Similar problems occurred with 2,4,6-OMe-PCBM (**3.8f**). Its low V_{OC} is attributed to these insolubility problems, leading to at best marginally successful bulk heterojunction morphology. When the domain sizes in the blend are too big, fewer charge carriers can be formed, resulting in a decreased splitting of the quasi-Fermi levels (see paragraph 3.1.1), hence lowering the observed V_{OC} at the same light intensity.

[I] For chlorobenzene 4 cells were averaged. For dichlorobenzene 2 experiments with both 4 cells were averaged.

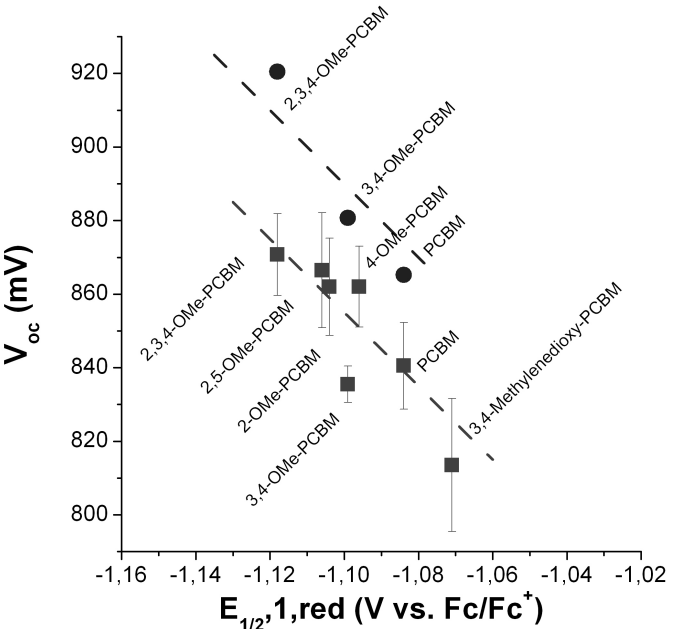

Fig. 3.5: V_{OC} of devices (average values) from MDMO-PPV blends vs the first reduction potential, $E_{1/2}$,1,red (V vs. Fc/Fc$^+$) of the PCBM derivatives: squares from ODCB; circles from chlorobenzene. The dashed lines are to guide the eye for a 1:1 relationship between V_{OC} and $E_{1/2}$,1,red.

All presented values here are, however, not obtained from fully optimized devices, since the optimization of ten completely new donor-acceptor combinations is an extremely time consuming process. Nevertheless, the trend is clearly visible, indicating that a higher LUMO level of the acceptor fullerene does give a higher V_{OC} in fullerene:polymer solar cells devices. Moreover that trend seems to be linear, in accordance with previous results.

3.5 Conclusions

A series of ten new fullerene derivatives were synthesized. All but one of the methoxy-substituted PCBM derivatives show a more negative first reduction potential than PCBM, clearly indicating a raise in the LUMO level. However, proof for a direct 'through space' interaction between the oxygen lone pair electrons and the fullerene π-system has not been found. The number of alkoxy substituents seems to be of more effect than their relative position on the phenyl ring. The thioether substituted PCBM derivatives gave no change in first reduction potentials

compared to PCBM, which is most likely due to the low donating power of the thioether groups. As expected the pentafluoro PCBM derivative gave a less negative first reduction potential.

Solar cell device measurements showed a linear trend when plotting the V_{OC} of the devices versus the first reduction potential of the corresponding fullerene. This is in accordance with previous results and gives further experimental proof that within the set conditions, the V_{OC} of a bulk heterojunction solar cell is determined by the distance between the donor HOMO level and the acceptor LUMO level.

This new library of fullerene adducts with different LUMO levels, might proof to be very useful in future optimization studies, although most of them exhibit solubility problems. The 3,4-OMe-PCBM and 2,3,4-OMe-PCBM derivatives, however, show very promising voltages combined with good processability. Further optimization studies with these two fullerenes should be very interesting and the performance of solar cell devices with these fullerenes as acceptors might even surpass performance of PCBM solar cells in the future.

3.6 Experimental

3.6.1 Device preparation

Photovoltaic devices were prepared by spincoating EL grade PEDOT:PSS (Bayer EG) layers of ~ 60 nm onto pre-cleaned, patterned ITO substrates. The photoactive layer was deposited by spincoating from the appropriate solvent. The spin coating conditions were adjusted to give photoactive layers between 60 and 90 nm. Finally, a 1nm layer of LiF (Sigma Aldrich) and 80 nm Al (5N, Sigma Aldrich) were evaporated at $1 \cdot 10^{-6}$ mbar through a shadow mask. Electrical device characterization was performed under a N_2 atmosphere. Current density-voltage measurements were carried out using a home-built (ECN) setup with a tungsten/halogen lamp (12V/50W) and a Keithley SMU 2400. From the overlap of the spectral response of the sample with the standard AM1.5 (1000 W/m2) spectrum we calculated the short circuit current density under AM1.5 conditions (Jsc,SR[II]) assuming a linear relation between the illumination intensity and the short circuit current density. The Jsc,SR is in this way largely insensitive to aging of Tungsten/halogen lamp, (long term) intensity variations and spectral mismatch errors.

[II] Spectral Response

3.6.2 Materials

All reagents and solvents were used as received or purified using standard procedures. [60]-Fullerene (99.5 %) was purchased from MTR, Ltd (Cleveland, Ohio) and used without further purification. Flash chromatography was performed using silica gel (Kieselgel Merck Type 9385 (230-400 mesh)). Melting points were determined with a Mettler FP1 melting point apparatus equipped with a Mettler FP2 microscope. ^{1}H NMR and ^{13}C NMR were performed on a Varian Unity Plus (500 MHz), on a Varian VXR-300 (300 MHz) or on a Varian VXR-200 (200 MHz) instrument as indicated, at 298 K using TMS as an internal standard. IR measurements were performed on a Nicolet Nexus FT-IR instrument. UV/VIS were performed on a Perkin-Elmer Instruments Lambda 900 spectrometer. High Resolution Mass Spectroscopy (HRMS) was performed on a JEOL JMS 600 spectrometer. HPLC analyses were performed on a Hewlett Packard HP LC-Chemstation 3D (HP 1100 Series) using an analytical Cosmosil Buckyprep® column (4.6 x 250 mm). Cyclic Voltammetry and Differential Pulse Voltammetry were performed using an Autolab PGStat 100. Elemental analysis was performed by the Microanalytical Department of this laboratory.

3.6.3 Synthesis

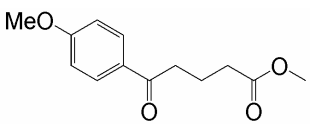

5-(4-Methoxy-phenyl)-5-oxo-pentanoic acid methyl ester (3.6a):

A flame dried three-necked flask equipped with N_2 inlet and parafin bubbler was charged with $AlCl_3$ (15.32 g, 115 mmol, 2.3 eq.) and 1,1,2,2-tetrachloroethane (40 ml). The resulting suspension was cooled in ice and then anisole (8.11 g, 75 mmol, 1.5 eq.) was added. After stirring for a few minutes methyl 5-chloro-5-oxopentanoate (8.23 g, 50 mmol) was added in portions over 1 minute. A slow stream of N_2 was passed over the solution. The resulting orange-red solution was allowed to reach RT and was stirred overnight. The mixture was then poured onto crushed ice (500 g) and CH_2Cl_2 (150 ml) was added. The two-layer system was separated and the aqeuous phase was extracted with CH_2Cl_2 (2 x 100 ml). The combined extracts were washed with dilute HCl (2N, 1 x 100 ml) and brine (1 x 100 ml) and then dried over Na_2SO_4. Evaporation of the solvents *in vacuo* yielded a pale yellow oil which crystallized upon standing. The solid was suspended in cold pentane (100 ml) and filtered through a glass funnel. The obtained solid was washed with cold pentane and dried in air. ^{1}H NMR ($CDCl_3$, 300 MHz): δ (ppm): 7.94 (d, *J* = 9.0 Hz, 2H), 6.93 (d, *J* = 9.0 Hz, 2H), 3.86 (s, 3H), 3.68 (s, 3H), 2.99 (t, *J* = 6.0 Hz, 2H), 2.43 (t, *J* = 6.0 Hz, 2H), 2.06 (m, 2H).

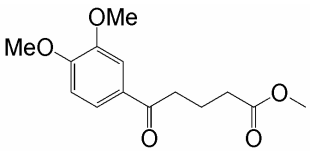

5-(3,4-Dimethoxy-phenyl)-5-oxo-pentanoic acid methyl ester (3.6b):

Glutaric anhydride (5.0 g, 43.8 mmol) was dissolved in veratrole (100 ml, 785 mmol). The remaining solution was cooled in an ice-bath. While stirred, $AlCl_3$ (13.0 g, 97.5 mmol) was added at once resulting in a dark purple mixture. The mixture was stirred at 0 ^{0}C for 1h and thereafter at RT overnight. The mixture was poured onto concentrated HCl/ice. The remaining orange mixture was extracted with ether (2 x 150 ml) and dichloromethane (1 x 150 ml). The orange organic layers were combined and extracted with Na_2CO_3 (3 x 100 ml). The combined basic aqueous extracts were combined and acidified with cold concentrated HCl. The crude acid precipitates as a sticky white solid and was isolated by extraction with dichloromethane (2 x 150 ml). The organic layers were dried over Na_2SO_4 and concentrated *in vacuo* yielding a yellow sticky solid. This crude acid was dissolved in methanol (100 ml) and dry HCl was bubbled through the solution for ~ 15 min. The resulting clear solution was stirred overnight at RT. The mixture was evaporated to dryness and the resulting oil was redissolved in ether (150 ml). The resulting solution was washed with $NaHCO_3$ (10% solution, 150 ml), dried over Na_2SO_4 and concentrated *in vacuo*, yielding a yellow oil. The crude ester was purified by kugelrohr distillation (180–185 ^{0}C, 0.04 mm Hg) yielding a colorless oil which crystallizes (3.0 g, 11.3 mmol, 26%). ^{1}H NMR ($CDCl_3$, 200 MHz): δ (ppm): 7.59 (dd, *J* = 8.5 Hz, *J* = 1.7 Hz, 1H), 7.53 (d, *J* = 1.7 Hz, 1H), 6.88 (d, *J* = 8.5 Hz, 1H), 3.95 (s, 3H), 3.94 (s, 3H), 3.68 (s, 3H), 3.02 (t, *J* = 7.9 Hz, 2H), 2.42 (t, *J* = 7.9 Hz, 2H), 2.05 (m, 2H).

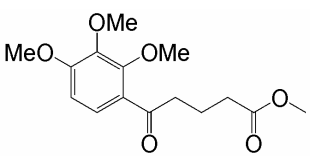

5-(2,3,4-Trimethoxy-phenyl)-5-oxo-pentanoic acid methyl ester (3.6c):

To a stirred solution of $AlCl_3$ (20.0 g, 150 mmol) in nitrobenzene (80 ml) were added trimethyl pyragallol trimethyl ester (8.0 g, 47.6 mmol) and glutaric anhydride (8.0 g, 70.2 mmol). An exothermic reaction occurred with a color change from yellow to dark brown. The mixture was stirred for 48 h. at RT. The solidified mixture was poured onto concentrated HCl/ice. A pink-purple mixture is obtained which contains a lot of precipitated material. This solid is filtered trough a glass funnel, dissolved in ether and extracted with aqeous Na_2CO_3. Acidification with concentrated HCl yielded a light brown precipitate which was filtered and dried at 50 ^{0}C *in vacuo*. The original filtrate was also extracted with ether (2 x 100 ml). The combined extracted were then extracted with aqueous Na_2CO_3. Acidification yielded a second batch of crude acid as a reddish powder after drying at 50 ^{0}C *in vacuo*. The crude acid was suspended in methanol (100 ml) and dry HCl gas was bubbled through the solution for ~ 15 min. After stirring the solution at RT overnight the methanol was removed and the residual oil was dissolved in ether (150 ml).

The organic solution was washed with water (1 x 50 ml), dried over Na_2SO_4 and concentrated *in vacuo*. The obtained oil contained partly deprotected phenol(s). Therefore the oil was dissolved in dry acetone (100 ml). K_2CO_3 (40 mmol) and MeI (40 mmol) were added and the mixture was refluxed overnight. After cooling to RT the mixture was filtered through Celite. The filtrate was evaporated to dryness. A silica gel column (5 x 10 cm) was prepared. Elution was started with a $CHCl_2/Et_2O$ (19/1) mixture. The product fractions were evaporated to dryness yielding a yellow oil (2.6 g, 8.8 mmol, 18%). ^{1}H NMR ($CDCl_3$, 200 MHz): δ (ppm): 7.48 (d, *J* = 9.3 Hz, 1H), 6.70 (d, *J* = 9.3 Hz, 1H), 3.94 (s, 3H), 3.89 (s, 3H), 3.85 (s, 3H), 3.66 (s, 3H), 3.09 (t, *J* = 6.4 Hz, 2H), 2.41 (t, *J* = 6.4 Hz, 2H), 2.01 (m, 2H).

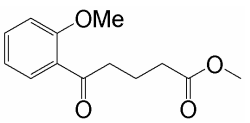

4-(2-methoxy-benzoyl)-butyric acid methyl ester (3.6d):

A solution of o-bromoanisole (4.5 g, 24.06 mmol) in dry THF (100 ml) was placed under nitrogen. Under stirring, a solution of BuLi (15 ml, 1.6 N in hexane, 24 mmol) was added dropwise while the mixture was kept at –78 ^{0}C. The resulting homogeneous solution was allowed to warm up to –55 ^{0}C in 30 min. Copper(I)iodide (2.38g, 12.49 mmol) was then added at once, resulting in a creamy brown solution. The mixture was allowed to warm up to –30 ^{0}C in 20 min. The obtained dark brown slurry was stirred for another 30 min, after which methyl 5-chloro-5-oxopentanoate (1.66 g, 10.09 mmol) was added, resulting in a green mixture. The mixture was allowed to warm up to 0 ^{0}C in 1 h. Dry MeOH (4 ml) was added, resulting in some precipitation. Aqueous NH_4Cl (50 ml) was added to the mixture. The mixture was then filtered through celite. The filtrate separated in a blue and a green layer, which were separated. The aqueous (blue) layer was extracted with ether (3x 50 ml). The combined organic extracts were washed with water (1x 100 ml) dried over Na_2SO_4 and concentrated *in vacuo* yielding a greenish liquid. To further purify the obtained product a silica gel column (7x 3 cm) was prepared. The Mixture was dissolved in toluene, deposited and eluted with toluene and 9:1 toluene:ether. Fractions containing product were concentrated *in vacuo*, yielding a yellow oil (1.92 g, 8.14 mmol, 80.6%). IR (neat) = ν (cm^{-1}): 2950 (m), 1737 (s), 1674 (m), 1597 (m), 1485 (m), 1437 (m), 1286 (m), 1246 (s), 1023 (m), 758 (m). ^{1}H NMR ($CDCl_3$, 300 MHz): δ (ppm): 7.68 (dd, *J* = 7.7 Hz, *J* = 1.8 Hz, 1H), 7.46 (m, 1H), 6.93–7.04 (m, 2H), 3.90 (s, 3H), 3.67 (s, 3H), 3.04 (t, *J* = 7.3 Hz, 2H), 2.41 (t, *J* = 7.3 Hz, 2H), 2.08–2.01 (m, 2H). ^{13}C NMR ($CDCl_3$, 75 MHz): δ (ppm): 201.7, 173.8, 158.4, 133.3, 130.1, 128.2, 120.5, 111.4, 97.9, 55.4, 51.4, 42.6, 33.3, 19.5. HRMS: Calcd for $C_{13}H_{16}O_4$: 236.1047. Found: 236.1048.

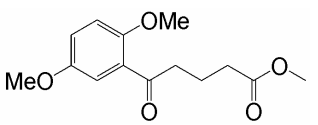

5-(2,5-dimethoxyphenyl)-5-oxo-pentanoic acid methyl ester (3.6e):

Aluminum trichloride (9.04 g, 67.8 mmol) was suspended in dichloroethane (50 ml), placed under nitrogen and cooled to 0 ^{0}C while stirred.

To the suspension p-dimethoxybenzene (6.29 g, 45.5 mmol) was added at once. Subsequently, methyl 5-chloro-5-oxopentanoate (5.05 g, 30.7 mmol) was added dropwise. The resulting mixture turned from green to brown and HCl gas formation was observed. The solution was allowed to warm up to RT and stirred for 20 h. The reaction mixture was poured out on ice (100 g). To the obtained yellow mixture 50 ml of dichloromethane was added and the mixture was stirred until all the ice had molten. The obtained mixture was then separated. The aqueous layer was extracted with dichloromethane (3x 50 ml). The organic layers were combined, washed with water (1x 75 ml) and brine (2x 75 ml) and dried over Na_2SO_4. Evaporation of the solvents afforded a yellow oil. The oil was redissolved in ether (200 ml) and washed with a NaOH solution (0.5 M, 4x 50 ml). The ethereal layer was then washed with water (1x 100 ml) and dried over Na_2SO_4. Concentration *in vacuo* afforded a light yellow liquid. The product was distilled using a kugelrohr apparatus (60 ^{0}C, 0.5 mTorr). The obtained residue was a somewhat yellow oil that crystallized upon standing. The residue was suspended in n-pentane and sonicated. The suspension was filtered by suction yielding a white powder (5.72 g, 21.5 mmol, 70%). IR (KBr) = ν (cm^{-1}): 2999 (m), 2951 (s), 2836 (s), 1737 (s), 1673 (s), 1609 (w), 1582 (w), 1495 (s), 1412 (m), 1279 (m), 1223 (m), 1048 (m), 1021 (m), 814 (m), 728 (m). ^{1}H NMR ($CDCl_3$, 300 MHz): δ (ppm): 7.24 (d, *J* = 3.3 Hz, 1H), 7.01 (dd, *J* = 9.2 Hz, *J* = 3.3 Hz, 1H), 6.89 (d, *J* = 9.2 Hz, 1H), 3.85 (s, 3H), 3.78 (s, 3H), 3.66 (s, 3H), 3.04 (t, *J* = 7.0 Hz, 2H), 2.40 (t, *J* = 7.3 Hz, 2H), 2.01 (m, 2H). ^{13}C NMR ($CDCl_3$, 75 MHz): δ (ppm): 201.2, 177.4, 173.7, 153.3, 152.9, 128.2, 119.8, 113.7, 112.9, 55.9, 55.7, 51.4, 42.6, 33.2, 19.4. HRMS: Calcd for $C_{14}H_{18}O_5$: 266.1154. Found: 266.1161. Melting point: 50.0 – 50.5 (^{0}C)

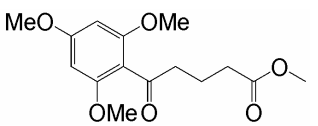

5-(2,4,6-trimethoxyphenyl)-5-oxo-pentanoic acid methyl ester (3.6f):

A dried 250 ml flask was charged with $AlCl_3$ (9.2 g, 69 mmol) under N_2. Dichloroethane (50 ml) was added and the suspension was cooled on ice while stirred.1,3,5-Trimethoxybenzene (7.57 g, 45 mmol) was added at once resulting in a homogeneous solution. After stirring for a few minutes methyl 5-chloro-5-oxopentanoate (4.94 g, 30 mmol) was added at once. The solution quickly turned dark brown. The cooling bath was removed and the mixture was stirred at RT for ~22 h. The reaction mixture was poured onto crushed ice and dichloromethane (50 ml) was added. The resulting mixture was separated. The aqueous layer was extracted with dichloromethane (3 x 50 ml). The combined organic layers were washed with H_2O (1 x 75 ml) and brine (2 x 75 ml), dried over Na_2SO_4 and concentrated *in vacuo* obtaining a purple oil. A silica gel column (5 x 11 cm) was prepared. Mixture was dissolved in toluene (50 ml) and dposited. Elution was started with toluene removing side products. Product was eluted with toluene:ether (9:1). Evaporation yielded a yellow viscous oil (7.58 g, 25.6 mmol, 85 %). ^{1}H NMR ($CDCl_3$, 300 MHz): δ (ppm): 6.08 (s, 2H), 3.71 (s, 3H), 3.66 (s, 6H), 3.57 (s, 3H), 2.69 (t, *J* = 6.7 Hz, 2H), 2.35 (t, *J* = 6.7 Hz, 2H), 1.98 (m, 2H).

^{13}C NMR ($CDCl_3$, 75 MHz): δ (ppm): 202.6, 173.7, 162.1, 161.3, 157.9, 113.2, 92.7, 90.4, 55.6, 55.2, 55.1, 51.3, 43.6, 33.0, 19.1.

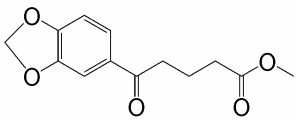

5-(3,4-(methylenedioxy)phenyl)-5-oxo-pentanoic acid methyl ester (3.6g):

A flame-dried three-necked flask, equipped with thermometer and stirr bar, was placed under a nitrogen atmosphere and charged with 1,2-(methylenedioxy)benzene (10 g, 81.88 mmol, 1.2 eq.) and methyl 5-chloro-5-oxopentanoate (1.2 g, 7.32 mmol). To this mixture was added 1,2-dichloroethane (40 ml). At 0 ^0C $Sn(IV)Cl_4$ (21 ml) was dropped to the solution. The mixture turned dark green and was stirred for 15 h, resulting in the formation of a deep purple suspension from which a deep purple solid had formed. The mixture was poured out on ice (100 g), the solid was transferred onto the ice using chloroform (50 ml). After all the ice had molten a green suspension was obtained. The aqueous layer was then extracted with chloroform (3 x 100 ml). The organic layers were collected and washed subsequently with $NaHCO_3$ (1 x 100 ml) and H_2O (1 x 100 ml), dried over Na_2SO_4 and concentrated *in vacuo* yielding a black oil. A silica gel column (2 x 20 cm) was prepared. The mixture was entered with a toluene : ether (1:1) mixture and eluted with a toluene : ether (1:1) mixture. An orange oil was obtained which solidified upon standing. ^1H NMR and ^{13}C NMR showed the product to be a mixture of product and starting material (2:1). The mixture was not further purified but used in the next reaction step.

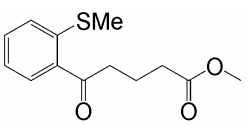

Methyl 5-[2-(methylthio)phenyl]-5-oxopentanoate (3.6h):

Magnesium turnings (6.11 g, 251 mmol) were mixed with some glasspearls and stirred under nitrogen atmosphere for 24 hours at room temperature THF (40 ml.) and an iodine crystal were added which resulted in a brown and then green/grey solution. A mixture of 2-bromo-thioanisole (10.00 g, 49.2mmol) in THF (40 ml.) was added over 70 minutes. The solution became grey/black and a temperature rise to 40ºC was observed. The solution was stirred for 2,5 hours and then added by Canula-manner to a solution of glutaric anhydride (10.98 g, 96.2 mmol) in THF (50 ml.) at -40 ºC. After 2 hours the mixture was allowed to warm up slowly to room temperature and was stirred overnight. The resulting mixture was poured onto a saturated solution of ammonium chloride (300 ml.). The aqueous layer was extracted with ether (3 x 100ml.) The combined colorless organic layers were washed with brine (2 x 200ml.), dried over sodium sulfate and concentrated invacuo yielding a yellow/brownish powder. The powder was suspended in ether, filtered and dried *in vacuo* yielding a white powder. Yield: 6.95g (29.1 mmol, 60%). MP = 118 ^0C; IR (KBr); ν (cm^{-1}): 2933 (m), 1698 (s), 1669 (s), 1587 (m), 1556 (m), 1467 (m), 1430 (s), 1332 (m), 1275(m), 1219(m), 1147(m) 961 (s), 746 (s); ^1H NMR ($CDCl_3$, 300 MHz): δ (ppm): 7.80 (d, *J* = 7.69 Hz, 1H), 7.45 (t, *J* = 7.69 Hz, 1H),

7.29 (d, *J* = 8.06 Hz, 1H), 7.16 (t, *J* = 7.69 Hz, 1H), 3.04 (t, *J* = 6.95 Hz, 2H), 2.48 (t, *J* = 7.33 Hz, 2H), 2.41 (s, 3H), 2.06 (m, 2H); ^{13}C NMR: ($CDCl_3$, 50 MHz): δ (ppm): 200.4, 179.0, 142.3, 134.4, 132.2, 130.0, 125.2, 123.5, 38.7, 33.0, 19.1, 16.0. HRMS: Calcd for $C_{12}H_{14}O_3S$: 238.0664. Found: 238.0677. The acid (6.37 g, 26.7mmol) was dissolved in of methanol (270 ml.). Some drops of concentrated hydrochloric acid were added. The resulting clear colorless mixture was stirred for 22 hours at room temperature. Subsequently the methanol was evaporated and the resulting brownish liquid was dissolved in ether (80 ml.), dried over sodium sulfate and concentrated *in vacuo* yielding a slightly yellow/golden solid. Yield: 5.56 g (22.0 mmol, 82.4 %). MP = 28 ^{0}C; IR: (KBr); ν (cm^{-1}): 2950 (m), 1735 (s), 1671 (s), 1587 (m), 1558 (m), 1434 (s), 1370 (m), 1212 (s), 1048 (m), 982 (m), 884 (w), 749 (s); ^{1}H NMR: ($CDCl_3$, 300 MHz): δ (ppm): 7.80 (d, *J* = 8.05 Hz, 1H), 7.44 (t, *J* = 8.05 Hz, 1H), 7.26 (d, *J* = 8.06 Hz, 1H), 7.15 (t, *J* = 7.69 Hz, 1H), 3.65 (s, 3H), 3.01 (t, *J* = 6.96 Hz, 2H), 2.43 (t, *J* = 7.32 Hz, 2H), 2.41 (s, 3H), 2.05 (q, *J* = 7.35 Hz, 2H); ^{13}C NMR. ($CDCl_3$, 50 MHz): δ (ppm): 200.7, 174.0, 142.6, 134.4, 132.4, 130.4, 125.3, 123.7, 51.8, 39.0, 33.3, 19.7, 16.2. HRMS: Calcd for $C_{13}H_{16}O_3S$: 252.0820. Found: 252.0834.

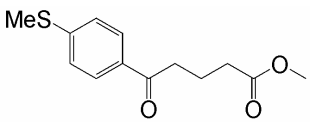

Ethyl 5-[4-(methylthio)phenyl]-5-oxopentanoate (3.6i):

A dry 3-neckled flask was charged with $AlCl_3$ (15.3 g, 115.0 mmol) and some glasspearls and was stirred for 2 hours. Subsequently, 1,1,2,2-tetracloroethane (40 ml.) vwas added. The resulting suspension was cooled with ice and thioanisole (9.32 g, 75.0 mmol) was added. After stirring for a few minutes, methyl 4-(chloroformyl)butyrate (8.23 g, 50.0 mmol) was added slowly by using a dropping funnel. A small flow of nitrogen was left over the solution to get rid of hydrochloric acid. The resulting green solution was allowed to reach room temperature and was stirred overnight. After 19 hours, the mixture was poured onto crushed ice and 1,1,2,2-tetracloroethane (150 ml.) was added. The two layer mixture was separated and the aqueous phase was extracted with 1,1,2,2-tetracloroethane (2 x 100 ml.). The combined organic layers were washed with 2M hydrochloric acid (100 ml.) and brine (100 ml.), dried over sodium sulfate and evaporated *in vacuo* yielding 20.0g of a purple/orange bilayer liquid which crystallize after upon standing. Subsequently, pentane (100 ml.) was added and the mixture was kept in ultrasonic bath for 45 minutes. The mixture was filtered and washed with cold pentane yielding a white powder. Yield: 11.8g (46.7mmol), 93.3%; MP = 55 ºC; IR (KBr); ν (cm^{-1}): 2962 (s), 1738 (s), 1670 (s), 1588 (m), 1383 (m), 1275 (m), 1168 (m), 753 (w); ^{1}H NMR ($CDCl_3$, 300 MHz): δ (ppm): 7.85 (d, *J* = 8.79 Hz, 2H), 7.24 (d, *J* = 8.79 Hz, 2H), 3.66 (s, 3H), 2.98 (t, *J* = 7.33 Hz, 2H), 2.49(s, 3H), 2.41 (t, *J* = 7.33 Hz, 2H), 2.06 (m, 2H); ^{13}C NMR: ($CDCl_3$, 50 MHz): δ (ppm): 196. 9, 172.2, 144.3, 131.6, 126.9, 123.5, 50.1, 35.7, 31.6, 17.9, 13.3. HRMS: Calcd for $C_{13}H_{16}O_3S$: 252.0820. Found: 252.0835.

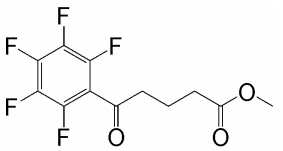

5-oxo-5-pentafluorophenyl-pentanoic acid methyl ester (3.6j):

A flame dried 3-necked flask equiped with: stirring egg, condensor, N_2-inlet, thermometer and dropping funnel, was charged with glutaric anhydride (5.63 g, 49.3 mmol, 2 eq.). The glutaric anhydride was dissolved in dry THF and brought to -35 ^{0}C with a cryostat apparatus, and ethanol as the cooling liquid. Then pentafluorobenzene magnesium bromide (50 ml, 0.5M in ether, 25 mmol) was dropped to the solution resulting in a brown reaction mixture which was allowed to warm up to RT and was stirred overnight. The reaction mixture was poured onto saturated aqueous NH_4Cl (40 ml). The layers were separated and the aqueous layer was extracted with Et_2O (1 x 150 ml). A thick gel formed and no separation was obtained (maybe NH_4Cl wasn't acidic enough?). The organic layer was dried over Na_2SO_4 and concentrated *in vacuo* yielding a brown oil. The thus obtained crude acid was esterified without further purification. The crude acid was dissolved in MeOH (200 ml) and a drop of foming hydrochloric acid (37%) was added. This mixture was stirred at RT for 4 days. The resulting mixture was concentrated *in vacuo* and the obtained brown oil was redissolved in Et_2O (100 ml). The ethereal solution was washed with 1 M NaOH (3 x 50 ml), dried over Na_2SO_4 and concentrated *in vacuo* yielding a brown oil. Purification by Kugelrohr destillation (140 – 190 ^{0}C, 15 mTorr) yielded a colorless oil (1.29 g, 4.35 mmol, 17,4 %). IR (neat) = ν (cm^{-1}): 2956 (w), 1740 (s), 1650 (m), 1522 (m), 1497 (s), 1439 (w), 1404 (w), 1382 (w), 1314 (m), 1201 (w), 1140 (m), 983 (m), 860 (w). ^{1}H-NMR ($CDCl_3$, 300 MHz); δ (ppm): 3.67 (s, 3H), 2.96 (t, *J* = 6.7 Hz, 2H), 2.42 (t, *J* = 7.3 Hz, 2H), 2.05 (q, *J* = 7.3 Hz, 2H). ^{13}C-NMR ($CDCl_3$, 50 MHz); δ (ppm): 173.2, 51.7, 43.9, 32.6, 18.6. ^{19}F-NMR ($CDCl_3$, 200 MHz); δ (ppm): -142.18 (dd, *J* = 6.9 Hz, *J* = 18.0 Hz, 2F), -150.31 – -150.53 (m, 1H), -160.75 – -161.05 (m, 2H).

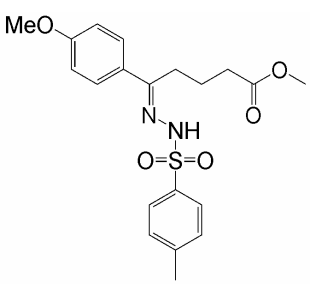

4-(methoxy-benzoyl)–methylbutyrate–*p*–tosylhydrazone (3.7a):

5-(4-Methoxy-phenyl)-5-oxo-pentanoic acid methyl ester (**3.6a**) (5.9 g, 25 mmol) and p-tosylhydrazide (5.6 g, 30 mmol) were solved in methanol (50 ml). The mixture was refluxed for 4 h. A yellow powder crystallized. This powder was then recrystallized from methanol obtaining pale-yellow crystals (7.8 g, 19.3 mmol, 77%) which were dried at 50 ^{0}C *in vacuo*. ^{1}H NMR ($CDCl_3$, 300 MHz): δ (ppm): 9.07 (s, 1H), 7.91 (d, *J* = 8.4 Hz, 2H), 7.61 (d, *J* = 8.8 Hz, 2H), 7.30 (d, *J* = 8.1 Hz, 2H), 6.85 (d, *J* = 8.8 Hz, 2H), 3.81 (s, 3H), 3.78 (s, 3H), 2.61 (t, *J* = 8.1 Hz, 2H), 2.40 (s, 3H), 2.32 (t, *J* = 6.6 Hz, 2H), 1.67 (m, 2H). ^{13}C NMR ($CDCl_3$, 75 MHz): δ (ppm): 174.6, 160.6, 153.6, 143.6, 135.8, 129.3, 128.6, 127.8, 127.5, 113.6, 55.2, 52.2, 32.0, 25.6, 21.4, 20.9.

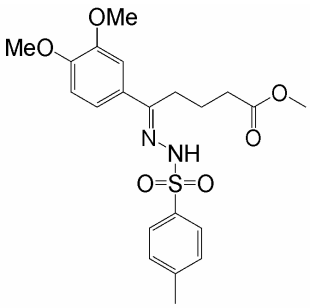

3,4-(Dimethoxy-benzoyl)–methylbutyrate–*p*–tosylhydrazone (3.7b):

5-(3,4-Dimethoxy-phenyl)-5-oxo-pentanoic acid methyl ester (**3.6b**) (1.6 g, 6.0 mmol) and p-tosylhydrazide (7.2 mmol) were dissolved in methanol (5 m). The mixture was refluxed for 5 h. After slightly cooling a white precipitate formed. Mixture was left at RT overnight. The precipitated material was filtered through a glass filter and washed with cold methanol (2 x 2 ml). The resulting white solid was dried at 40 ^{0}C *in vacuo*. A two component mixture was obtained. The solid material was therefore recrystallized from boiling ethanol (200 ml). A precipitate was formed. The mixture was cooled to RT and then put in fridge at –18 ^{0}C overnight. A white solid was collected wich was dried at 40 ^{0}C *in vacuo*. The obtained solid was recrystallized from methanol (40 ml) obtaining a white solid which was dried at 40 ^{0}C *in vacuo* (1.6 g, 3.68 mmol, 61 %). ^{1}H NMR ($CDCl_3$, 300 MHz): δ (ppm): 9.02 (s, 1H), 7.91 (d, *J* = 8.5 Hz, 2H) 7.30 (m, 3H), 7.09 (dd, *J* = 8.4 Hz, *J* = 2.2 Hz, 1H), 6.79 (d, *J* = 8.4 Hz), 3.90 (s, 3H), 3.88 (s, 3H), 3.80 (s, 3H), 2.60 (t, *J* = 7.7 Hz, 2H), 2.40 (s, 3H), 2.33 (t, *J* = 6.2 Hz, 2H), 1.67 (m, 2H). ^{13}C NMR ($CDCl_3$, 75 MHz): δ (ppm): 174.4, 153.7, 150.3, 148.7, 143.6, 135.7, 129.3, 129.2, 128.8, 127.8, 119.1, 110.1, 108.7, 55.7, 55.5, 52.0, 32.0, 25.5, 21.4, 20.9. HRMS: calcd for $C_{21}H_{26}N_2O_6S$: 434.15112. Found: 434.15329.

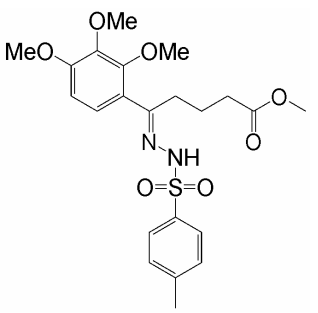

2,3,4-(Trimethoxy-benzoyl)–methylbutyrate-*p*-tosylhydrazone (3.7c):

5-(2,3,4-Trimethoxy-phenyl)-5-oxo-pentanoic acid methyl ester (**3.6c**) (2.6 g, 8.78 mmol) and p-tosylhydrazide (1.9 g, 10.2 mmol) were dissolved in toluene (40 ml). The resulting mixture was refluxed using a Dean-Stark setup. The first 20 ml. of the liquid which distilled over was removed. After 4 h. the mixture was allowed to cool to RT and was evaporated to dryness. The slightly yellow solid material that was obtained was recrystallized from methanol with stirring. A fine white precipitate was obtained while the solution was stirred in an ice-bath for 1 h. The solid was collected by filtration through a glass filter. The obtained solid was washed with cold methanol and dried at 50 ^{0}C *in vacuo*. From the mother liquor a second fraction was obtained after storing at –18 ^{0}C. (combined yield: 2.91 g, 6.27 mmol, 71 %). ^{1}H NMR ($CDCl_3$, 300 MHz): δ (ppm): 7.81 (d, *J* = 8.1 Hz, 2H), 7.6 (s, 1H), 7.31 (d, *J* = 8.1 Hz, 2H), 6.69 (d, *J* = 8.4 Hz, 1H), 6.61 (d, *J* = 8.4 Hz, 1H), 3.86 (s, 3H), 3.85 (s, 3H), 3.63 (s, 3H),

3.53 (s, 3H), 2.48 (t, *J* = 7.3 Hz, 2H), 2.42 (s, 3H), 2.19 (t, *J* = 7.3 Hz, 2H), 1.74 (m, 2H). ^{13}C NMR ($CDCl_3$, 75 MHz): δ (ppm): 173.5, 155.0, 154.7, 149.8, 143.7, 142.3, 135.3, 129.3, 127.8, 122.3, 119.0, 108.2, 97.8, 61.2, 60.9, 56.0, 51.4, 37.0, 32.8, 21.5, 21.2. HRMS: calcd for $C_{22}H_{28}N_2O_7S$: 464.16168. Found: 464.16031.

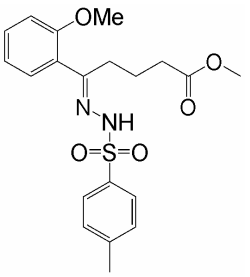

2-methoxy-benzoyl-methylbutyrate-*p*-tosylhydrazone (3.7d):

4-(2-methoxy-benzoyl)-butyric acid methyl ester (**3.6d**) (1.61 g, 6.82 mmol) was dissolved in methanol (25 ml). $TsNHNH_2$ (1.52 g, 8.16 mmol) was added at once and the mixture was brought to reflux for 12 h. The mixture was put in freezer for 48 h and crystallization was observed. The crystals were filtered by suction and dried in air. White crystals remained (1.69 g, 4.2 mmol, 61.3%). The filtrate was put in the freezer. A second fraction was obtained (0.38 g, 0.9 mmol, 13.8%). Combined yield: 2.17 g, 5.12mmol, 75.1%. IR (KBr) = ν (cm^{-1}): 3177 (s), 2948 (s), 2830 (m), 1723 (s), 1598 (m), 1493 (m), 1336 (m), 1026 (m), 758 (m), 593 (m), 555 (m). ^{1}H NMR ($CDCl_3$, 300 MHz); δ (ppm): 7.80 (d, *J* = 8.1 Hz, 2H), 7.28–7.42 (m, 4H), 6.99 (t, *J* = 8.1 Hz, 1H), 6.92 (d, *J* = 8.8 Hz, 2H), 3.62 (s, 6H), 2.49 (t, *J* = 7.3 Hz, 2H), 2.45 (s, 3H), 2.18 (t, *J* = 7.3 Hz, 2H), 1.73 (q, *J* = 7.3 Hz, 2H). ^{13}C NMR ($CDCl_3$, 75 MHz): δ (ppm): 117.4, 173.6, 155.0, 154.9, 143.7, 135.5, 131.2, 129.3, 128.0, 127.8, 121.5, 121.5, 111.4, 55.3, 51.3, 36.9, 32.7, 21.5, 20.9. HRMS: Calcd for $C_{20}H_{24}N_2O_5S$: 404.1406. Found: 404.1411. Melting point: 86.5 – 87.5 (^{0}C). Elemental Analysis: Calcd for $C_{20}H_{24}N_2O_5S$: C: 59.39%, H: 5.98%, N: 6.93%, S: 7.93%. Found: C: 59.23%, H: 6.00%, N: 6.90%, S: 7.88%.

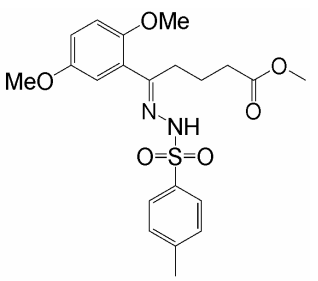

***Cis*-2,5-(dimethoxy-benzoyl)–methylbutyrate-*p*-tosylhydrazone (3.7e):**

5-(2,5-dimethoxy-phenyl)-5-oxo-pentanoic acid methyl ester (**3.6e**) (3.02 g, 11.35 mmol) was dissolved in methanol (25 ml). p-Tosylhydrazide (2.57 g, 13.8 mmol) was added at once. The remaining yellow solution was heated to reflux for 12 h. The mixture was concentrated to ~10 ml and cooled to 0 ^{0}C resulting in crystallization. The obtained crystals were filtered by suction and a white powder remained (0.78 g, 1.73 mmol) with a cis:trans ratio of 1:13.5 (by ^{1}H NMR). The filtrate was left in the freezer overnight and filtered by suction. A white powder remained (2.76 g, 6.13 mmol) with a cis:trans ratio of 9.7:1. Combined yield 3.54 g (7.85 mmol), 69.2%. The cis product (2.76 g, 6.13 mmol) was recrystallized from a mixture of ethylether (50 ml) and t-butylmethyl-ether (3 ml). The obtained crystals were filtered by suction and dried *in vacuo* at 50 ^{0}C. White crystals were obtained (1.78 g, 3.95 mmol, 34.8%). IR (KBr) = ν (cm^{-1}): 3239 (s), 2973 (s), 2841 (m),

1728 (s), 1597 (w), 1501 (m), 1343 (m), 1172 (s), 1041 (s), 748 (m), 571 (m). ^{1}H NMR ($CDCl_3$, 300 MHz): δ (ppm): 7.82 (d, *J* = 8.4 Hz, 2H), 7.44 (s, 1H), 7.33 (d, *J* = 8.1 Hz, 2H), 6.92 (dd, *J* = 9.2 Hz, *J* = 2.9 Hz, 1H), 6.85 (d, *J* = 9.2 Hz, 1H), 6.48 (d, *J* = 2.6 Hz, 1H), 3.75 (s, 3H), 3.64 (s, 3H), 3.58 (s, 3H), 2.49 (t, *J* = 7.1 Hz, 2H), 2.45 (s, 3H), 2.18 (t, *J* = 7.5 Hz, 2H), 1.73 (m, 2H). ^{13}C NMR ($CDCl_3$, 75 MHz): δ (ppm): 173.6, 154.6, 154.1, 148.9, 143.7, 135.5, 129.3, 127.8, 122.2, 115.9, 113.5, 112.7, 97.9, 55.8, 55.7, 51.4, 36.9, 32.7, 21.5, 21.0. HRMS: Calcd for $C_{22}H_{30}N_2O_6S$: 434.1511. Found: 434.1514. Melting point: 77.0 – 79.0 (^{0}C). Element Analysis: Calcd for $C_{22}H_{30}N_2O_6S$: C: 58.65%, H: 6.71%, N: 6.22%, S: 7.12%. Found: C: 58.36%, H: 6.44%, N: 6.33%, S: 6.93%.

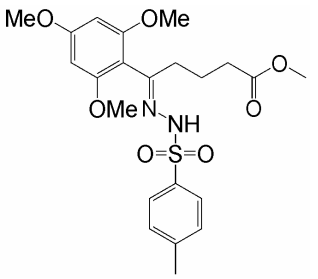

2,4,6-(Trimethoxy-benzoyl)–methylbutyrate–*p*–tosylhydrazone (3.7f):

5-(2,4,6-trimethoxyphenyl)-5-oxo-pentanoic acid methyl ester (**3.6f**) (4.45 g, 15 mmol) was dissolved in methanol (25 ml) and p-tosylhydrazide (3.36 g, 18 mmol, 1.2 eq.) was added at once. The resulting mixture was refluxed for 12 h. After cooling to RT no crystallization took place. Mixture was concentrated *in vacuo*. During concentration crystallization started. Mixture was left in the fridge (4 ^{0}C) overnight. The obtained crystals were filtered off yielding a white microcrystalline powder which was washed with cold methanol (2 x 2 ml). The obtained powder was dried in air. A second batch was obtained from the motherliquor. Combined yield: 5.81 g (12.5 mmol, 83 %). ^{1}H NMR ($CDCl_3$, 300 MHz): δ (ppm): 7.80 (d, *J* = 8.4 Hz, 2H), 7.32 (d, *J* = 8.4 Hz, 2H), 7.26 (s, 1H), 6.08 (s, 2H), 3.80 (s, 3H), 3.62 (s, 3H), 3.56 (s, 6H), 2.42 (m, 5H), 2.12 (t, *J* = 7.2 Hz, 2H), 1.66 (m, 2H).

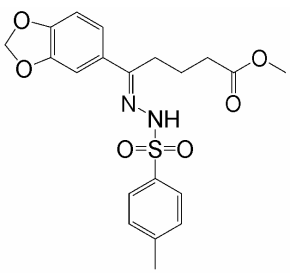

3,4-(methylenedioxy)benzoyl–methylbutyrate–*p*–tosylhydrazone (3.7g):

A 25 ml round bottom flask was placed under nitrogen and charged with crude 5-(3,4-(methylenedioxy)phenyl)-5-oxo-pentanoic acid methyl ester (**3.6g**) (0.52 g, 2.08 mmol), p-tosylhydrazide (0.465 g, 2.49 mmol, 1.2 eq.) and methanol (6 ml). The resulting yellow mixture was brought to reflux and allowed to react for 4 h. The reaction mixture was then cooled to RT and an off-white solid crystallized. The crystals were filtered of by suction. ^{1}H NMR analysis showed that this product was 1,2-(methylenedioxy)benzene. The filtrate was put in the freezer overnight and more crystallization was observed. White crystals were obtained. Yield: 130 mg (0.31 mmol, 15%).

^{1}H NMR ($CDCl_3$, 200 MHz); δ (ppm): 9.08 (s, 1H), 7.91 (d, *J* = 8.3 Hz, 2 H), 7.33 – 7.24 (m, 3H), 7.08 (dd, *J* = 8.3 Hz, 1.9 Hz, 1H), 6.75 (d, *J* = 8.3 Hz, 1H), 5.98 (s, 2H), 3.80 (s, 3H), 2.58 (m, 2H), 2.41 (s, 3H), 2.33 (m, 2H), 1.63 (m, 2H). ^{13}C NMR (DMSO-d6, 75MHz); δ (ppm): 173.1, 154.8, 148.4, 147.6, 143.4, 136.2, 130.5, 129.6, 127.5, 120.7, 108.0, 105.8, 101.4, 51.4, 32.7, 25.9, 21.2, 21.1.

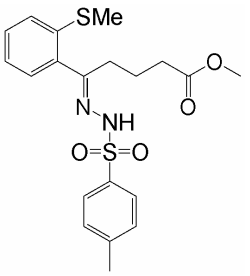

2-(methylthio)–benzoyl–methylbutyrate–*p*–tosylhydrazone (3.7h):

Compound **3.6h** (2.50 g, 9.91 mmol) and toluene-4-sulfonohydrazide (2.32 g, 12.4 mmol) were dissolved in dry methanol (30 ml.) brought to reflux and stirred overnight. The reaction was followed by TLC using chloroform as the eluens. Subsequently, the mixture was cooled down slowly and placed in the refrigerator over the weekend resulting in crystallization. A white powder was obtained which was washed with cold methanol and dried *in vacuo* at 50 ^{o}C. Yield: 2.73 g (6.49 mmol, 65.5 %); MP = 85 ºC; IR: (KBr): ν (cm^{-1}): 3257 (s), 3065 (m), 2983 (m), 2934 (m), 2891 (m), 1735 (s), 1595 (m), 1433 (m), 1378 (m), 1333 (m), 1164 (s), 1074 (w), 997 (w), 752 (m); ^{1}H NMR: ($CDCl_3$, 200 MHz): δ (ppm): 9.05 (s, 1H), 7.85(d, *J* = 8.05 Hz, 2H), 7.52(d, *J* = 8.42 Hz, 2H), 7.24(d, *J* = 8.06 Hz, 2H), 7.13(d, *J* = 8.42 Hz, 2H), 3.74 (s, 3H), 2.54(t, *J* = 7.68 Hz, 2H), 2.43 (s, 3H), 2.35 (s, 3H), 2.67 (t, *J* = 6.23 Hz, 2H), 1.61 (m, 2H); ^{13}C NMR: ($CDCl_3$, 50 MHz): δ (ppm): 173.7, 155.8, 143.9, 135.8, 135.4, 131.8, 130.3, 129.3, 128.1, 127.3, 126.2, 125.9, 51.4, 36.5, 33.1, 21.6, 20.8, 15.3. HRMS: Calcd for $C_{20}H_{24}O_4S_2N_2$: 420.1177. Found: 420.1198.

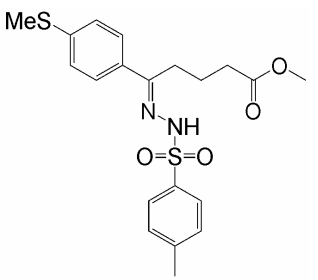

4-(methylthio)–benzoyl–methylbutyrate–*p*–tosylhydrazone (3.7i):

4.00 g. (15.9 mmol) of **3.6i,** toluene-4-sulfonohydrazide (3.74 g, 20.0mmol) and dry methanol (30 ml.) were mixed and refluxed for 4 hours. Subsequently, the mixture was cooled down and placed in the refrigerator over the weekend resulting in white crystals. The powder was washed with cold methanol and dried *in vacuo* at 50 ^{0}C. Yield: 5.50 g (13.1 mmol) 82.3%. MP = 135ºC; IR (KBr); ν (cm^{-1}): 3234 (s), 2947 (m), 1738 (s), 1595 (m), 1480 (m), 1390 (m), 1168 (s), 1060 (m), 815 (m); ^{1}H NMR: ($CDCl_3$, 300 MHz): δ (ppm): 9.05 (s, 1H), 7.85 (d, *J* = 8.05 Hz, 2H), 7.52 (d, *J* = 8.42 Hz, 2H), 7.24 (d, *J* = 8.06 Hz, 2H), 7.13 (d, *J* = 8.42 Hz, 2H), 3.74 (s, 3H), 2.54 (t, *J* = 7.68 Hz, 2H), 2.43 (s, 3H), 2.35 (s, 3H), 2.67 (t, *J* = 6.23 Hz, 2H), 1.61 (m, 2H); ^{13}C-NMR. ($CDCl_3$, 50 MHz): δ (ppm): 174.7, 153.1, 143.7, 140.6, 136.0, 132.7, 129.4, 127.9, 126.5 125.8, 52.4, 32.0, 25.6, 21.6, 20.9, 15.3. HRMS: Calcd for $C_{20}H_{24}O_4S_2N_2$: 420.1177. Found: 420.1195.

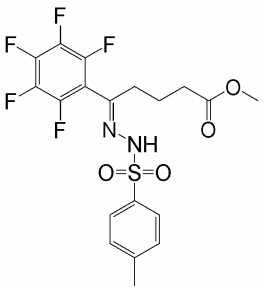

Pentafluorobenzoyl-methylbutyrate-*p*-tosylhydrazone (3.7j):

A 25 ml roundflask, equiped with stirring egg, condensor and N_2-inlet was charged with pentafluorophenyl-5-oxo-pentanoic acid methyl ester (**3.6j**) (1.0 g, 3.38 mmol), p-tosylhydrazide (755 mg, 4.05 mmol, 1.2 eq.) and methanol (15 ml). The resulting mixture was refluxed for 17 h. Then cooled to RT, no crystals were observed and the mixture was put in the fridge. After no crystallization was observed the mixture was concentrated to ¼ volume and crystallization commenced after 3 h in the fridge. Two fractions of white crystals were obtained. Total yield: 680 mg (1.46 mmol, 43,3 %). IR (KBr) = ν (cm^{-1}): 3077 (s), 1700 (s), 1655 (m), 1596 (m), 1500 (s), 1351 (s), 1288 (m), 1253 (m), 1171 (s), 1084 (s), 984 (s), 926 (m), 881 (m), 848 (m), 817 (m), 668 (m), 549 (s). ^{1}H-NMR ($CDCl_3$, 200 MHz); δ (ppm): 9.83 (s, 1H), 7.84 (d, *J* = 8.3 Hz, 2H), 7.31 (d, *J* = 8.1 Hz, 2H), 3.79 (s, 3H), 2.51 (t, *J* = 7.3 Hz, 2H), 2.47 (s, 3H), 2.26 (t, *J* = 6.4 Hz, 2H), 1.66 (m, 2H). ^{13}C-NMR ($CDCl_3$, 50 MHz); δ (ppm): 173.4, 142.6, 134.2, 128.0, 126.3, 51.1, 30.1, 28.1, 20.1, 18.1. ^{19}F-NMR ($CDCl_3$, 200 MHz); δ (ppm): -142.43 (dd, *J* = 6.7 Hz, *J* = 16.0 Hz, 2H*),* -153.81 *(t, J* = 21.4 Hz, 1F), -162.32 (dt, *J* = 6.7 Hz, *J* = 21.4 Hz, 2H). HRMS: Calcd. for $C_{19}H_{17}O_4N_2SF_5$: 464.0828. Found: 464.0829.

General method for a diazomethane addition to C_{60}: A mixture of methoxy-substituted benzoyl-methylbutyrate-p-tosylhydrazone (449 mg, 1.11 mmol), sodium methoxide (60 mg, 1.07 mmol) and dry pyridine (15 ml) was placed under nitrogen and stirred at RT for 30 min. To the mixture a solution of C_{60} (735 mg, 1.02 mmol) in 1,2-dichlorobenzene (75 ml) was added. The mixture was deoxygenated using ultrasound and three vacuum/N_2 purge cycles. Irradiation was started using a 150 W Na-lamp, no cooling was applied. The mixture was stirred and allowed to reach thermal equilibrium (T~86 ^{0}C). The reaction was allowed to continue for 12 h during which the color turned from purple to brown. The obtained mixture was concentrated *in vacuo* to 25 ml. A silica gel column was prepared (2.5x 20 cm) with 1,2-dichlorobenzene. The mixture was admitted and eluted with 1,2-dichlorobenzene. The fraction containing mono-adduct was collected and concentrated *in vacuo*, redissolved in a minimal amount of 1,2-dichlorobenzene and transferred to a centrifugal tube (100 ml). The product was precipitated with MeOH, centrifuged and decanted. The remaining pellet was washed twice with methanol. The obtained pellet was dried under vacuo at 40 ^{0}C for 24 h.

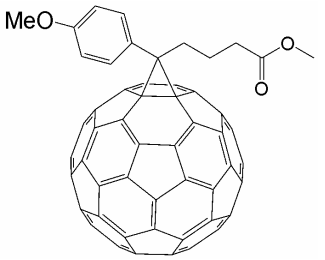

4-methoxy-[6,6]-PCBM (3.8a):

IR (KBr) = ν (cm^{-1}): 2946 (m), 2828 (m), 2323 (w), 1731 (s), 1610 (m), 1512 (s), 1456 (m), 1431 (s). 1302 (w), 1247 (s), 1174 (s), 1109 (m), 1032 (m), 832 (m), 744 (w), 525 (s), 428 (m). UV-vis (toluene); λ_{max} (nm): 330, 433, 498, 697. ^{1}H NMR (CS_2/D_2O, 500 MHz); δ (ppm): 7.89 (d, *J* = 8.4 Hz, 2H), 7.13 (d, *J* = 8.4 Hz, 2H), 4.02 (s, 3H), 3.75 (s, 3H), 2.99 (br.t, *J* = 8.1 Hz, 2H), 2.59 (t, *J* = 7.3 Hz, 2H), 2.27 (m, 2H). ^{13}C NMR (CS_2/D_2O); δ (ppm): 171.2, 159.2, 148.5, 147.6, 145.6, 145.0, 145.0, 144.9, 144.6, 144.5, 144.3, 143.9, 143.6, 142.9, 142.9, 142.8, 142.8, 142.1, 142.0, 141.9, 140.8, 140.6, 137.9, 137.6, 132.9, 128.0, 113.8, 79.9, 54.8, 51.2, 50.9, 33.6, 33.5, 22.5. Elemental Analysis: Calcd for $C_{73}H_{16}O_3$: C: 92.78%, H: 1.71%. Found: C: 92.94%, H: 1.65%.

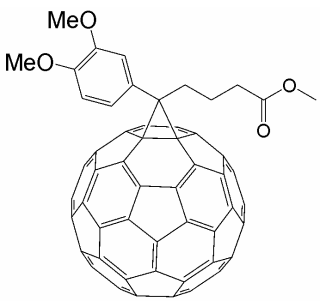

3,4-dimethoxy-[6,6]-PCBM (3.8b):

IR (KBr) = ν (cm^{-1}): 2946 (s), 2832 (m), 2326 (w), 1737 (s), 1589 (m), 1516 (s), 1462 (s), 1430 (s), 1251 (s), 1187 (s), 1140 (s), 1028 (s), 853 (w), 742 (m), 526 (s). UV (cyclohexane): λ_{max} (nm): 215, 262, 333. VIS (toluene): λ_{max} (nm): 433, 493, 698. ^{1}H NMR (CS_2/D_2O, 500 MHz); δ (ppm): (dd, *J* = 8.2, 2.2 Hz, 1H), 7.43 (d, *J* = 2.2 Hz, 1H), 7.06 (d, *J* = 8.2 Hz, 1H), 4.02 (s, 6H), 3.75 (s, 3H), 3.00 (m, 2H), 2.60 (t, *J* = 2.60 Hz, 2H), 2.27 (m, 2H). ^{13}C NMR (CS_2/D_2O, 125 MHz): δ (ppm): 171.3, 149.4, 149.2, 148.5, 147.6, 145.6, 145.0, 144.98, 144.95, 144.9, 144.8, 144.6, 144.4, 144.3, 143.9, 143.6, 142.9, 142.84, 142.82, 142.75, 142.74, 142.0, 141.94, 137.91, 137.7, 128.4, 125.0, 115.6, 111.3, 78.0, 55.8, 55.4, 53.6, 51.0, 33.7, 33.5, 22.7. Elemental Analysis: Calcd for $C_{74}H_{18}O_4$: C: 91.54%, H: 1.87%. Found: C: 91.35%, H: 1.93%.

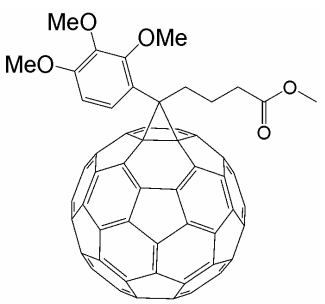

2,3,4-trimethoxy-[6,6]-PCBM (3.8c):

IR (KBr) = ν (cm^{-1}): 2939 (s), 1738 (s), 1599 (w), 1494 (m), 1463 (m), 1412 (m), 1303 (w), 1235 (w), 1103 (m), 1017 (m), 526 (s). VIS (toluene): λ_{max} (nm): 434, 497, 698. ^{1}H NMR ($CDCl_3$, 500 MHz); δ (ppm): 6.75 (d, *J* = 8.6 Hz), 4.31 (s, 3H), 4.07 (s, 3H), 4.02 (s, 3H), 3.75 (s, 3H), 3.03 (m, 1H), 2.89 (m, 1H), 2.58 (m, 2H), 2.20 (m, 2H). ^{13}C NMR (CS_2/D_2O, 125 MHz): δ (ppm): 171.4, 154.2, 152.4, 149.5, 149.4, 148.1, 145.9, 145.8, 145.3, 145.0, 144.93, 144.89, 144.85, 144.62, 144.60, 144.54, 144.51, 144.4, 144.3, 144.2,

143.9, 143.7, 143.6, 143.5, 142.9, 142.84, 142.81, 142.76, 142.71, 142.1, 142.0, 140.9, 140.8, 140.7, 140.4, 138.0, 137.9, 137.7, 136.3, 128.1, 120.3, 105.5, 81.2, 78.1, 61.3, 60.1, 55.5, 50.9, 48.3, 33.6, 31.8, 22.8. Elemental Analysis: Calcd for $C_{75}H_{20}O_5$: C: 89.99%, H: 2.01%. Found: C: 89.93%, H: 2.14%.

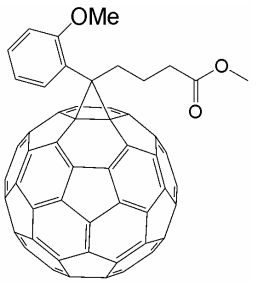

2-methoxy-[6,6]-PCBM (3.8d):

IR (KBr) = ν (cm^{-1}): 2945 (m), 2328 (w), 1739 (s), 1599 (w), 1492 (m), 1430 (s), 1246 (s), 1186 (m), 1159 (m), 1026 (m), 758 (m), 574 (w), 527 (s). UV-vis (chloroform); λ_{max} (nm): 260 (ε = 127410), 328 ($\varepsilon = 38648$), 432 ($\varepsilon = 2626$), 495 ($\varepsilon = 1498$), 697 (ε = 261). ^{1}H NMR (CS_2/D_2O, 500 MHz); δ (ppm): 7.89 (dd, *J* = 7.6 Hz, *J* = 1.6 Hz, 1H), 7.60 (dt, *J* = 8.2 Hz, *J* = 1.6 Hz, 1H), 7.25 (m, 2H), 4.19 (s, 3H), 3.76 (s, 3H), 3.06–2.97 (m, 2H), 2.61 (t, *J* = 7.6 Hz, 2H), 2.29–2.24 (m, 2H). ^{13}C NMR (CS_2, 125 MHz): δ (ppm): 171.6, 158.1, 150.0, 149.4, 148.3, 148.1, 146.3, 146.2, 145.5, 145.3, 145.1, 144.9, 144.8, 144.7, 144.6, 144.5, 144.2, 144.0, 143.98, 143.94, 143.90, 143.8, 143.12, 143.06, 143.0, 142.42, 142.38, 142.31, 142.26, 142.21, 142.15, 141.2, 141.1, 141.0, 140.7, 138.3, 138.2, 138.0, 136.3, 134.3, 130.0, 124.0, 120.7, 111.7, 81.0, 78.1, 55.6, 51.1, 47.9, 33.9, 31.6, 30.4, 23.1. Melting Point: > 300 ^{0}C. Elemental Analysis: Calcd for $C_{73}H_{16}O_3$: C: 93.18%, H: 1.71%. Found: C: 92.78%, H: 1.63%.

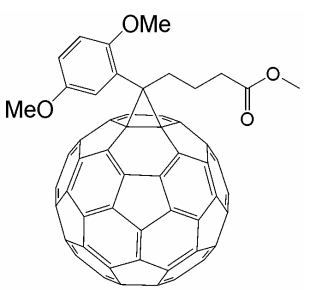

2,5-dimethoxy-[6,6]-PCBM (3.8e):

IR (KBr) =ν (cm^{-1}): 2945 (m), 2328 (w), 1737 (s), 1613 (w), 1498 (s), 1463 (m), 1427 (s), 1218 (s), 1186 (m), 1047 (m), 1025 (m), 808 (m), 735 (w), 573 (w), 526 (s). UV-vis (chloroform); λ_{max} (nm): 260 (ε = 132106), 328 ($\varepsilon = 41385$), 433 ($\varepsilon = 2795$), 495 ($\varepsilon = 1611$), 697 ($\varepsilon = 262$). ^{1}H NMR (CS_2/D_2O, 500 MHz): δ (ppm): 7.38 (br. s, 1H), 7.11 (d, *J* = 8.8 Hz, 1H), 7.04 (br. d, *J* = 8.1 Hz, 1H), 4.09 (s, 3H), 3.95 (s, 3H), 3.74 (s, 3H), 2.98 (m, 2H), 2.59 (t, *J* = 7.3 Hz, 2H), 2.25 (m, 2H). ^{13}C NMR (CS_2, 125 MHz): δ (ppm): 171.4, 152.8, 151.8, 149.8, 149.0, 148.0, 147.8, 146.1, 145.9, 145.2, 145.0, 144.90, 144.87, 144.8, 144.61, 144.55, 144.51, 144.45, 144.4, 144.3, 144.2, 144.0, 143.7, 143.6, 143.5, 142.9, 142.8, 142.8, 142.7, 142.11, 142.05, 142.0, 141.93, 141.86, 140.9, 140.8, 140.7, 140.4, 138.0, 137.9, 137.8, 136.0, 124.6, 120.6, 113.3, 112.0, 80.7, 77.8, 55.6, 55.1, 50.9, 47.7, 33.6, 31.3, 22.7. Melting Point: > 300 ^{0}C. Elemental Analysis: Calcd for $C_{74}H_{18}O_4$: C: 91.54%, H: 1.87%. Found: C: 90.84%, 1.80%.

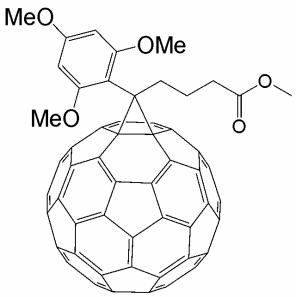

2,4,6-trimethoxy-[6,6]-PCBM (3.8f):

IR (KBr) = ν (cm^{-1}): 2928 (s), 2835 (m), 1729 (s), 1611 (s), 1588 (m), 1457 (s), 1429 (m), 1340 (m), 1276 (w), 1226 (s), 1207 (s), 1159 (s), 1128 (s), 1037 (m), 811 (m), 526 (s). UV-vis (toluene); λ_{max} (nm): 329, 435, 498, 701. ^{1}H NMR (CS_2/D_2O, 300 MHz); δ(ppm): 6.39 (s, 2H), 4.06 (s, 6H), 4.04 (s, 3H), 3.75 (s, 3H), 2.96 (t, *J* = 7.7 Hz, 2H), 2.63 (t, *J* = 7.3 Hz, 2H), 2.27 (m, 2H).). ^{13}C NMR (CS_2, 75 MHz): δ (ppm): 170.0, 159.4, 157.4, 149.3, 146.4, 144.3, 142.82, 142.79, 142.7, 142.6, 142.50, 142.45, 142.3, 142.19, 142.16, 142.0, 141.6, 141.4, 140.64, 140.61, 140.51, 140.48, 140.3, 140.1, 139.8, 139.6, 138.6, 138.3, 135.9, 133.3, 102.9, 89.1, 77.0, 53.3, 52.6, 48.6, 40.3, 31.7, 29.3, 20.5. Elemental Analysis: Calcd for $C_{75}H_{20}O_5$: C: 89.99%, H: 2.01%. Found: C: 89.86%, H: 1.91%.

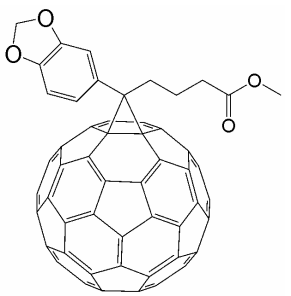

3,4-methylenedioxy-[6,6]-PCBM (3.8g):

IR (KBr) = ν (cm^{-1}): 2942.60 (s), 2772.38 (w), 2328.35 (m), 1738.08 (s), 1607.12 (w), 1501.06 (s), 1487.00 (s), 1346.29 (w), 1240.51 (s), 1187.53 (s), 1039.54 (s), 938.07 (m), 812.02 (m), 742.35 (m), 585.83 (w), 526.25 (s), 441.97 (w). UV-vis (toluene); λ_{max} (nm): 330, 432, 496, 696. ^{1}H NMR (CS_2/D_2O, 300 MHz); δ(ppm): 7.45 – 7.41 (m, 2H), 7.02 (d, *J* = 7.7 Hz, 1H), 6.18 (s, 2H), 3.74 (s, 3H), 2.99 – 2.94 (m, 2H), 2.56 (t, *J* = 7.3 Hz, 2H), 2.29 – 2.24 (m, 2H). ^{13}C NMR (CS_2, 75MHz); δ(ppm): 170.9, 148.0, 147.1, 147.0, 145.3, 144.7, 144.6, 144.5, 144.31, 144.28, 144.0, 143.7, 143.3, 142.6, 142.50, 142.45, 141.7, 141.61, 141.59, 140.5, 140.3, 137.6, 137.3, 129.5, 125.4, 111.7, 107.8, 101.0, 79.4, 51.1, 50.6, 33.4, 33.2, 29.8, 22.2. Melting Point: > 300 ^{0}C. Elemental Analysis: Calcd for: $C_{73}H_{14}O_3$: C: 91.82%, H: 1.48%. Found: C: 92.01%, H: 1.44%.

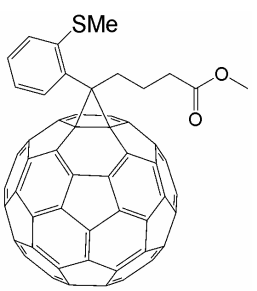

2-thiomethyl-[6,6]-PCBM (3.8h):

IR: (KBr) = ν (cm^{-1}): 2943 (w), 2859 (w), 1733 (s), 1583 (w), 1464 (m), 1431 (m), 1360 (w), 1247 (w), 1187 (m), 1155 (m), 737 (m), 526 (s); UV-VIS (toluene); λ_{max} (nm): 331 (ε = 43793), 435 (ε = 3063), 493 (ε = 1732), 697 (ε = 290); ^{1}H NMR: ($CDCl_3$, 300 MHz): δ (ppm): 7.97 (d, *J* = 7.69 Hz, H), 7.63 (d, *J* = 6.96 Hz, H), 7.46 (d, *J* = 7.69 Hz, H), 3.78 (s, 3H), 3.11 (m, 2H), 2.82 (s, 3H), 2.60 (t, *J* = 7.33 Hz, 2H), 2.22 (m, 2H); ^{13}C NMR: ($CDCl_3$, 50 MHz): δ (ppm): 173.5, 150.2, 150.0, 148.7, 148.6, 147.2, 146.7, 146.0, 145.89, 145.85, 145.82, 145.78, 145.6, 145.4, 145.3, 145.23, 145.20, 144.88, 144.87, 144.7,

144.6, 144.5, 144.4, 143.8, 143.8, 143.7, 143.7, 143.6, 143.0, 142.9, 142.8, 141.9, 141.7, 141.5, 141.3, 141.1, 139.2, 138.80, 138.76, 136.75, 135.0, 125.0, 111.0, 81.9, 78.4, 52.1, 51.4, 34.6, 30.8, 24.0, 16.7. Melting Point: > 295 ºC. Elemental Analysis: Calcd for $C_{73}H_{16}O_2S$: C: 91.6 %, H: 1.69%. Found: C: 91.20 , H: 1.51%

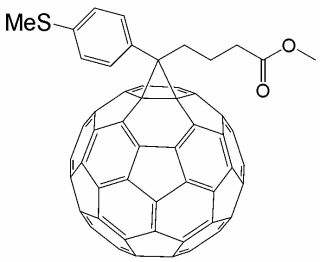

4-thiomethyl-[6,6]-PCBM (3.8i):

IR (KBr) = ν (cm^{-1}): 2947 (m), 2912(m), 1730 (s), 1431 (s), 1187(m), 819(m), 742 (m), 548 (m), 525 (s); UV-VIS (toluene); λ_{max} (nm): 334 (ε = 43538), 433 (ε = 2835), 497 (ε = 1700), 696 (ε = 282); ^{1}H NMR: ($CDCl_3$, 300 MHz): δ (ppm): 7.78 (d, *J* = 8.05 Hz, 2H), 7.34 (d, *J* = 8.42 Hz, 2H), 3.63 (s, 3H), 2.83 (m, 2H), 2.52 (s, 3H), 2.48 (t, *J* = 7.69 Hz, 2H), 2.12 (m, 2H); ^{13}C NMR: ($CDCl_3$, 75 MHz): δ (ppm): 173.5, 148.6, 147.7, 145.82 145.20, 145.15, 145.1, 143.8, 143.04, 143.00, 142.9, 142.20, 142.17, 142.11, 140.99, 138.8, 138.0, 137.7, 133.2, 132.4, 125.9, 51.7, 51.3, 33.9, 33.6, 22.4, 15.4. Melting Point: > 295 ºC. Elemental Analysis: Calcd for $C_{73}H_{16}O_2S$: C: 91.62%, H: 1.69%. Found: C: 91.4%, H: 1.47%.

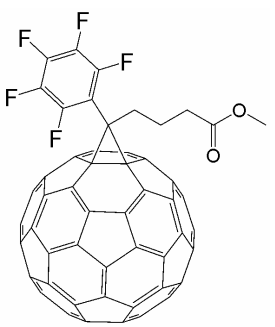

pentafluoro-[6,6]-PCBM (3.8j):

IR (KBr) = ν (cm^{-1}): 2946 (m), 2330 (w), 1738 (s), 1652 (w), 1514 (s), 1495 (s), 1464 (m), 1430 (m), 1350 (w), 1324 (w), 1254 (w), 1187 (m), 1070 (w), 995 (m), 986 (m), 956 (w), 915 (w), 838 (w), 791 (w), 775 (w), 743 (w), 711 (w), 678 (w), 581 (w), 573 (w), 553 (w), 527 (s). ^{1}H NMR (D_2O, 400 MHz); δ (ppm): 3.70 (s, 3H), 2.97 (t, *J* = 8.4 Hz, 2H), 2.59 (t, *J* = 7.0 Hz, 2H), 2.24 (m, 2H). ^{19}F NMR (D_2O, 400 MHz); δ (ppm): –137.54 (dd, *J* = 16.8 Hz, *J* = 6.9 Hz, 2F), –151.79 (t, *J* = 22.1 Hz, 1F), –159.79 (m, 2F). ^{13}C NMR (CS_2, 100 MHz); δ (ppm): 170.8, 147.3, 146.7, 145.7, 144.9, 144.83, 144.80, 144.5, 144.29, 144.27, 144.24, 144.15, 144.04, 143.97, 143.4, 143.3, 142.59, 142.56, 142.54, 142.52, 141.7, 141.64, 141.60, 141.58, 140.7, 140.6, 138.9, 138.1, 136.4, 135.8, 75.0, 50.8, 32.8, 31.4, 21.8.

3.7 References

1. N. Camaioni, G. Ridolfi, G. Casalbore-Miceli, A. Possamai, and M. Maggini, *Adv.Mater.*, 2002, **14**, 1735.

2. D. Chirvase, Z. Chiguvare, M. Knipper, J. Parisi, V. Dyakonov, and J. C. Hummelen, *J.Appl.Phys.*, 2003, **93**, 3376.
3. G. Li, V. Shrotriya, J. Huang, Y. Yao, T. Moriarty, K. Emery, and Y. Yang, *Nat.Mater.*, 2005, **4**, 864.
4. F. Padinger, R. S. Rittberger, and N. S. Sariciftci, *Adv.Funct.Mater.*, 2003, **13**, 85.
5. P. Schillinsky, C. Waldauf, and C. J. Brabec, *Appl.Phys.Lett.,* 2002, **81**, 3885.
6. M. M. Wienk, J. M. Kroon, W. J. H. Verhees, J. Knol, J. C. Hummelen, P. A. van Hal, and R. A. J. Janssen, *Angew.Chem.Int.Ed.*, 2003, **42**, 3371.
7. L. M. Popescu, P. van 't Hof, A. B. Sieval, H. T. Jonkman, and J. C. Hummelen, *Appl.Phys.Lett.*, 2006, **89**, 213507.
8. S. E. Shaheen, C. J. Brabec, N. S. Sariciftci, F. Padinger, T. Fromherz, and J. C. Hummelen, *Appl.Phys.Lett.*, 2001, **78**, 841.
9. A. Gadisa, M. Svensson, M. R. Andersson, and O. Inganäs, *Appl.Phys.Lett.*, 2004, **84**, 1609.
10. K. L. Mutolo, E. I. Mayo, B. P. Rand, S. R. Forrest, and M. E. Thompson, *J.Amer.Chem.Soc.,* 2006, **128**, 8108.
11. C. M. Ramsdale, J. A. Barker, A. C. Arias, J. D. MacKenzie, R. H. Friend, and N. C. Greenham, *J.Appl.Phys.*, 2002, **92**, 4266.
12. M. C. Scharber, D. Mühlbacher, M. Koppe, P. Denk, C. Waldauf, A. J. Heeger, and C. J. Brabec, *Adv.Mater.,* 2006, **18**, 789.
13. H. Antoniadis, B. R. Hsieh, M. A. Abkowitz, M. Stolka, and S. A. Jenekhe, *Abstracts of Papers of the American Chemical Society*, 1993, **206**, 105.
14. J. Liu, Y. Shi, and Y. Yang, *Adv.Funct.Mater.,* 2001, **11**, 420.
15. C. J. Brabec, A. Cravino, D. Meissner, N. S. Sariciftci, T. Fromherz, M. T. Rispens, L. Sanchez, and J. C. Hummelen, *Adv.Funct.Mater.*, 2001, **11**, 374.
16. C. J. Brabec, A. Cravino, D. Meissner, N. S. Sariciftci, M. T. Rispens, L. Sanchez, J. C. Hummelen, and T. Fromherz, *Thin Solid Films*, 2002, **403-404**, 368.
17. V. D. Mihailetchi, P. W. M. Blom, J. C. Hummelen, and M. T. Rispens, *J.Appl.Phys.*, 2003, **94**, 6849.
18. L. J. A. Koster, PhD Thesis, University of Groningen, 2007.
19. L. J. A. Koster, V. D. Mihailetchi, R. Ramaker, and P. W. M. Blom, *Appl.Phys.Lett.*, 2005, **86**, 123509.
20. P. Würfel, *Physics of Solar Cells*, WILEY-VCH Verlag GmbH & Co., Weinheim, 2005, Chapter 3, pp. 37-84.
21. H. Frohne, S. E. Shaheen, C. J. Brabec, D. C. Müller, N. S. Sariciftci, and K. Meerholz, *CHEMPHYSCHEM*, 2007, **3**, 799.
22. J. Cremer, P. Bäuerle, M. M. Wienk, and R. A. J. Janssen, *Chem.Mater.,* 2006, **18**, 5832.
23. C. J. Brabec, N. S. Sariciftci, and J. C. Hummelen, *Adv.Funct.Mater.*, 2001, **11**, 15.
24. V. D. Mihailetchi, L. J. A. Koster, and P. W. M. Blom, *App.Phys.Lett.*, 2004, **85**, 970.

25. L. J. A. Koster, V. D. Mihailetchi, and P. W. M. Blom, *Appl.Phys.Lett.,* 2006, **88**, 093511.
26. R. M. Williams, J. M. Zwier, and J. W. Verhoeven, *J.Amer.Chem.Soc.*, 1995, **117**, 4093.
27. M. Eiermann, R. C. Haddon, B. Knight, Q. C. Li, M. Maggini, N. Martin, T. Ohno, M. Prato, T. Suzuki, and F. Wudl, *Angew.Chem.Int.Ed.*, 1995, **34**, 1591.
28. a) I. Riedel, N. Martín, F. Giacalone, J. L. Segura, D. Chirvase, J. Parisi, and V. Dyakonov, *Thin Solid Films*, 2004, **451-452**, 43. b) I. Riedel, E. von Hauss, J. Parisi, N. Martín, F. Giacalone, V. Dyakonov. *Adv.Funct.Mater.*, 2005, **15**, 1979
29. J. O'Leary and J. D. Wallis, *Chem.Eur.J.*, 2006, **12**, 7724.
30. J. C. Hummelen, B. W. Knight, F. Lepeq, F. Wudl, J. Yao, and C. L. Wilkins, *J.Org.Chem.*, 1995, **60**, 532.
31. D. M. Guldi and M. Prato, *Acc.Chem.Res.*, 2000, **33**, 695.
32. D. M. Guldi and K. D. Asmus, *J.Phys.Chem.A.*, 1997, **101**, 1472.

Chapter 4

Air Stable Organic Field Effect Transistors

In this Chapter two different methods of achieving air-stability for Organic Field Effect Transistors (OFETs) are discussed. First [84]PCBM was used as the organic semiconductor. For the first time air and light-stable ambipolar FETs were fabricated with electron mobilities of 3 x 10^{-3} cm^2/Vs and hole mobilities in the range of 10^{-4} – 10^{-5} cm^2/Vs. Complementary voltage inverters were fabricated to determine the environmental stability. After exposure to light and air for three months the devices still operated with voltage gain as high as 14. Second, a series of fluorinated PCBM analogues was synthesized. The fluorine atoms should act as a barrier for air and water penetration into the semiconductor layer of the FET. The FET devices prepared with these compounds, however, show no air-stability. Nevertheless, quite high electron mobilities approaching 10^{-1} cm^2/Vs were obtained.

*Part of this chapter was published:

Thomas D. Anthopoulos, Floris B. Kooistra, Harry J. Wondergem, David Kronholm, Jan C. Hummelen and Dago M. de Leeuw, *Advanced Materials*, **2006**, 18, 1679–1684.

Paul Wöbkenberg, Donal D. C. Bradley, David F. Kronholm, Floris B. Kooistra, Jan C. Hummelen, Michael Cölle, Dago M. de Leeuw, and Thomas D. Anthopoulos, *submitted for publication.*

4.1 Introduction

Organic Field Effect Transistors (OFETs) have received much attention in recent years and have shown to possess great potential for use in low-end electronic applications.[1-6] Obvious advantages over their silicium based counterparts are flexibility and low processing costs. In order to use organic materials for FET applications one must be able to fabricate large-scale integrated circuits at low cost. One way of achieving this is by use of complementary technology,[4] as is known from silicon microelectronics. However, this is not at all an established process in organic FETs. The fabrication of organic complementary circuits is very challenging and requires the separate deposition of p- and n-channel semiconductors by vacuum sublimation techniques.[4,7] Alternatively, inkjet printing is a potentially low cost method, processing separate p- and n-channel OFET's.[8,9] Applying ambipolar materials would simplify processing even more. It is crucial in this case to use environmentally stable organic semiconductors. Especially n-type materials are scarce and air-stability is even rarer with these type of materials. Among the most promising organic molecules that show n-type mobility are the fullerenes. Electron mobilities in the order of 1 cm^2/Vs have been measured.[10-16] Since fullerenes are usually very insoluble, derivitization is necessary.[17,18] The application of soluble fullerene derivatives has led to good results.[19-22] However FETs fabricated with fullerenes rapidly decay in air.[12,15,19,21]

In the next subparagraphs air stable p- and n-type and ambipolar organic semiconducting materials will be discussed. The general FET principle has been discussed in paragraph 1.3.2.

The research presented in this chapter was a collaboration between our labs and Dr. Thomas Anthopoulos, first at Philips Research labs Eindhoven, and later at Imperial College London.

4.1.1 Air-Stable p-type organic semiconductors

Air stability is not a major concern when using p-type organic semiconductors. A large number of p-type organic semiconducting materials that show environmental stability as well as high mobilities in excess of 0.1 cm^2/Vs have been demonstrated (examples are compounds **4.1** and **4.3,** see figure 4.1).[23-26] One of the most promising p-type materials is polythiophene. Although regioregular poly(3-hexyl)thiophene (P3HT **4.2**) shows high mobilities up to 0.1 cm^2/Vs it is not very stable under ambient conditions, due to its low ionization potential (4.8 eV).[27-29] However, adding some alkyl chains to some thienyl moieties (**4.4**) successfully

increases the ionization potential thus obtaining environmentally stable polythiophenes with high hole mobilities.[30]

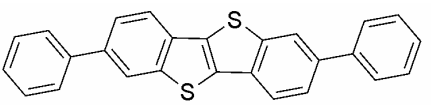

4.1: DPh-BTBT

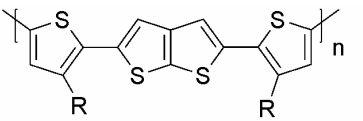

Thiene[2,3-b]thiophenes

4.3a: R = C_8H_{17}
4.3b: R = $C_{10}H_{21}$
4.3c: R = $C_{12}H_{25}$

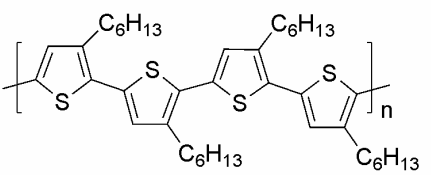

4.2: RR-P3HT

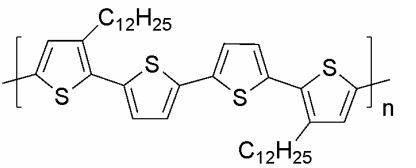

4.4: PQT-12

Fig. 4.1: Thiophene based hole conductors

4.1.2 Air-stable n-type organic semiconductors

The development of complementary organic circuits has been slowed down to some extent by the scarcity of n-type organic semiconductors. Fortunately, the availability of electron conducting organic materials is increasing rapidly in recent years.[31,32] However, there are only few environmentally stable n-type materials known as of now (see figure 4.2).[31,33-35] The main problem is the formation of anions at positive gate voltages. These anions have considerable reducing powers and can reduce oxygen and water molecules that have diffused into the semiconducting layer. One can think of two ways of circumventing this problem. First, protecting the active layer from diffusion of oxygen and water. This might be possible by introducing fluorine atoms which, due to their hydrophobic nature, might prevent the diffusion of water (and oxygen dissolved in water) into the semiconducting layer. A second possibility is tuning the redox properties of the semiconducting material itself in such a way that reactivity with respect to water and oxygen is low.[36,37]

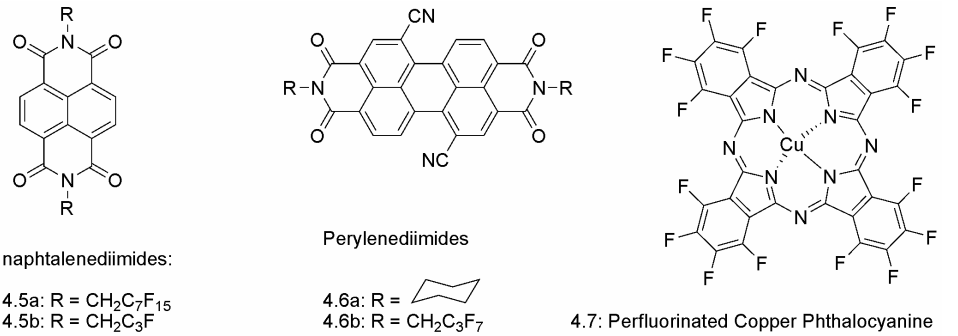

Fig. 4.2: Examples of air-stable n-type semiconductors.

4.1.3 Air-stable ambipolar organic semiconductors

Some materials are able to conduct both holes and electrons and show FET mobility for both charges. These materials are called ambipolar. When a negative gate voltage is applied, holes are conducted. Applying a positive gate voltage, in turn, causes electron conduction. These type of materials have been extensively reviewed by Zuamseil and Sirringhaus.[32] Fig 4.3 gives an overview of organic ambipolar semiconducting materials that have been applied most successsfully.

One of the major drawbacks of using organic materials in complementary circuits is that the deposition of two different organic materials requires advanced patterning techniques, which increases the costs of such circuitry. Using one material that can act as both n- and p-type would greatly simplify circuit fabrication and thus result in a large cost reduction. Ideally the hole and electron mobility would both be high. This, however, is rarely observed. Although PCBM does show high mobilities for both charges[19,20] its air stability is low. The availability of an air-stable ambipolar materials would greatly simplify production. In this chapter the first air-stable ambipolar OFET will be shown.

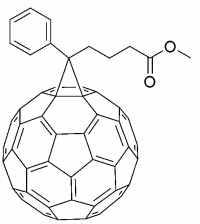

4.9: PCBM

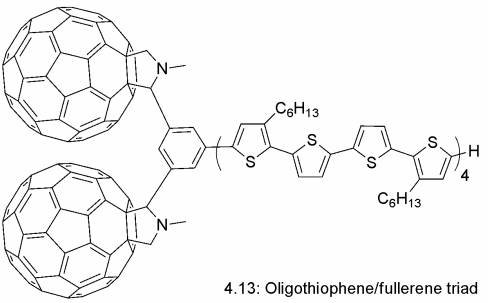

4.13: Oligothiophene/fullerene triad

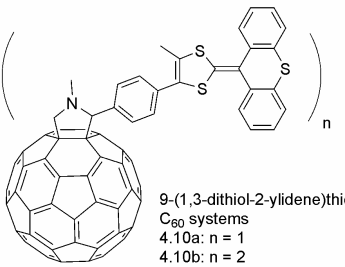

9-(1,3-dithiol-2-ylidene)thioxane-C_{60} systems
4.10a: n = 1
4.10b: n = 2

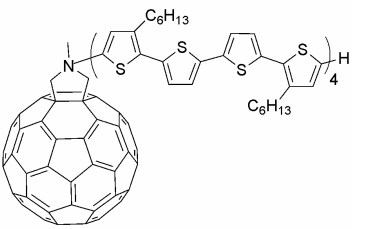

4.14: Oligothiophene/fullerene diad

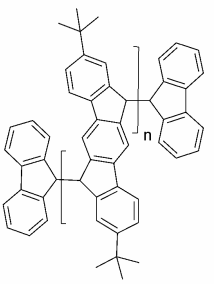

4.11: poly(3,9-di-tert-butylindeno[1,2-*b*]fluorene (PIF)

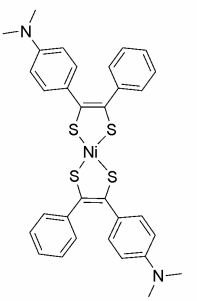

4.15: bis[4-dimethylaminodithiobenzyl]nickel

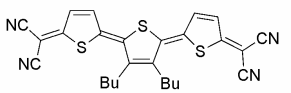

4.12: quinoidal terthiophene (DCMT)

*Fig. 4.3.: Ambipolar organic semiconductors: PCBM (**4.9**)[19]; 9-(1,3-dithiol-2-ylidene)thioxanthene-C_{60} system **4.10**[38]; poly(3,9-di-tert-butylindeno[1,2-b]fluorene) **4.11** (PIF)[39]; quinoidal terthiophene **4.12** (DCMT)[40]; oligothiophene/fullerene triad **4.13** [41]; oligothiophene/fullerene diad **4.14**[41]; bis[4-dimethylaminodithiobenzyl]nickel **4.15**.[42]*

4.1.4 Research Goal

The goal of this investigation was to synthesize new fullerene n-type organic semiconductors which are solution processable under ambient conditions for use in fabrication of complementary circuits. We choose two different paths to achieve this goal. First we used [84]PCBM (see chapter 2) as an n-type organic material since its low lying LUMO level was believed to render it stable to reduction with oxygen and water. Also the photostability of C_{84} was expected to be benificial to device stability.[43] Secondly a series of fluorine containing fullerenes was synthesized to test whether the presence of fluorine atoms in the semiconducting layer would prevent water and oxygen from diffusing into the layer.

4.2 Synthesis

The synthesis and characterization of [84]PCBM has been described in detail in chapter 2. The synthesis of F5-PCBM (**4.21**) has been discussed in chapter 3. In the next paragraphs the synthesis of several new fluorine containing fullerene derivatives will be discussed. The target molecules were choosen to differ both in fluorinated chain length and in position of the fluorine atoms (see figure 4.4).

Characterization of the compounds can be found in the experimental section. All compounds showed clean ^{19}F spectra. H–F coupling was observed in all ^{1}H NMR. C–F coupling was only visible for carbon atoms neighboring carbon centra containing fluorine atoms. Carbon atom resonances in the middle of fluorinated side chains are usually split up too much and are not visible anymore. Further structural proof was obtained from IR spectra, which all show a characteristic fullerene vibration at ~ 526 cm^{-1}. Mass spectra, obtained from the LC-MS used to follow reactions, furthermore confirmed formation of the desired products. The analytical department of this lab does not have the necessary equipment to perform elemental analysis on fluorine containing compounds. Elemental analysis was performed, but could only give accurate analysis for carbon and nitrogen and not for fluorine and hydrogen.

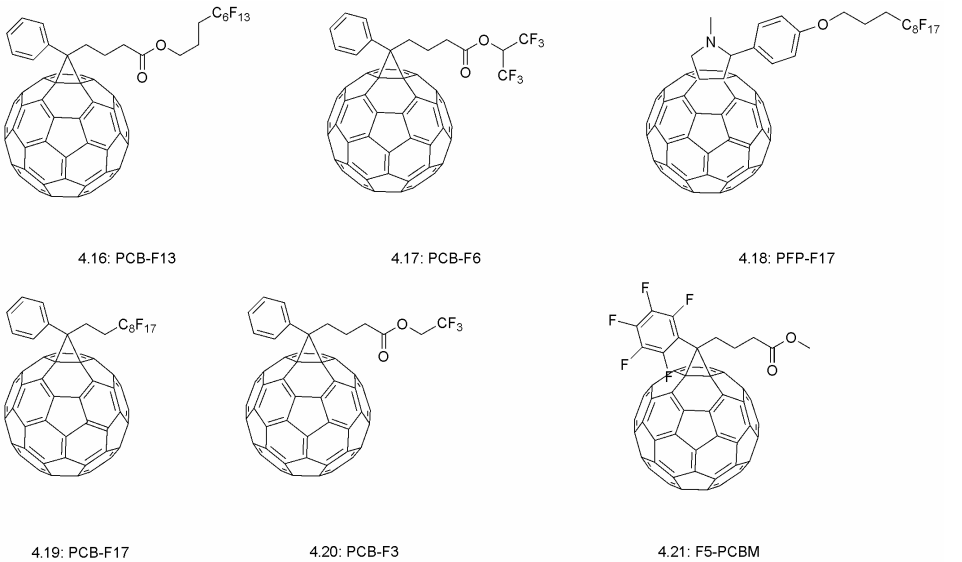

Fig. 4.4: Targeted fluorine containing fullerenes

4.2.1 Synthesis of PCB-F13 (4.16), PCB-F6 (4.17) and PCB-F3 (4.20)

The compounds discussed here are all PCBM analogues and are synthesized in a similar way. Purification and reaction conditions do differ at times and are discussed in the experimental section of this chapter.

As a first step benzoylbutyric acid was esterified with the appropriate alcohols. Nextly, the ketone functionality can easily undergo a condensation reaction with p-tosylhydrazide forming a tosylhydrazone. Subsequently, the tosylhydrazone is transformed *in situ* to the active diazo species which can undergo a 1,3-dipolar addtion reaction with a double bond of C_{60}, thus obtaining the desired fluorine containing fullerene derivatives (see scheme 4.1).

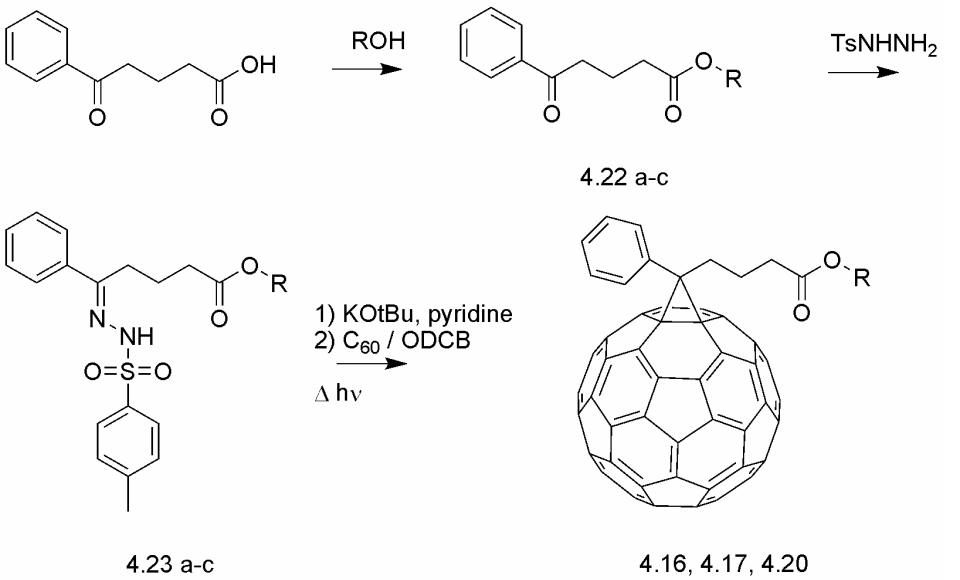

Scheme 4.1.: Synthetic scheme. a) R = $-CH_2CH_2C_6F_{13}$; b) R = $-CH(CF_3)_2$; c) R = $-CH_2CF_3$. ***4.16****) R = $-CH_2CH_2C_6F_{13}$.* ***4.17****) R = $-CH(CF_3)_2$.* ***4.20****) R = $-CH_2CF_3$.*

4.2.2 Synthesis of PFP-F17 (4.18)

A fairly straightforward Prato reaction[44] was used in this synthesis. PFP-F17 (4-(4,4,5,5,6,6,7,7,8,8,9,9,10,10,11,11,11,-heptadecafluoroundecyloxy)phenyl fulleropyrolidine) was obtained by a reaction of C_{60} with sarcosine (**4.25**) and commercially available 4-(4,4,5,5,6,6,7,7,8,8,9,9,10,10,11,11,11-heptadecafluoroundecyloxy)benzaldehyde (**4.26**) in good yield of 32%. (see Scheme 4.1) The sarcosine first forms an iminium ion with the aldehyde. After subsequent loss of CO_2, the resulting ylide can then react with a fullerene C=C bond via a 1,3-dipolar cycloaddition reaction.

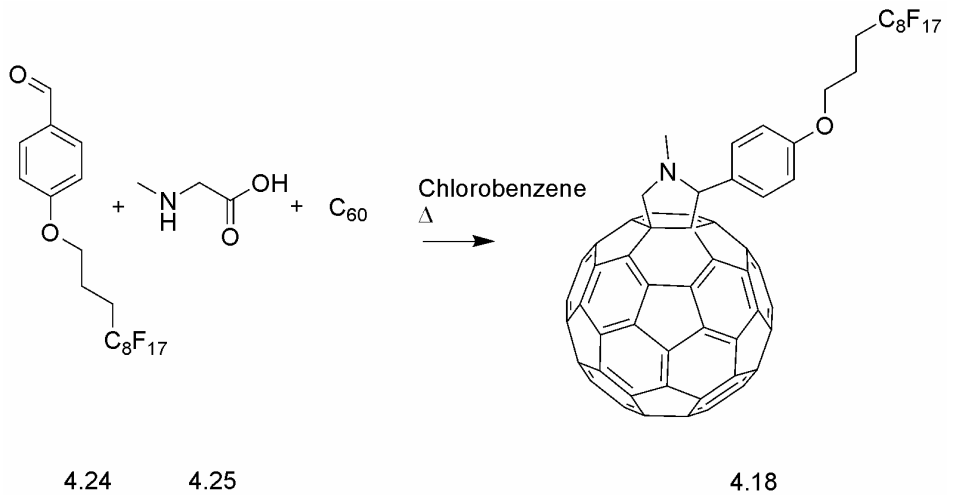

*Scheme 4.1: Synthesis of PFP-F17 (**4.18**)*

4.2.3 Synthesis of PCB-F17 (4.19)

A Friedel-Crafts acylation between benzene and commercially available 4,4,5,5,6,6,7,7,8,8,9,9,10,10,11,11,11-heptadecafluoro-undecanoyl chloride (**4.26**) was performed, quantitatively yielding 4,4,5,5,6,6,7,7,8,8,9,9,10,10,11,11,11-heptadecafluoro-phenyl-undecan-1-one (**4.27**). Next the ketone functionality was subjected to a condensation reaction with p-tosylhydrazide obtaining the corresponding tosylhydrazone (**4.25**) in 49% yield. In the last step, sodium methoxide was used to generate the diazo species *in situ*, which reacted with a fullerene double bond in a 1,3-dipolar cycloaddition reaction, resulting in the formation of PCB-F17 (**4.19**) in 15% yield (see scheme 4.3). The yield was low since purification proved extremely difficult. Multiple silica gel columns were necessary to remove all unreacted C_{60} from the product. It is well known in our labs that for separation purposes the introduction of some polarity in the fullerene adduct is necessary. Compound **4.19** is very apolar, causing these severe purification problems.

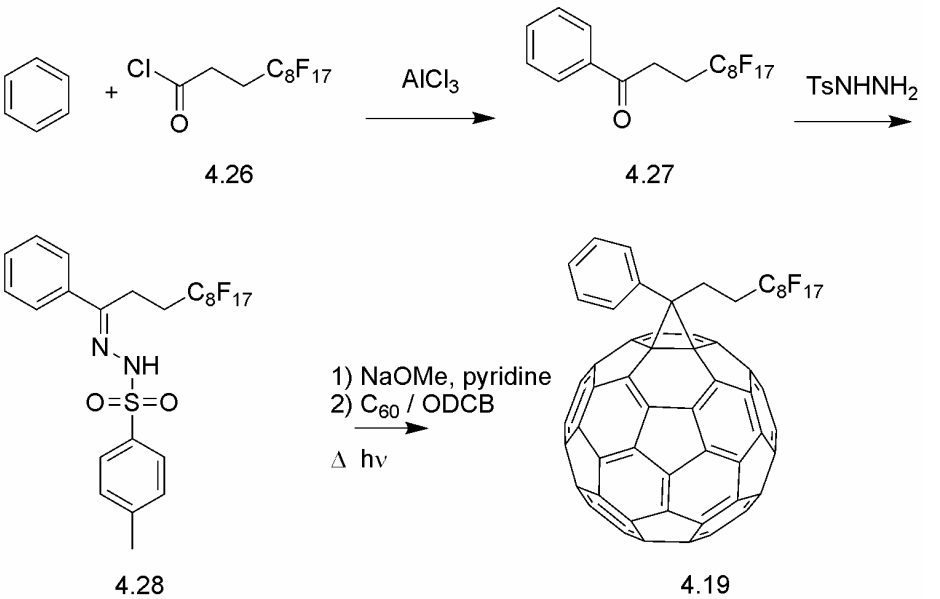

*Scheme 4.2: Synthesis of PCB-F17 (**4.19**)*

4.3 [84]PCBM Organic Field-Effect Transistors

As discussed in paragraph 4.1.5 we expected [84]PCBM to be an interesting material for n-channel FETs. Its low LUMO level when compared to its C_{60} and C_{70} analogues (paragraph 2.3.3) should allow for easy electron injection. Earlier work by Shibata already showed good electron mobilities of 2.1 x 10^{-3} cm^2/Vs for crystalline C_{84}.[45] However, C_{84} itself is not solution processable due to its low solubility in organic solvents. [84]PCBM on the other hand is soluble enough for solution processing. Besides the expected ease of electron injection we also hypothesized that [84]PCBM FETs could show environmental stability. Again, its low LUMO level could play a favorable role since the [84]PCBM anion is not able to undergo redox reactions with ambient water and air.[36] Also the photostability of C_{84} should be of great benefit to device stability.[43]

4.3.1 Film Morphology

The morphology of the [84]PCBM films that were used in FET devices was studied by X-ray diffraction (XRD) measurements. (see Fig. 4.5)

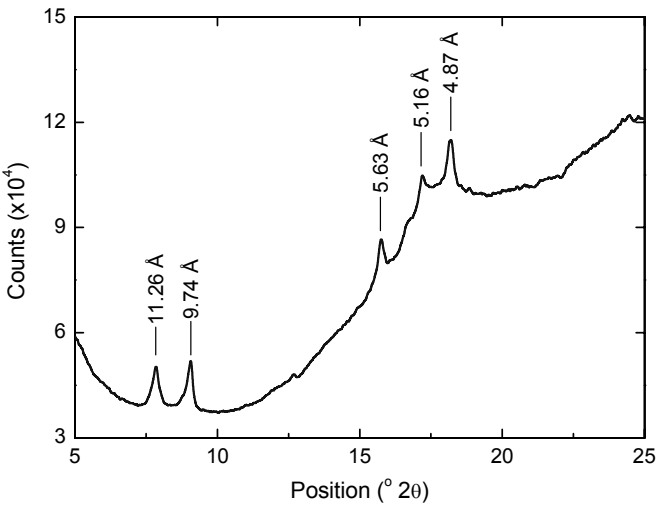

Fig. 4.5 XRD spectra for a drop-cast [84]PCBM film after recrystallization from dichlorobenzene. The corresponding d-spacings are shown for each peak.

The peaks are of rather low intensity indicating poor crystallinity in the films, especially when compared to its [60]PCBM analogue.[46] It seems that the films consist of small crystallites embedded in an amorphous background of randomly orientated [84]PCBM molecules.[I] Recrystallization from dichlorobenzene does not alter the film structure, but the FET performance differs to a great extent with the recrystallized films operating best. Due to the limited availability of [84]PCBM the film morphology was not optimized.

[I] From the full width at half the maximum of the peaks the crystallite size can be estimated using the Scherrer equation ($D = k\lambda/\beta\cos\Theta$), yielding in this case ca. 40 nm. The presence of the much wider peaks at $10^0 < 2\theta < 25^0$ is attributed to amorphous regions.

4.3.2 Field Effect Transistor properties

[84]PCBM transistors were prepared in a bottom-contact configuration and measured under ambient air and light. The output curves for a freshly prepared device can be seen in figure 4.6. Small hysteresis can be observed. The electon mobilities are calculated in saturation and give a value in the order of 0.5 x 10^{-3} cm^2/Vs. The room temperature[II] onset-voltage (V_{OS}) was estimated to be –10 V. This value was obtained from the $I_D^{1/2}$ versus V_G plot by extrapolating the linear region of the plot to the V_G axis at $(I_D)^{1/2} = 0\ A^{1/2}$. (see figure 4.7)

The current on/off ratio was calculated[III] to be approximately 10^4. This relatively low value is contributed to the high background conductivity of the films at negative V_G. The electron mobility remains the same after storage in ambient air for six months. This is to the best of our knowledge the first example of an air-stable methanofullerene based FET and one of the very few environmentally stable soluble n-type conducting organic semiconductors. We attribute the stability of these transistors to the stability of the [84]PCBM radical anion and to the fact that C_{84}, in contrast to C_{60} and C_{70}, does not convert to the triplet excited state upon optical excitation. Therefore [84]PCBM can not act as a singlet oxygen sensitizer. Self-sensitized degradation by singlet oxygen formation is strongly inhibited, at least.

The influence of annealing on the semiconductor layer was studied by annealing the layer in high vacuum (10^{-7} mbar) at 373 K for 24h. The resulting FET characteristics can be seen in figure 4.6b. It can be clearly seen that hysteresis is reduced and that the mobility is greatly enhanced by a factor of six to $\mu > 3 \times 10^{-3}$ cm^2/Vs. Since contact effects are known to play an important role in mobility determination[47] we attribute this enhancement of the effective mobility to a lowering of the injection barrier (and therefore the contact resistance) at the Au/[84]PCBM interface.

[II] Measurements mentioned to be performed at room temperature, are measured at 40 ^{0}C to ensure reproducibility.

[III] The on/off ratio is defined as the ratio of I_D at maximum V_G to I_D at V_G=V_{OS}

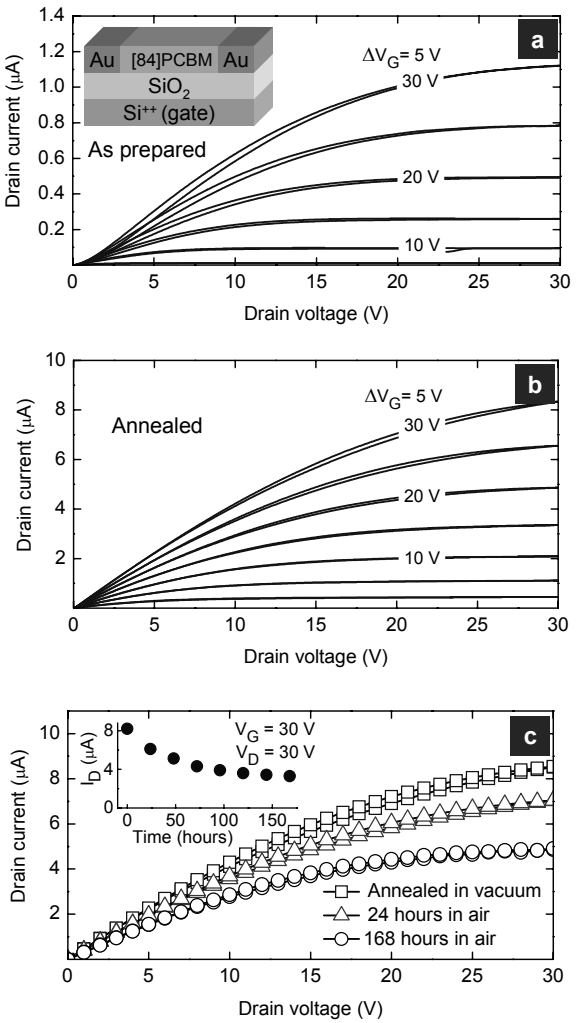

Fig. 4.6: Output characteristics of a [84]PCBM transistor (L = 20 μm and W = 10 mm) in the forward and backward sweep direction. (a) Output curves obtained from an as-prepared device under ambient conditions. Inset: Schematic diagram of the bottom contact transistor configuration employed. V_G: gate voltage. (b) Room temperature output characteristics of the same transistor measured in high vacuum after annealing at 100 ^{0}C for 24 hours. (c) room temperature output characteristics, at V_G = 30 V, measured after annealing at 100 ^{0}C in vacuum (squares), after exposure to ambient air for 24 hours (triangles) and 168 hours (circles). Inset: Evolution of the drain current (I_D) versus exposure time to ambient air. V_D: drain voltage.

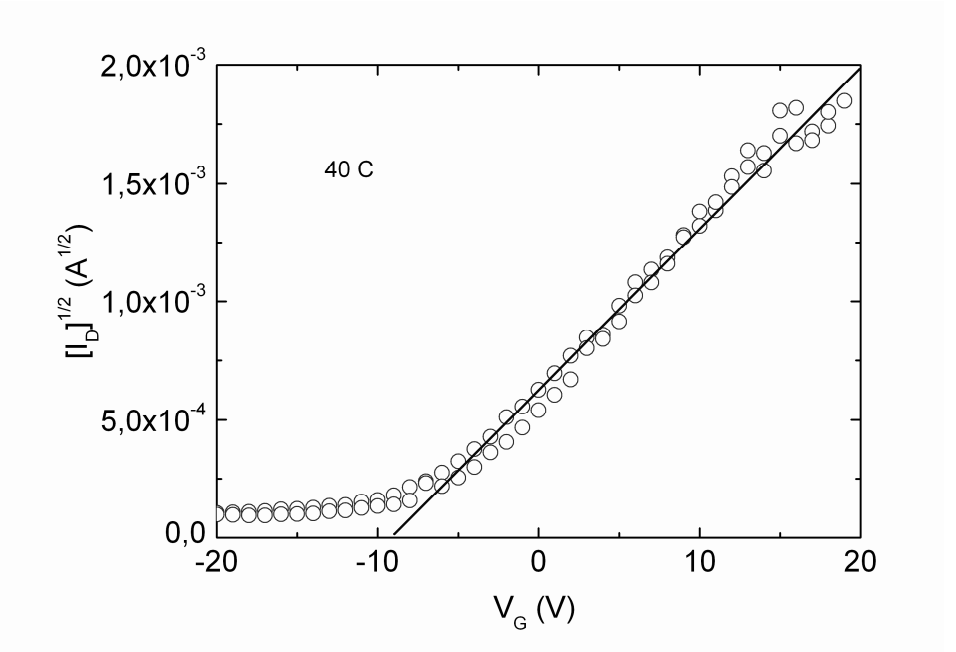

Fig. 4.7: Plot of $(I_D)^{1/2}$ vs V_G at 40 ^{0}C. The linear region of the plot is extrapolated to the V_G at $(I_D)^{1/2} = 0\ A^{1/2}$. This point is the onset-voltage (V_{OS}).

In figure 4.6c the FET characteristics of the annealed device are shown after re-exposure to air. It is clearly visible that the good transporting properties are retained. The inset in figure 4.6c shows how the drain current evolves in time at a gate voltage of 30V. We can see that the drain current is reduced to about half its original value with $\mu \sim 1.5 \times 10^{-3}$ cm^2/Vs, but it seems to remain stable. The mobility values both before and after exposure to air are higher than any previously obtained value from C_{84}[45] and endohedral C_{82}, and C_{80} metallofullerene-based OFETs.[10,16] Although the mobility stays good the on/off current reduces by two orders of magnitude to 3×10^2. Most likely this drop in on/off current is caused by degassing of oxygen during annealing. Oxygen is known to act as an electron trap and thus leads to a higher electron bulk current. Overall annealing seems to benefit the transporting materials of the material eventhough the on/off current is reduced.

Figure 4.8 shows the temperature dependence of the transistors. Interestingly at T < 273K the FET shows ambipolar transfer characteristics with a strong hole accumulation observed at $V_G < -55$V.

The dashed line in the figure shows the low leakage current of the gate, providing clear evidence that the observed current is caused by hole transport. Since the V_{OS} shifts significantly with T, the pinch-off point moves with T as well. This is most likely caused by thermally activated traps at the insulator/semiconductor interface. At higher T more traps are filled by thermally activated charges (electrons) and therefore they do not influence the transport. At lower T these traps are empty and thus influence the charge transport. The hole mobility, deduced from the saturation curves at low temperature, has a value of 10^{-5} – 10^{-4} cm^2/Vs and is slightly temperature dependent. This value is much lower (2 orders of magnitude) than the hole mobility of [60]PCBM[19] and comparable to [70]PCBM.[21] This is, however, the first time that ambipolar charge transport has been demonstrated in a C_{84}–based compound.

We propose that the low hole mobility in [70]PCBM and [84]PCBM is due the fact that these molecules are used as an isomeric mixture. Although cyclic voltammetry shows clean first reduction potentials in both cases, indicating that all isomers have the same LUMO level, it is possible that the HOMO levels are not the same. A difference in HOMO level could result in hole traps in the semiconducting layer, thus hindering hole transport.

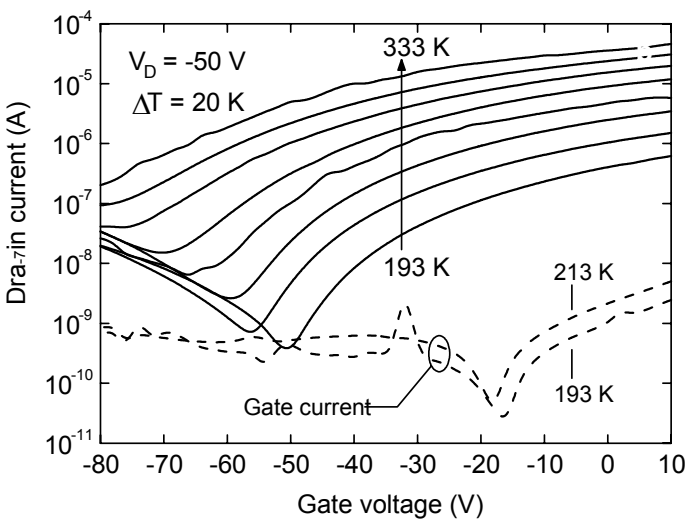

Fig. 4.8: Transfer characteristics (solid lines) of a [84]PCBM transistor (L= 20 µm, W = 10 nm) at 193 K < T < 333 K (ΔT = 20 K). Dashed lines are the gate leakage current (I_G) as a function of V_G measured at 193 and 213 K.

4.3.3 [84]PCBM complementary voltage inverters

In order to prove that these transistors can lead to environmentally stable complementary circuits, voltage inverters with an n-channel fabricated from [84]PCBM and a p-channel fabricated from poly[2-methoxy-5-(3',7'-dimethyloctyloxy)]-*p*-phenylene vinylene (MDMO-PPV) were made. The characteristics of such an inverter measured after exposure to ambient air for three months(!!) is shown in figure 4.9. Voltage gain as high as 14 is obtained. However transfer hysteresis does increase significantly when increasing the V_{DD} form 30 to 60V. In figure 4.10 the response of the inverter is shown when driven by a sinusoidal input voltage of 5V. These results cleary show that we can indeed use [84]PCBM as a solution processable n-type organic air-stable semiconductor for complementary circuits.

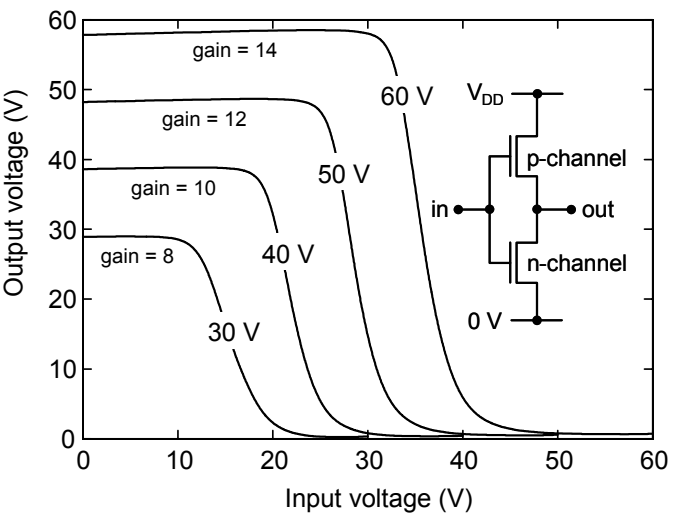

Fig. 4.9: Quasistatic transfer characteristics of a complementary voltage inverter consisting of an n-channel ([84]PCBM) transistor and a p-channel (MDMO-PPV) one (L = 10 µm, W = 2.5 mm) at different biasing conditions. Inset shows the complementary circuitry of the inverter.

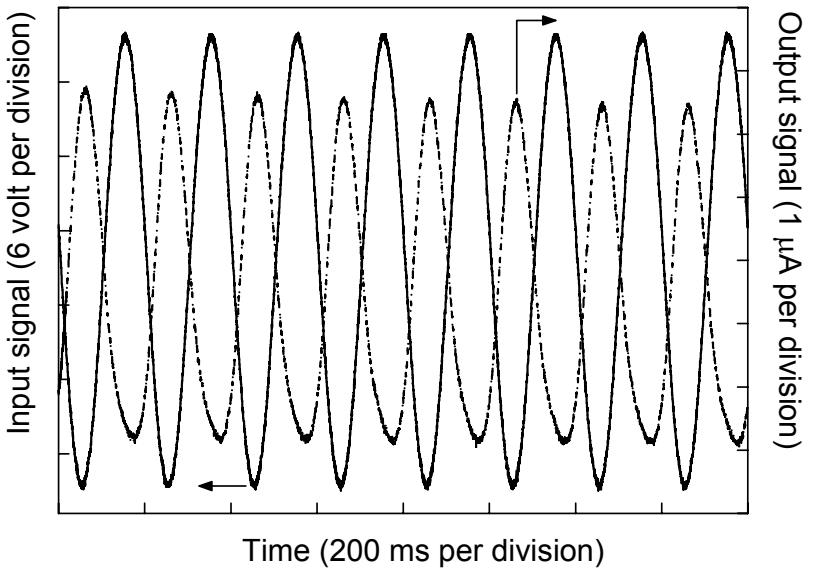

Fig. 4.10: Inverter response to a sinusoidel input signal of 5 Hz with the straigt and dotted lines the input and output signals, respectively.

4.4 Field Effect Transistors of fluorine containing fullerene derivatives.

In total a series of six fullerene derivatives containing varying amounts of fluorine atoms was synthesized. Of these fullerenes three (**4.16, 4.18** and **4.21**) were tested in FET devices. Work on the other three derivatives is part of ongoing research. The preliminary results obtained with **4.16**, **4.18** and **4.21** will be discussed in this section.

4.4.1 PCB-F13 (4.16) based Field Effect Transistors

First, the n-channel characteristics for a device, based on PCB-F13 (**4.16**), that has been placed in high vacuum (10^{-7} mbar) for 2 hours, were measured at room temperature (see Fig. 4.11).

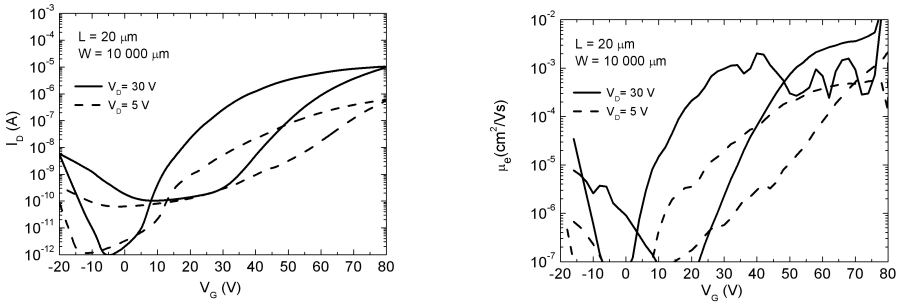

*Fig. 4.11: n-channel characteristics of **4.16** prepared in high vacuum and measured at RT.*

Quite large hysteresis was observed and relatively low mobilities in the order of 10^{-3} cm^2/Vs were found. Next the device was annealed at 115 ^{0}C in high vacuum for 2 hours after which its characteristics were measured at RT (see Fig. 4.12).

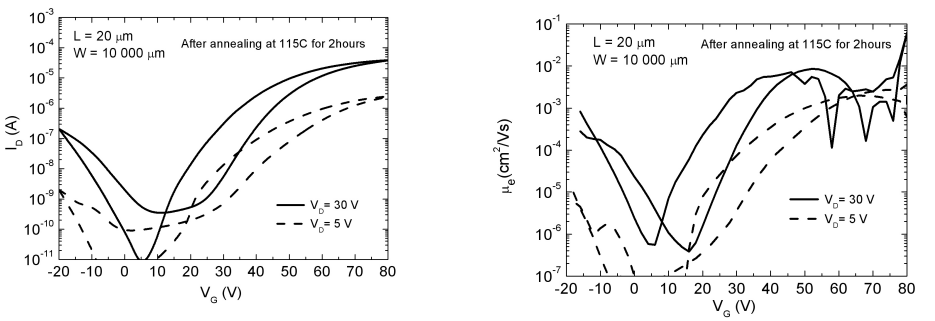

*Fig. 4.12: n-channel characteristics of **4.16** after annealing at 115 ^{0}C. Width (W) in micrometers.*

It is obvious that annealing resulted in improved device performance. The hysteresis priorly observed, had significantly decreased. Furthermore the mobilities had increased by a factor 10 to approximately 10^{-2} cm^2/Vs.

Finally, the characteristics for a FET that had been re-exposed to air for 10 minutes were measured at RT (see Fig. 4.13).

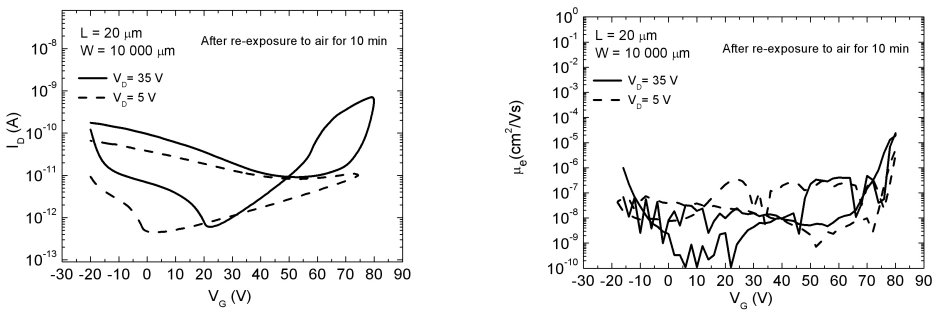

*Fig. 4.13: n-channel characteristics of **4.16** after re-exposure to air for 10 minutes. Width (W) in micrometers.*

Clearly the FET behaviour of PCB-F13 dramatically decreased due to exposure to ambient air.

4.4.2 PFP-F17 (4.18) based Field Effect Transistors

The same experiments, as described for PCB-F13, were performed with FET devices based on PFP-F13.

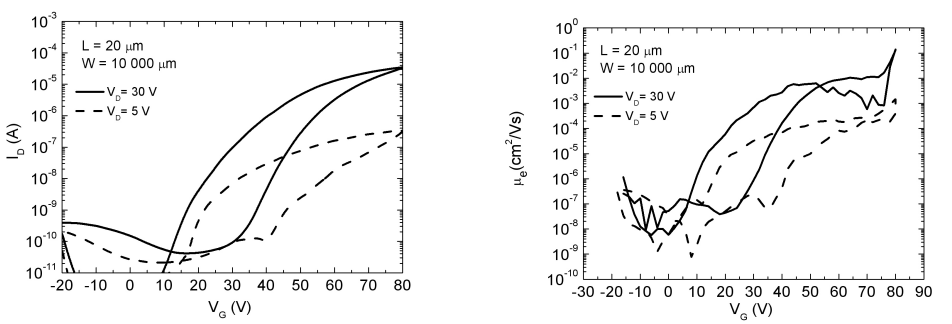

*Fig. 4.14: n-channel characteristics of **4.18**, prepared under high vacuum for 2 hours and measured at room temperature. Width (W) in micrometers.*

Also in this case the FET characteristics were rather poor. Large hysteresis was observed and the mobility was rather low, around 10^{-3} cm^2/Vs. Annealing the device at 115 ^0C resulted in minor improvements. The mobility was increased again by one order of magnitude to 10^{-2} cm^2/Vs and the hysteresis had decreased somewhat (see Fig. 4.15).

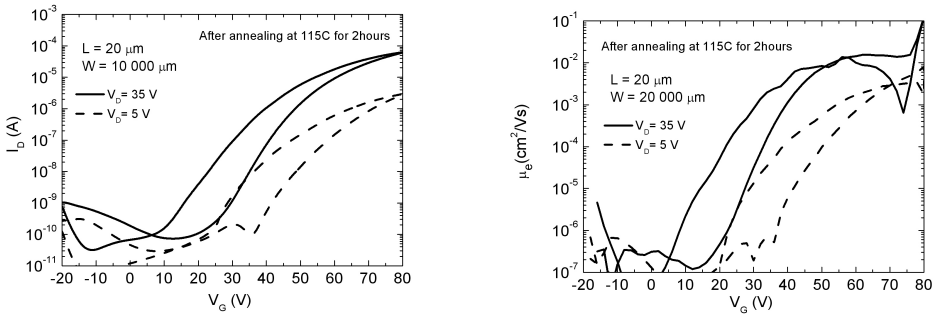

*Fig. 4.15: n-channel characteristics of **4.18** prepared under vacuum and annealed at 115 ^{0}C. Width (W) in micrometers.*

The devices also showed very poor air-stability as can be seen from the data presented in figure 4.16.

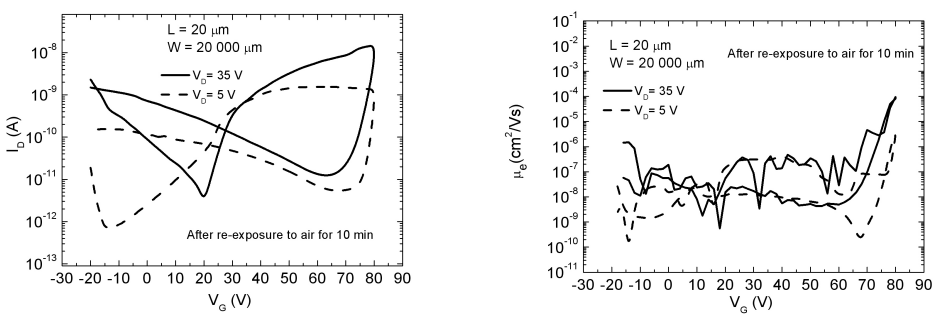

*Fig. 4.16: n-channel characteristics of **4.18** after exposure to air for 10 minutes. Width (W) in micrometers.*

4.4.3 F5-PCBM (4.21) based Field Effect Transitors

The previously reported experiments were also performed using 4.21 as the semiconductor. When prepared under high vacuum the devices showed quite some hysteresis, comparable to **4.16** and **4.18**. However, the mobility was significantly higher, approaching 10^{-2} cm^2/Vs.

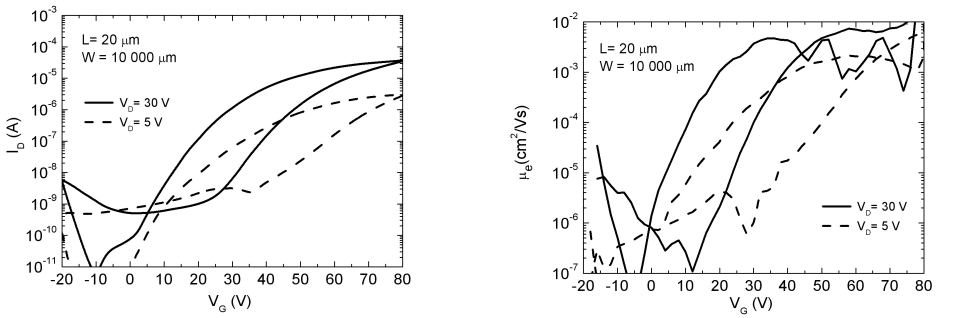

*Fig. 4.17: n-channel characteristics of **4.21** prepared under high vacuum and measured at RT. Width (W) in micrometers.*

Annealing the device increased the device performance just like for **4.16** and **4.18**. The hysteresis decreased significantly and the mobility was increased by one order of magnitude to ~10^{-1} cm^2/Vs, which surpasses the mobility of [60]PCBM.

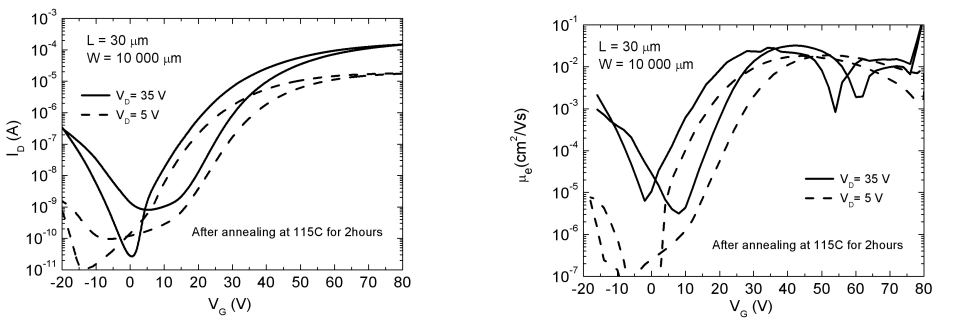

*Fig. 4.18: n-channel characteristics of **4.21** after annealing at 115 ^{0}C. Width (W) in micrometers.*

The air-stability of this device, unfortunately, was very poor again as can be seen in figure 4.19.

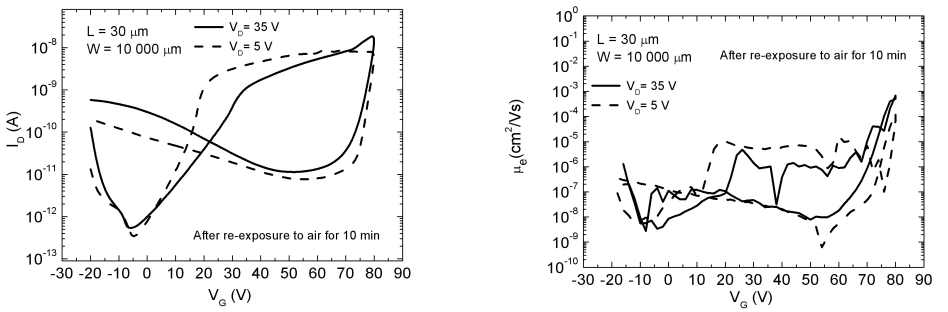

*Fig. 4.19: n-channel characteristics of **4.21** after exposure to air for 10 minutes. Width (W) in micrometers.*

4.5 Conclusions

The use of fullerenes containing fluorine atoms did not result in air-stable FET devices. Apparently, the fluorine atoms do not prevent oxygen and water from diffusion into the semiconducting layer. Some promising results were obtained with respect to electron mobilities. The mobilities obtained with F5-PCBM (**4.21**) are very promising, already exceeding those of [60]PCBM. Optimization of FET devices with this methanofullerene are currently under way. Very promising results are being obtained.[48]

Air-stable FET devices were obtained using [84]PCBM as the semiconducting layer. This air-stability is attributed to the low LUMO level of [84]PCBM. For the first time ambipolar transport was observed in a C_{84} fullerene. The transistors were combined with a polymeric p-type device to construct a complementary voltage inverter. This inverter was able to operate under ambient conditions, without encapsulation, due to the stability of the [84]PCBM semiconducting layer. These air-stable complementary inverters respresent a significant breakthrough in the search for air-stable molecular electronics.

4.6 Experimental

4.6.1 X-ray diffraction measurements

X-ray diffraction measurements have been performed using a PANalytical X'Pert PRO MPD θ-θ diffractometer equipped with an X'Celerator scanning, position sensitive, solid-state detector.

The θ-2θ scan was made using the Bragg-Brentano geometry. A θ-compensating slit was used resulting in an irradiated area of 5 × 15 mm throughout the measurement. A scanning speed of 60s / 0.05° 2θ was used.

4.6.2 Field Effect Transistors

Field effect transistors were made using heavily doped Si wafers as the common gate electrode with a 200 nm thermally oxidized silica gel layer as the gate dielectric. Using conventional photolithography, gold source and drain electrodes were defined in a bottom contact configuration. A 10 nm layer of titanium was used acting as an adhesion layer for the gold on SiO_2. The SiO_2 layer was treated with the primer hexamethyldisilazane prior to semiconductor deposition in order to passivate its surface. Films were drop cast from a 10 mg/ml solution of [84]PCBM in chlorobenzene (CB) with substrate temperature maintained at 55 ^{0}C in ambient conditions. Films were then recrystallized by applying few drops of ODCB on the top of the films at the same substrate temperature. Electrical characterization was performed using an HP 4156B semiconductor parameter analyzer. Complementary voltage inverters where fabricated and tested in ambient conditions. The p-channel (MDMO-PPV) and an n-channel ([84]PCBM) transistors were fabricated in two separate silicon substrate chips. Films of MDMO-PPV were spun from a 2 mg/ml solution in CB. The two devices were then interconnected in a complementary configuration (figure 4.9, inset) using coaxial cables. Quasistatic characterisation of the inverters was performed using an HP 4156B semiconductor parameter analyser while dynamic characterisation was done using a 1 MΩ input impedance oscilloscope connected directly to the output node of the inverter circuit.

4.6.3 Synthesis

General: See paragraph 3.6.2

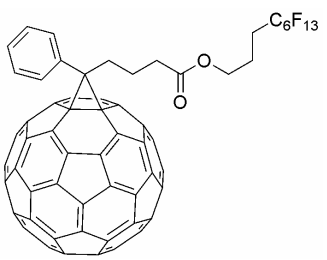

Phenyl–C_{61}–Butyric Acid 3,3,4,4,5,5,6,6,7,7,8,8,8-tridecafluoro-octyl ester (PCB–F13) (4.16):

A flame dried 500 ml three-necked flask, equiped with stirring egg, condensor, thermometer and septum, was charged with 3,3,4,4,5,5,6,6,7,7,8,8,8-tridecafluoro-octyl-5-{(Z)-2-[(4-methylphenyl)sulfonyl]hydrazono}-5-phenyl-pentanoate (**4.23a**) (1.54 g, 2.18 mmol, 1.09 eq.), pyridine (30 ml) and KOtBu (271 mg, 2.22 mmol, 1.11 eq.). This dark brown mixture was stirred for 1 h. Then a solution of C_{60} (1.44 g, 2.0 mmol) in *ortho*-dichlorobenzene (ODCB) (200 ml) was added.

The resulting purple mixture was degassed by three N_2/vacuum purges and then heated to 80 ^{0}C with a hotgun and subsequently irradiated with a Na-lamp (400 W). After 21 h. the reaction was stopped and the mixture was concentrated in vacuo to dryness and then redissolved in CS_2. A silica gel column (5 x 30 cm) was prepared with toluene. The column was pre-eluted with 125 ml of CS_2. Then the reaction mixture was deposited and eluted with CS_2 obtaining a purple C_{60} fraction. The C_{60} fraction was concentrated in vacuo, redissolved in ODCB and precipitated in MeOH. The resulting brown pellet was washed twice with MeOH and dried *in vacuo* at 50 ^{0}C. Elution was continued with cyclohexane:toluene (1:1) obtaining two brown mono-adduct fractions. The first fraction had a HPLC purity of 100%, the second fraction of 93.1%. Therefore the second fraction was columned once more with a silica gel column (2.5 x 10 cm) and elution with cyclohexane:toluene (1:1). Both now pure mono-adduct fractions were concentrated *in vacuo* and redissolved in ODCB. Precipitation with MeOH resulted in a brown pellet, which was washed with MeOH (2x) then dried *in vacuo* at 50 ^{0}C, washed again once with pentane, dried *in vacuo* at 50 ^{0}C and washed once more with MeOH yielding a brown pellet which was dried *in vacuo* at 50 ^{0}C. The bis-adducts were obtained by elution with toluene, precipitation from ODCB with MeOH and washing with MeOH. Yield recovered C_{60}: 712 mg (0.99 mmol, 49.4 %). Yield bis-adducts: 62 mg (3.5 10^{-2} mmol, 1.8 %). Yield mono-adduct: 687 mg (0.55 mmol, 27.7 %). IR (KBr); ν (cm^{-1}): 2960 (m), 2329 (m), 1742 (s), 1495 (w), 1464 (w), 1428 (m), 1347 (w), 1237 (s), 1204 (s), 1145 (s), 1081 (w), 1005 (w), 843 (w), 810 (w), 743 (w), 732 (w), 699 (m), 652 (w), 586 (w), 573 (w), 559 (w), 550 (w), 526 (s), 480 (w), 424 (w), 408 (w). ^{1}H NMR ($CDCl_3$, 200 MHz); δ (ppm): 7.93 (d, *J* = 7.6 Hz, 2H), 7.58–7.47 (m, 3H), 4.38 (t, *J* = 6.6 Hz, 2H), 2.95–2.87 (m, 2H), 2.59–2.46 (m, 4H), 2.23–2.19 (m, 2H). ^{19}F NMR ($CDCl_3$, 200 MHz); δ (ppm): –81.9 (t, *J* = 10.1 Hz, 3F), –114.6 – –114.8 (m, 2F), –123.0 (br., 2F), –124.0 (br., 2F), –124.7 (br., 2F), –127.2 (br., 2F). ^{13}C NMR ($CDCl_3$, 75 MHz); δ (ppm): 171.56, 147.74, 146.73, 144.82, 144.19, 144.16, 144.05, 143.80, 143.74, 143.67, 143.51, 143.43, 143.01, 142.75, 142.12, 142.04, 142.01, 141.94, 141.91, 141.20, 141.17, 141.10, 140.00, 139.76, 137.01, 136.57, 135.66, 131.07, 127.44, 127.28, 78.81, 76.19, 55.38, 50.73, 32.82, 32.61, 29.50 (t, *J* = 20.8 Hz, 1C), 21.18. Elemental Analysis: calcd. for $C_{79}H_{15}O_2F_{13}$: C: 76.34 %, Found: C: 75.86 %. Mass m/z: calcd: 1242.97, Found 1242.3.

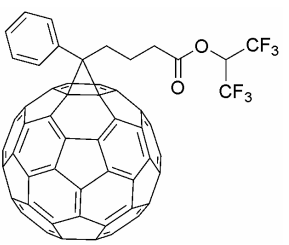

Phenyl–C_{61}–Butyric Acid 1,1,1-3.3.3 hexafluoro isopropanol ester (PCB–F6) (4.17):

A flame dried 250 ml three-necked flask, equiped with stirring egg, condensor, thermometer and septum, was charged with 2,2,2-trifluoro-1-(trifluoromethyl)ethyl-5-(Z)-2-[4(-methylphenyl)sulfonyl] (**4.23b**) (285 mg, 0.6 mmol, 1.1 eq.), pyridine (7.5 ml) and KOtBu (66,2 mg, 0.59 mmol, 1.09 eq.). This light yellow mixture was stirred for 1 h.

Then a solution of C_{60} (390 mg, 0.54 mmol) in ODCB (50 ml) was added. The resulting purple mixture was heated to 85 ^{0}C with a hotgun and subsequently irradiated with a Na-lamp (400 W) reaching a T_{eq} of 103 ^{0}C. After 20 h. the reaction was stopped and the mixture was concentrated *in vacuo* to dryness and then redissolved in CS_2. A silica gel column (5 x 23 cm) was prepared with toluene. The column was pre-eluted with 125 ml of CS_2. Then the reaction mixture was deposited and eluted with CS_2 obtaining a purple C_{60} fraction and a brown mono-adduct fraction. Since the mono-adduct fraction still contained some C_{60} a second silica gel column (3 x 15 cm) was prepared with toluene. Elution with CS_2 resulted in a brown mono-adduct fraction with a HPLC purity of 99.7 %. Both the C_{60} fraction from the first column and the mono-adduct fraction were concentrated *in vacuo* to dryness and redissolved in a minimal amount of ODCB. This was then transferred to a centrifugal tube and both the C_{60} and the mono-adduct were precipitated with MeOH, washed twice with MeOH and once with n-pentane. The resulting brown pellets were dried *in vacuo* at 50 ^{0}C overnight. The next day they were washed once more with methanol and dried again *in vacuo* at 50 ^{0}C. Yield recovered C_{60}: 155 mg (0.22 mmol, 40 %). Yield mono-adduct: 73.7 mg (0.07 mmol, 13 %). IR (KBr); ν (cm^{-1}): 3026 (w), 2961 (m), 2926 (m), 2329 (m), 1781 (s), 1601 (w), 1540 (w), 1495 (w), 1463 (w), 1428 (s), 1385 (m), 1356 (s), 1289 (w), 1265 (s), 1228 (s), 1200 (w), 1110 (s), 1026 (w), 988 (w), 924 (m), 906 (m), 797 (w), 755 (w), 731 (w), 698 (m), 585 (m), 573 (m), 527 (s), 481 (w). ^{1}H NMR ($CDCl_3$, 200 MHz); δ (ppm): 7.93 (dd, *J* = 6.4 Hz, 2.0 Hz, 2H), 7.61–7.49 (m, 3H), 5.78 (quintet, *J* = 6.1 Hz, 1H), 2.97–2.67 (m, 2H), 2.72 (t, *J* = 7.3 Hz, 2H), 2.33 – 2.21 (m, 2H). ^{19}F NMR ($CDCl_3$, 200 MHz); δ (ppm): –74.5 (d, *J* = 5.6 Hz, 6F). ^{13}C NMR ($CDCl_3$, 100 MHz); δ (ppm): 169.28, 148.11, 146.98, 145.28, 144.71, 144.68, 144.56, 144.51, 144.31, 144.25, 144.18, 144.03, 143.97, 143.54, 143.26, 142.64, 142.56, 142.52, 142.45, 142.43, 141.72, 141.66, 141.63, 140.55, 140.27, 137.55, 137.10, 135.95, 131.54, 128.04, 127.92, 79.12, 66.35 – 65.66 (m, 1C), 50.90, 32.88, 32.51, 21.39. Mass m/z: calcd: 1046.90, Found: 1047.6

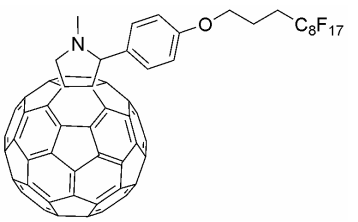

4-(4,4,5,5,6,6,7,7,8,8,9,9,10,10,11,11,11-heptadecafluoroundecyloxy)phenyl fulleropyrolidine (PFP–17) (4.18):

A 250 ml round flask was charged with C_{60} (1.255 g, 1.74 mmol, 2 eq.), sarcosine (385 mg, 4.32 mmol, 5 eq) and 4-(4,4,5,5,6,6,7,7,8,8,9,9,10,10,11,11,11-heptadecafluoroundecyloxy)benzaldehyde (0.5 g, 0.859 mmol). Chlorobenzene (150 ml) was added and the mixture was brought to reflux in the dark. The reaction was stopped after 20 h. and the mixture was concentrated to dryness *in vacuo*. All was redissolved in CS_2. A silica gel column (6 x 30 cm) was prepared with toluene. Elution with CS_2 yielded unreacted C_{60}. Elution was continued with cyclohexane:toluene (1:1) to obtain the mono adduct. Work up C_{60}: The C_{60} fraction was concentrated *in vacuo*, redissolved in ODCB and precipitated with

MeOH resulting in a brown pellet. This was then washed with MeOH (2x) and pentane (1x). The resulting brown pellet was dried *in vacuo* at 50 ^{0}C. Then washed once more with MeOH and dried *in vacuo* at 50 ^{0}C. Work up mono-adduct: The mono adduct fraction was concentrated *in vacuo*, redissolved in ODCB and precipitated with MeOH resulting in a brown pellet, which was washed twice with MeOH. Drying *in vacuo* at 50 ^{0}C yielded a brown powder, which was washed once with MeOH and dried *in vacuo* at 50 ^{0}C. Yield recovered C_{60}: 736 mg (1.02 mmol, 59 %). Yield mono-adduct: 366 mg (0.275 mmol, 32 %). IR (KBr): ν (cm^{-1}): 3425 (s), 2782 (w), 1611 (w), 1512 (w), 1463 (w), 1428 (w), 1332 (w), 1244 (s), 1211 (s), 1151 (s), 1030 (w), 842 (w), 832 (w), 788 (w), 766 (w), 737 (w), 704 (w), 656 (w), 574 (w), 553 (w), 527 (s). ^{1}H NMR ($CDCl_3$, 300 MHz): δ (ppm): 7.71 (br. 2H), 6.94 (d, *J* = 8.4 Hz, 2H), 4.98 (d, *J* = 9.5 Hz, 1H), 4.89 (s, 1H), 4.05 (t, *J* = 5.5 Hz, 2H), 2.79 (s, 3H), 2.34–2.29 (m, 2H), 2.12–2.07 (m, 2H). ^{19}F NMR ($CDCl_3$, 200 MHz); δ (ppm): -82.0 (t, *J* = 10.1 Hz, 3F), -115.5 (br., 2F), -123.0 (br., 6F), -123.8 (br., 2F), -124.5 (br., 2F), -127.2 (br., 2F). ^{13}C NMR ($CDCl_3$, 75 MHz); δ (ppm): 157.56, 155.34, 153.08, 152.57, 146.30, 145.76, 145.49, 145.29, 145.19, 145.11, 144.94, 144.76, 144.53, 144.45, 144.30, 144.27, 144.22, 143.69, 143.58, 143.37, 142.14, 141.97, 141.67, 141.55, 141.25, 141.15, 141.12, 141.08, 141.02, 140.95, 140.78, 140.68, 140.52, 139.16, 139.13, 138.88, 138.53, 135.79, 135.50, 134.80, 134.72, 129.55, 128.36, 113.46, 82.11, 76.30, 76.20, 68.97, 67.95, 65.20, 38.97, 27.00 (t, *J* = 23.2 Hz, 1C), 19.60. Elemental Analysis: calcd. for $C_{80}H_{16}ONF_{17}$: C: 72.25 %, N: 1.05 %, Found: C: 71.98 %, N: 1.18 %. Mass m/z: calcd: 1329.99, Found: 1330.3.

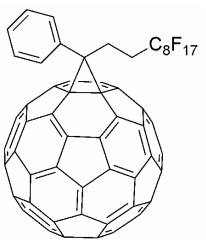

1-phenyl-1-[60]fullerene–4,4,5,5,6,6,7,7,8,8,9,9,10,10,11,-11,11-heptadeca-fluoroundecane (PCB–F17) (4.19):

A 100 ml flame-dried three-necked flask, equiped with condensor, stirring egg, N_2-inlet and thermometer, was charged with 1-phenyl-4,4,5,5,6,6,7,7,8,8,9,9,10,10,11,11,11-heptadecafluoroundecane-1-tosylhydrazone (**4.28**) (367 mg, 0.51 mmol, 1.02 eq.), Sodium methoxide (30 mg, 0.55 mmol, 1.1 eq.) and pyridine (7.5 ml). The resulting suspension was stirred at RT for 1 hour. Then a solution of C_{60} (360 mg, 0.5 mmol) in ODCB (50 ml) was added. The resulting mixture was degassed with three N_2 / vacuum purges. The reaction mixture was heated to 80 ^{0}C with a hotgun and irradiation with a 150 W Na-lamp was started. After 4 hours the mixture was allowed to cool to RT under illumination. The reaction mixture was concentrated *in vacuo* to dryness. The resulting black solid was redissolved in CS_2. A silica gel column (2,5 x 35 cm) was prepared with toluene. Elution with CS_2 gave enriched product/C_{60} fractions. The enriched fractions were collected and redissolved in CS_2 (200 ml). Precipitation with THF (400 ml) was attempted without success. The entire mixture was concentrated *in vacuo* and redissolved in ODCB (25 ml). Addtion of THF (50 ml) resulted in precipitation.

The entire mixture was transferred to a 100 ml centrifugal tube and centrifuged for 20 min. A brown pellet and a dark brown supernatant were obtained. The supernatant consists of enriched product/C_{60} (HPLC: 73/17, and 7% bis-adducts) and the pellet of enriched C_{60} (HPLC: 31/69). The supernatant was concentrated *in vacuo* and redissolved in ODCB (10 ml). Precipitation with THF (30 ml) and centrifugation gave a brown pellet (49% mono, 51% C_{60}) and a dark brown supernatant (70 % mono, 12% bis, 15% C_{60}). The supernatant was concentrated *in vacuo* and THF (50 ml) was added. This suspension was stirred overnight and then centrifuged obtaining a dark supernatant (3% C_{60}, 64% mono, rest is bis and solvent peaks). This supernatant was purified by column chromatography (2 times) with CS_2 as the eluent. All the pellets were combined and stirred overnight in THF and centrifuged (78% mono, 12% C_{60}). The supernatant was concentrated *in vacuo* and purified by column chromatography with CS_2 as the eluent. The purest fractions (97%) were combined and concentrated *in vacuo*. These fractions were combined with the previous almost pure fractions and purified by column chromatography (silica gel 2.5 x 25 cm) with CS_2 as the eluent. Yielding 92.6 mg mono-adduct (7.4 10^{-2} mmol, 14.7 %). HPLC purity 98.8 %. IR (KBr) = ν (cm^{-1}): 1450 (m), 1428 (m), 1240 (s), 1207 (s), 1148 (s), 1134 (m), 1116 (m), 1022 (m), 764 (w), 742 (w), 733 (w), 721 (w), 700 (m), 655 (m), 586 (m), 572 (m), 559 (m), 550 (m), 528 (s).^{1}H NMR ($CDCl_3$, 300 MHz); δ(ppm): 7.92 (d, *J* = 7.3 Hz, 2H), 7.61—7.52 (m, 3H), 3.23—3.17 (m, 2H), 2.64—2.59 (m, 2H). ^{19}F NMR ($CDCl_3$, 200 MHz); δ (ppm): -81.93 (t, *J* = 10.1 Hz, 3F), -114.63 (m, 2F), -122.96 (m, 6F), -123.87 (m, 4F), -127.20 (m, 2F). ^{13}C NMR ($CDCl_3$, 75 MHz); δ(ppm): 147.17, 145.71, 144.63, 144.22, 144.09, 143.88, 143.82, 143.72, 143.58, 143.53, 143.11, 142.73, 142.07, 141.97, 141.26, 141.12, 141.08, 140.13, 139.79, 137.15, 136.67, 134.64, 130.89, 127.80, 127.77, 78.16, 76.19, 48.84, 27.80 (t, *J* = 23 Hz, 1C), 24.61. Elemental Analysis: calcd. for $C_{77}H_9F_{17}$: C: 73.58 %. Found: 72.44 %. Mass m/z: calcd: 1256.89, Found: 1256.6

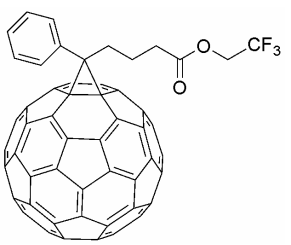

Phenyl-C_{61}-butyric acid 2,2,2-trifluoroethanol ester (PCB–F3) (4.20):

A flame dried 3-necked flask equiped with stirring egg, condensor, thermometer and septum was charged with 2,2,2-trifluoroethyl-5-{(*Z*)-2-[(4-methylphenyl) sulfonyl] hydrazono} -5-phenyl-pentanoate (**4.22c**) (491 mg, 1.1 mmol, 1.1 eq), KOtBu (122.4 mg, 1.09 mmol, 1.09 eq.) and dry pyridine (15 ml). This yellowish solution was stirred for 45 min. Then C_{60} (720 mg, 1 mmol) in ODCB (100 ml), which was sonicated for 2 h, was added. The resulting purple solution was heated to 80 ^{0}C with a hotgun. Irradiation was started with a 400 Na lamp. T_{eq} ~ 85 ^{0}C. After 2 h, reaction was complete and the mixture was concentrated to 1/3 rd volume. A silica gel column was prepared (6 x 40 cm) with toluene. Elution with CS_2 yielded unreacted C_{60} and elution was continued with cyclohexane:toluene (1:1) mono-adduct. The mono-adduct fractions were concentrated to dryness. The resulting solid was redissolved in a minimal amount

of ODCB and precipitated with MeOH. Centrifugation yielded a brown pellet. The supernatant was decanted. The pellet was then washed twice with MeOH and once with pentane. The resulting pellet was dried *in vacuo* at 50 ^{0}C overnight and then washed once more with MeOH. The obtained pellet was dried *in vacuo* at 50 ^{0}C. Yield: 378 mg (0.386 mmol, 38,6 %). IR (KBr); ν (cm^{-1}): 3425 (w), 2961 (w), 1759 (s), 1494 (w), 1434 (w), 1446 (w), 1428 (w), 1410 (w), 1281 (s), 1168 (s), 1142 (s), 1076 (w), 1026 (w), 976 (w), 841 (w), 755 (w), 742 (w), 731 (w), 715 (w), 699 (w), 586 (w), 573 (w), 550 (w), 527 (s), 480 (w), 443 (w), 424 (w), 417 (w), 407 (w). ^{1}H NMR ($CDCl_3$, 400 MHz); δ (ppm): 7.95–7.91 (m, 2H), 7.60–7.48 (m, 3H), 4.47 (q, *J* = 8.5 Hz, 2H), 2.97–2.89 (m, 2H), 2.64 (t, *J* = 7.3 Hz, 2H), 2.26–2.18 (m, 2H). ^{13}C NMR ($CDCl_3$, 100 MHz); δ (ppm): 170.40, 147.68, 146.63, 144.80, 144.19, 144.16, 144.03, 143.78, 143.74, 143.66, 143.51, 143.44, 143.01, 142.75, 142.12, 142.04, 141.99, 141.92, 141.20, 141.15, 141.11, 140.01, 139.74, 137.02, 136.57, 135.56, 131.06, 123.26, 120.50, 78.71, 59.31 (m, 1C), 50.60, 32.49, 32.36, 21.05. ^{19}F NMR ($CDCl_3$, 200 MHz); δ (ppm): –74.94 (t, *J* = 9.1 Hz, 3F). HPLC purity: 99,8 %. Elemental Analysis: calcd. for $C_{73}H_{14}O_2F_3$: C: 89.57 %, Found: C: 88.91 %. Mass m/z: calcd: 979.91, Found: 978.7

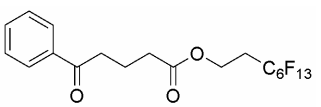

5-Oxo-5-phenyl-pentanoic acid 3,3,4,4,5,5,6,6,7,7,8,8,8-tridecafluoro-octyl ester (4.22a):

1H,1H,2H,2H-perfluoro-1-octanol (4 g, 11 mmol) was dissolved in toluene (20 ml). Added was benzoyl butyric acid (2.11 g, 11 mmol) and two drops of concentrated sulfuric acid. The solution was refluxed using a Dean-Stark setup for 17 h. The resulting yellow solution was dissolved in ethyl acetate (25 ml) and washed with 10 % $NaHCO_3$ solution (2 x 25 ml). The obtained organic layer was then washed with water (3 x 50 ml), dried over Na_2SO_4 and concentrated *in vacuo* to 15 ml volume. A silica gel column (2 x 20 cm) was prepared with toluene. The mixture was deposited and eluted with toluene:EtOAc (up to 5 % EtOAc). A yellow oil was obtained, which crystallized upon standing into an off-white wax-like solid. (5.01 g, 9.31 mmol, 85 %). IR (KBr): ν (cm^{-1}): 3057 (w), 2970 (s), 2911 (m), 1740 (s), 1676 (s), 1599 (m), 1581 (m), 1475 (m), 1415 (m), 1402 (m), 1380 (m), 1367 (m), 1320 (m), 1283 (s), 1235 (s), 1207 (s), 1145 (s), 1089 (s), 1001 (w), 940 (w), 895 (w), 843 (w), 809 (w), 781 (w), 771 (w), 736 (s), 696 (s), 652 (w), 567 (w), 533 (w). ^{1}H NMR ($CDCl_3$, 200 MHz); δ (ppm): 7.98–7.93 (m, 2H), 7.60–7.41 (m, 3H), 4.39 (t, *J* = 6.6 Hz, 2H), 3.06 (t, *J* = 7.1 Hz, 2H0, 2.59–2.35 (m, 4H), 2.15–2.01 (m, 2H). ^{13}C NMR ($CDCl_3$, 50 MHz); δ (ppm): 198.19, 171.84, 135.74, 132.13, 127.60, 126.97, 55.26, 36.24, 29.46 (t, *J* = 21.4 Hz, 1C), 18.08. ^{19}F NMR ($CDCl_3$, 200 MHz); δ (ppm): -82.03 (t, *J* = 10.1 Hz, 3F), -114.75 – -114.92 (m, 2F), -123.06 (br, 2F), -124.03 – -124.77 (m, 2F), -127.21 – -127.36 (m, 2F). HRMS calcd. for $C_{19}H_{15}O_3F_{15}$: 538.08131 Found: 538.08296.

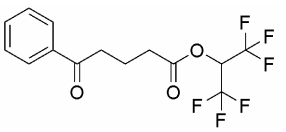

5-Oxo-5-phenyl-pentanoic acid 2,2,2-trifluoro-1-trifluoro methyl-ethyl ester (4.22b):

Benzoylbutyric acid (2.4 g, 12,5 mmol) was dissolved in 1,1,1-3,3,3-hexafluoro-isopropanol (30 ml), two drops of concentrated sulfuric acid were added and the resulting solution was refluxed for 48 h. The crude reaction mixture was purified by column chromatography (silica gel 2 x 20 cm). Elution was carried out with toluene : EtOAc (9:1). Two fractions were obtained. The second fraction was purified by column chromatography again over a small silica gel column (2 x 5 cm) with toluene as the eluent. Both fractions were now combined and concentrated *in vacuo* yielding an off-white wax like solid (2.37 g, 6.9 mmol, 55.4 %). IR (KBr) = ν (cm^{-1}): 3066 (m), 2970 (m), 2946 (m), 2916 (m), 1773 (s), 1677 (s), 1641 (w), 1597 (m), 1581 (m), 1449 (m), 1412 (s), 1385 (s), 1355 (m), 1321 (m), 1272 (s), 1204 (s), 1175 (m), 1163 (m), 1134 (s), 1107 (s), 1062 (m), 1050 (m), 1001 (w), 980 (w), 934 (m), 907 (m), 864 (m), 773 (m), 745 (m), 734 (m), 691 (s), 661 (w), 578 (w), 531 (w), 481 (w). ^{1}H NMR ($CDCl_3$, 300 MHz); δ (ppm): 7.95 (d, *J* = 8.4 Hz, 2H), 7.58 (t, *J* = 7.7 Hz, 1H), 7.47 (t, *J* = 8.1 Hz, 2H), 5.79 (t, *J* = 6.2 Hz, 1H), 3.08 (t, *J* = 7.0 Hz, 2H), 2.68 (t, *J* = 7.3 Hz, 2H), 2.20 – 2.13 (m, 2H). ^{13}C NMR ($CDCl_3$, 50 MHz); δ (ppm): 197.16, 168.52, 135.10, 131.77, 127.16, 126.43, 121.73, 65.59, 64.90, 35.24, 30.88, 17.31. ^{19}F NMR ($CDCl_3$, 200 MHz); δ (ppm): –74.60 (d, *J* = 6.8 Hz, 6F). HRMS calcd. for $C_{14}H_{12}O_3F_6$: 342.06903 Found: 342.06741

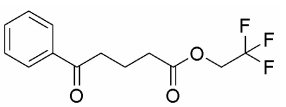

5-Oxo-5-phenyl-pentanoic acid 2,2,2-trifluoro-ethyl ester (4.22c):

Benzoylbutyric acid (2.5 g, 13 mmol) was dissolved in 2,2,2-trifluoroethanol (23 ml), two drops of concentrated sulfuric acid were added and the resulting solution was refluxed for 48 h. The crude reaction mixture was purified by column chromatography (silica gel 2 x 20 cm). Elution was carried out with toluene : EtOAc (9:1). A clear oil was obtained, which solidified upon standing. (2.76 g, 10.07 mmol, 77.5 %). IR (KBr) = ν (cm^{-1}): 2977 (s), 2947 (m), 2921 (m), 2905 (w), 1755 (s), 1676 (s), 1597 (m), 1580 (m), 1449 (s), 1413 (s), 1385 (s), 1320 (m), 1288 (s), 1210 (m), 1178 (s), 1150 (s)m 1089 (m), 1063 (m), 1052 (m), 1033 (m), 968 (s), 942 (m), 921 (m), 845 (m), 772 (m), 736 (s), 696 (m), 659 (m), 640 (m), 572 (w). ^{1}H NMR ($CDCl_3$, 300 MHz); δ (ppm): 7.96 (d, *J* = 7.7 Hz, 2H), 7.57 (t, *J* = 7.3 Hz, 1H), 7.47 (t, *J* = 7.7 Hz, 2H), 4.48 (quartet, *J* = 8.4 Hz, 2H), 3.07 (t, *J* = 7.0 Hz, 2H), 2.57 (t, *J* = 7.0 Hz, 2H), 2.12 (quintet, J = 7.0 Hz, 2H). ^{13}C NMR ($CDCl_3$, 50 MHz); δ (ppm): 197.97, 170.60, 150.00, 135.70, 132.15, 127.60, 126.96, 59.92, 59.44, 58.95, 36.05, 31.70, 17.99. ^{19}F NMR ($CDCl_3$, 200 MHz); δ (ppm): –75.11 (t, *J* = 7.9 Hz, 3F). HRMS calcd. for $C_{13}H_{13}O_3F_3$: 274.08165 Found: 274.08242.

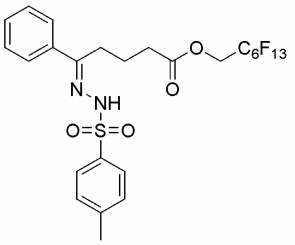

5-Oxo-5-phenyl-pentanoic acid 3,3,4,4,5,5,6,6,7,7,8,8,8-tridecafluoro-octyl ester p-tosyl hydrazone (4.23a):

Compound **4.22a** (3 g, 5.58 mmol) and p-tosylhydrazide (1.25 g, 6.7 mmol, 1.2 eq.) were dissolved in methanol (35 ml). The resulting solution was refluxed for 10 h. and then placed in the freezer. Product crystallized as a white powder consisting of two isomers in a 4:1 (Z:E) ratio (3.46 g, 4.9 mmol, 88%). IR (KBr): ν (cm^{-1}): 3186 (s), 2977 (m), 1734 (m), 1712 (s), 1600 (w), 1471 (w), 1445 (w), 1402 (m), 1364 (m), 1346 (m), 1289 (m), 1231 (s), 1202 (s), 1167 (s), 1143 (s), 1121 (s), 1081 (m), 1046 (m), 1020 (m), 992 (w), 930 (m), 879 (w), 839 (w), 811 (w), 770 (w), 752 (w), 732 (w), 697 (w), 671 (w), 582 (w), 548 (w), 527 (w). Major Z-isomer: ^{1}H NMR ($CDCl_3$, 200 MHz); δ (ppm): 9.0 (s, 1H), 7.91 (d, *J* = 8.3 Hz, 2H), 7.67–7.61 (m, 2H), 7.45–7.05 (m, 5H), 4.49 (t, *J* = 6.4 Hz, 2H), 2.67–2.26 (m, 9H), 1.80–1.64 (m, 2H). ^{13}C NMR ($CDCl_3$, 50 MHz); δ (ppm): 172.96, 152.57, 142.81, 135.05, 128.96, 128.67, 128.54, 128.48, 127.44, 126.92, 125.64, 125.17, 56.07, 36.05, 31.11, 29.81, 29.38, 28.96, 24.70, 20.55, 19.69. ^{19}F NMR ($CDCl_3$, 200 MHz); δ (ppm): -81.99 (t, *J* = 10.1 Hz, 3F), -114.69 – -114.85 (m, 2F), -123.01 (br. s, 2F), -124.02 (br. s, 2F), -124.69 (br. s, 2F), -127.28 (br. s, 2F). HRMS calcd. for $C_{26}H_{23}O_4F_{13}SN_2$: 706.1170 Found: 706.1156.

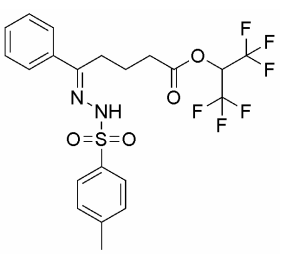

5-Oxo-5-phenyl-pentanoic acid 2,2,2-trifluoro-1-trifluoro methyl-ethyl ester *p*-tosylhydrazone (4.23b):

5-Oxo-5-phenyl-pentanoic acid 2,2,2-trifluoro-1-trifluoro methyl-ethyl ester (**4.22b**) (1.0 g, 2.92 mmol) was dissolved in methanol (17 ml). p-Tosylhydrazide (663 mg, 3.51 mmol, 1.2 eq.) was added and the resulting mixture was refluxed for 18 h. After cooling to RT crystallization commenced and the mixture was put in the refrigerator yielding white powder. Combined yield: 1.162 g (2.28 mmol, 78%). IR (KBr); ν (cm^{-1}): 3235 (s), 2975 (m), 1775 (s), 1599 (m), 1482 (m), 1445 (m), 1404 (m), 1387 (m), 1352 (m), 1337 (m), 1316 (m), 1304 (m), 1275 (s), 1257 (s), 1238 (s), 1193 (s), 1166 (s), 1129 (s), 1107 (s), 1086 (m), 1059 (m), 1028 (m), 978 (m), 937 (m), 907 (w), 860 (w), 815 (w), 781 (w), 763 (w), 745 (w), 962 (m), 674 (m), 617 (w), 590 (w), 557 (w), 529 (w). ^{1}H NMR (DMSO, 200 MHz); δ (ppm): 10.70 (br.s, 1H), 7.75 (d, *J* = 8.1 Hz, 2H), 7.60 – 7.56 (m, 2H), 7.39–7.32 (m, 5H), 6.77 (quintet, *J* = 6.1 Hz, 1H), 2.68–2.61 (m, 4H), 2.33 (s, 3H), 1.63–1.56 (m, 2H). ^{19}F NMR (DMSO, 200 MHz); δ (ppm): –73.75 (d, *J* = 5.6 Hz, 6F). ^{13}C NMR (DMSO, 50 MHz); δ (ppm): 168.69, 153.44, 142.34, 135.11, 135.07, 128.47, 128.39, 127.42, 126.35, 124.94, 122.44,

116.84, 64.8 (m, 1C), 30.97, 24.53, 19.92, 19.67. HRMS calcd. for $C_{21}H_{20}O_4N_2SF_6$: 510.10475, Found: 510.10463.

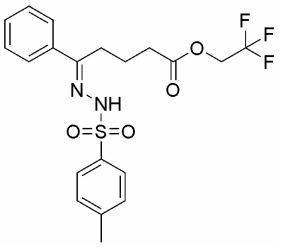

5-Oxo-5-phenyl-pentanoic acid 2,2,2-trifluoro-ethyl ester *p*-tosylhydrazone (4.23c):

5-Oxo-5-phenyl-pentanoic acid 2,2,2-trifluoroethyl ester (**4.22c**) (822 mg, 3.0 mmol) was dissolved in methanol (17 ml). p-tosylhydrazide (670 mg, 3.6 mmol, 1.2 eq.) was added and the resulting mixture was refluxed for 18 h. After cooling to RT no crystallization commenced. The mixture was concentrated to 2/3 rd volume and put in the refrigerator yielding white crystals. Combined yield: 1.12 g (2.53 mmol, 84.5%). IR (KBr); ν (cm^{-1}): 3219 (s), 2966 (m), 1755 (s), 1598 (w), 1483 (w), 1450 (w), 1416 (m), 1385 (m), 1353 (m), 1329 (m), 1306 (m), 1282 (s), 1250 (m), 1162 (s), 1085 (m), 1061 (m), 1025 (m), 978 (m), 940 (m), 855 (m), 816 (m), 786 (m), 771 (m), 700 (m), 672 (m), 637 (m), 624 (m), 615 (m), 571 (m), 551 (m), 528 (w). ^{1}H NMR (DMSO, 200 MHz); δ (ppm): 10.68 (br.s, 1H), 7.75 (d, *J* = 8.1 Hz, 2H), 7.60–7.56 (m, 2H), 7.39–7.31 (m, 5H), 4.70 (quartet, *J* = 9.0 Hz, 2H), 2.69–2.62 (m, 2H), 2.47–2.45 (m, 2H), 2.33 (s, 3H), 1.57 (m, 2H). ^{19}F NMR (DMSO, 200 MHz); δ (ppm): –73.65 (t, *J* = 9.1 Hz, 3F). ^{13}C NMR (DMSO, 50 MHz); δ (ppm): 170.13, 153.72, 142.33, 135.14, 128.47, 128.35, 127.42, 126.37, 125.23, 124.97, 119.71, 58.63 (quartet, *J* = 35.1 Hz, 1C), 31.33, 24.60, 19.93, 19.84. HRMS calcd. for $C_{20}H_{21}O_4N_2SF_3$: 442.11738, Found: 442.11643.

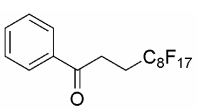

4,4,5,5,6,6,7,7,8,8,9,9,10,10,11,11,11-Heptadecafluoro-phenyl-undecan-1-one (4.27):

A 250 ml three-necked flask equiped with stirring egg, thermometer, condensor (with $CaCl_2$ tube) and dropping funnel, was charged with $AlCl_3$ (1.38 g, 10.35 mmol, 2.6 eq.) and 10 ml benzene (a.g.). The orange suspension was cooled to 0 ^{0}C with ice and stirred for 1 h. Then 4,4,5,5,6,6,7,7,8,8,9,9,10,10,11,11,11-heptadecafluoro-undecanoyl chloride (2.0 g, 3.92 mmol) in benzene (25 ml) was dropped to the solution. Heat and HCl gas formation was observed. The mixture was allowed to warm up to RT and was stirred for 20 h. The resulting black mixture was poored onto ice/water and $CHCl_3$ (50 ml) was added. After all the ice had molten, 25 ml of water and three drops of HCl were added to dissolve all salts. The layers were separated and the aqeous layer was extracted with $CHCl_3$ (2 x 50 ml). The combined organic (orange) layers were washed with water (1 x 50 ml) and brine (2 x 50 ml), dried over Na_2SO_4 and concentrated *in vacuo* yielding a light orange solid (2.45 g). A silica gel column (2 x 10 cm) was prepared with petroleum ether (40:60). Mixture was deposited in $CHCl_3$ and eluted with EtOAc: petroleum ether (40:60) 1:4. An off-white solid was obtained, but not completely pure.

A second silica gel column (2 x 15 cm) with $CHCl_3$. Solid was deposited and eluted with chloroform, obtaining a white powder: 2.14 g (3.88 mmol, 99%). IR (KBr) = ν (cm^{-1}): 3091 (w), 3064 (w), 2965 (w), 2925 (w), 1686 (s), 1649 (w), 1599 (m), 1583 (m), 1450 (s), 1436 (s), 1424 (m), 1372 (m), 1337 (s), 1302 (s), 1202 (s), 1146 (s), 1116 (s), 1099 (s), 1077 (m), 1059 (m), 1001 (s), 979 (s), 953 (m), 926 (m), 873 (w), 853 (w), 800 (w), 744 (s), 721 (w), 705 (s), 689 (s), 658 (s), 620 (w), 576 (m), 560 (m), 530 (m), 478 (w). ^{1}H NMR ($CDCl_3$, 200 MHz); δ (ppm): 8.0 – 7.97 (m, 2H), 7.65–7.45 (m, 3H), 3.36–3.28 (m, 2H), 2.75–2.48 (m, 2H). ^{19}F NMR ($CDCl_3$, 200 MHz); δ (ppm): –82.03 (t, *J* = 10.1 Hz, 3F), –115.2 – –115.39 (m, 2F), –123.02 (br., 6F), –123.86 (br., 2F), –124.55 (br., 2F), –127.24 (br., 2F). ^{13}C NMR ($CDCl_3$, 50 MHz); δ (ppm): 195.44, 132.65, 127.78, 127.02, 28.51, 24.53. HRMS calcd. for $C_{17}H_8OF_{17}$: 551.0303, Found: 551.0294.

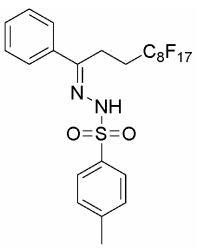

1-Phenyl-4,4,5,5,6,6,7,7,8,8,9,9,10,10,11,11,11-heptadecafluoroundecane-1-tosylhydrazone (4.28):

To a solution of 4,4,5,5,6,6,7,7,8,8,9,9,10,10,11,11,11-heptadecafluoro-phenyl-undecan-1-one (**4.27**) (1.1 g, 2.0 mmol) in toluene (25ml) was added *p*-tosylhydrazide (447 mg, 2.4 mmol, 1.2 eq) and a spatula tip of *p*-toluenesulfonic acid. The mixture was refluxed under Dean-Stark conditions for 19h obtaining a light yellow suspension. The suspension was placed in the refrigerator allowing crystallization to take place. After filtration a white powder (1.06 g) was obtained which was dried on air. The thus obtained powder was recrystallized from methanol. The obtained solid however was not completely pure. Therefore a silica gel column was prepared with chloroform. A sticky white solid was obtained (710 mg, 0.98 mmol, 49%). ^{1}H NMR (DMSO-d_6, 200 MHz); δ (ppm): 10.88 (s, 1H), 7.78 (d, *J* = 8.1Hz, 2H), 7.55 – 7.52 (m, 2H), 7.41 – 7.35 (m, 5H), 3.04–2.96 (m, 2H), 2.35 (br., 5H). ^{19}F NMR (DMSO-d6, 200 MHz); δ (ppm): –81.59 (t, *J* = 9.0 Hz, 3F), –115.15 (br., 2F), –122.90 (br., 6F), –123.72 (br., 2F), –124.12 (br., 2F), –126.94 (br., 2F). HRMS calcd. for $C_{24}H_{17}O_2N_2SF_{17}$: 720.0739, Found: 720.0751.

4.7 References

1. D. M. de Leeuw, C. M. Hart, and M. Matters. USPatent: 6133835. 1999.
2. T. Shimoda, Y. Matsuki, M. Furusawa, T. Aoki, I. Yudasaka, H. Tanaka, H. Iwasawa, D. Wang, M. Miyasaka, and Y. Takeuchi, *Nature*, 2006, **440**, 783.
3. M. Muccini, *Nat.Mater.*, 2006**, 5**, 605.
4. B. Crone, A. Dodabalapur, Y.-Y. Lin, R. W. Filas, Z. Bao, A. LaDuca, R. Sarpeshkar, E. A. Katz, and W. Li, *Nature*, 2000, **403**, 521.

5. A. Facchetti, *Mater.Today*, 2007, **10**, 28.
6. G. H. Gelinck, H. E. A. Huitema, E. van Veenendaal, E. Cantatore, L. Schrijnemakers, J. B. P. H. van der Putten, T. C. T. Geuns, M. Beenhakkers, J. B. Giesbers, B. H. Huisman, E. J. Meijer, E. M. Benito, F. J. Touwslager, A. W. Marsman, B. J. E. van Rens, and D. M. de Leeuw, *Nat.Mater.*, 2004, **3**, 106.
7. H. Sirringhaus, N. Tessler, and R. H. Friend, *Science*, 1998, **280**, 1741.
8. M. M. Ling and Z. Bao, *Chem.Mater.*, 2004, **16**, 4824.
9. A. Knobloch, A. Manuelli, A. Bernds, and W. Clemens, *J.Appl.Phys.*, 2007, **96**, 2286.
10. S. Kobayashi, S. Mori, S. Iida, H. Ando, T. Takenobu, Y. Taguchi, A. Fujiwara, A. Taninaka, H. Shinohara, and Y. Iwasa, *J.Amer.Chem.Soc.*, 2003, **125**, 8116.
11. Th. B. Singh, N. Marjanovic, G. J. Matt, S. Günes, N. S. Sariciftci, A. Montaigne Ramil, A. Andreev, H. Sitter, R. Schwödiauer, and S. Bauer, *Org.Electron.*, 2005, **6**, 105.
12. R. C. Haddon, A. S. Perel, R. C. Morris, T. T. M. Palstra, A. F. Hebard, and R. M. Fleming, *Appl.Phys.Lett.*, 1995, **67**, 121.
13. R. Kumashiro, K. Tanigaki, H. Ohashi, N. Tagmatarchis, H. Kato, H. Shinohara, T. Akasaka, K. Kato, S. Aoyagi, S. Kimura, and M. Takata, *Appl.Phys.Lett.*, 2004, **84**, 2154.
14. K. Shibata, Y. Kubozono, T. Kanbara, T. Hosokawa, A. Fujiwara, Y. Ito, and H. Shinohara, *Appl.Phys.Lett.,* 2004, **84**, 2572.
15. R. C. Haddon, *J.Amer.Chem.Soc.,* 1996, **118**, 3041.
16. T. Kanbara, K. Shibata, S. Fujiki, Y. Kubozono, S. Kashino, T. Urisu, M. Sakai, A. Fujiwara, R. Kumashiro, and K. Tanigaki, *Chem.Phys.Lett.*, 2003, **379**, 223.
17. J. C. Hummelen, B. W. Knight, F. Lepeq, F. Wudl, J. Yao, and C. L. Wilkins, *J.Org.Chem.,* 1995, **60**, 532.
18. M. M. Wienk, J. M. Kroon, W. J. H. Verhees, J. Knol, J. C. Hummelen, P. A. van Hal, and R. A. J. Janssen, *Angew.Chem.Int.Ed.*, 2003, **42**, 3371.
19. T. D. Anthopoulos, C. Tanase, S. Setayesh, E. Meijer, J. C. Hummelen, P. W. M. Blom, and D. M. de Leeuw, *Adv.Mater.*, 2004, **16**, 2174.
20. T. D. Anthopoulos, D. M. de Leeuw, E. Cantatore, S. Setayesh, E. J. Meijer, C. Tanase, J. C. Hummelen, and P. W. M. Blom, *Appl.Phys.Lett.*, 2004, **85**, 4205.
21. T. D. Anthopoulos, D. M. de Leeuw, E. Cantatore, P. van 't Hof, J. Alma, and J. C. Hummelen, *J.Appl.Phys.*, 2005, **98**, 054503.
22. C. Waldauf, P. Schillinsky, M. Perisutti, J. Hauch, and C. J. Brabec, *Adv.Mater.*, 2003, **15**, 2084.
23. C. D. Dimitrakopoulos and P. R. L. Malenfant, *Adv.Mater.*, 2002**,** **14**, 99.
24. K. Takimiya, H. Ebata, K. Sakamoto, T. Izawa, T. Otsubo, and Y. Kunugi, *J.Amer.Chem.Soc.*, 2006, **128**, 12604.
25. J. Veres, S. Ogier, and G. Lloyd, *Chem.Mater.*, 2004, **16**, 4543.
26. M. Heeney, C. Bailey, K. Genevicius, M. Shkunov, D. Sparrowe, S. Tierney, and I. McCulloch, *J.Amer.Chem.Soc.*, 2005, **127**, 1078.

27. H. Sirringhaus, P. J. Brown, R. H. Friend, M. M. Nielsen, K. Bechgaard, B. M. W. Langeveld-Voss, A. J. H. Spiering, R. A. J. Janssen, E. W. Meijer, P. Herwig, and D. M. de Leeuw, *Nature*, 1999, **401**, 685.
28. J.-F. Chang, B. Sun, D. W. Breiby, M. M. Nielsen, T. I. Sölling, M. Giles, I. McCulloch, and H. Sirringhaus, *Chem.Mater.*, 2004, **16**, 4772.
29. R. J. Kline, M. D. McGehee, E. N. Kadnikova, J. Liu, J. M. J. Fréchet, and M. F. Toney, *Macromolecules*, 2005, **38**, 3312.
30. B. S. Ong, Y. Wu, P. Liu, and S. Gardner, *J.Amer.Chem.Soc.*, 2004, **126**, 3378.
31. Z. Bao, A. J. Lovinger, and J. Brown, *J.Amer.Chem.Soc.*, 1998, **120**, 207.
32. J. Zaumseil and H. Sirringhaus, *Chem.Rev.*, 2007, **107**, 1296.
33. E. A. Katz, A. J. Lovinger, J. Johnson, C. Kloc, T. Siegrist, W. Li, Y.-Y. Lin, and A. Dodabalapur, *Nature*, 2000, **404**, 478.
34. B. A. Jones, M. J. Ahrens, M.-H. Yoon, A. Facchetti, T. J. Marks, and M. R. Wasielewski, *Angew.Chem.Int.Ed.*, 2004, **43**, 6363.
35. C. R. Newman, C. D. Frisbie, D. A. da Silva Filho, J. L. Brédas, P. C. Ewbank, and K. R. Mann, *Chem.Mater.*, 2004, **16**, 4436.
36. D. M. de Leeuw, M. M. J. Simenon, A. R. Brown, and R. E. F. Einerhand, *Synth.Met.,* 1997, **87**, 53.
37. T. D. Anthopoulos, G. C. Anyfantis, G. C. Papavassiliou, and D. M. de Leeuw, *Appl.Phys.Lett.*, 2007, **90**, 122105.
38. Y. Kunugi, K. Takimiya, N. O. Negishi, T. Otsubo, and Y. Aso, *J.Mater.Chem.*, 2004, **14**, 2840.
39. E. J. Meijer, D. M. de Leeuw, S. Setayesh, E. van Veenendaal, B. H. Huisman, P. W. M. Blom, J. C. Hummelen, U. Scherf, J. Kadam, and T. M. Klapwijk, *Nat.Mater.*, 2005, **2**, 678.
40. R. J. Chesterfield, C. R. Newman, T. M. Pappenfus, P. C. Ewbank, M. H. Haukaas, K. R. Mann, L. L. Miller, and C. D. Frisbie, *Adv.Mater.*, 2003, **15**, 1278.
41. S. Amriou, A. Metha, and M. R. Bryce, *J.Mater.Chem.,* 2005, **15**, 1232.
42. T. D. Anthopoulos, S. Setayesh, E. Smits, M. Cölle, E. Cantatore, B. de Boer, P. W. M. Blom, and D. M. de Leeuw, *Adv.Mater.*, 2006, **18**, 1900.
43. L. Juha, B. Ehrenberg, S. Couris, E. Koudoumas, S. Leach, V. Hamplova, Z. Pokorna, A. Mullerova, and P. Kubat, *Chem.Phys.Lett.*, 2001, **335**, 539.
44. M. Prato and D. M. Guldi, *Acc.Chem.Res.*, 1998, **31**, 519.
45. K. Shibata, Y. Kubozono, T. Kanbara, T. Hosokawa, A. Fujiwara, Y. Ito, and H. Shinohara, *Appl.Phys.Lett.,* 2004, **84**, 2572.
46. M. T. Rispens, A. Meetsma, R. Rittberger, C. J. Brabec, N. S. Sariciftci, and J. C. Hummelen, *Chem.Commun.,* 2003, 2116.
47. E. J. Meijer, G. H. Gelinck, E. van Veenendaal, B. H. Huisman, D. M. de Leeuw, and T. M. Klapwijk, *Appl.Phys.Lett.*, 2007, **82**, 4576.
48. T. D. Anthopoulos, F. B. Kooistra, P. Wöbkenberg, D. D. C. Bradley, J. C. Hummelen, and D. M. de Leeuw, *Manuscript in Preparation,* 2007.

Chapter 5

Fullerenes for Time-Gated Holographic Imaging

In this Chapter the use of fullerenes in time-gated holographic imaging (TGHI) will be discussed. Two different roles of the fullerene were investigated. First, fullerenes were used as sensitizer materials in conventional organic photorefractive materials for holographic imaging. (meaning: based on hole-transporting molecules/polymers)). We show here that by lowering the LUMO level of the fullerene sensitizer we can enhance the hologram sensitivity and decrease the response time of the hologram. Second, we applied fullerenes with low glass temperatures in inverted photorefractive materials for holographic imaging (meaning: based on electron transporting molecules/polymers). We show that promising holographic properties can be achieved when using fullerenes as the holographic matrix.

*Part of this work was published:

Sebastian Köber, Floris B. Kooistra, Francisco Gallego-Gomez, Michael Salvador, Felix Mielke, Oscar Nuyken, Jan C. Hummelen and Klaus Meerholz. *Submitted for publication.*

Sebastian Köber, Floris B. Kooistra, Francisco Gallego-Gomez, Michael Salvador, Felix Mielke, Oscar Nuyken, Jan C. Hummelen and Klaus Meerholz. *OSA proceedings, 2007, accepted.*

Sebastian Köber, Floris B. Kooistra, Johannes Beerlink, Franceico Gallego-Gomez, Michael Salvador, Felix Mielke, Oscar Nuyken, Jan C. Hummelen and Klaus Meerholz. *Inverted photorefractive materials, to be published.*

5.1 Introduction

As described in section 1.3.3 TGHI offers great potential in the area of non-invasive medical diagnostic tools. A short introduction was given in chapter 1 concerning the basic operating principle of TGHI. In the following paragraphs a more in depth introduction will be given concerning the different materials that make up the total holographic composite.

The work presented in this chapter has been a collaboration between our labs and Sebastian Köber of the labs of Klaus Meerholz at the University of Cologne, Germany.

5.1.1 Photorefractive effect and materials

The photorefractive (PR) effect can be defined as a light induced change of the refractive index. The change is caused by the redistribution of charge carriers in the material by drift and/or diffusion processes.[1] The PR effect was observed for the first time in a $LiNbO_3$ crystal in 1966 by Ashkin et al.[2] A big advantage of the PR effect is that it is reversible because uniform illumination of the material will redistribute the charges. It is therefore possible to write, erase, and rewrite a hologram. A theoretical model for this process in organic materials was first developed by Schildkraut and Buettner[3] and further extended by Ostroverkhova and Singer.[4] The build-up of an internal space-charge field E_{SC} depends on several parameters: photogeneration of charges, charge migration, trapping/detrapping, and recombination. In organic materials all of these parameters are field dependent and they are influenced greatly by the material properties of the composite.

The PR effect has been observed in photorefractive crystals[5] and photorefractive multiple quantum wells.[6] Amorphous PR polymeric materials offer the advantage of easy processability, low costs, and good reproducibility. The first polymeric PR material was reported in 1991. It consisted of a NLO epoxy polymer bisphenol A-diglycidyl ether 4-nitro-1,2-phenylenediamine (bisA-NPDA),[7] which was doped by a hole conducting material, diethylamino-benzaldehyde diphenylhydrazone (DEH).[8] Some typical amorphous high performance PR polymeric materials are shown in figure 5.1. PVK (**5.1**) and PSX (**5.2**) have quite similar charge mobilities. PVK however, has a lower glass temperature (T_g) which allows for less plasticizer in the composite in order to lower the T_g of the entire composite. PPV type polymers have mobilities of several factors higher than PVK, which should lead to a higher PR effect.[1] All of the polymers shown and discussed here are hole transporting materials and are thus used for photorefractive composites. Up until now no organic photorefractive material based on electron transporting materials have

been described in literature that can act in inverted photorefractive materials. In this chapter we will show the first examples of inverted photorefractive materials which can be used for TGHI.

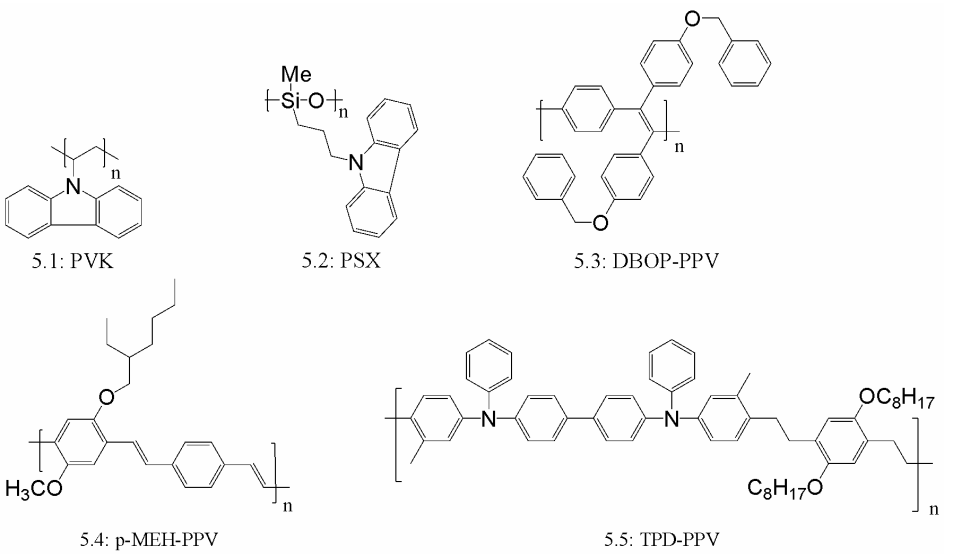

Fig. 5.1: PR polymers. ***5.1****) poly(N-vinylcarbazole) (PVK)*[9] *,* ***5.2****) poly[methyl(3-carbazol-9-ylpropyl)siloxane] (PSX)*[10]*,* ***5.3****) poly[1,4]phenylene-1,2-di(benzyloxyphenyl)vinylene] (DBOP-PPV)*[11]*,* ***5.4****) poly[o(p)-phenylenevinylene-alt-2-methoxy-5-(2-ethylhexyloxy)-p-phenylenevinylene] (p-PMEH-PPV),*[12] ***5.5****) Triphenyldiamine-phenylenevinylene polymer TPD-PPV.*[13,14]

5.1.2 Sensitizers

Although only 1% of the total composite usually consists of a molecular sensitizer, it does play a crucial role in the hologram formation process. The main task of the sensitizer molecule is to absorb at the desired wavelength (in the case of gating, see paragraph 1.3.3.1) and assist in charge photogeneration.[1] Because the interaction of the sensitizer with the charge transporting material will affect the photoconductivity of the composite and thus the temporal evolution of the hologram (see 5.1.1) the choice of sensitizer is of critical importance. The best results are obtained when the charge-transfer properties between the sensitizer and the transporting material are tuned well. Several ways of tuning these materials have been described. It is possible to incorporate sensitizers (metal complexes of phtalocyanines and porphyrins) into polymers.[15-18] Other groups used semiconductor quantum dots like CdS and CdSe as sensitizers.[12,19-23] The most successful sensitizers as of now are molecules that form charge transfer

complexes with the polymeric material and molecules that show efficient photo induced charge transfer (see fig. 5.2). In short, a donor-like material in combination with an acceptor-like material. The most common such sensitizer molecules are C_{60}[24], PCBM[1,11,14], TNF[11] and TNFM[25-27] (see figure 5.2).

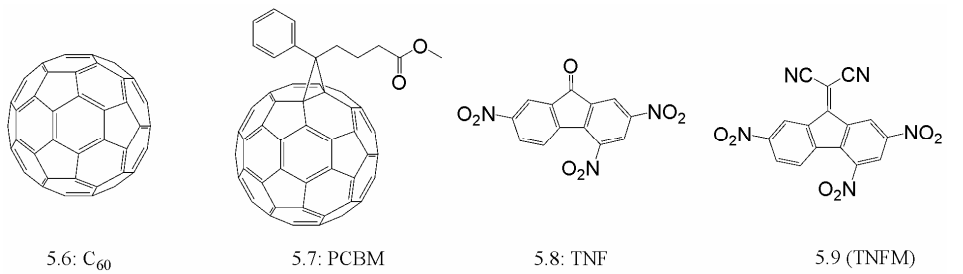

5.6: C_{60} 5.7: PCBM 5.8: TNF 5.9 (TNFM)

*Fig. 5.2: Sensitizers for photorefractive materials: **5.6**) C_{60}, **5.7**) phenyl–C_{61}– butyric acid methyl ester (PCBM), **5.8**) 2,4,7-trinitro-9-fluorenone (TNF), **5.9**) (2,4,7-trinitro-9-fluorenylidene)malononitrile (TNFM).*

When comparing all different sensitizers, fullerene based sensitizers give the best results. This is most likely due to a combination of strong accepting capabilities, thus inducing fast charge transfer with high quantum yield, and the long lifetime of its charged state providing stable traps for electrons. This high stability of its anion is caused by its low reorganization energy. Moreover, fullerenes are excellently compatible to and soluble in non-polar or less polar polymers, which is a critical point in sample preparation. In this chapter different fullerenes as sensitizers are investigated.

5.1.3 NLO Chromophores

The most important role of the NLO chromophores in the composite is to re-orientate according to the induced internal field, thus locally changing the refractive index of the material. It is favorable to have a large concentration of chromophores in the composite to enhance the change in refractive index. However, one must be careful that components of the composite do not undergo phase separation.[28-30] Furthermore it is of importance to tune the ionization potential (I_P) of the chromophore with respect to that of the sensitizer and the charge transporting material, since the chromophore can play a part in absorption, transport and

trapping.[4,9,24,31] Some of the most successful chromophores are shown in figure 5.3 with their names and commonly used abbreviations.

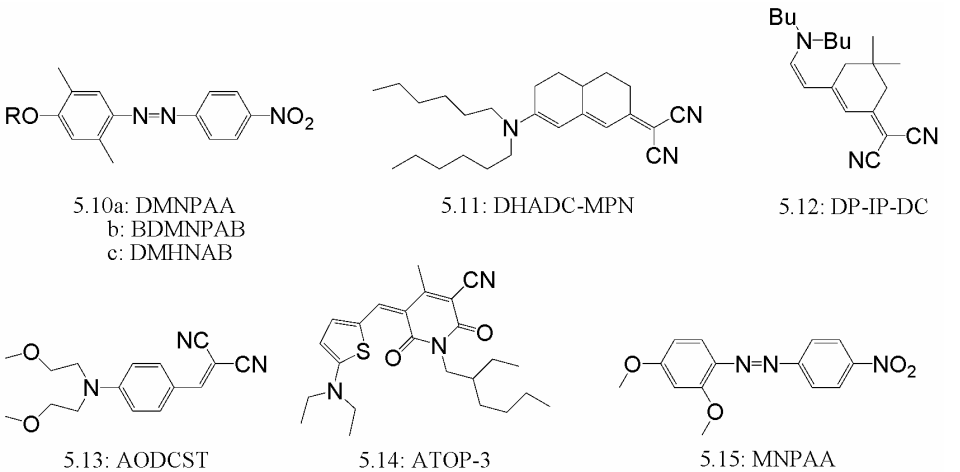

Fig. 5.3:: NLO Chromophores: ***5.10a****) R = CH_3: 2,5-dimethyl-(4-p-nitrophenylazo)anisole (DMNPAA)* ***b****) R = n-C_4H_9: 1-n-butoxy-2,5-dimethyl-(4-p-nitrophenyl-azo)benzene (BDMNPAB)* ***c****) R = CH_2CH_2OH: 2,5-dimethyl-4-(2-hydroxyethoxy)4'-nitro-azobenzene (DMHNAB).* ***5.11****) 2,N,N-dihexylamino-7-dicyanomethylidenyl-3,4,5,6,10-pentahydronaphthalene (DHADC-MPN).* ***5.12****)2-{3-[(E)-2-(dibutyl-amino)ethen-1-yl]-5,5-dimethylcyclohex-2-enylidene}-malononitrile (DP-IP-DC).* ***5.13****) 2-[4-bis(2-methoxyethyl)amino]benzylidene]-malononitrile (AODCST).* ***5.14****) 1-(2-ethylhexyl)-5-[2-diethylaminothienyl)methylene-]-4-methyl-[2,6-dioxy-1,2,5,6-tetrahydropyridine]-3-carbonitrile (ATOP-3).* ***5.15****)3-methoxy-(4-p-nitrophenylazo)anisole (MNPAA).*[1]

5.1.4 Measurement setup

Fig. 5.4 shows the measurement setup. Both two-beam coupling (2BC) and degenerate[I] four wave mixing (DFWM) techniques were used. In 2BC two optical beams are used, a probe beam and a pump beam (both writing beams). Both have a different incident angle and interfere in the holographic material, creating a diffraction grating. One beam will be amplified (energy gain) while the other will be attenuated (energy loss) when diffracted. In DFWM there is an additional beam next to the two writing beams. This third beam (probe, reading beam) is diffracted

[I] All waves have the same frequency

by the grating creating a fourth beam, which is detected. Usually the probe beam is counterpropagating to one of the writing beams and has the same wavelength, which allows for background free detection of weak signals.[1]

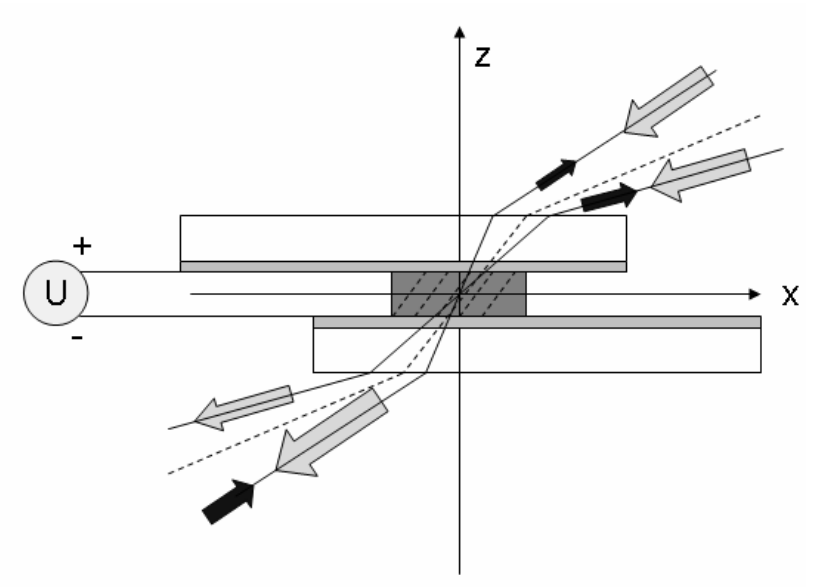

Fig. 5.4: Measurement setup. For 2BC no counterpropagating beam (dark arrow) is used. Picture by Sebastian Köber (University of Cologne).

5.1.5 Research Goal

Investigations on two different systems are described in this chapter. First the influence of the LUMO level of the sensitizer on the response time of the holographic material was studied. We hypothesized that a lower LUMO level would result in faster charge transfer and deeper electron traps which should increase the hologram build up speed. Second, we tried to develop fullerene based materials for inverted photorefractive materials. This means that fullerenes will be used as the matrix material instead of a hole conducting polymer. The difficulty here is the high T_g of fullerenes. We tried to tackle this problem by introducing large alkyl chains.

5.2 Fullerene Sensitizers for TGHI

5.2.1 Synthesis

Fullerenes with different LUMO levels were choosen as sensitizer molecules. Fullerenes are known to be the best sensitizers for photorefractive polymers as of now, as was determined by the Meerholz group in a collaborative effort previously.[13] Besides that, fullerenes allow for chemical modification and thus tunability of their LUMO level. The synthesis of the fullerenes used for this study have been described in detail in Chapter 2 (**5.16**) and 3 (**5.19**, **5.20**) or in literature (**5.17**, **5.18**, **5.21**, **5.22**).[32-34] All the fullerenes used as sensitizers are shown in figure 5.5.

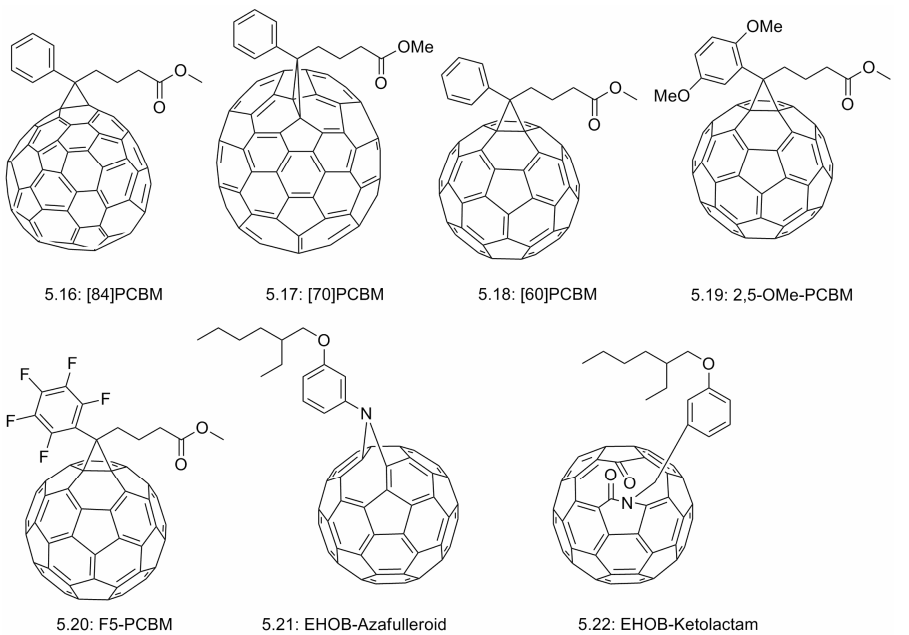

5.16: [84]PCBM 5.17: [70]PCBM 5.18: [60]PCBM 5.19: 2,5-OMe-PCBM

5.20: F5-PCBM 5.21: EHOB-Azafulleroid 5.22: EHOB-Ketolactam

*Fig. 5.5: Fullerene sensitizers. **5.16**) [84]PCBM.[35] **5.17**) [70]PCBM.[34] **5.18**) [60]PCBM.[33] **5.19**) 2,5-OMe-PCBM.[36] **5.20**) F5-PCBM.[36] **5.21**) EHOB-Azafulleroid.[32] **5.22**) EHOB-Ketolactam.[32]*

5.2.2 TGHI measurements

The composite used for measurements consisted for 49 wt.% PF6-TPD, which is a high molecular weight hole conducting polymer. An eutectic mixture (25 wt.% each) of two different NLO chromophores (DMNPAA and MNPAA) was used for the electro-optic response (see figure 5.6). The use of this mixture avoids the formation of crystals in the film.[32,37] Finally 1 wt.% of fullerene sensitizer was added. The thus obtained mixture had a T_g of 6 ^{0}C, rendering the addition of plasticizers unnecessary. The material shows good optical quality and unmatched resistivity towards dielectric breakdown. The chromophores were chosen in such a way that their ionisation potentials are higher than the hole conducting polymer matrix. Therefore they can not form hole traps within the hole conducting matrix, consequently preventing deterioration of the holographic response under prolonged light exposure.[32,38,39]

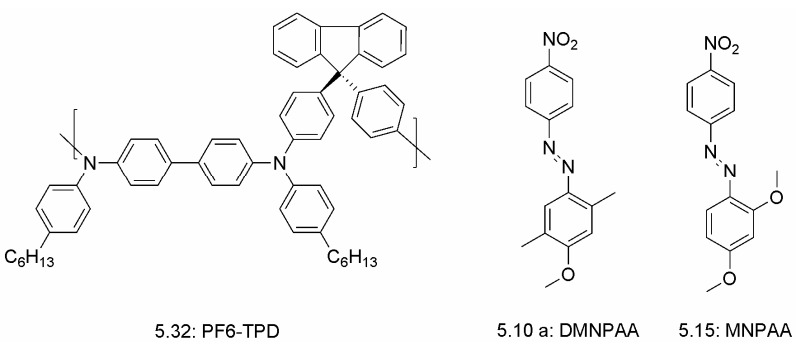

5.32: PF6-TPD 5.10 a: DMNPAA 5.15: MNPAA

Fig. 5.6: Hole-conducting matrix PF6-TPD and electro-optic chromophores DMNPAA and MNPAA.

Both the DFWM and 2BC techniques discussed in section 5.1.4 were applied to follow the temporal evolution of the hologram build-up. All measurements were carried out at 830 nm, I_{ext} = 0.64 W/cm^2 and E_{ext} = 56.6 V/μm applied dc-field. The samples were pre-poled for 60 s at E_{ext} prior to measurements. The PF6-TPD matrix was doped with the different fullerenes as sensitizers which differ greatly in their first reduction potentials. The spectral response is negligable at 830 nm except for [84]PCBM (**5.16**) which shows significant absorption. All discussed parameters and the sensitivities are shown in Table 5.1.

Table 5.1: Sensitizer data

Compound	$E_{1/2}$, red (V)	α_{830} (cm^{-1})	$S_{1\%}$ (cm^2/J)
5.19	–1.106	6	3
5.17	–1.089	5	9
5.18	–1.084	8	6
5.21	–1.058	12	6
5.20	–1.042	6	8
5.22	–0.918	16	10
5.15	–0.730	68	15

First reduction potential $E_{1/2}$, red vs. ferrocene, absorption coefficient α_{830}, For calculation of sensitivity $S_{1\%}$ for 1% external diffraction efficiency see experimental section.

The relation between build-up speed $(1/\tau_{50})$[II] and first reduction potential is plotted in Fig 5.7. The τ_{50} value is defined as the time necessary to build up half the maximum external diffraction efficiency of the hologram. However, one must keep in mind that a much lower external diffraction efficiency (10^{-3} %) is enough for a good CCD to extract information. Therefore, when operating continuously, the CCD extracts information from the hologram before half the maximum external diffraction efficiency is reached. The values presented in figure 5.7 are therefore not the times necessary for the hologram to build up in order to extract enough information. This process is, in fact, much faster and at video rate speeds.[40] The plot clearly shows that the best acceptor ([84]PCBM) induced the fastest response of the holographic material. The true measure of the material performance for technical applications is the sensitivity which is shown in table 5.2.

[II] See experimental: paragraph 5.1.1

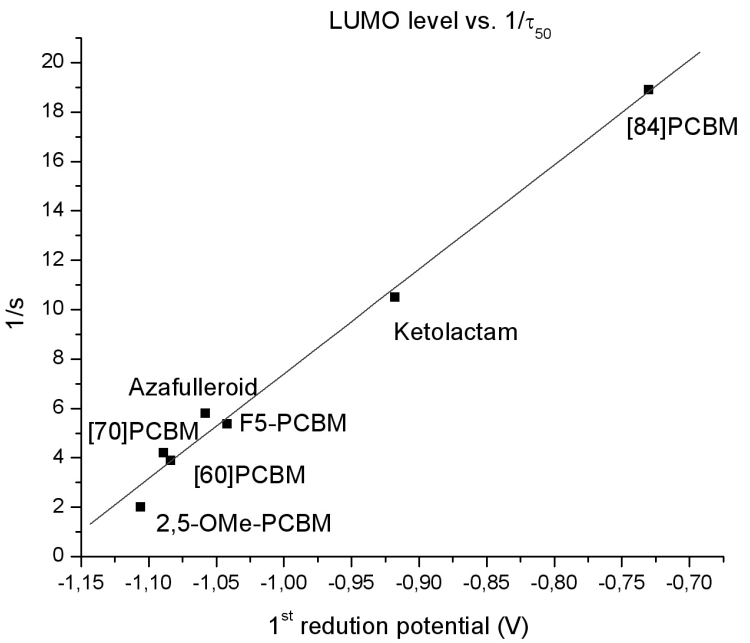

Fig. 5.7: Plot of reduction potential vs $1/\tau_{50}$ for the different fullerene sensitizers. The linear fit is a guide to the eye.

5.2.3 Increased sensitizer content

Usually only 1% wt. of sensitizer is used in the composite. It was investigated whether increasing the sensitizer content would have a favorable effect. Care must be taken however, that there is no electron conduction in the material since electrons have to be trapped in order to create an internal space charge field. Two series of PF6-TPD composites were made, one with [60]PCBM as the sensitizer and one with [84]PCBM as the sensitizer ranging from 1 to 5 wt.%. The increased wt.% of fullerene was subtracted from the wt.% PF6-TPD. No difference in T_g was observed throughout the series and no solubility problems of the fullerenes in the PF6-TPD matrix were encountered. Data extracted from DFWM measurements are shown in Fig. 5.8. In the [60]PCBM series we see an increase in holographic performance when increasing the sensitizer content.

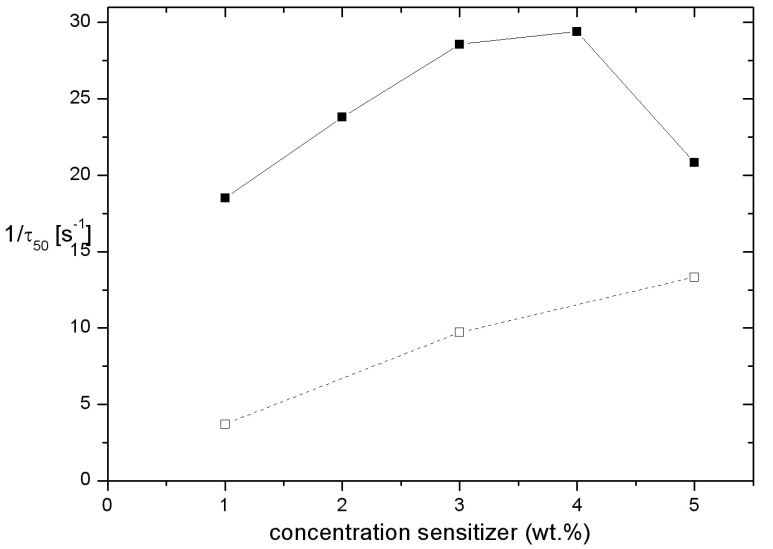

Fig. 5.8: Sensitizer concentration vs hologram build up speed. Closed squares: [84]PCBM, open squares: [60]PCBM

This increase in performance is attributed to a rise in NIR light absorption of the materials with increased sensitizer content, which consequently increases along with the density of charge transfer complexes. In accordance with previously reported data[11,41] it was found in steady state measurements that a decreased applied field is needed to reach the same refractive index modulation, which is most likely caused by an increased electron trap density. The same trend is found for [84]PCBM sensitized composites. However, at 5 wt.% a reduced performance of the holographic composites was observed. The formation of Coulombic hole traps by radical anions of the sensitizers upon illumination hampers the hole transport and thus reduces the composite performance.[41] These findings stress the importance of balancing an increased charge generation with a concomitant increase in recombination. The response time decreases for both series with an increase in sensitizer content with the exception of 5 wt.% [84]PCBM, most likely caused by the strong rise in absorption in this case. The sensitivity increases for the [60]PCBM series but it decreases for [84]PCBM > 2 wt.% This decrease is due to the large increase in absorption of these composites.(seeTable 5.2)

Table 5.2: Data of sensitivity and absorption for different wt.% sensitizer

	α_{830} (cm^{-1})	$S_{1\%}$ (cm^2/J)
[60]PCBM		
1 wt.%	8	6
3 wt.%	9	11
5 wt.%	11	16
[84]PCBM		
1 wt.%	68	15
2 wt.%	110	17
3 wt.%	158	12
4 wt.%	199	9
5 wt.%	258	2

Absorption coefficient α_{830}, Sensitivity $S_{1\%}$, calculated for 1% external diffraction efficiency.

5.2.4 Conclusion

The experiments clearly show a linear relationship between the LUMO level of the sensitizer and the build-up speed of the holographic image. These findings are attributed to more efficient charge separation, deeper electron traps which potentially reduce geminate recombination, and the increased absorption of the sensitizer at 830 nm (for [84]PCBM only). A C_{84} fullerene was incorporated in a photorefractive material for the first time. The incorporation of [84]PCBM instead of the standard [60]PCBM leads to a more than 4–fold increase in the build-up speed. It was furthermore found that an increase in sensitizer content can improve the holographic performance even more, however one must take into account that fullerene anions can act as Coulombic traps for holes which has detrimental effects on the hologram build-up. A maximum performance was found for 4 wt.% [84]PCBM sensitizer.

5.3 Low T_g Fullerenes for inverted photorefractive materials

5.3.1 Synthesis of long tail PCBM analogues

In order to investigate the feasability of reverse phase TGHI, low T_g acceptors were made. First bis-PCBM (**5.23**) was isolated from a crude reaction mixture and purified. This is a side product from the standard preparation of PCBM. Besides a single adduct, higher adducts are formed in the reaction, which are normally discarded. We considered the isomeric mixture of bis-adducts to be of interest for the application described in this chapter and therefore a batch for use in reverse phase TGHI was purified.

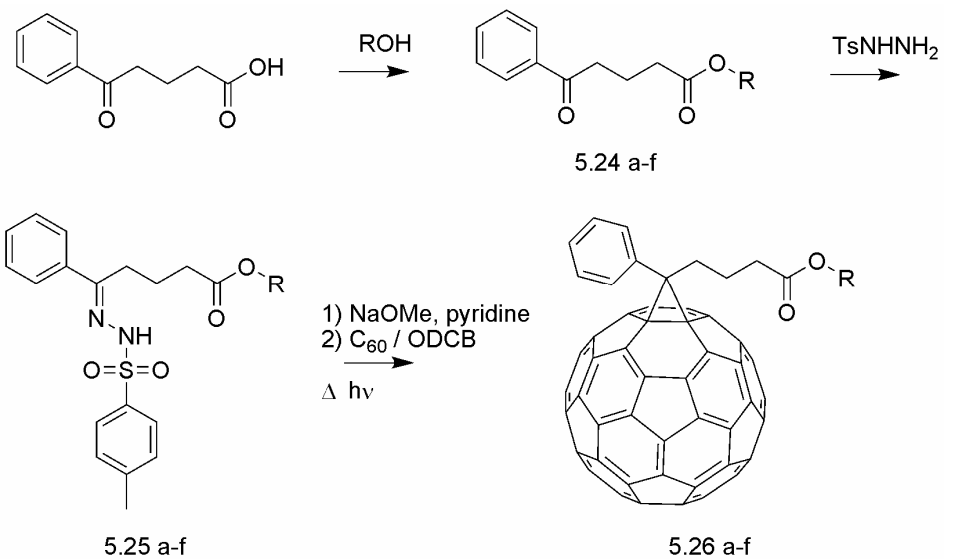

Scheme 5.1:Synthesis of long alkyl chain PCBM analogues. a) R = butyl (PCBB). b) R = hexyl (PCBH). c) R = octyl (PCBO). d) R = decyl (PCBD). e) R = 2-ethylhexyl (PCBMEH). f) R = 2-butyloctyl (PCBBO).

To further induce a lower T_g we choose to increase the length of the ester tail as well as inducing branching of the standard PCBM molecule. A series of different methanofullerenes with increasing ester tail size were synthesized. Esterification of benzoylbutyric acid with the corresponding alcohol yielded the desired keto-esters. The keto functionality underwent a condensation reaction with p-tosylhydrazide obtaining the matching tosylhydrazones. The tosylhydrazones were then

transformed *in situ* to diazo compounds which underwent a 1,3-dipolar addition reaction to C_{60} yielding the final fullerene products.

A second series of 'double' tail PCBM analogues was synthesized in order to increase the 'greasiness' even more. The synthesis was performed parallel to the aforementioned long tail PCBM analogues. The only difference being that the necessary alcohols had to be synthesized. This was done starting from 1,3-dichloro-2-propanol. A Williamson ether synthesis was performed between long chain alcohols and the chloride functionalities. The obtained secondary alcohols were then used for esterification reactions with benzoylbutyric acid. Subsequent tosylhydrazone formation was followed by a 1,3-dipolar addition reaction to C_{60}.

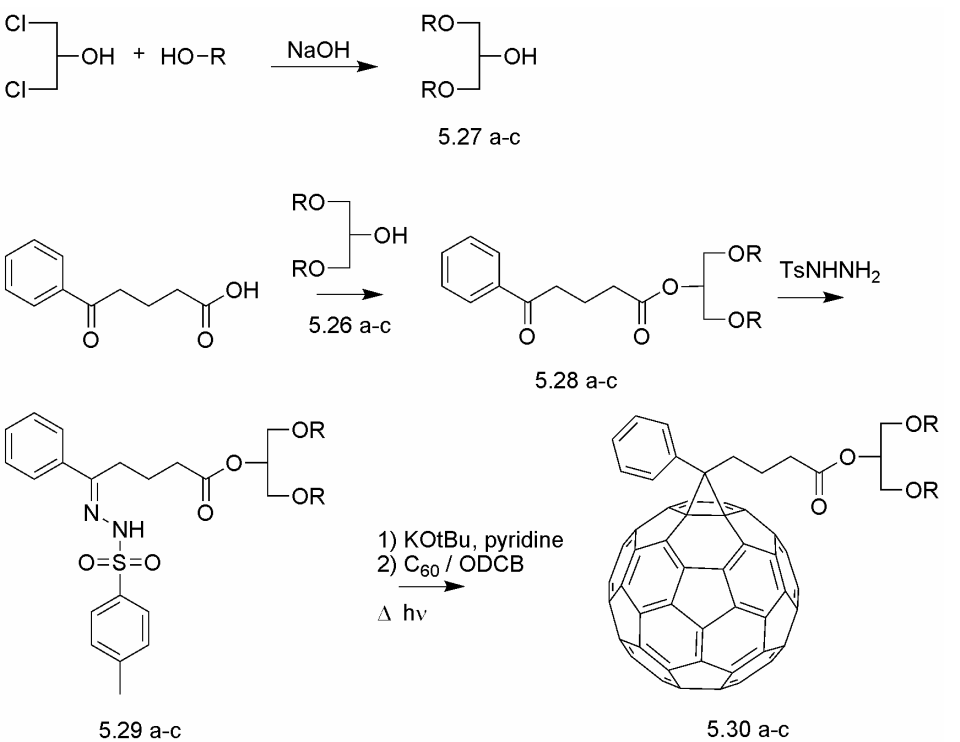

Scheme 5.2: Synthesis of 'double' tail PCBM analogues. a) R = hexyl (PCB-dihexyl). b) R = octyl (PCB-dioctyl). c) R = decyl (PCB-didecyl).

5.3.2 Glass transition temperatures

The glass transition temperatures of the long and double alkyl chain PCBM analogues were measured by differential scanning calorimetry (DSC) measurements. As exptected, the T_g lowers with increasing tail lenghts and branching. The exact values are tabulated in Table 5.3.

Table 5.3: T_g results from DSC measurements.

Compound	Tg (^{0}C)
PCBM (**5.18**)	256.4
Bis-PCBM (**5.23**)	153.0
PCBB (**5.26a**)	88.3
PCBH (**5.26b**)	60.9
PCBMEH (**5.26e**)	56.8
PCBO (**5.26c**)	50.5
PCBBO (**5.26f**)	43.5
PCBD (**5.26d**)	38.2
PCB-dihexyl (**5.30a**)	6.0
PCB-dioctyl (**5.30b**)	4.3
PCB-didecyl (**5.30c**)	–2.3

From these results it is clear that we can vary the T_g of fullerene compounds to a great extent by simply adjusting the chain length and/or branching of the ester moiety. These results allow for more flexibility in the preparation of the photorefractive materials (regarding T_g and composition), which might result in better material durability under application conditions (i.e. high fields).

5.3.3 Photorefractive-composite performance

As a first test, composites consisting of the mixture of bis-PCBM:DMNPAA:MNPAA:TPD (45:25:25:5 wt.%) were fabricated. In this composite the bis-PCBM serves as the electron conducting matrix, DMNPAA and MNPAA as the NLO chromophores, and TPD as the hole trap. The electron conduction can be confirmed by measuring the gain (see figure 5.9), the sign of which depends on the nature of the charge carrier and the applied field direction.

Under identical experimental conditions the gain is always positive under the same biasing conditions. In this case a clear negative sign is obtained, proving that electron conduction is taking place through the matrix.

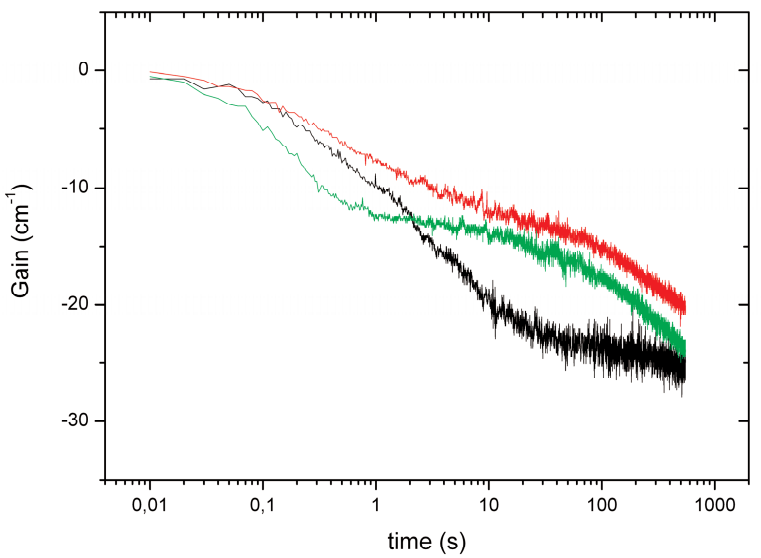

Fig. 5.9: The gain vs. time of a bis-PCBM:DMNPAA:MNPAA:TPD (45:25:25:5 wt.%) composite. Black line: unpreilluminated, red line: gated at 633 nm, green line: gated at 532 nm. For experimental conditions see inset of fig.5.10.

Dynamic measurements after pre-elumination show some interesting effects. (see figure 5.10) That is, a considerable green gating effect. To the best of our knowledge this is the first material in which any considerable green gating is observed. Upon this gating, the temporal response improves nicely. Since fullerenes absorb in this region, this effect is attributed to charge generation in the fullerene matrix. The existence of these charges prior to the measurements increases the build-up speed of the hologram, which is clearly visible since the internal diffraction efficiency increases most rapidly when the sample is pre-illuminated with green light. Please note that an internal diffraction efficiency of 10^{-3} % is sufficient for a good CCD to extract sufficient information. This device is therefore easily capable of operating at video rate.

The material does suffer from a major drawback, which surfaces when the samples are heated to dissolve the chromophores during preparation. The composite is not transparent when the material is heated to 135 ^{0}C due to the formation of

chromophore crystals. These crystals dissolve when the sample is heated to 145 ^{0}C, but upon heating to 145 ^{0}C air bubbles appear in the material, this causes the material not to be field resistive and no measurements can be made. The measurements shown here were done in duplicate from the same sample, which was the only successful sample out of a series of 15.

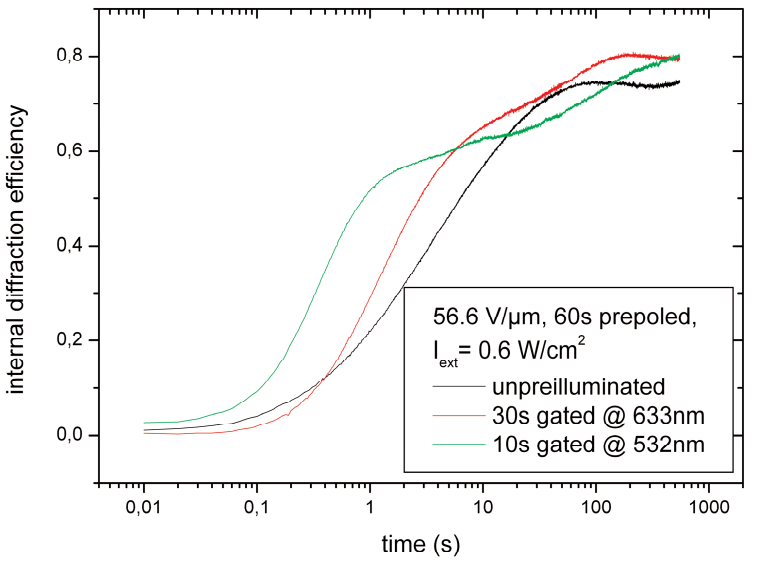

Fig. 5.10: Dynamics of a PCBM:DMNPAA:MNPAA:TPD (45:25:25:5 wt.%) composite. Black (without gating), red (standard gating), green (green light gating).

5.3.4 Conclusions

Although some major problems arise when using bis-PCBM as the electron conducting matrix, some very interesting properties have been observed. First, electron conduction through the matrix was confirmed by measuring the gain, which gives a negative sign. Second, a green-gating effect was observed. This material is the first material showing a green gating effect. These promising results give a first proof of principle that organic inverted photorefractive materials are feasible.

Furthermore, a large library of fullerenes was synthesized with a big variety in T_g. Further measurements with these fullerenes will allow for optimization of material behavior and durability.

5.4 Conclusions

Two different photorefractive materials were investigated in this chapter. We have shown that for conventional photorefractive materials, meaning a hole conducting matrix, the LUMO level of the sensitizer plays a crucial role in the build-up speed of the hologram. A linear relation was found between the LUMO level of the sensitizer and the build-up time of the hologram. This increase in response time is attributed to better accepting capabilities of the sensitizers, deeper electronic traps and increased absorption of the sensitizer at 830 nm (for [84]PCBM). One must be aware though that the increased absorption can also have some detrimental effects.

For the first time a C_{84} derivative was applied in a photorefractive material resulting in a four fold increase in the build-up time of the hologram when compared to the standard C_{60} derivative PCBM.

A proof of principle was given for organic inverted photorefractive materials. The observation of negative gain proofs that electron transport is taking place in the matrix. Furthermore, for the first time, green-gating was observed. Although the material still suffers from some major problems, very promising results were obtained. A library of fullerenes with varying T_g was synthesized and will hopefully allow for further optimization of these materials. These measurements are currently underway.

5.5 Experimental

5.5.1 Holographic setup

All components were dissolved in spectroscopy grade dichloromethane. The solvent was evaporated and the materials homogenized. The composite was sandwiched between two ITO-coated glass sheets with a uniform thickness d of d=106 µm, ensured by glassy spacer beads.

The write beams (830 nm, 40 mW laser diode, s-polarized) illuminated the sample from the positive side of the applied field. The angle of incidence was 50^0 for write beam 1 and 70^0 for write beam 2, with regard to the sample normal. The total write beam intensity was 0.64 W/cm^2.

The index grating was probed by a weak p-polarized read beam (approx. 3 mW/cm^2), counterpropagating with write beam 1, which lead to a transmitted component RB_{trans} counterpropagating write beam 1 and a diffracted component

RB_{diff}, counterpropagating write beam 2, whose intensities were collected additionally to both transmitted write beam intensities by standard Si-photodiodes. The internal diffraction efficiency is given by:

$$\eta_{\text{int}} = \frac{I_{RB_{diff}}}{I_{RB_{trans}} + I_{RB_{diff}}} \tag{1}$$

The gain by (for α_1 and α_2 internal angles of WB_1 and WB_2 respectively) :

$$\Gamma = \frac{1}{d}\left[\cos\alpha_1 \ln\left(\frac{I_{WB_1}(E)}{I_{WB_1}(E=0)}\right) - \cos\alpha_2 \ln\left(\frac{I_{WB_2}(E)}{I_{WB_2}(E=0)}\right)\right] \tag{2}$$

To calculate the sensitivity, one has to consider absorption losses, taken into account by the external diffraction energy given by:

$$\eta_{ext} = \exp\left(-\frac{\alpha d}{\cos\alpha_1}\right)\eta_{\text{int}} \tag{3}$$

With α the absorption coefficient of the composite. The sensitivity is given through:

$$S = \frac{\sqrt{\eta_{ext}(t_{\text{exp}})}}{I_{WB,ext}\, t_{\text{exp}}} \tag{4}$$

with I_{WB} the total intensity of the write beams and $\eta_{exp}(t_{exp})$ the external diffraction efficiency after a certain exposure time t_{exp}. For direct comparison of the dynamic behavior τ_{50} values were considered, which is the time needed for building up half the normalized quasi steady-state diffraction efficiency. Steady-state data was collected after 60s of exposure to write beams.

5.5.2 Absorption measurements

Absorption measurements were carried out on 37 μm thick samples with a Cary Variant Bio 50 spectrometer. The absorption coefficient is given by:

$$\alpha = \ln(10) A / d \tag{5}$$

wherein A is the measured absorbance and d the thickness of the film.

5.5.3 Differential Scanning Calorimetry

The glass transition temperature of the materials was measured by means of Differential Scanning Calorimetry (DSC) by a Mettler Toledo calorimeter, model 821^e, calibrated through the melting-point of Indium. Materials were measured from –50 ^{0}C to 280 ^{0}C, heating rate 20 K/min.

5.5.4 Materials

General method for the ester synthesis (5.24 a-f): A suspension of 4-benzoyl butyric acid (5.0 g, 26 mmol, 1 eq.) in toluene (30 ml) and the corresponding alcohol (30 mmol, 1.15 eq) with 2 drops sulfur acid (H_2SO_4) as catalyst were stirred and refluxed over night. A Dean-Stark trap was used to collect the condensed water. After cooling down to RT the product was dissolved in ethyl acetate (50 ml), washed with 10% sodium carbonate water (Na_2CO_3) (2x50 ml) and with distilled water (3x50 ml). The organic layer was collected, dried over sodium sulfate (Na_2SO_4) and concentrated *in vacuo*. The product was purified by column chromatography over silica gel. Elution with petroleum ether/ ethyl acetate 9:1 yielded pure products.

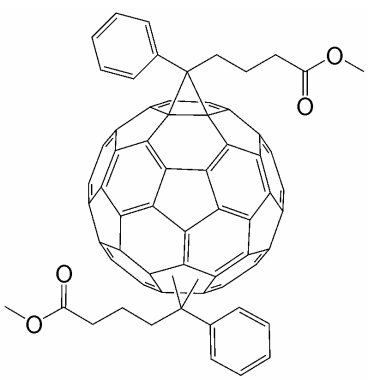

Bis-PCBM (5.23) was obtained as a byproduct from regular PCBM synthesis.[33]

IR (KBr); ν (cm^{-1}): 3450 (s) (H_2O in KBr), 3056 (w), 3025 (w), 2945 (s), 2329 (w) (CO_2), 1737 (s), 1601 (w), 1581 (w), 1538 (w), 1495 (m), 1446 (m), 1433 (m), 1335 (w), 1250 (m), 1194 (m), 1156 (m), 1076 (w), 1026 (w), 1002 (w), 884 (w), 841 (w), 799 (w), 753 (m), 700 (m), 670 (w), 572 (w), 546 (m), 527 (s), 481 (w). ^{1}H NMR ($CDCl_3$, 300 MHz); δ(ppm): 8.15 – 7.19 (broad signals; 10H, phenyl ring), 3.75 – 3.57 (mixture of singlets, 6H, -OCH_3), 3.13 – 2.05 (broad signals, 12H, -CH_2's). ^{13}C NMR ($CDCl_3$, 75 MHz); δ(ppm): 173.47, 149.87, 149.28, 148.94, 148.33, 147.95, 147.84, 147.41, 147.12, 147.04, 146.98, 146.90, 146.75, 146.57, 146.51. 146.38, 146.35, 146.27, 146.18, 146.12, 146.06, 145.99, 145.84, 145.67, 145.60, 145.50, 145.39, 145.26, 145.15, 145.00, 144.92, 144.83, 144.78, 144.68, 144.53, 144.47, 144.39, 144.23, 144.16, 144.05, 143.92, 143.81, 143.64, 143.50, 143.43, 143.35, 143.27, 143.19, 143.13, 142.98, 142.92,

142.77, 142.58, 142.49, 142.14, 142.07, 141.99, 141.90, 141.80, 141.67, 141.60, 141.44, 141.36, 141.14, 141.07, 140.92, 140.88,140.80, 140.67, 140.62, 140.59, 140.42, 140.13, 138.98, 138.11, 137.74, 137.46, 137.35, 137.20, 137.04, 136.81, 136.60, 136.47, 136.44, 132.27, 132.01, 131.94, 131.91, 131.77, 131.70, 131.49, 131.39, 130.50, 128.53, 128.37, 128.24, 128.08, 128.01, 127.90, 127.69, 80.53, 80.48, 80.22, 79.80, 79.74, 79.27, 78.89, 78.78, 78.62, 78.42, 78.18, 77.21, 53.66, 53.41, 51.62, 50.88, 50.83, 50.78, 50.67, 50.52, 49.26, 49.20, 49.13, 49.07, 48.99, 48.91, 34.23, 34.03, 33.87, 33.81, 33.76, 33.52, 33.21, 33.11, 22.46, 22.38, 22.24, 22.16, 22.07. MALDI-TOF m/z: 1100.

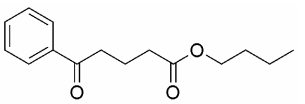

4-benzoylbutyric acid 1-butyl ester (5.24 a):

Yield: 87.9 % of a yellow oil. IR (KBr) = ν (cm^{-1}): 3061 (s), 2960 (w), 2873 (m), 1732 (w), 1687 (w), 1598 (s), 1449 (m), 1372 (s), 1069 (s), 1206 (m), 1002 (s), 748 (s), 691 (m). ^{1}H NMR ($CDCl_3$, 200 MHz); δ (ppm): 7.92 (d, *J* = 7.1 Hz, 2H), 7.41 – 7.52 (m, 3H), 4.05 (t, *J* = 6.6 Hz, 2H), 3.02 (t, *J* = 7.1 Hz, 2H), 2.40 (t, *J* = 7.1 Hz, 2H), 2.05 (quart., *J* = 7.7 Hz, 2H), 1.50 – 1.60 (m, 2H), 1.28 – 1.39 (m, 2H), 0.88 (t, *J* = 7.1 Hz, 3H). ^{13}C NMR ($CDCl_3$, 50 MHz); δ (ppm):199.2, 173.2, 136.7, 132.9, 128.4, 127.9, 64.1, 33.3, 30.5, 19.3, 19.0, 13.6. HRMS: Calcd. for: $C_{15}H_{20}O_3$: 248.14123. Found: 248.14436.

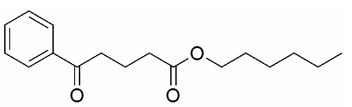

4-benzoylbutyric acid 1-hexyl ester (5.24 b):

Yield 87.1 % of a yellow oil. IR (KBr); ν (cm^{-1}): 2956 (m), 2859 (s), 1733 (w), 1687 (w), 1598 (s), 1449 (m), 1373 (s), 1211 (m), 1001 (s), 747 (s), 691 (m). ^{1}H NMR ($CDCl_3$, 200 MHz); δ (ppm): 7.93 (d, *J* = 8.3 Hz, 2H), 7.37 – 7.57 (m, 3H), 4.05 (t, *J* = 6.9 Hz, 2H), 3.03 (t, *J* = 7.1 Hz, 2H), 2.41 (t, *J* = 7.1 Hz, 2H),1.91 – 2.11 (m, 2H), 1.52 – 1.61 (m, 2H), 1.19 – 1.34 (m, 6H), 0.82 – 0.88 (m, 3H). ^{13}C NMR ($CDCl_3$, 50 MHz); δ (ppm): 199.3, 179.2, 136.7, 132.9, 128.5, 127.9, 64.5, 37.4, 33.3, 31.3, 28.50 25.5, 22.4, 19.3, 13.8. HRMS: Calcd. for: $C_{17}H_{24}O_3$: 276.17253. Found: 276.17408.

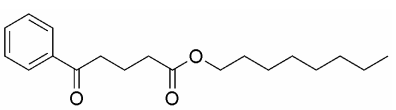

4-benzoylbutyric acid 1-octyl ester (5.24 c):.

Yield: 77.2 % of a yellow oil. IR (KBr); ν (cm^{-1}): 2928 (w), 2856 (m), 1733 (w), 1687 (w), 1598 (s), 1449 (m), 1372 (s), 1208 (m), 1002 (s), 747 (s), 690 (m). ^{1}H NMR ($CDCl_3$, 200 MHz); δ (ppm): 7.96 (d, *J* = 7.1 Hz, 2H), 7.40 – 7.59 (m, 3H), 4.06 (t, *J* = 6.1 Hz, 2H), 3.05 (t, *J* = 7.0 Hz, 2H), 2.43 (t, *J* = 7.1 Hz, 2H), 1.99 – 2.14 (m, 2H), 1.60–1.73 (m, 2H), 1.25 – 1.27 (m, 10H), 0.83 – 0.90 (m, 3H).

^{13}C NMR ($CDCl_3$, 50 MHz); δ (ppm): 199.2, 173.2, 136.7, 132.9, 128.4, 127.9, 64.5, 37.3, 33.3, 31.6, 29.1, 29.0, 28.5, 25.8, 22.5, 19.3, 14.0. HRMS: Calcd. for: $C_{19}H_{28}O_3$: 304.20383. Found: 304.20352.

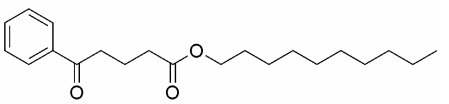

4-benzoylbutyric acid 1-decyl ester (5.24 d):

Yield 74.3 % of a yellow oil. IR (KBr); ν (cm^{-1}): 2925 (w), 2845 (w), 1733 (w), 1688 (w), 1598 (m), 1581 (s), 1449 (w), 1413 (s), 1372 s), 1209 (w), 1179 (w), 1073 (s), 1001 (m), 747 (m), 690 (m). ^{1}H NMR ($CDCl_3$, 200 MHz); δ (ppm): 7.96 (d, *J* = 7.3 Hz, 2H), 7.43 – 7.55 (m, 3H), 4.07 (t, *J* = 6.8 Hz, 2H), 3.05 (t, *J* = 7.1 Hz, 2H), 2.43 (t, *J* = 7.1 Hz, 2H), 2.05 – 2.09 (m, 2H), 1.61 (t, *J* = 6.9 Hz, 2H), 1.25 - 1.29 (m, 14H), 0.85 – 0.82 (m, 3H). ^{13}C NMR ($CDCl_3$, 50 MHz); δ (ppm): 198.4, 172.3,135.9, 132.0, 127.6, 127.0, 63.6, 63.5. 32.4. 30.9. 28.5. 27.6. 24.9. 21.6. 18.4. 13.1. HRMS: Calcd. for: $C_{21}H_{32}O_3$: 332.23513. Found: 332.23339.

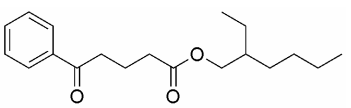

(2-ethyl)-1-hexyl-4-benzoylbutyrate (5.24 e):

Yield 93%. IR (neat); ν (cm^{-1}): 2959, 2930, 2872, 2861, 1731, 1688, 1598, 1580, 1449, 1414, 1377, 1310, 1276, 1230, 1208, 1178, 1156, 1001, 875, 749, 691, 568. ^{1}H NMR ($CDCl_3$, 300 MHz); δ (ppm): 7.95 (d, *J* = 7.2 Hz, 2H), 7.55 (t, *J* = 7.2 Hz, 1H), 7.45 (t, *J* = 7.2 Hz, 2H), 4.00 (d, *J* = 6.0 Hz, 2H), 3.06 (t, *J* = 7.2 Hz, 2H), 2.44 (t, *J* = 7.2 Hz, 2H), 2.07 (q, *J* = 6.3 Hz, 2H), 1.58 (m, 1H), 1.32 (m, 8H), 0.87 (t, *J* = 7.2 Hz, 6H). ^{13}C NMR ($CDCl_3$, 75 MHz); δ (ppm): 198.9, 173.1, 136.6, 132.7, 128.3, 127.7, 66.5, 38.5, 37.1, 33.1, 30.1, 28.6, 23.5, 22.7, 19.5, 13.8, 10.7. HRMS calcd. for $C_{19}H_{28}O_3$: 304.2038 Found: 304.2028. Elemental Analysis calcd. for $C_{19}H_{28}O_3$: C: 74.96 % H: 9.27 %. Found: C: 75.00 % H: 9.22 %.

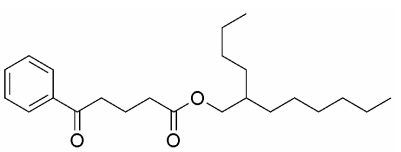

4-benzoylbutyric acid 2-butyl-1-octyl ester (5.24 f):

Yield 96.8 % of a yellow oil. IR (KBr); ν (cm^{-1}): 2928 (w), 2857 (w), 1734 (w), 1688 (w), 1598 (s), 1449 (m), 1376 (s), 1208 (w), 1052 (s), 1002 (m), 747 (m), 690 (m). ^{1}H NMR ($CDCl_3$, 200 MHz); δ (ppm): 7.93 – 7.98 (m, 2H), 7.40 – 7.55 (m, 3H), 3.98 (d, *J* = 6.1 Hz, 2H), 3.05 (t, *J* = 7.1 Hz, 2H), 2.42 (t, *J* = 7.1 Hz, 2H), 2.03 – 2.10 (m, 2H), 1.25 (m, 17 H), 0.83 – 0.88 (m, 6H). ^{13}C NMR ($CDCl_3$, 50 MHz); δ (ppm): 199.3, 173.4, 136.8, 133.0, 128.5, 128.0, 67.2, 37.5, 37.3, 33.4, 31.8, 31.2, 30.9, 29.6, 28.9, 26.6, 22.9, 22.6, 19.9, 14.0. HRMS: Calcd. for: $C_{23}H_{36}O_3$: 360.26643. Found: 360.26505.

General method for tosylhydrazone synthesis (5.25 a-f): A round bottom flask was charged with the ester (**5.24 a-f**), *p*-tosylhydrazide (1.2 eq) and absolute ethanol (1g ester / 25 ml). The resulting solution was refluxed over night, concentrated to 25% volume and purified by column chromatography over silica gel.

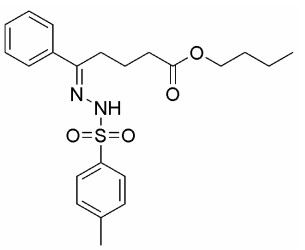

Butyl-4-benzoylbutyrate *p*-tosylhydrazone (5.25 a):

Elution with petrol ether/ ethyl acetate 4:1. Yield 59.1 % of a light yellow solid (E/Z 4:1). IR (KBr); ν (cm^{-1}): 3429 (s), 3211 (w), 2954 (w), 2871 (w), 1927 (s), 1725 (w), 1597 (m), 1384 (s), 1330 (s), 1258 (s), 1165 (m), 1059 (m), 1019 (s), 934 (m), 855 (s), 815 (s), 768 (m), 661 (m), 623 (s), 550 (m). ^{1}H NMR (E isomer) ($CDCl_3$, 200 MHz); δ (ppm): 9.32 (s, 1H), 7.91 (d, *J* = 8.1 Hz, 2H), 7.62 – 7.67 (m, 2H), 7.26 – 7.34 (m, 5H), 4.18 (t, *J* = 6.7 Hz, 2H), 2.63 (t, *J* = 8.1 Hz, 2H), 2.24 – 2.44 (m, 5H), 1.57 – 1.74 (m, 4H), 1.33 – 1.44 (m, 2H), 0.94 (t, *J* = 6.6 Hz, 3H). ^{13}C NMR (E/Z mixture) ($CDCl_3$, 50 MHz); δ (ppm): 174.4, 153.6, 143.6, 136.1, 136.0, 129.9, 129.6, 129.5, 129.4, 128.4, 127.9, 126.6, 126.2, 65.2, 64.2, 37.2, 33.2, 32.2, 30.5, 25.8, 25.5, 21.5, 21.2, 20.9, 19.0 13.7. HRMS: Calcd. for: $C_{22}H_{28}N_2O_4S$: 416.17695. Found: 416.17834. Melting point: 122–124 °C

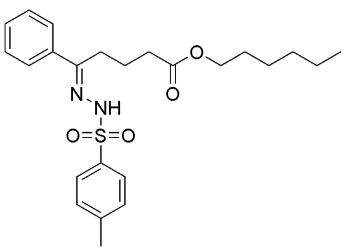

Hexyl-4-benzoylbutyrate *p*-tosylhydrazone (5.25 b):

Elution with petrol ether/ ethyl acetate 9:2 (Z isomer). Yield 87.3 % of yellow precipitate. IR (KBr);ν (cm^{-1}): 3149 (w), 2959 (w), 2918 (w), 1740 (w), 1597 (m), 1421 (s), 1327 (s), 1234 (s), 1167 (m), 1084 (m), 1018 (s), 985 (s), 937 (s), 812 (m), 778 (m), 759 (m), 667 (m), 615 (s), 549 (m). ^{1}H NMR ($CDCl_3$, 200 MHz); δ (ppm): 9.30 (s, 1H), 7.91 (d, J = 8.2 Hz, 2H), 7.62 – 7.67 (m, 2H), 7.31 – 7.37 (m, 5H), 4.20 (t, *J* = 7.2 Hz, 2H), 2.63 (t, *J* = 8.1 Hz, 2H), 2.40 (s, 3H), 2.30 (t, *J* = 6.0 Hz, 2H), 1.57 – 1.66 (m, 4H), 1.22 – 1.32 (m, 6H), 0.87 – 0.94 (m, 3H). ^{13}C NMR ($CDCl_3$, 50 MHz); δ (ppm): 174.52, 153.49, 143.61, 136.17, 136.08, 129.42, 128.38, 127.91, 126.65, 126.16, 65.57, 64.54, 32.19, 31.39, 28.50, 25.82, 25.51, 22.60, 21.55, 20.96, 13.97. HRMS: Calcd. for: $C_{24}H_{32}N_2O_4S$: 444.20825. Found: 444.21015. Melting point: 74–78 °C.

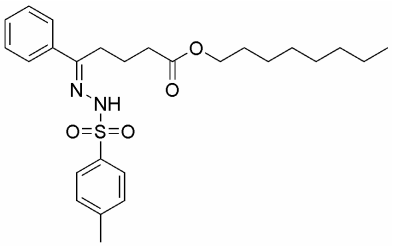

Octyl-4-benzoylbutyrate *p*-tosylhydrazone (5.25 c):

Elution with petrol ether/ ethyl acetate 9:2. Yield 76.6 % of yellow precipitate (Z isomer). IR (KBr); ν (cm^{-1}): 3135 (l), 2921 (w), 2853 (w), 1699 (w), 1598 (m), 1479 (s), 1417 (s), 1395 (s), 1354 (s), 1162 (m), 1083 (m), 1021 (s), 986 (s), 940 (s), 814 (m), 765 (m), 705 (m), 670 (m), 615 (s), 551 (m), 528 (s). ^{1}H NMR ($CDCl_3$, 200 MHz); δ (ppm):, 9.31 (s, 1H), 7.91 (d, *J* = 8.3 Hz, 2H), 7.62 – 7.67 (m, 2H), 7.26 – 7.35 (m, 5H), 4.10 – 4.22 (m, 2H), 2.61 (t, *J* = 8.1 Hz, 2H), 2.27 – 2.44 (m, 5H), 1.66 (m, 4H), 1.22 – 1.29 (m, 10H), 0.88 – 0.91 (m, 3H). ^{13}C NMR ($CDCl_3$, 50 MHz); δ (ppm): 174.6, 153.5, 143.6, 136.1, 129.9, 129.5, 129.4, 128.4, 127.9, 126.6, 126.1, 65.5, 64.5, 60.3, 37.2, 33.2, 32.2, 31.7, 29.1, 28.5, 25.8, 22.6, 21.5, 21.2, 21.0, 14.2, 14.0. HRMS calcd for $C_{26}H_{36}O_4N_2S$: 472.2396, Found: 472.2413. Melting point: 62.8–63.3 °C.

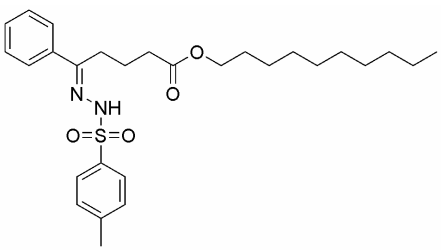

Decyl-4-benzoylbutyrate *p*-tosylhydrazone (5.25 d):

Elution with petrol ether/ ethyl acetate 9:2. Yield 93.8 % of yellow precipitate (E isomer). IR (KBr); ν (cm^{-1}): 3135 (w), 2921 (w), 2853 (w), 1699 (w), 1598 (m), 1479 (s), 1417 (s), 1395 (s), 1354 (s), 1162 (m), 1083 (m), 1021 (s), 986 (s), 940 (s), 814 (m), 765 (m), 705 (m), 670 (m), 615 (s), 551 (m), 528 (s). ^{1}H NMR ($CDCl_3$, 200 MHz); δ (ppm): 9.30 (s, 1H), 7.92 (d, *J* = 8.2 Hz, 2H), 7.62 – 7.67 (m, 2H), 7.27 – 7.35 (m, 5H), 4.10 – 4.23 (m, 2H), 2.62 (t, *J* = 8.1 Hz, 2H), 2.27 – 2.40 (m, 5H), 1.66 (m, 4H), 1.22 – 1.27 (m, 14H), 0.85 – 0.88 (m, 3H). ^{13}C NMR ($CDCl_3$, 50 MHz); δ (ppm): 174.5, 153.5, 143.6, 136.3, 129.5, 129.4, 128.4, 127.9, 126.7, 126.2, 65.6, 64.6, 37.2, 33.3, 32.2, 31.9, 29.5, 29.2, 28.6, 25.9, 22.8, 21.6, 21.2, 21.0, 14.1. HRMS calcd for $C_{28}H_{40}O_4N_2S$: 500.2708, Found: 500.2694. Melting point: 63.6–66.6°C

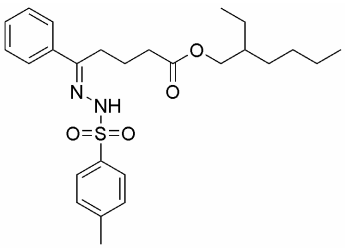

(2-ethyl)-1-hexyl-4-benzoylbutyrate *p*-tosylhydrazone (5.25 e):

Elution with chloroform. Yield 95% of a light yellow solid (E/Z 8:1). IR (neat); ν (cm^{-1}): 3213, 3064, 2958, 2930, 2872, 1729, 1709, 1597, 1462, 1393, 1350, 1329, 1306, 1218, 1184, 1168, 1085, 813, 758, 694, 668, 550. ^{1}H NMR (E isomer) ($CDCl_3$, 300 MHz); δ (ppm): 9.33 (s, 1H), 7.90 (d, *J* = 8.1 Hz, 2H), 7.64 (m, 2H), 7.34 (m, 3H), 7.29 (d, *J* = 8.1 Hz, 2H), 4.11 (d, *J* = 5.7 Hz, 2H), 2.62 (m, 2H), 2.39 (s, 3H), 2.29 (t, *J* = 6.0 Hz, 2H), 1.67 (m, 2H), 1.62 (m, 1H), 1.38 (m, 8H), 0.92 (t, *J* = 7.2 Hz, 6H). ^{13}C NMR (E isomer) ($CDCl_3$, 75 MHz); δ (ppm): 174.5, 153.7, 143.5, 136.0, 135.9, 129.3, 129.2, 128.2, 127.7, 126.0, 67.5, 38.5, 32.5, 28.7, 23.6, 22.8, 21.4, 21.1, 13.9, 10.8. HRMS calcd. for $C_{19}H_{28}O_3$: 472.2395 Found: 472.2406.

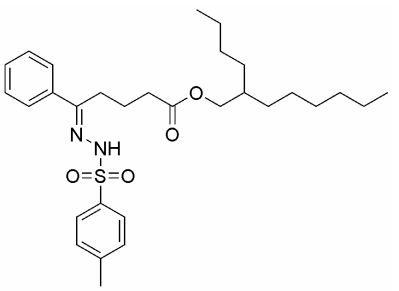

2-butyl-1-octyl-4-benzoylbutyrate *p*-tosylhydrazone (5.25 f):

Elution with petrol ether/ ethyl acetate 9:2. Yield 55.7% of a light yellow wax-like solid as a E/Z mixture (3:1). IR (KBr); ν (cm^{-1}): 3212 (m), 3064 (s), 2928 (w), 2857 (w), 1731 (w), 1598 (m), 1467 (s), 1393 (s), 1352 (s), 1169 (m), 1085 (m), 983 (s), 930 (s), 814 (m), 767 (s), 668 (m), 613 (s), 550 (m). ^{1}H NMR (E isomer) ($CDCl_3$, 200 MHz); δ (ppm):,9.23 (s, 1H), 7.86 (d, *J* = 8.0 Hz, 2H), 7.58 – 7.61 (m, 2H), 7.21 – 7.29 (m, 5H), 4.05 (d, *J* = 5.9 Hz, 2H), 2.55 – 2.60 (t, *J* = 8.1 Hz, 2H), 2.34 (s, 3H), 2.18 – 2.27 (m, 2H), 1.60 – 1.62 (m, 2H), 1.18 – 1.24 (m, 17H), 0.76 – 0.85 (m, 6H). ^{13}C NMR (E/Z mixture) ($CDCl_3$, 50 MHz); δ (ppm): 174.7, 153.5, 143.6, 136.2, 129.5, 129.4, 128.4, 127.9, 126.7, 126.2, 68.3, 67.17, 67.21, 37.2, 33.6, 32.2, 31.8, 31.2, 30.8, 29.6, 28.9, 26.6, 25.8, 23.0, 2.6, 21.6, 21.3, 21.0, 14.1, 14.0. HRMS calcd for $C_{30}H_{44}O_4N_2S$: 528.3021, Found: 528.3019.

General method for dipolar addition reaction to C_{60} (5.26 a-f): A flame-dried three-necked flask, equipped with, stirring egg, N_2-inlet, condensor and thermometer, was charged with tosylhydrazone (**5.25 a-f**, 1.07eq.), NaOMe (1.1 eq.) and dry pyridine (30 mg/ml; tosylhydrazone/pyridine). The resulting mixture was stirred for 45 minutes, resulting in a yellowish clear solution. To this solution was added a solution of C_{60} (1 eq.) in ODCB (~10 mg/ml; C_{60}/ODCB). The resulting solution was degassed by N_2/vacuum purges (3x). The reaction mixture was rapidly heated to ~90 ^{0}C, after which irradiation with a 400 W Na lamp was started. The reaction was followed by HPLC and stopped when about 50 % mono-adduct was formed. The reaction mixture was then concentrated to 25% volume and purified by column chromatography over silica gel. Elution was started with CS_2 to obtain unreacted C_{60}. Elution was then continued with cyclohexane/toluene

mixtures (indicated for each fullerene) to obtain pure mono-adduct. The obtained pure fractions were concentrated *in vacuo* and redissolved in a minimal amount of ODCB, precipitated with methanol and centrifuged. The thus obtained brown pellets were washed with methanol (2x), dried *in vacuo* at 50 ^{0}C, washed again with pentane and once more with methanol before being dried again *in vacuo* at 50 ^{0}C, yielding a brown powder.

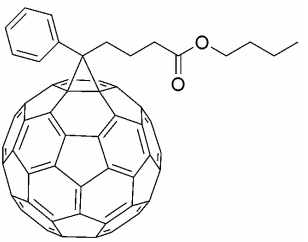

Phenyl–C_{61}–butyric acid butyl ester (PCBB, **5.26 a):** Elution with toluene/cyclohexane 1:2 yielded mono-adduct (51.3%). IR (KBr); ν (cm^{-1}): 3025 (s), 2955 (w), 2867 (m), 2328 (m), 1733 (w), 1600 (s), 1539 (s), 1494 (s), 1428 (m), 1249 (m), 1186 (m), 1074 (s), 964 (s), 755 (m), 698 (m), 573 (m), 526 (w), 481 (m). ^{1}H NMR ($CDCl_3$, 400 MHz), δ (ppm): 7.93 (d, *J* = 7.1 Hz, 2H), 7.47–7.57 (m, 3H), 4.08 (t, *J* = 6.6 Hz, 2H), 2.91 (t, *J* = 8.0 Hz, 2H), 2.51 (t, *J* = 7.5 Hz, 2H), 2.16 – 2.20 (m, 2H), 1.56 – 1.62 (m, 2H), 1.33 – 1.37 (m, 2H), 0.91 – 0.95 (m, 3H). ^{13}C NMR ($CDCl_3$, 100 MHz), δ (ppm): 173.1, 148.8, 147.8, 145.8, 145.1, 145.1, 145.0, 145.0, 144.7, 144.64, 144,61, 144.5, 144.4, 143.9, 143.7, 143.1, 143.0, 142.9, 142.2, 142.1, 142.08, 140.9, 140.7, 138.0, 137.5, 136.7, 132.1, 128.4, 128.2, 79.8, 64.5, 51.9, 34.1, 30.6, 22.4, 19.2, 13.8. Elemental analysis: Calcd. for $C_{75}H_{20}O_2$: C: 94.52 %, H: 2.12 %. Found C: 94.65 %, H: 2.09 %.

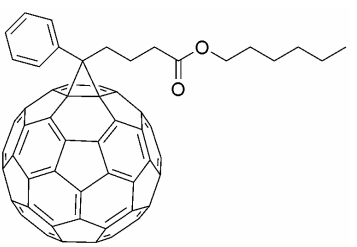

Phenyl–C_{61}–butyric acid hexyl ester (PCBH, **5.26 b):**

Elution with toluene/cyclohexane 1:2 yielded mono-adduct (44.1%). IR (KBr); ν (cm^{-1}): 3025 (s), 2951 (w), 2854 (m), 2328 (m), 1733 (w), 1600 (s), 1539 (s), 1494 (s), 1463 (m), 1248 (m), 1187 (m), 1076 (s), 891 (s), 742 (m), 705 (m), 573 (m), 526 (w), 480 (m). ^{1}H NMR ($CDCl_3$, 400 MHz), δ (ppm): 7.93 (d, *J* = 7.1 Hz, 2H), 7.47 – 7.57 (m, 3H), 4.07 (t, *J* = 7.2 Hz, 2H), 2.92 (t, *J* = 8.2 Hz, 2H), 2.51 (t, *J* = 7.3 Hz, 2H), 2.18 – 2.21 (m, 2H), 1.55 – 1.61 (m, 2H), 1.30 (m, 6H), 0.87 – 0.91 (m, 3H). ^{13}C NMR ($CDCl_3$, 100 MHz), δ (ppm): 173.1, 148.8, 147.8, 145.8, 145.2, 145.1, 145.6, 145.0, 144.8, 144.7, 144.5, 144.4, 144.0, 143.7, 143.1, 143.0, 142.96, 142.9, 142.2, 142.14, 142.10, 141.0, 140.7, 138.0, 137.5, 136.7, 132.1, 128.4, 128.2, 79.9, 64.8, 51.9, 34.1, 33.7, 31.4, 28.6, 25.6, 22.6, 22.4, 14.0. Elemental Analysis: Calcd. for: $C_{77}H_{24}O_2$: C: 94.27 %, H: 2.47 %. Found: C: 94.20 %, H: 2.44 %.

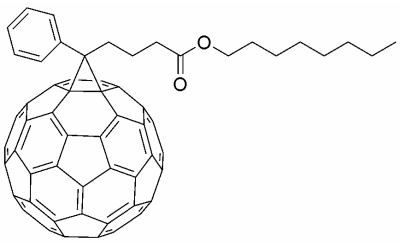

Phenyl–C_{61}–butyric acid octyl ester (PCBO, 4.26 c):

Elution with toluene/cyclohexane 1:2 yielded mono-adduct (41.7%). IR (KBr); ν (cm^{-1}): 3025 (s), 2919 (w), 2850 (m), 2328 (m), 1730 (w), 1540 (s), 1493 (s), 1463 (m), 1410 (m), 1207 (m), 1187 (s), 1161 (m), 1075 (s), 1035 (s), 983 (s), 742 (m), 698 (m), 573 (m), 526 (w), 480 (s). ^{1}H NMR ($CDCl_3$, 400 MHz), δ (ppm): 7.93 (d, *J* = 7.1 Hz, 2H), 7.46 – 7.58 (m, 3H), 4.06 (t, *J* = 6.8 Hz, 2H), 2.90 (t, *J* = 8.1 Hz, 2H), 2.51 (t, *J* = 7.1 Hz, 2H), 2.14 – 2.21 (m, 2H), 1.55 – 1.60 (m, 2H), 1.28 (m, 10H), 0.85 – 0.91 (m, 3H). ^{13}C NMR ($CDCl_3$, 100 MHz), δ (ppm): 173.1, 148.8, 147.8, 145.8, 145.2, 145.0, 144.8, 144.6, 144.5, 144.4, 144.0, 143.7, 143.0, 142.96, 142.9, 142.2, 142.14, 142.10, 141.0, 140.7, 138.0, 137.5, 136.7, 132.1, 128.4, 128.2, 79.9, 64.8, 51.9, 34.1, 33.7, 31.8, 29.2, 29.19, 28.6, 25.9, 22.7, 22.4, 14.1. Elemental Analysis: Calcd. for: $C_{79}H_{28}O_2$: C: 94.03 %, H: 2.80 %. Found: C: 93.5 %, H: 2.75 %.

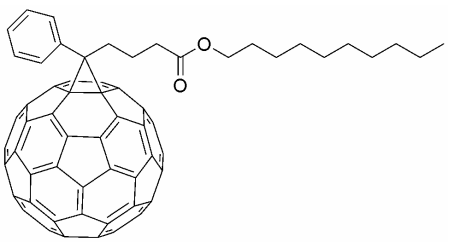

Phenyl–C_{61}–butyric acid decyl ester (PCBD, 5.26 d):

Elution with toluene/cyclohexane 1:2 yielded mono-adduct (22.2%). IR (KBr) = ν (cm^{-1}): 3025 (s), 2923 (w), 2850 (m), 2329 (m), 1733 (w), 1600 (s), 1539 (s), 1494 (s), 1463 (m), 1428 (m), 1250 (s), 1186 (m), 1076 (s), 988 (s), 698 (m), 906 (s), 698 (w), 573 (m), 526 (w), 480 (s). ^{1}H NMR ($CDCl_3$, 300 MHz), δ (ppm): 7.93 (d, *J* = 7.1 Hz, 2H), 7.47 – 7.57 (m, 3H), 4.06 (d, *J* = 6.8 Hz, 2H), 2.92 (t, *J* = 8.1 Hz, 2H), 2.51 (t, *J* = 7.4 Hz, 2H), 2.16 – 2.21 (m, 2H), 1.54 – 1.63 (m, 2H), 1.27 – 1.29 (m, 14H), 0.86 – 0.93 (m, 3H). ^{13}C NMR ($CDCl_3$, 100 MHz), δ (ppm): 173.1, 148.8, 147.8, 145.8, 145.2, 145.0, 144.8, 144.6, 144.5, 144.4, 144.0, 143.7, 143.0, 142.96, 142.9, 142.2, 142.1, 142.1, 141.0, 140.7, 138.0, 137.5, 136.7, 132.1, 128.4, 128.2, 79.9, 51.9, 34.1, 33.7, 31.9, 29.6, 29.3, 28.6, 25.9, 22.7, 22.4, 14.1. Elemental Analysis: Calcd. for $C_{81}H_{32}O_2$: C: 93.80 %, H: 3.11 %. Found: C: 93.70 %, H: 3.06 %.

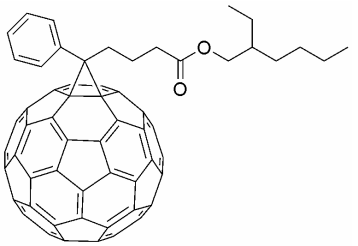

Phenyl–C_{61}–butyric acid 1-hexyl-2-ethyl ester (PCBMEH, **5.26 e):**

Elution with 1:1 cyclohexane:toluene yielded mono-adduct (47.7 %): IR (KBr) = ν (cm^{-1}): 2954 (s), 2925 (s), 2967 (m), 1733 (s), 1494 (w), 1463 (m), 1446 (m), 1428 (m), 1377 (w), 1338 (w),1305 (w), 1248 (m), 1186 (m), 1148 (m), 1076 (w), 1051 (w), 1026 (w), 765 (w), 755 (w), 742 (w), 731 (w), 715 (w), 699 (m), 586 (w), 550 (w), 527 (s). ^{1}H NMR ($CDCl_3$, 200 MHz); δ(ppm): 7.93 (d, *J* = 7.7 Hz, 2H), 7.57 – 7.47 (m, 3H), 3.99 (d, *J* = 5.9 Hz, 2H), 2.94 — 2.89 (m, 2H), 2.52 (t, *J* = 7.3 Hz, 2H), 2.21 — 2.16 (m, 2H), 1.36 — 1.28 (m, 9H), 0.91 — 0.86 (m, 6H). ^{13}C NMR ($CDCl_3$, 125 MHz); δ (ppm): 173.2, 148.8, 147.7, 145.8, 145.13, 145.09, 145.03, 144.97, 144.7, 144.6, 144.4, 144.36, 143.9, 143.7, 143.1, 143.0, 142.9, 142.87, 142.2, 142.1, 142.07, 140.9, 140.7, 138.0, 137.5, 136.7, 132.1, 128.4, 128.2, 79.9, 67.0, 51.9, 38.7, 34.2, 33.7, 30.4, 28.9, 23.8, 23.0, 22.5, 14.2, 11.1. Elemental Analysis: Calcd. for: $C_{73}H_{16}O_2$: C: 94.03 %, H: 2.80 %. Found: C: 93.28 %, H: 2.90 %.

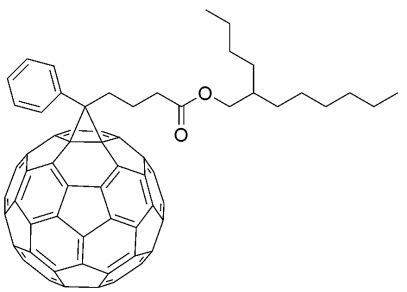

Phenyl–C_{61}–butyric acid 2-butyloctyl ester (PCBBO. 5.26 f):

Elution with toluene/cyclohexane 1:1 gave 91% pure product. A second column (silica gel) using toluene/cyclohexane 1:2 as the eluent yielded pure mono-adduct (34.6 %). IR (KBr) ν (cm^{-1}): 3025 (s), 2924 (w), 2853 (m), 2329 (s), 1733 (w), 1600 (s), 1539 (s), 1494 (s), 1463 (m), 1428 (m), 1250 (s), 1186 (m), 1076 (s), 698 (m), 906 (s), 698 (w), 573 (m), 527 (w), 480 (s), 434 (s). ^{1}H NMR ($CDCl_3$, 400 MHz), δ (ppm): 7.93 (d, *J* = 7.1 Hz, 2H), 7.54 (t, *J* = 7.4 Hz, 2H), 7.26 – 7.49 (m, 1H), 3.98 (d, *J* = 6.9 Hz, 2H), 2.90 (t, *J* = 7.1 Hz, 2H), 2.52 (t, *J* = 7.2 Hz, 2H), 2.16 – 2.21 (m, 2H), 1.55 – 1.61 (m, 1H), 1.27 – 1.35 (m, 16H), 0.86 – 0.90 (m, 6H). ^{13}C NMR ($CDCl_3$, 100 MHz), δ (ppm): 173.23, 148.78, 147.76, 145.81, 145.81, 145.15, 145.10, 145.04, 144.99, 144.74, 144.64, 144.45, 144.38, 143.96, 143.71, 143.07, 142.98, 142.94, 142.88, 142.20, 142.14, 142.08, 140.95, 140.70, 138.00, 137.52, 136.70, 132.06, 130.50, 128.40, 128.20, 127.67, 79.85, 51.88, 37.22, 34.20, 33.67, 31.82, 31.24, 30.91, 29.63, 28.88, 26.67, 22.99, 22.66, 22.45, 14.11. Elemental Analysis: Calcd. for: $C_{83}H_{36}O_2$: C: 93.59 %, H: 3.41 %. Found: C: 92.7 %, H: 3.36 %.

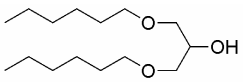

1,3-bis-hexyloxy-propan-2-ol (5.27a):

A 250 ml. three-necked flask equipped with N_2-inlet and mechanical stirrer was charged with NaOH pellets (6.6 g, 165 mmol, 2.1 eq) and glass splinters. The pellets were ground to a powder and hexanol was added (70 ml) resulting in a cloudy suspension. This was allowed to stir for 30 min. Then a solution of 1,3-dichloro-2-propanol in 15 ml hexanol was dropped to the suspension resulting in a white suspension which was refluxed for 1h. The mixture was neutralized with concentrated HCl (0.5 ml). The suspension was filtered and a clear solution was obtained which was concentrated *in vacuo* yielding a light yellow oil. The oil was distilled through a 5 cm vigreux (4 mm Hg, 105 ^{0}C). IR (neat); ν (cm^{-1}): 3441 (s), 2931 (s), 2860 (s), 1467 (m), 1379 (w), 1117 (s), 726 (w). ^{1}H NMR ($CDCl_3$, 300 MHz); δ (ppm): 3.93 – 3.89 (m, 1H), 3.68 – 3.61 (m, 1H), 3.52 – 3.37 (m, 7H), 2.54 (br., 1H), 1.59 – 1.49 (m, 4H), 1.38 – 1.27 (m, 12H), 0.87 (t, *J* = 6.4 Hz, 6H). ^{13}C NMR ($CDCl_3$, 75 MHz); δ (ppm): 71.47, 70.88, 70.67, 69.49, 68.48, 63.25, 30.66, 28.56, 24.76, 21.60, 13.00.

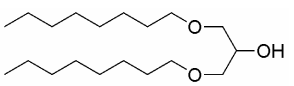

1,3-bis-octyloxy-propan-2-ol (5.27b):

A flame dried three-necked flask equipped with condensor, N_2-inlet, stirring egg and dropping funnel, was charged with powdered NaOH (13.02 g, 326 mmol, 2.1 eq.) and Octanol (170 ml). The resulting suspension was stirred for 2 h. 1,3-dichloro-2-propanol (20.0 g, 155 mmol) dissolved in octanol (30 ml) was dropped to the suspension. The suspension turned cloudy white and was refluxed for 1 h. The mixture was then cooled to RT and acidified with concentrated HCl. All remaining NaCl salts were filtered off. All remaining octanol was removed by distillation. At 2 mTorr and 160 ^{0}C a light yellow residue remained: 35.95 g (113.8 mmol, 73.4 %). IR (neat); ν (cm^{-1}): 3450 (s), 2927 (s), 2857 (s), 1467 (m), 1378 (w), 1117 (s). ^{1}H NMR ($CDCl_3$, 300 MHz); δ (ppm): 3.94 – 3.93 (m, 1H), 3.50 – 3.40 (m, 8H), 2.52 – 2.50 (m, 1H), 1.59 – 1.52 (m, 4H), 1.27 (br., 20H), 0.87 (t, *J* = 7.0 Hz, 6H). ^{13}C NMR ($CDCl_3$, 50 MHz); δ (ppm): 70.9, 70.7, 68.5, 30.8, 28.6, 28.4, 28.2, 25.1, 23.6, 13.1.

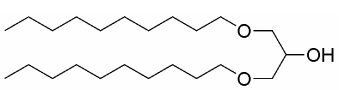

1,3-Bis-decyloxy-propan-2-ol (5.27 c):

A 250 ml three-necked flask equipped with condensor, N_2-inlet, stirring egg and dropping funnel was charged with NaOH pellets (6.6 g, 165 mmol, 2.1 eq) and glassplinters. The NaOH was ground to a powder for 3 h. Then decanol (85 ml) was added yielding a white suspension. This supsension was stirred for 45 min. Then 1,3-dichloropropanol (10.0 g, 77.5 mmol) in decanol (15 ml) was added drop-wise. The mixture was then refluxed for 1 h resulting in a thick white suspension. Concentrated HCl was added until a pH ~1 was reached. The remaining solids were filtered off (difficult) leaving a clear liquid. Remaining decanol was removed by vacuum distillation. At 0 mTorr and 155 ^{0}C a solid sublimed in the cooling tube. This solid was scraped out yielding a waxy white

solid (4.75 g, 12.8 mmol, 16.5 %. The residue was transferred to a sublimation tube (30 cm) using acetone. The aceton was removed by the vacuum line. 2.3 g of a white solid was obtained by the sublimation. Combined yield: 7.05 g. (18.98 mmol, 25 %). IR (KBr): ν (cm^{-1}): 3465 (s), 2924 (s), 2853 (s), 1466 (s), 1378 (m), 1332 (m), 1241 (m), 1117 (s), 722 (w). ^{1}H NMR ($CDCl_3$, 200 MHz); δ (ppm): 3.95 (br., 1H), 3.53 – 3.40 (m, 8H), 2.50 (br., 1H), 1.63 – 1.51 (m, 4H), 1.27 (br., 28H), 0.92 – 0.85 (m, 6H). ^{13}C NMR ($CDCl_3$, 50 MHz); δ (ppm): 70.3, 70.2, 68.0, 30.4, 28.1, 28.0, 27.8, 24.6, 21.2, 12.6.

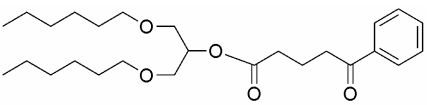

5-Oxo-5-phenyl-pentanoic acid 2-hexyloxy-1-hexyloxymethyl-ethyl ester (5.28a):

A 100 ml round bottom flask, equipped with stirring egg and Dean-Stark setup was charged with benzoyl butyric acid (5.0 g, 26 mmol), 1,3-Bis-hexyloxy-propan-2-ol (7.45 g, 28.6 mmol, 1.1 eq.) and toluene (60 ml). Two drops of concentrated H_2SO_4 were added and the mixture was refluxed for ~18h. To the obtained solution ethyl acetate (25 ml) was added. The organic layer was then washed with 10% $Na_2CO_{3\,(aq)}$ (50 ml) and three times with H_2O (50 ml). The organic layer was separated, dried over Na_2SO_4 and concentrated *in vacuo* yielding a yellow oil. A silica gel column (2.5 x 20 cm) was prepared with toluene. Elution with 19:1 toluene:petroleum ether (40/60) yielded a light yellow oil. Another silica gel column (2.5 x 20 cm) was prepared with hexane. Elution with 4:1 cyclohexane:ethyl acetate yielded a light yellow oil (4.59 g, 10.6 mmol, 41%). IR (KBr) = ν (cm^{-1}): 2932 (s), 2860 (s), 1735 (s), 1688 (s), 1598 (w), 1581 (w), 1449 (m), 1377 (m), 1122 (s), 1002 (w), 749 (m), 691 (m). ^{1}H NMR ($CDCl_3$, 200 MHz); δ(ppm): 7.95 (d, *J* = 7.3 Hz, 2H), 7.54 — 7.52 (m, 1H), 7.46 — 7.41 (m, 2H), 5.17 — 5.12 (m, 1H), 4.06 (t, *J* = 7.0 Hz, 1H), 3.54 (d, *J* = 5.1 Hz, 4H), 3.47 — 3.34 (m, 3H), 3.07 — 3.02 (m, 2H), 2.49 — 2.40 (m, 2H), 2.09 — 2.02 (m, 2H), 1.60 — 1.46 (m, 4H), 1.28 (br., 12H), 0.87 — 0.83 (m, 6H). ^{13}C NMR ($CDCl_3$, 75 MHz); δ (ppm): 198.3, 171.7, 132.8, 127.5, 127.0, 70.5, 68.2, 63.5, 36.3, 32.5, 32.3, 30.3, 28.5, 27.5, 24.6, 24.5, 21.5, 18.4, 12.9. HRMS calcd for $C_{26}H_{42}O_5$: 434.30320 Found: 434.30392.

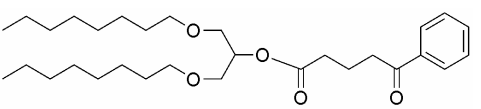

5-Oxo-5-phenyl-pentanoic acid 2-octyloxy-1-octyloxymethyl-ethyl ester (5.28 b):

A 100 ml round-bottom flask equipped with a Dean-Stark setup was charged with benzoylbutyric acid (5.39 g, 28.06 mmol, 1.2 eq.), 1,3-bis-octyloxy-propan-2-ol (7.39 g, 23.39 mmol), dry toluene (40 ml) and three drops of concentrated sulfuric acid. The mixture was refluxed for 20 h. Then EtOAc (25 ml) was added. The organic layer was washed with 10 % Na_2CO_3 (2x 100 ml, 1x 50 ml), dried over

Na_2SO_4 and concentrated *in vacuo*. A silica gel column (6 x 20 cm) was prepared with toluene. Elution with 3:1 toluene/EtOAc yielded a brownish liquid. This liquid was dissolved in ether and carbon black was added. The mixture was stirred for 30 min and the charcoal was filtered off. The resulting solution was concentrated *in vacuo* yielding a light yellow oil (8.40 g, 17.14 mmol, 73.3%). IR (neat); ν (cm^{-1}): 2928 (s), 2857 (s), 1737 (s), 1689 (s), 1598 (w), 1581 (w), 1449 (m), 1414 (w), 1377 (m), 1307 (w), 1212 (s), 1180 (s), 1121 (s), 1002 (m), 988 (w), 877 (w), 748 (m), 691 (s), 569 (w). ^{1}H NMR ($CDCl_3$, 300 MHz); δ (ppm): 7.95 (d, *J* = 7.3 Hz, 2H), 7.54 (t, *J* = 7.3 Hz, 1H), 7.44 (t, *J* = 7.7 Hz, 2H), 5.15 (quin, *J* = 5.1 Hz, 1H), 3.54 (d, *J* = 5.1 Hz, 4H), 3.46 – 3.37 (m, 4H), 3.06 (t, *J* = 7.0 Hz, 2H), 2.47 (t, *J* = 7.0 Hz, 2H), 2.07 (quin, *J* = 7.0 Hz, 2H), 1.52 – 1.49 (m, 4H), 1.25 (br., 20H), 0.86 (t, *J* = 7.0 Hz, 6H). ^{13}C NMR ($CDCl_3$, 50 MHz); δ (ppm): 198.3, 171.7, 135.8, 131.9, 127.5, 127.0, 70.7, 70.6, 68.3, 36.4, 32.5, 30.8, 28.5, 28.4, 28.2, 25.0, 23.6, 18.5, 18.3, 13.0. HRMS calcd for $C_{30}H_{50}O_5$: 490.36580, Found: 490.36704.

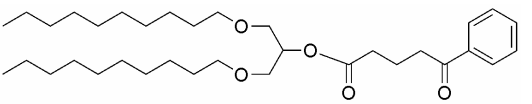

5-Oxo-5-phenyl-pentanoic acid 2-decyloxy-1-decyloxymethyl-ethyl ester (5.28 c):

A 100 ml round bottom flask equipped with Dean-Stark setup was charged with 1,3-bis-decyloxy-propan-2-ol (4.0 g, 10.75 mmol, 1.1 eq.), benzoyl butyric acid (9.78 mmol), toluene (60 ml) and 2 drops of concentrated sulfuric acid. The mixture was brought to reflux for ~18 h. The mixture was then cooled to RT and 25 ml of EtOAc were added. The mixture was washed with 10 % Na_2CO_3 (50 ml), washing with water (50 ml) gives a soapy solution. Addition of EtOAc (30 ml) doesn't help but 50 ml of 10 % Na_2CO_3 (2 x) did give a clear two layer system. The yellow organic layer was collected and the aqueous layer was extracted with 75 ml EtOAc. The combined organic layers were dried over Na_2SO_4 and concentrated *in vacuo*. The resulting oil was purified by a silica gel column (2 x 30 cm). Column was made with hexane and elution with 4:1 hexane: EtOAc yielded a yellowish oil (4.6 g, 8.4 mmol, 86%). IR (neat); ν (cm^{-1}): 2926 (s), 2855 (s), 1738 (s), 1690 (s), 1598 (w), 1449 (m), 1414 (w), 1377 (m), 1211 (w), 1179 (w), 1120 (s), 1001 (w), 748 (w), 691 (m). ^{1}H NMR ($CDCl_3$, 300 MHz); δ (ppm): 7.96 (d, *J* = 7.3 Hz, 2H), 7.55 (t, *J* = 7.3 Hz, 1H), 7.45 (t, *J* = 7.3 Hz, 2H), 5.16 (quin, *J* = 5.1 Hz, 1H), 3.55 (d, *J* = 5.1 Hz, 4H), 3.48 – 3.37 (m, 4H), 3.06 (t, *J* = 7.0 Hz, 2H), 2.48 (t, *J* = 7.0 Hz, 2H), 2.08 (quin, *J* = 7.0 Hz, 2H), 1.57 – 1.50 (m, 4H), 1.25 (br., 28 H), 0.87 (t, *J* = 6.6 Hz, 6H). ^{13}C NMR ($CDCl_3$, 50 MHz); δ (ppm): 198.4, 171.8, 135.8, 132.0, 127.6, 127.0, 70.6, 70.5, 68.2, 36.4, 32.5, 30.9, 28.6, 28.56, 28.5, 28.3, 25.0, 21.7, 18.4, 13.1. HRMS calcd for $C_{34}H_{58}O_5$: 546.42840, Found: 546.42848.

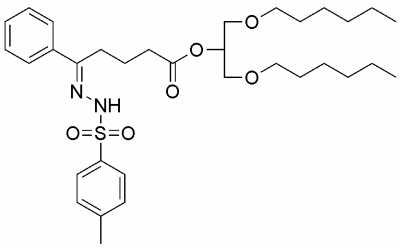

5-p-tosylhydrazone-5-phenyl-pentanoic acid 2-hexyloxy-1-hexyloxymethyl-ethyl ester (5.29 a):

A 100 ml round bottom flask was charged with *p*-tosylhydrazide (1.03 g, 5.53 mmol, 1.2 eq) and toluene (50 ml). 5-Oxo-5-phenyl-pentanoic acid 2-hexyloxy-1-hexyloxymethyl-ethyl ester (**5.28a**) (2.0 g, 4.61 mmol) was added to this solution together with a spatula tip of *p*-toluenesulfonic acid. The resulting mixture was brought to reflux. All formed water was removed by a Dean Stark setup. After 19 h. the mixture was concentrated *in vacuo* yielding a reddish slurry. A silica gel column (2.5 x 15 cm) was prepared with $CHCl_3$. Elution with $CHCl_3$ yielded a yellow oil which crystallized upon standing (2.43 g, 4.04 mmol, 88%). IR (KBr); ν (cm^{-1}): 3212 (m), 2931 (s), 2860 (s), 1732 (s), 1598 (w), 1446 (w), 1380 (w), 1350 (w), 1219 (w), 1169 (s), 1085 (w), 982 (w), 930 (w), 814 (w), 757 (s), 694 (w), 668 (w), 614 (w), 550 (w). ^{1}H NMR (major isomer) ($CDCl_3$, 300 MHz); δ (ppm): 9.20 (s, 1H), 7.91 (d, J = 8.1 Hz, 2H), 7.67 – 7.62 (m, 2H), 7.45 – 7.27 (m, 5H), 5.34 – 5.31 (m, 1H), 4.20 (t, J = 6.8 Hz, 1H), 3.72 – 3.37 (m, 6H), 2.67 – 2.59 (m, 2H), 2.55 – 2.25 (m, 6H), 1.82 – 1.64 (m, 2H), 1.56 – 1.50 (m, 4H), 1.32 – 1.25 (m, 12H), 0.91 – 0.83 (m, 6H). ^{13}C NMR (isomeric mixture) ($CDCl_3$, 50 MHz); δ (ppm): 174.1, 173.2, 153.0, 152.9, 143.1, 135.7, 135.6, 135.5, 132.5, 129.1, 129.0, 128.9, 128.0, 127.9, 127.5, 127.4, 126.2, 125.7, 71.4, 71.1, 68.7, 65.1, 36.9, 33.0, 32.4, 31.7, 31.1, 30.9, 29.0, 28.0, 25.3, 25.2, 25.0, 22.1, 22.0, 21.1, 20.6, 13.5. HRMS calcd for $C_{33}H_{50}O_6N_2S$: 602.3389, Found: 602.3414.

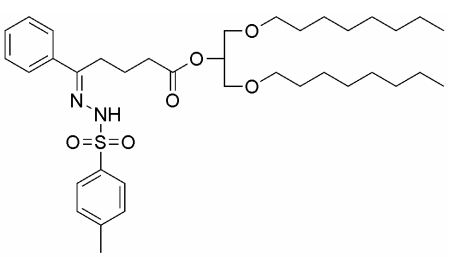

5-p-tosylhydrazone-5-phenyl-pentanoic acid 2-octyloxy-1-octyloxymethyl-ethyl ester (5.29 b):

A 50 ml round bottom flask was charged with 5-Oxo-5-phenyl-pentanoic acid 2-octyloxy-1-octyloxymethyl-ethyl ester (2.46 g, 5.02 mmol), p-tosylhydrazide (1.12 g, 6.02 mmol, 1.2 eq.) and methanol (30 ml). The mixture was refluxed for 18 h under N_2 atmosphere. Concentration *in vacuo* yielded a brown oil. A silica gel column (2 x 15 cm) was prepared with chloroform. Elution with chloroform yielded a red oil. The red oil was dissolved in ether and carbon black was added. The suspension was stirred for 30 min and the carbon black was filtered off. Concentration *in vacuo* yielded a yellowish oil. A second silica gel column (2 x 25 cm) was prepared with toluene/EtOAc 3:1.

Elution with 3:1 toluene/EtOAc yielded an unpure oil. Another silica gel column (2,5 x 20 cm) was prepared with hexane/EtOAc 4:1. Elution with 4:1 hexane/EtOAc yielded a colorless oil which was dried *in vacuo* at 50 ^{0}C yielding a thick somewhat crystalline oil (1.33 g, 2.02 mmol, 40 %) consisting of a 7:1 isomeric cis/trans mixture. IR (KBr); ν (cm^{-1}): 3212 (m), 2926 (s), 2856 (s), 1735 (s), 1598 (m), 1466 (m), 1379 (w), 1351 (w), 1275 (w), 1220 (w), 1167 (s), 1118 (m), 1085 (m), 981 (w), 931 (w), 813 (w), 757 (w), 694 (m), 668 (m), 613 (w), 550 (m). ^{1}H NMR (main isomer) ($CDCl_3$, 300 MHz); δ (ppm): 9.20 (s, 1H), 7.92 (d, *J* = 8.4 Hz, 2H), 7.67 – 7.64 (m, 2H), 7.45 – 7.28 (m, 5H), 5.38 – 5.31 (m, 1H), 3.84 – 3.59 (m, 4H), 3.55 – 3.07 (m, 4H), 2.64 (t, *J* = 7.7 Hz, 2H), 2.41 (s, 3H), 2.38–2.30 (m, 2H), 1.81 – 1.73 (m, 2H), 1.54 – 1.52 (m, 4H), 1.26 – 1.25 (m, 20H), 0.87 (t, *J* = 6.6 Hz, 6H). ^{13}C NMR ($CDCl_3$, 50 MHz); δ (ppm): 172.6, 152.4, 142.6, 135.3, 135.2, 128.6, 128.4, 127.4, 127.0, 125.7, 125.2, 71.0, 70.6, 68.3, 31.9, 30.8, 28.6, 28.4, 28.2, 25.1, 24.7, 21.6, 20.5, 20.1, 13.1.

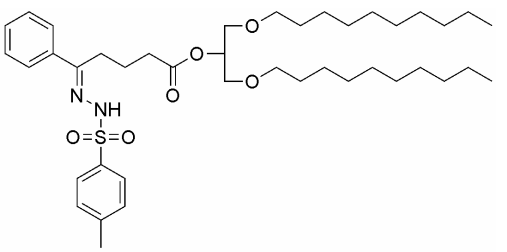

5-p-tosylhydrazone-5-phenyl-pentanoic acid 2-decyloxy-1-decyloxymethyl-ethyl ester (5.29 c):

A 100 ml round bottom flask equipped with a Dean-Stark setup was charged with 5-Oxo-5-phenyl-pentanoic acid 2-decyloxy-1-decyloxymethyl-ethyl ester (4.0 g, 7.3 mmol), p-tosylhydrazide (1.64 g, 8.8 mmol, 1.2 eq.), toluene (60 ml) and a spatula tip of p-toluenesulfonic acid monohydrate. The resulting mixture was refluxed for 20 h. The obtained yellow suspension was filtered to remove unreacted hydrazide. The filtrate was concentrated *in vacuo* to 1/3 rd volume. A silica gel column (4 x 20 cm) was prepared with hexane. Elution with hexane/EtOAc 3:1 yielded a light yellow oil. A second silica gel column (2,5 x 40 cm) was prepared with hexane. Elution with hexane/EtOAc 6:1 yielded a white oil (3.38 g, 4.73 mmol, 64.8 %). IR (neat): ν (cm^{-1}): 3213 (m), 2926 (s), 2855 (s), 1737 (s), 1598 (w), 1466 (w), 1379 (w), 1351 (w), 1305 (w), 1275 (w), 1241 (w), 1221 (w), 1185 (w), 1170 (w), 1119 (w), 1085 (w), 1020 (w), 982 (w), 930 (w), 814 (w), 757 (w), 722 (w), 694 (w), 669 (w), 613 (w), 550 (w). ^{1}H NMR ($CDCl_3$, 300 MHz); δ (ppm): 9.20 (s, 1H), 7.90 (d, *J* = 7.3 Hz, 2H), 7.68 – 7.59 (m, 2H), 7.36 – 7.20 (m, 5H), 5.36 – 5.26 (m, 1H), 3.71 – 3.54 (m, 4H), 3.54 – 3.33 (m, 4H), 2.65 – 2.56 (m, 2H), 2.43 – 2.24 (m, 5H), 1.76 – 1.61 (m, 2H), 1.60 – 1.42 (m, 4H), 1.22 (br., 28H), 0.92 – 0.78 (m, 6H). ^{13}C NMR ($CDCl_3$, 50 MHz); δ (ppm): 172.1, 151.9, 142.1, 134.8, 134.7, 128.4, 128.1, 128.1, 127.9, 126.9, 126.5, 125.2, 124.7, 70.5, 70.1, 67.8, 31.4, 30.4, 28.1, 28.0, 27.8, 24.6, 24.3, 21.2, 20.0, 19.6, 12.6.

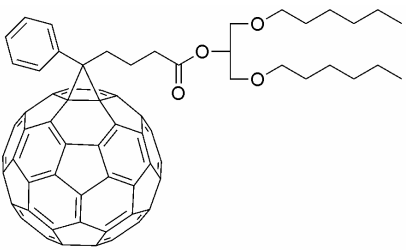

Phenyl–C_{61}–Butyric acid 2-hexyloxy-1-hexyloxymethyl-ethyl ester (PCB-dihexyl, 5.30 a):

A flame dried 500 ml three-necked flask equipped with condensor, N_2-inlet, stirring egg and thermometer was charged with 5-p-tosylhydrazone-5-phenyl-pentanoic acid 2-hexyloxy-1-hexyloxymethyl-ethyl ester (**5.29a**) (1.33 g, 2.2 mmol, 1.1 eq), KOtBu (0.25 g, 2.23 mmol, 1.11 eq.) and dry pyridine (30 ml). The resulting solution was stirred for ~45 min. A solution of C_{60} (1.44g, 2.0 mmol) in ODCB (200 ml) was added resulting in a purple solution. The solution was degassed by N_2/vacuum purges (3x). The mixture was rapidly heated to 85 ^{0}C and irradiation with a 400 W Na lamp was started. The reaction was followed by HPLC and stopped at 50% conversion. The resulting brown solution was concentrated to 25% volume. A silica gel column was prepared with toluene. The reaction mixture was eluted with CS_2 to remove unreacted C_{60}. Elution was continued with a mixture of toluene/cyclohexane 1:1 to obtain mono-adduct in 96% purity (HPLC). A second column was performed with toluene/cyclohexane 1:1 yielding pure mono-adduct. The mono-adduct fractions were concentrated *in vacuo* and redissolved in a minimal amount of ODCB. Precipitation with methanol and subsequent centrifugation yields a sticky black solid. The solid was washed with methanol (2x) and pentane (1x) and dried *in vacuo* at 50 ^{0}C. The resulting black oily substance was washed once more with methanol and once with pentane before drying again at 50 ^{0}C *in vacuo*. A sticky black solid was obtained (618 mg, 0.54 mmol, 27%). IR (KBr); ν (cm^{-1}): 3764 (w), 3751 (w), 2981 (s), 2866 (s), 2186 (w), 2027 (w), 1721 (s), 1436 (w), 1184 (w), 712 (s), 521 (s), 422 (s). ^{1}H NMR ($CDCl_3$, 300 MHz); δ (ppm): 7.92 (d, *J* = 7.0 Hz, 2H), 7.54 (m, 3H), 5.13 (m, 1H), 3.54 (m, 4H), 3.47 (m, 4H), 2.91 (m, 2H), 2.54 (q, *J* = 7.7 Hz, 2H), 2.19 (m, 2H), 1.55 (m, 4H), 1.31 (m, 12H), 0.88 (t, *J* = 7.0 Hz, 6). ^{13}C NMR ($CDCl_3$, 75 MHz); δ (ppm): 172.6, 148.8, 147.8, 145.8, 144.8, 144.0, 143.0, 141.0, 138.1, 137.6, 136.8, 132.1, 130.5, 128.4, 127.7, 79.9, 69.2, 51.9, 34.2, 33.7, 31.6, 30.9, 29.5, 22.6, 22.4, 14.1. Elemental Analysis Calcd for: $C_{86}H_{42}O_4$: C: 90.67 %, H: 3.72 %. Found: C: 89.48 %, H: 3.62 %.

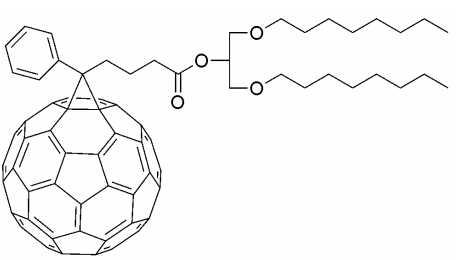

Phenyl–C_{61}–Butyric acid 2-octyloxy-1-octyloxymethyl-ethyl ester (PCB-dioctyl, 5.30 b):

A flame dried 250 ml three-necked flask equipped with condensor, N_2-inlet, stirring egg and thermometer was charged with 5-p-tosylhydrazone-5-

phenyl-pentanoic acid 2-octyloxy-1-octyloxymethyl-ethyl ester (**5.29b**) (717 mg, 1.09 mmol, 1.09 eq.), pyridine (15 ml) and KOtBu (123 mg, 1.1 mmol, 1.1 eq.). The resulting yellow suspension was stirred for 40 min. C_{60} (720 mg, 1.0 mmol) in ODCB (100 ml) was added to the mixture. The resulting mixture was degassed with three N_2/vacuum purges. Then the mixture was heated to 85 ^{0}C by a hotgun and irradiation with a 400 W Na-lamp was started (T_{eq} ~ 105 ^{0}C). After 1,5 h the reaction mixture was allowed to cool to RT under illumination and the mixture was concentrated *in vacuo* to 1/3 rd volume. A silica gel column (5 x 18 cm) was prepared with toluene and pre-eluted with CS_2 (25 ml). The mixture was brought on and eluted with CS_2 to obtain unreacted C_{60}. Elution with toluene yielded the mono-adduct fraction. Work up C_{60}: The C_{60} fraction was concentrated *in vacuo* and redissolved in ODCB. Precipitation with MeOH and subsequent centrifugation yielded a brown pellet which was washed with MeOH (2x) and once with pentane. The resulting brown pellet was dried *in vacuo* at 50 ^{0}C. The pellet was then washed once more with MeOH and dried *in vacuo* at 50 ^{0}C. Yield: 205 mg (0.28 mmol, 28.5 %). Work up mono-adduct: The mono-adduct fraction was concentrated *in vacuo* and redissolved in ODCB. Precipitation with MeOH and subsequent centrifugation yielded a dark oil. This was washed with MeOH (2x) and once with pentane. The subsequent oily substance was dried *in vacuo* at 50 ^{0}C. The obtained sticky black solid was washed once more with MeOH and dried *in vacuo* at 50 ^{0}C. Yield: 480 mg (0.4 mmol, 40 %). IR (KBr); ν (cm^{-1}): 3026 (w), 2924 (s), 2854 (s), 1737 (s), 1601 (w), 1539 (w), 1495 (m), 1464 (s), 1428 (s), 1376 (m), 1248 (m), 1186 (s), 1121 (s), 988 (w), 963 (w), 882 (w), 843 (w), 798 (w), 766 (m), 756 (m), 742 (m), 731 (w), 714 (m), 699 (m), 586 (w), 573 (m), 559 (w), 550 (m), 527 (s), 481 (w), 436 (w). ^{1}H NMR ($CDCl_3$, 300 MHz); δ (ppm): 7.92 (d, *J* = 7.0 Hz, 2H), 7.56 – 7.43 (m, 3H), 5.14 (quin, *J* = 5.1 Hz, 1H), 3.55 (t, *J* = 4.4 Hz, 4H), 3.47 – 3.39 (m, 4H), 2.94 – 2.89 (m, 2H), 2.55 (t, *J* = 7.3 Hz, 2H), 2.22 – 2.16 (m, 2H), 1.55 – 1.52 (m, 4H), 1.27 (br., 20H), 0.88 (t, *J* = 7.0 Hz, 6H). ^{13}C NMR ($CDCl_3$, 75 MHz); δ (ppm): 171.6, 147.8, 146.8, 144.8, 144.2, 144.1, 144.07, 144.0, 143.8, 143.7, 143.5, 143.4, 143.0, 142.8, 142.1, 142.0, 142.0 141.9, 141.2, 141.17, 141.1, 140.0, 139.7, 137.1, 136.6, 135.8, 131.1, 129.5, 127.4, 127.2, 126.7, 78.9, 70.7, 70.66, 68.2, 50.9, 33.2, 32.7, 30.9, 28.6, 28.4, 28.3, 25.1, 21.7, 21.4, 13.1. Elemental Analysis calcd for $C_{90}H_{50}O_4$: C: 90.43 %, H: 4.22 %, Found: C: 90.20 %, H: 4.07 %.

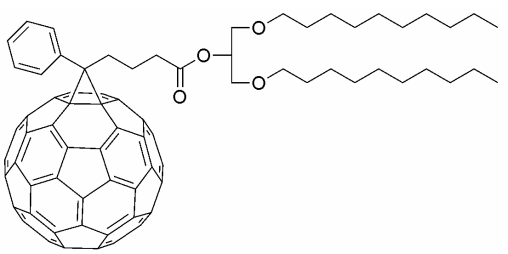

Phenyl–C_{61}–Butyric acid 2-decyloxy-1-decyloxymethyl-ethyl ester (PCB-didecyl, 5.30 c):

A flame dried 250 ml three-necked flask, equipped with condensor, thermometer and stirring egg, was charged with *5*-p-tosylhydrazone-5-phenyl-pentanoic acid 2-decyloxy-1-decyloxymethyl-ethyl ester (**5.29c**) (720 mg, 1.0 mmol) and pyridine (15 ml). Then KOtBu (122 mg, 1.0 mmol) was added resulting in a light yellow solution which was

stirred for 30 min. C_{60} dissolved in ODCB was added. The resulting purple mixture was degassed by three N_2/vacuum purges and then heated to 80 ^{0}C by a hotgun. Irradiation with a 400 W Na-lamp was started (T_{eq} ~ 100 ^{0}C). After 2 h. the reaction was stopped and the reaction mixture was concentrated to approximately 1/5th volume. A silica gel column (3 x 25 cm) was prepared with toluene. Pre-elution with 50 ml. CS_2. Mixture was brought on and eluted with CS_2 to obtain unreacted C_{60}. Elution was continued with 1:1 toluene/cyclohexane yielding an impure band. Elution was then continued with toluene to obtain the mono-adduct fraction. Elution with CH_2Cl_2 yielded the bis-adduct fraction. Work up C_{60}: The C_{60} fraction was concentrated *in vacuo* and redissolved in ODCB. Precipitation with MeOH and subsequent centrifugation yielded a brown pellet which was washed with MeOH (2x). The resulting pellet was dried *in vacuo* at 50 ^{0}C and then washed once with pentane and once with MeOH. The resulting brown pellet was dried *in vacuo* at 50 ^{0}C. Yield: 246 mg (0.34 mmol, 34,2%). Work up mono-adduct: The mono adduct fraction was concentrated *in vacuo*, redissolved in ODCB and precipitated with MeOH yielding a dark black tarr like solid. This was washed with MeOH, but no suspension was formed during sonication. Washing with 50 ml pentane gave a brown suspension which was centrifuged yielding a brown pellet and a dark brown pentane solution. The pellet was dried *in vacuo* at 50 ^{0}C. This pellet was washed with MeOH and dried *in vacuo* at 50 ^{0}C yielding a sticky brown solid. This solid was transferred to a vile using liquid nitrogen. Isolated yield: 457 mg (0.37 mmol, 37%). IR (KBr): ν (cm^{-1}): 3430 (s), 2924 (s), 2852 (s), 1737 (s), 1633 (s), 1464 (m), 1428 (m), 1187 (m), 1121 (m), 756 (w), 699 (w), 676 (w), 586 (w), 573 (w), 551 (w), 526 (s). ^{1}H NMR ($CDCl_3$, 400 MHz); δ (ppm): 7.92 (d, *J* = 7.3 Hz, 2H), 7.56 (t, *J* = 7.3 Hz, 1H), 7.49 – 7.45 (m, 2H), 5.13 (quin, *J* = 5.1 Hz, 1H), 3.59 – 3.51 (m, 4H), 3.48 – 3.37 (m, 4H), 2.93 – 2.89 (m, 2H), 2.55 (t, *J* = 7.3 Hz, 2H), 2.23 – 2.15 (m, 2H), 1.54 – 1.51 (m, 4H), 1.26 (br., 28H), 0.88 (t, *J* = 6.6 Hz, 6H). ^{13}C NMR ($CDCl_3$, 100 MHz); δ (ppm): 171.5, 147.8, 146.8, 144.8, 144.2, 144.1, 144.05, 144.0, 143.8, 143.7, 143.5, 143.4, 143.0, 142.7, 142.0, 141.97, 141.9, 141.2, 141.16, 141.11, 141.10, 140.0, 139.7, 137.1, 136.5, 135.8, 131.1, 127.4, 127.2, 78.9, 70.7, 70.6, 68.1, 50.9, 33.2, 32.7, 30.9, 28.64, 28.60, 28.5, 28.3, 25.1, 21.7, 21.4, 13.1. Elemental Analysis calcd for $C_{94}H_{58}O_4$: C: 90.22 %, H: 4.67%, Found: C: 89.73 %, H: 4.55 %.

5.6 References

1. O. Ostroverkhova and W. E. Moerner, *Chem.Rev.,* 2004, **104**, 3267.
2. A. Ashkin, G. D. Boyd, J. M. Dziedzic, R. G. Smith, A. A. Ballman, J. J. Levinstein, and K. Nassau, *Appl.Phys.Lett.*, 1966, **9**, 72.
3. J. S. Schildkraut and A. V. Buettner, *J.Appl.Phys.*, 1992, **72**, 1888.
4. O. Ostroverkhova and K. D. Singer, *J.Appl.Phys.*, 2002, **92**, 1727.
5. V. M. N. Passaro and F. Magno, *Laser Physics*, 2007, **17**, 231.

6. R. Jones, S. C. W. Hyde, M. J. Lynn, N. P. Barry, J. C. Dainty, P. M. W. French, K. M. Kwolek, D. D. Nolte, and M. R. Melloch, *Appl.Phys.Lett.*, 1996, **69**, 1837.
7. M. Eich, B. Reck, D. Y. Yoon, C. G. Willson, and G. C. Bjorklund, *J.Appl.Phys.*, 1989, **66**, 3241.
8. S. Ducharme, J. C. Scott, R. J. Twieg, and W. E. Moerner, *Phys.Rev.Lett.*, 1991, **66**, 1846.
9. M. A. Diaz-Garcia, D. Wright, J. D. Casperson, B. Smith, E. Glazer, and W. E. Moerner, *Chem.Mater.*, 1999, **11**, 1784.
10. L. Paelke, H.-S. Kitzerow, and P. Strohriegl, *Appl.Phys.Lett.*, 2005, **86**, 031104.
11. E. Mecher, C. Bräuchle, H. H. Hörhold, J. C. Hummelen, and K. Meerholz, *Phys.Chem.Chem.Phys.*, 1999, **1**, 1749.
12. D. J. Suh, O. O. Park, T. Ahn, and H. K. Shim, *Jap.J.Appl.Phys.Part 2*, 2002, **41**, L428.
13. E. Mecher, F. Gallego-Gómez, H. Tillman, H. H. Hörhold, J. C. Hummelen, and K. Meerholz, *Nature*, 2002, **418**, 959.
14. E. Mecher, F. Gallego-Gómez, K. Meerholz, H. Tillman, H. H. Hörhold, and J. C. Hummelen, *CHEMPHYSCHEM*, 2004, **5**, 277.
15. W. You, L. Wang, Q. Wang, and L. Yu, *Macromolecules*, 2002, **35**, 4636.
16. I. Aiello, D. Datillo, M. Ghedini, A. Bruno, R. Termine, and A. Golemne, *Adv.Mater.*, 2002, **14**, 1233.
17. Q. Wang, L. Wang, J. Yu, and L. Yu, *Adv.Mater.*, 2000, **12**, 974.
18. Z. Peng, A. R. Gharavi, and L. Yu, *J.Amer.Chem.Soc.*, 1997, **119**, 4622.
19. J. Winiarz and P. Prasad, *Opt.Lett.*, 2002, **27**, 1330.
20. J. G. Winiarz, L. Zhang, M. Lal, C. S. Friend, and P. N. Prasad, *J.Amer.Chem.Soc.*, 1999, **121**, 5287.
21. D. J. Binks, D. P. West, S. Norager, and P. O'Brien, *J.Chem.Phys.*, 2002, **117**, 7335.
22. Y. Wang and N. Herron, *Chem.Phys.Lett.*, 1992, **200**, 71.
23. J. G. Winiarz, L. M. Zhang, M. Lal, C. S. Friend, and P. N. Prasad, *Chem.Phys.*, 1999, **245**, 417.
24. E. Hendrickx, B. Kippelen, S. Thayumanavan, S. R. Marder, A. Persoons, and N. Peyghambarian, *J.Chem.Phys.,* 2000, **112**, 9557.
25. S. J. Zilker and U. Hofmann, *Appl.Opt.,* 2000, **39**, 2287.
26. O. Ostroverkhova, W. E. Moerner, M. He, and R. J. Twieg, *Appl.Phys.Lett.,* 2003, **82**, 3602.
27. O. Ostroverkhova, D. Wright, U. Gubler, W. E. Moerner, M. He, A. Sastre-Santos, and R. J. Twieg, *Adv.Funct.Mater.*, 2002, **12**, 621.
28. K. Meerholz, Y. De Nardin, R. Bittner, R. Wortmann, and F. Würthner, *Appl.Phys.Lett.,* 1998, **73**, 4.
29. K. Meerholz, R. Bittner, Y. De Nardin, C. Bräuchle, E. Hendrickx, B. L. Volodin, B. Kippelen, and N. Peyghambarian, *Adv.Mater.*, 1997, **9**, 1043.
30. E. Hendrickx, B. L. Volodin, D. D. Steele, J. L. Maldonado, J. F. Wang, B. Kippelen, and N. Peyghambarian, *Appl.Phys.Lett.,* 1997, **71**, 1159.

31. D. Van Steenwinckel, E. Hendrickx, A. Persoons, K. Van den Broek, and C. Samyn, *J.Chem.Phys.*, 2000, **112**, 11030.
32. C. J. Brabec, A. Cravino, D. Meissner, N. S. Sariciftci, T. Fromherz, M. T. Rispens, L. Sanchez, and J. C. Hummelen, *Adv.Funct.Mater.*, 2001, **11**, 374.
33. J. C. Hummelen, B. W. Knight, F. Lepeq, F. Wudl, J. Yao, and C. L. Wilkins, *J.Org.Chem.*, 1995, **60**, 532.
34. M. M. Wienk, J. M. Kroon, W. J. H. Verhees, J. Knol, J. C. Hummelen, P. A. van Hal, and R. A. J. Janssen, *Angew.Chem.Int.Ed.*, 2003, **42**, 3371.
35. F. B. Kooistra, V. D. Mihailetchi, L. M. Popescu, D. Kronholm, P. W. M. Blom, and J. C. Hummelen, *Chem.Mater.*, 2006, **18**, 3068.
36. F. B. Kooistra, J. Knol, F. Kastenberg, L. M. Popescu, W. J. H. Verhees, J. M. Kroon, and J. C. Hummelen, *Org.Lett.*, 2007, **9**, 551.
37. K. Meerholz, Y. De Nardin, and R. Bittner, *Mol.Cryst.Liq.Cryst.*, 1998, **315**, 99.
38. A. Grunnet-Jepsen, D. Wright, B. Smith, M. S. Bratcher, M. S. DeClue, J. S. Siegel, and W. E. Moerner, *Chem.Phys.Lett.*, 1998, **291**, 553.
39. J. Thomas, C. Fuentes-Hernandez, M. Yamamoto, K. Cammack, K. Matsumoto, G. A. Walker, S. Barlow, B. Kippelen, G. Meredith, S. R. Marder, and N. Peyghambarian, *Adv.Mater.*, 2004, **16**, 2032.
40. S. Köber, F.B. Kooistra, F. Gallego-Gomez, M. Salvador, F. Mielke, O. Nuyken, J.C. Hummelen and K. Meerholz. *OSA proceedings, 2007, accepted*
41. D. Van Steenwinckel, E. Hendrickx, and A. Persoons, *J.Chem.Phys.*, 2001, **114**, 9557.

Chapter 6

π-Conjugated Fullerene Adducts

This Chapter describes the synthesis and characterization of fullerene derivatives with addends connected to the parent fullerene in such a way that the π-system of the parent fullerene is extended to the addend. In order to accomplish this continuation of the π-system from the fullerene to the addend, [5,6] bridged benzylideno fulleroids were synthesized. For comparison reasons we synthesized both [5,6] and [6,6] bridged benzylidenofullerenes. The [5,6] and the [6,6] benzylidenofullerenes are compared by UV-Vis measurements as well as by semi-empirical PM3 calculations. We show that interactions between the addend and the fullerene can clearly be seen in both [5,6] and [6,6] benzylidenofullerenes. The [5,6] benzylidenofullerene compounds discussed here are the first fullerenes where a functional group has been added to the fullerene cage with alternating single and double bonds separating the fullerene moiety from the addend.

*Part of this work was published:

Floris B. Kooistra, Tessa M. Leuning, Enrique Maroto Martinez, and Jan C. Hummelen, *submitted for publication.*

6.1 Introduction

Over the years many synthetic methodologies have been developed to functionalize fullerenes.[1-5] Besides improving solubility and processability of fullerenes these methodologies also allow tuning of the electronic properties of the fullerenes. The ability to efficiently alter the electronic properties of fullerenes would signify a major advance in the field of molecular electronics. However, altering these electronic properties has been a tough challenge so far. We have shown in chapter 3 that placing electron donating and withdrawing groups on the phenyl ring of PCBM results in small variations of the fullerene LUMO level.[6] We aimed for a through-space interaction between lone-pair electrons of oxygen and sulphur atoms with the π-system of the parent fullerene, but only found a small inductive 'through-bond' effect. Another possible way to influence the electronic properties of fullerenes, which was initially explored by Wudl and co-workers, is by peri-conjugation.[7] They observed an electronic overlap of two π-systems, separated by two sp^3 carbons, in spiroannelated methanofullerenes. Peri-conjugation results from the overlap between p_z orbitals which are alligned in a perpendicular way, this in contrast to spiroconjugation where all orbitals are oriented in one plane (see paragraphs 6.1.1 and 6.1.2).[8] In theory, the most efficient method to alter the electronic properties of fullerenes (as with any π-conjugated system) would be by direct π-conjugated pathways from the addend to the fullerene. As we will show, this π-conjugated pathway, however, since it can not lay in one plane, results in limited overlap of the involved π-orbitals. In this chapter such fullerenes are presented for the first time.

6.1.1 Spiroconjugation

When two cyclic systems are linked by one central atom we speak of spiro compounds. If these cycles contain π-electron systems they are called spiro-polyenes or spirenes.[8,9] An overlap between the two π-systems is possible, which has been termed spiroconjugation.[10,11] The overlap in spiroconjugation involves four interacting p orbitals. A Newman projection and a 3D projection can be seen in Fig 6.1. Some examples of spiroconjugation are given by Maslak et al.[12] and more recently by Wu et al. and the group of Martín.[13] An extensive review was published as early as 1978.[8]

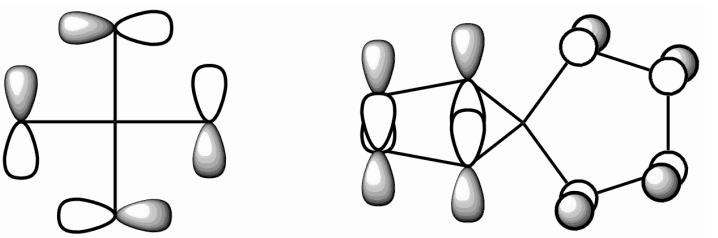

Fig. 6.1: Two 'spiro' connected butadiene units. Left: Newman projection of interacting HOMO p orbitals. Right: 3D projection of interacting HOMO –1 p orbitals.

6.1.2 Periconjugation

The term periconjugation was introduced for the first time by Wudl et al., describing substituent effects in spiroannelated fulleroid compounds.[14] They later showed similar effects in spiromethanofullerenes.[7] These spiromethanofullerenes were further investigated by computational methods, showing a large calculated influence by peri-conjugation, surpassing effects observed for spiroconjugation.[15] The most important difference between spiroconjugation and periconjugation is the geometric allignment of the interacting p orbitals as well as the number of involved p-orbitals (4 and 10 respectively). Although not discussed by Wudl et al., we expect the bottom p orbitals (not shown) in the fluorene (dotted) structure (i.e. on the 1 and 8 position of the fluorene) to show overlap with the fullerene p-orbitals as well.

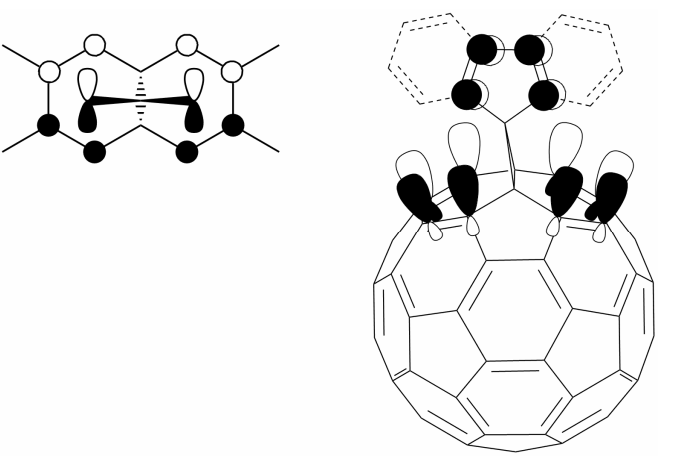

Fig. 6.2: Periconjugation (HOMO) in a spiromethanofullerene.[7] Left: Newman projection. Right: 3D projection. Dotted: actual synthesized compound, the "solid" structure was subjected to calculation.

Another noticeable difference is the fact that in these periconjugated fullerenes both π-systems are separated by two sp^3 carbons whereas in the spiroconjugated molecules the π-systems are separated by only one sp^3 carbon. A maximum effect of a 70 mV reduction of the first reduction potential was observed, when comparing spiromethanofullerenes with and without possible peri-conjugation.

6.1.3 1,6-bridged [10]annulenes

A reasonable model compound for the study of [5,6] fulleroids is a 1,6-bridged [10]annulene. The interactions between the bridge atoms and the 'perimeter' 10 π-system has been studied extensively.[16-21] Although not entirely the same, [5,6] fulleroids can be expected to show similar interactions ([6,6] fulleroids are not known).

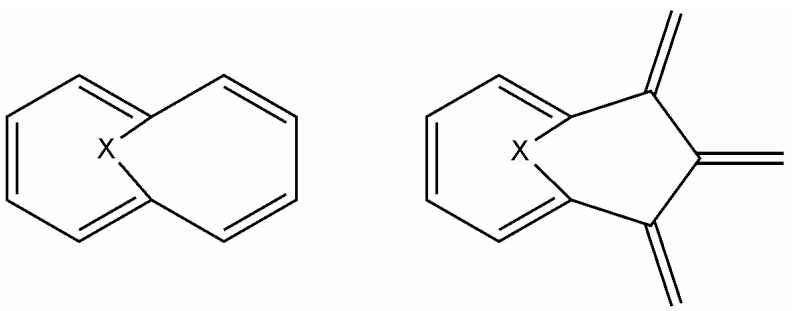

Fig. 6.3: Left: 1,6-bridged [10]annulene. Right: [5,6] bridged fulleroid region.

11-methylene-1,6-methano[10]annulene (**6.1**) was synthesized by Vogel et al.[16] but showed virtually no interaction between the two π-systems. Similarly 1,6-methano[10]annulene-11-one (**6.2**) shows no interaction at all.[17] However, when a heteroatom is used as the bridging atom, interactions can be observed (**6.3a-c**). The reason why the lone pairs of either nitrogen or oxygen atoms can influence the 'perimeter' π-system, while the π-orbitals of the methylene and ketone functionality can not,[20] are not clear. The main difference between the systems is the hybridization of the bridging atom, which is sp^2 for **6.1** and **6.2**, while the bridging nitrogen or oxygen atom is sp^3 hybridized in **6.3**. The sp^3 orbitals might overlap with the perimeter π-system, thus explaining the observed interaction.

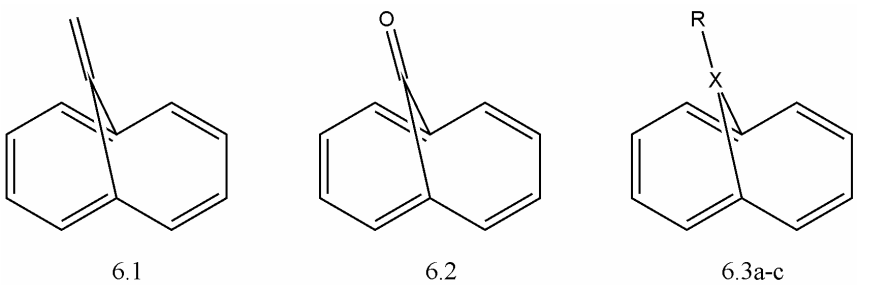

Fig. 6.4.: ***6.1****: 11-methylene-1,6-methano[10]annulene,* ***6.2****: 1,6-methano[10]annulene-11-one,* ***6.3a****: X = O,* ***6.3b****: X = N, R = H,* ***6.3c****: X =N, R =* CH_3.

6.1.4 Fullerenes and Fulleroids

The interaction that was found in compounds **6.3a-c** might also be visible in azafulleroids and possibly in oxidized C_{60}. In the first case a heteroatom bridges a 5 and 6 membered ring, while in the second case the heteroatom bridges two six membered rings. A fullerene epoxide (**6.4**) was synthesized for the first time by the group of Cox.[22] The UV-spectra presented in that work as well as later work[23], however, show no difference between a methanofullerene and the fullerene epoxide, indicating that there is no inductive effect from the oxygen atom. This is not entirely surprising since the oxygen lone pairs are quite far away from the fullerene π-system. The synthesis of azafulleroids (**6.5a-c**) was pioneered by the group of Wudl.[24] Although no special attention was paid to the UV spectra of these compounds one might deduct at least a small influence of the nitrogen atom. An absorption maximum around 550 nm is observed for three of the presented azafulleroids. These azafulleroids all have a phenyl functionality attached to the nitrogen atom. The observed absorption is slightly red shifted (~ 8 nm) when compared to [5,6]PCBM (**6.6**) which has an absorption maximum at 542 nm.[25] The main difference between the azafulleroid and the [5,6]PCBM is the bridging atom being a nitrogen or a carbon atom (see figure 6.5). One might conclude therefore that a small influence of the nitrogen lone pair is visible.

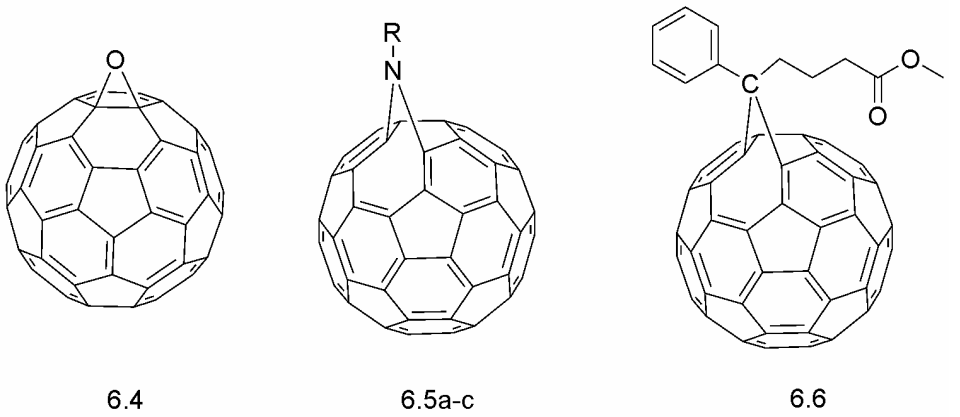

Fig. 6.5.: ***6.4****: fullerene epoxide,* ***6.5****: azafulleroids, a: R = benzyl, b: R = 4-methoxybenzyl, c: R = 4-bromobenzyl,* ***6.6****: [5,6]PCBM.*

A different solvent[I] was used for both measurement however, which might account for the difference as well. Depending on the type of transition, either a blue or red shift is expected. π-π* Transitions usually give a redshift while n-π* transitions give a blue shift when using a more polar solvent. The observed red shift might therefore also be a solvent effect.

Calculations regarding the electronic structure of fulleroids and the occurrence of homoconjugation in bridged C_{60} derivatives have been performed by Haddon.[26] The calculations performed on these C_{60} derivatives can be seen as an extension of earlier work on calculations of nonplanar conjugated organic molecules.[27] The interaction of bridge atoms on 'perimeter' π-systems can be analyzed by using π-Orbital Axis Vector Analysis (POAV). In the case of [6,6] bridged systems it is shown that the pyramidilization, that occurs due to [6,6] bridging, leads to an increase in the π-overlap in the periphery. The opposite is observed for [5,6] bridging, where the pyramidalization is much greater, resulting in π-orbital misalignment. Another important factor in the [5,6] bridged structures is the violation of Bredt's rule, which forbids placement of a double bond at the bridgehead of small ring systems. Since double bonds are placed at the bridgeheads of a small ring system here, a further π-orbital misallignment is expected. Placement of double bonds in 5 membered rings however, seems to be energetically even more unfavorable. The high reactivity of [5,6] fulleroids at the bridgehead position can thus be explained by this violation of Bredt's rule.

[I] The azafulleroids (**6.5)** were measured in dichloromethane while the [5,6]PCBM (**6.6**) was measured in hexane.

6.1.5 Research Goal

When trying to influence the electronic properties of fullerenes one should, ideally, functionalize fullerenes with electron donating and electron withdrawing groups in a conjugated way to the parent fullerene. This is an extremely challenging task since this would require the synthesis of a [5,6]bridged fullerene addend, which, in turn, should contain an alkene functionality directly attached to the fullerene. (Fig. 6.6)

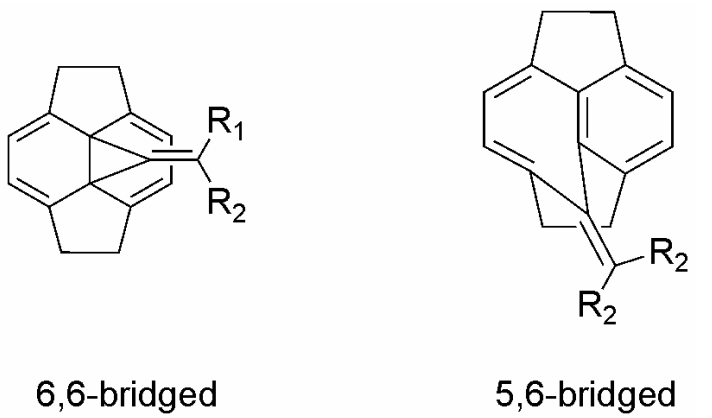

Fig. 6.6: peracylene unit of a [6,6] and a [5,6]bridged fullerene. In the [5,6]bridged fulleroid a continuous pathway of alternating single and double bonds from the addend R groups to the fullerene cage is apparent.

The synthesis of π-conjugated [5,6]bridged fulleroids with both electron donating and electron withdrawing functional groups was the subject of study of this chapter. The [6,6]bridged analogues will be discussed as well, in order to compare both. The targeted molecules can be seen in Fig. 6.7. The target molecules will be compared by UV-Vis absorption and semi-emperical PM3 calculations.

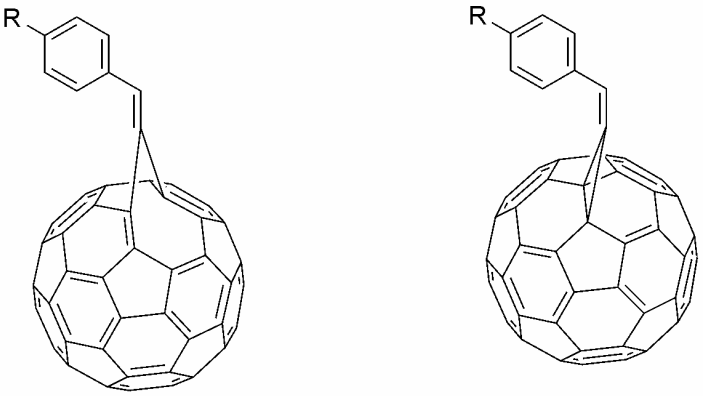

Fig. 6.7: Target molecules: 6.7:'conjugated' [5,6]bridged fulleroids, 6.8: 'conjugated' [6,6]bridged fullerenes. a: R = H, b: R = NO_2.

6.2 Synthesis

As a precursor for the fullerene addition reaction we choose to use diazirines.[28] It is well known that diazirines decay under photolytical or thermolytical conditions with expulsion of nitrogen.[29-34] Two interesting intermediate species are formed during this decay i.e. a carbene species and a diazo species. In order to study this decay pathway, Nagase et al. have used C_{60} as a mechanistic trap. Carbene species react with C_{60} to form a [6,6] adduct. Diazo intermediates on the other hand form [5,6] adducts (see Fig. 6.8).[35] When 3-chloro-3-alkyldiazirines are used, both the [6,6] and the [5,6] adduct are obtained with the chlorine atom situated at the cyclopropane ring.[36] The ratio of [5,6] and [6,6] addition product is determined by the substituent on the diazirine.[37] In our synthetic approach we used 3-chloro-3-phenyldiazirines as precursors for addition reactions to C_{60}. When a subsequent HCl elimination is performed an alkene functionality is obtained 'on top of' the cyclopropane ring. The advantage of using a diazirine is that it allows for the introduction of a leaving group on the cyclopropane ring that is formed upon addition to the fullerene.

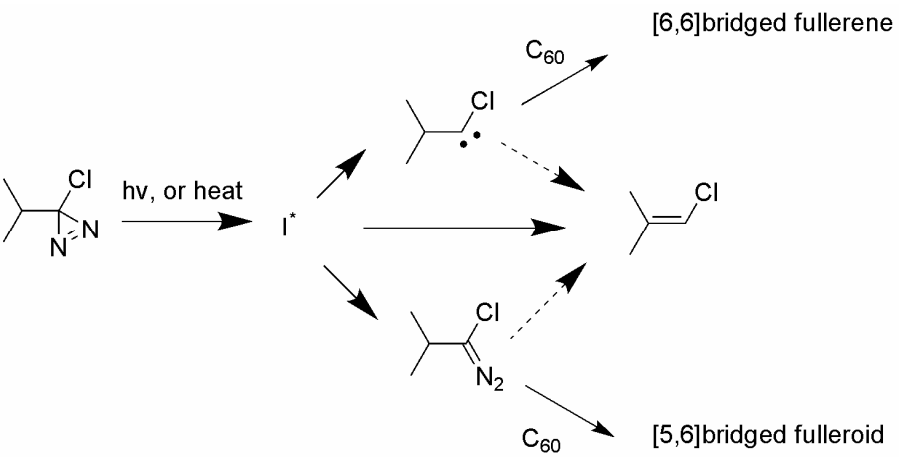

Fig. 6.8: Decay pathway of 3-alkyl-3-chlorodiazirines. When C_{60} is used as a mechanistic trap the carbene species results in a [6,6]bridged fullerene and the diazo species in a [5,6]bridged fulleroid. (I^*: excited intermediate)

Other synthetic precursors used for the formation of diazo compounds are azides and tosylhydrazones.[5] However both azide and tosylhydrazone precursors do not allow for the introduction of an effective leaving group at the introduced cyclopropane moiety. This leaving group is essential for the desired subsequent elimination reaction, forming an alkene moiety 'on top of' the cyclopropane ring.

6.2.1 Synthetic Pathway

Two different [5,6] adducts and two corresponding [6,6] adducts were synthesized via diazirine addition reactions. The diazirines were prepared according to literature procedures.[38-41] The necessary substituted phenylacetonitril (**6.9a,b**) was transformed to a benzylamidate ester hydrochloride (**6.10a,b**) by reaction with dry hydrochloric acid gas and ethanol. The thus obtained benzylamidate ester hydrochloride was allowed to react with ammonia to afford benzylamidine hydrochloride (**6.11a,b**). A subsequent Graham's oxidation[40] yielded the desired 3-benzyl-3-chloro-diazirines (**6.12a,b**). The diazirines were thermally decomposed in the dark and in the presence of a concentrated solution of C_{60}. In the reaction both [6,6] and [5,6] adducts are obtained, however, the percentage of [5,6] adducts is extremely low (see Scheme 6.1). Separation of the [5,6] and [6,6] adducts obtained from the diazirine addition was done by preparative HPLC. Interestingly, the two isomers of the [5,6]adduct separated on the column (but were collected as one fraction). One isomer has the chlorine atom above a pentagon while the other has the chlorine above a hexagon.

The subsequent HCl elimination was performed with KOtBu as a strong non-nucleophilic base in order to prevent nucleophilic substitution reactions involving chlorine atom as a leaving group (see scheme 6.1). Separation of the resulting fullerenes was achieved by preparative HPLC. In case of [5,6] adduct **6.7b** we were not able to isolate a pure fraction since only a trace amount of products was observed. In the case of **6.8a** we were able to obtain a pure fraction by HPLC, however, not enough material was obtained for full characterization. UV-Vis and Mass spectra however, were obtained.

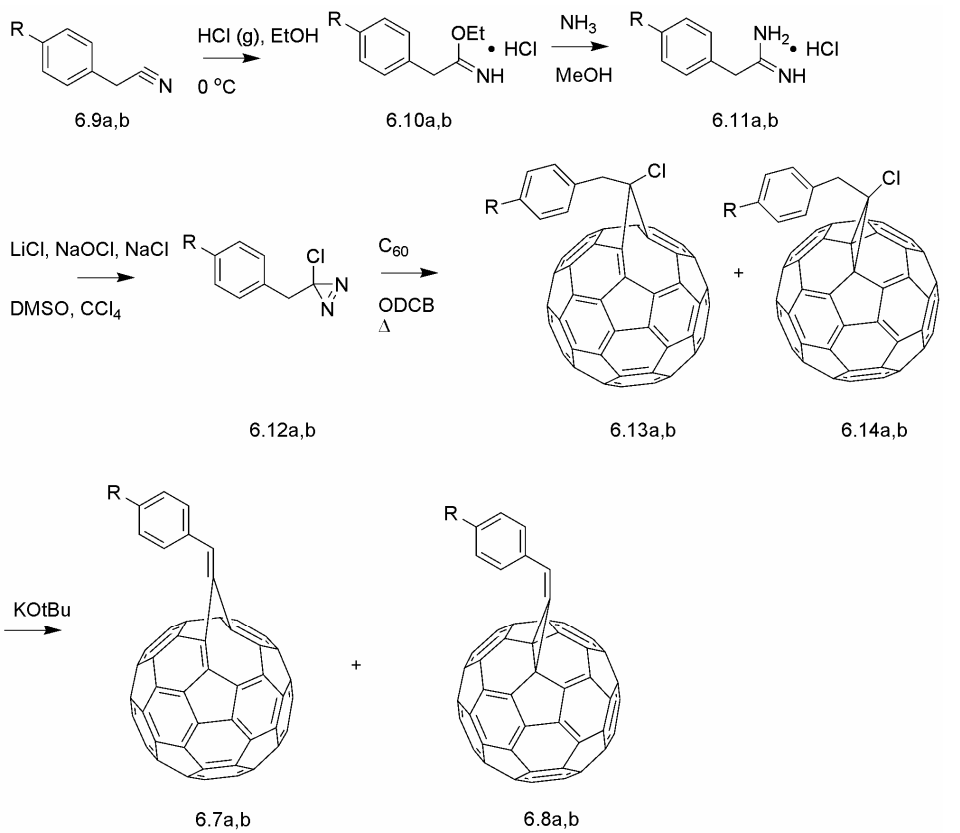

Scheme 6.1: Synthetic scheme for the synthesis of [5,6]bridged fulleroids and [6,6]bridged benzylidene fullerenes containing an 'alkene' functionality 'on top of' the cylopropane ring. a: R = H, b: R = NO_2

6.2.2 HCl elimination reaction

In order to obtain the alkene functionality on top of the cyclopropane ring an elimination reaction on **13a,b** and **14a,b** is needed. Generally, the elimination of HCl proceeds via an E2 mechanism. This means that the reaction is concerted and proceeds best in a non-protic polar solvent with a strong non-nucleophilic base. Furthermore, an antiperiplanar allignment of the proton and chlorine atom is necessary. As a solvent we used dichlorobenzene which is a non-protic polar solvent. As a base KOtBu is used, which is known to be a strong non-nucleophilic base. The necessary antiperiplanar allignment is also possible in this case, but it is expected that the fullerene cage will cause severe steric hindrance. It would therefore be preferable to use a small base. However, we have not been able to find a small strong non-nucleophilic base which is also unreactive towards fullerenes. After extensive optimilization experiments, good reaction conditions were found, which are described in the experimental section of this chapter. The elimination was followed by LC-MS. The appearance of a signal with a mass of ~36 smaller is observed, consistent with the elimination of HCl (see Table 6.1).

Table 6.1: Mass Spectrometry data

Compound	Mass[a]	Difference
6.13a	858.5	36.4
6.7a	822.1	
6.13b	903.8	36
6.7b	867.8	
6.14a	858.5	36
6.8a	822.5	
6.14b	904.0	36.1
6.8b	867.9	

[a] *main peak*

The elimination reactions proceeded cleanly without problems in the case of the [6,6]bridged fullerenes. The [5,6]bridged fulleroids (**6.14a,b**) however, did not give clean eliminated products. The desired product is observed, but only in small quantities. The appearance of eliminated [6,6]bridged fullerenes is observed next to the eliminated [5,6]bridged fulleroid, indicating that a rearrangement takes place during the reaction. Furthermore, a strong signal is observed with a mass of two higher than that of the eliminated product, indicating the presence of two additional hydrogen atoms.

Identification of this by-product has not been possible due to the low quantities that were obtained. We can speculate, however, on the identity of this byproduct. We suggest that the formation of a phenonium ion (third structure in figure 6.9) causes the formation of this byproduct, a subsequent addition of a hydride ion would result in a structure with a mass of two higher than that of the regular elimination product. The origin of this hydride ion however is unclear. The existence of phenonium ions in benzylic systems is well documented however, and not unlikely to occur in these structures.[42]

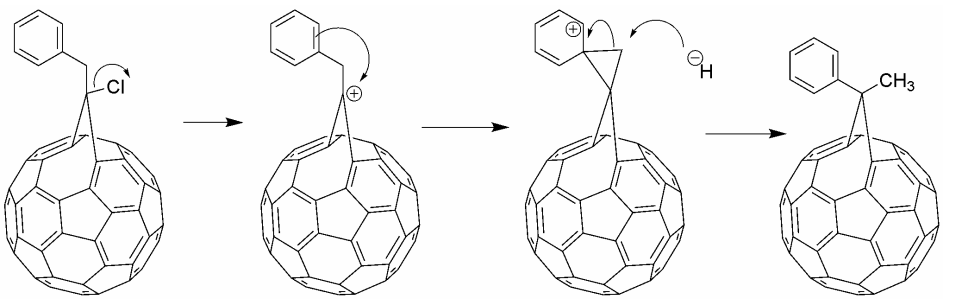

Fig. 6.9: Suggested mechanism of byproduct formation in elimination reactions on [5,6]bridged fulleroids.

The idea of a hydride ion is, however, quite unsatisfactory since the origin of such a hydride ion is not clear and even unlikely to be present. A more like possibility is that the cation (2nd structure from the left in figure 6.9), being extremely electonegative, is immedeately reduced, resulting in a radical structure, which might then abstract a hydrogen radical from, for example, dichlorobenzene.

6.3 [6,6]Bridged Fullerenes

6.3.1 NMR Characterization

After the elimination reaction, performed on the [6,6]adducts (**6.14a,b**), the ^{1}H NMR signal of the benzylic protons dissapears and a singlet with intensity of 1 proton appears 3 ppm downfield, clearly indicating the formation of a vinylic proton (see Fig. 6.10 and Fig. 6.11). Carbon NMR shows an upfield shift of ~70 ppm of the benzylic carbon as well as for the 'top' cyclopropane carbon. Only a slight upfield shift of 3 ppm of the bridgehead carbons is observed upon introduction of the alkene functionality.

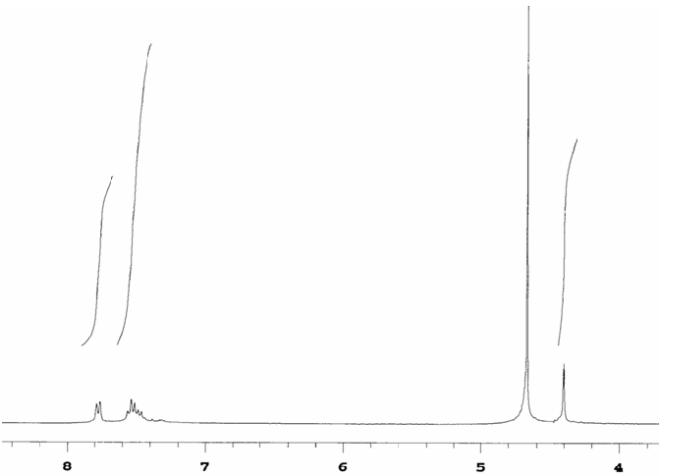

*Fig. 6.10: ^{1}H NMR (D_2O/CS_2) spectrum of **6.14a**, before elimination of HCl. The benzylic protons are clearly visible as a singlet around 4.4 ppm. D_2O is visible at 4.7 ppm.*

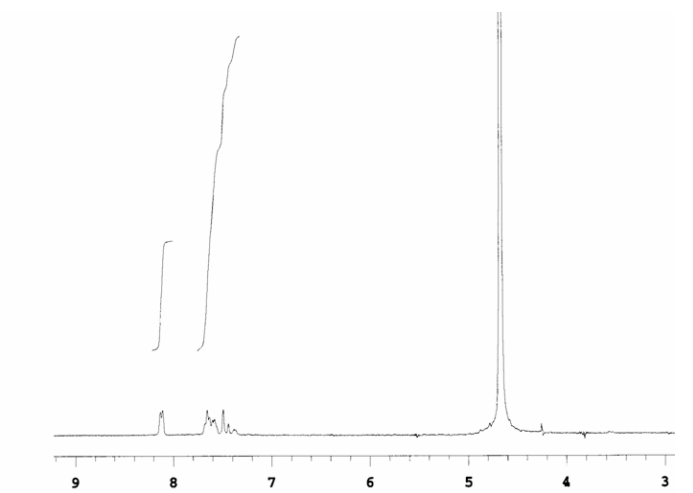

*Fig. 6.11: ^{1}H NMR (D_2O/CS_2) spectrum of **6.8a** after HCl elimination. The benzylic protons around 4.4 ppm have clearly dissapeared, instead the intensity of the multiplet around 7.5 ppm has increased due to the formation of the alkene bond. The expected singlet apparently appears in the same region as the aromatic protons and therefore the corresponding expected singlet can not be assigned with certainty. D_2O is visible at 4.7 ppm.*

6.3.2 UV-Vis Spectroscopy

The influence of introducing an alkene moiety 'on top of' the cyclopropane ring can be most clearly seen in the UV/Vis absorption spectra. A large red shift was observed indicating an effective overlap between both π-systems. The unsubstituted fullerene (**6.8a**) shows a red shift of ~18 nm while the nitro substituted fullerene (**6.8b**) shows a red shift of ~ 21 nm (see Table 6.2). These values correspond to a change in a transition responsible for absorption around 500 nm of 87 meV and 104 meV.

Table 6.2: UV/Vis Absorption maxima

Compound	Absorption (nm)	Bathochromic Shift (nm)
6.14a	497	18
6.8a	515	
6.14b	490	21
6.8b	511	

We believe that these changes are due to an effective peri-conjugation between both π-systems. The difference, when compared to the results of the Wudl group, is most likely due to the closer proximity and different orientation of both π-systems in the compounds presented here. (see Fig. 6.12) The shift in the Wudl system are seen in the HOMO-LUMO transition, while the shifts, presented here, are in π-π^* transitions responsible for absorption in the 500 nm region. We observe no shift of the lowest energy transition in our UV-Vis spectra. Since, we have not been able to isolate sufficient quantities of product, cyclic voltammetry measurements were not possible. We can therefore not draw any conclusions regarding possible shifts in the first reduction potential, which would also be relevant for the band gap of the material.

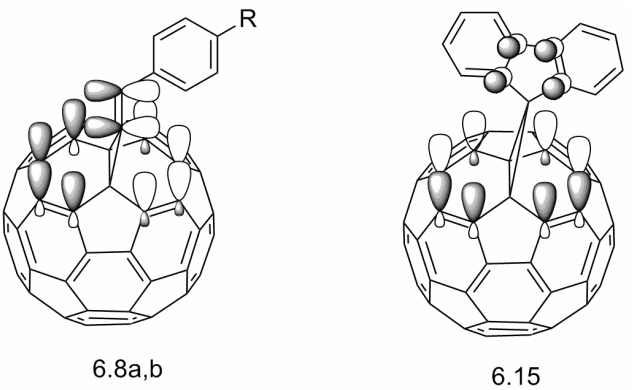

*Fig. 6.12: Peri-conjugation in **6.8a,b** (left) and right peri-conjugation in the fluorene substituted fullerene by Wudl (right).[7] (orbital signs are chosen as to give maximal overlap)*

Note that in the compound synthesized by the Wudl group (**6.15**) both π-systems are separated by two sp^3 carbons while in our case (**6.8a,b**) both π-systems are separated by only one sp^3 carbon. Besides being in closer proximity, the p_z orbitals are orientated in a different way, by a 90 degree angle, in both compounds. This means that the symmetry of the involved molecular orbitals is completely different, most likely causing a different interaction. We suggest that the overlap of the alkene p_z orbitals and the fullerene p_z orbitals in compounds **6.8a** and **6.8b** is more favorable than the overlap of the phenyl p_z orbitals and the fullerene p_z orbitals in the compound synthesized by Wudl. (see Fig. 6.12). The introduction of an electron withdrawing nitro group at the para position of the phenyl ring causes an additional red-shift of 3 nm. These results unequivocally demonstrate that we are able to tune the properties of a fullerene by introduction of a functional group which is connected to a fullerene in a peri-conjugated way.

6.3.3 Semi-emperical PM3 calculations

To further confirm the experimental results, semi-emperical PM3 calculations on the fullerenes discussed in this section (6.3) were performed with Hyperchem 7.5 Professional. Both the not eliminated (**6.14a,b**) and the eliminated (**6.8a,b**) structures were optimalized. The bond lengths and local charges show some interesting differences. The largest changes are observed close to the cyclopropane ring. The important regions are shown in Fig. 6.13. In order to examine the effect of the chlorine atom, the same structure was calculated, with the chlorine atom replaced by a hydrogen atom (**6.16a,b**).

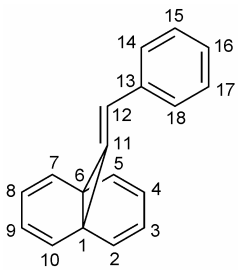

6.8a

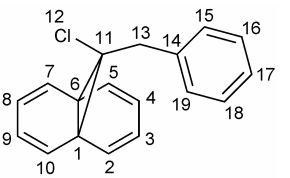

6.14a

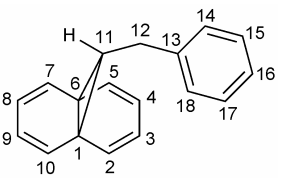

6.16a

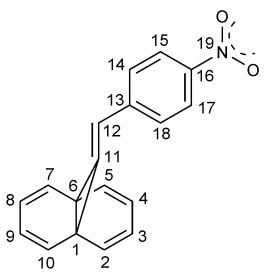

6.8b

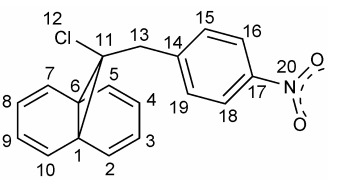

6.14b

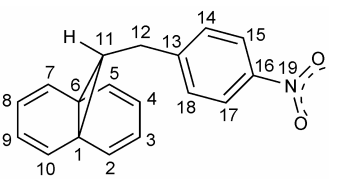

6.16b

Fig. 6.13: Regions in the 6,6-methano- and 6,6-benzylidenofullerenes for which atomic charges and bond lengths were calculated.

Table 6.3: Atomic charges calculated by semi-emperical PM3 calculations

		Charge	
Atom	**6.8a**	**6.14a**	**6.16a**
1	0.020	-0.043	-0.042
6	0.006	-0.039	-0.044
11	-0.103	-0.008	0.002
Atom	**6.8b**	**6.14b**	**6.16b**
1	0.011	-0.041	-0.040
6	0.010	-0.038	-0.043
11	-0.084	-0.017	-0.002

The calculated molecular charges are given in the table 6.3. Only the most striking changes are shown. Not surprisingly, the bridgehead carbons of the fullerene and

the carbon atoms in the bond on top of the cyclopropane ring are affected most strongly by the formation of a double bond due to the elimination of HCl.

The bridgehead carbon atoms 1 and 6 convert from partial negatively charged atoms to partial positively charged atoms when the alkene functionality is introduced on top of the cyclopropane ring. This change is attributed to a small electron withdrawing effect of the alkene functionality. This small effect indicates that the two π-systems interact to some extent. We can furthermore see that the chlorine atom has only little influence on atoms 1 and 6.

Table 6.4: Bond lengths calculated by semi-emperical PM3 calculations

		Bond Length (Å)	
Bond	**6.8a**	**6.14a**	**6.16a**
1-11	1.462	1.5089	1.5066
1-6	1.5778	1.553	1.5545
6-11	1.4611	1.5072	1.5062
11-12	1.3168		1.505
11-13		1.5069	
Bond	**6.8b**	**6.14b**	**6.16b**
1-11	1.4625	1.5059	1.5054
1-6	1.5761	1.5535	1.554
6-11	1.4616	1.5073	1.5063
11-12	1.3203		1.5077
11-13		1.5082	

The bond lengths of the cyclopropane moiety were affected to some extent as well, and are shown in table 6.4. A good indication of interaction between the two π-systems is the reduction in bondlength of bonds 1,11 and 6,11 which we attribute to an increase in electron delocalization. However, the bond length of the alkene moiety on top of the cyclopropane ring is somewhat smaller than standard double bonds (1.34 Å), indicating fairly poor electron delocalization. Again the chlorine atom seems to have little influence.

6.3.4 Conlusions

Both the experimental and computational results show that the introduction of an exo double bond on a cyclopropane ring in [6,6]bridged fullerenes causes a small but significant interaction between the two π-systems. Bathochromic shifts of 18 and 21 nm were observed in the absorption at ~500 nm, corresponding to an energy change of respectively 87 meV and 104 meV. This change is attributed to an effective periconjugation as drawn in Fig. 6.12. The observed changes are quite different from previously reported values, since Wudl et al. report changes in the HOMO-LUMO gap by cyclic voltammetry measurements, while we have not been able to measure the HOMO-LUMO gap. In contrast to Wudl. we see a large change in the absorption area at ~500 nm, caused by a change in a π-π^* transition.

6.4 [5,6]bridged Fulleroids

During the diazirine addition reaction only a very small amount of [5,6]bridged fullerenes (i.e. fulleroids) is formed. Especially the synthesis of **6.13b** was very troublesome. We have never been able to isolate enough product for full characterization, although HPLC gives the correct mass and a characteristic UV-Vis for [5,6]bridged fulleroids. All isolated product was immedeately used for elimination reactions. In case of **6.13a** we were able to isolate sufficient quantities and its characterization is reported in the experimental section of this chapter. In contrast to the [6,6]bridged fullerenes, elimination reactions with the [5,6]fulleroids gave little product and mainly sideproducts, which were highly insoluble. Fortunately, small amounts of product were observed and could be investigated by mass spectroscopy (data presented in Table 6.1) and UV-Vis absorption measurements.

6.4.1 UV-Vis Spectroscopy

The UV-Vis spectra of both **6.7a** and **6.7b** show a small bathochromic shift. The observed shifts, however, are quite a bit smaller than observed for the [6,6]bridged fullerenes (**6.8a,b**). The absorption maxima before and after the elimination reaction are presented in Table 6 5. The benzylidene [5,6] fulleroid (**6.7a**) could be isolated by preperative HPLC, but in insufficient quantities for further characterization. The UV-Vis spectrum shows a small bathochromic shift of 11 nm. Interesting however, is the appearance of a new shoulder at 664 nm, which might be caused by a previously forbidden π-π^* transition. We are tempted to attribute these changes to an interaction between the two π-systems. The 4-nitrobenzylidene [5,6] fulleroid (**6.7b**) was only observed as a small peak by HPLC, a clear mass signal, however, was obtained (see Table 6.1). The UV-Vis spectra

however, gave a very low signal to noise ratio. The presented data therefore is only indicative, but seems to show a small shift of 7 nm, indicating a small interaction as well.

Table 6 5: UV-Vis absorptions

Compound	Absorption (nm)	Bathochromic Shift (nm)
6.13a	537, 602(s)	11
6.7a	548, 603 (s), 664 (s)	
6.13b	540, 603 (s)	7
6.7b[a]	547	

[a] *Very low intensity signal*

6.4.2 Semi-emperical PM3 calculations

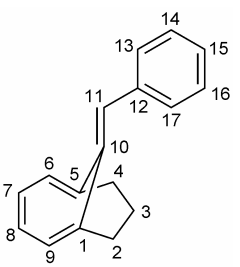

6.7a

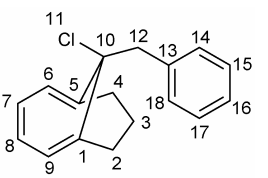

6.13a

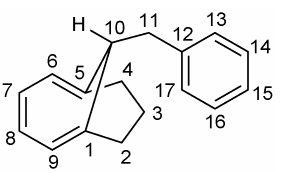

6.17a

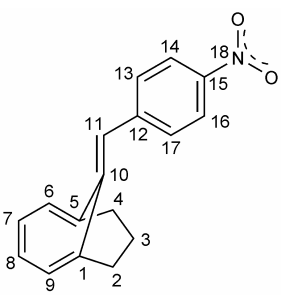

6.7b

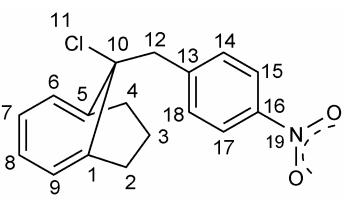

6.13b

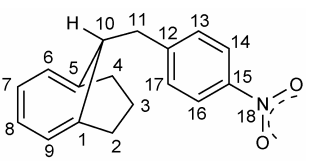

6.17b

Fig. 6.14: Regions for 5,6-methano- and 5,6-benzylidenofulleroids which atomic charges and bond lengths were calculated.

Calculations of the bond lengths and atomic charge densities were performed, and show similar effects as in the [6,6]bridged benzylidenofullerenes discussed in paragraph 6.3.3

The atomic charges of the carbon atoms 5 and 10 show significant changes (see Table 6.6). In both **6.7a** and **6.7b** the bridgehead carbons 1 and 5 become slightly positively charged when the alkene functionality is introduced. The 'bridging' carbon atom 10 shows the largest change. As can be expected, all 'bridging' carbons (1,5 and 10) are more negatively charged in **6.7a** than in **6.7b**, clearly showing the effect of the electron withdrawing nitro functionality. In both cases it is clear that the chlorine atom has an effect which was not seen in **6.8a** and **6.8b** (see paragraph 6.3.3 This is most likely due to the closer proximity of the π-system to the chlorine atom in the [5,6]bridged fulleroids.

Table 6.6: Atom charges calculated by semi-emperical PM3 calculations

	Atomic Charges		
Atom	**6.7a**	**6.13a**	**6.17a**
1	0.025	-0.018	0.001
5	0.039	0.006	-0.009
10	-0.103	0.037	0.000
Atom	**6.7b**	**6.13b**	**6.17b**
1	0.013	-0.029	-0.011
5	0.012	-0.039	-0.017
10	-0.059	0.035	0.003

The bond length calculations (see Table 6.7) show a clear shortening of the 1-10 and 5-10 bonds, indicating that some electron delocalization is taking place when the alkene functionality is introduced. Contrarily, the 10-11 bond shows clear double bond character in **6.7a,b**, which implies little electron delocalization is taking place. The chlorine atom has little influence on the bond lengths. Finally we see a significant change in the distance between atom 1 and 5 when the alkene bond is introduced. This change is expected since the bond angles increase around carbon 10 when going from a sp^3 hybridized situation to a sp^2 hybridized situation.

Table 6.7: Bond lengths calculated by semi-emperical PM3 calculations

	Bond Length (Å)		
Bond	**6.7a**	**6.13a**	**6.17a**
1-10	1.4642	1.4991	1.497
5-10	1.4601	1.4962	1.4977
1-5[a]	2.235	2.208	2.204
10-11	1.3348		1.5245
10-12		1.5259	
Bond	**6.7b**	**6.13b**	**6.17b**
1-10	1.4626	1.4962	1.4975
5-10	1.4613	1.4988	1.497
1-5[a]	2.241	2.208	2.206
10-11	1.333		1.525
10-12		1.5256	

[a] *Distance between atom 1 and 5, this is not an actual bond*

6.4.3 Conclusion

For the first time a fullerene has been functionalized in such a way that there is an alternating single–double bond pathway going from the addend to the fullerene moiety. The experimental data shows however, that the overlap between both systems is fairly small, most likely due to orbital misallignment. The largest red-shift of 11 nm was observed in the case of the benzylidene [5,6] fulleroid (**6.7a**). An interesting change in the spectrum is the appearance of an additional shoulder at 664 nm, which might be caused by a previously forbidden π-π* transition. The calculation data confirm the small effect that was observed in UV-Vis measurements.

6.5 Conclusions

We have successfully synthesized fullerenes with addends which are connected to the fullerene sphere via alternating single-double bonds. In theory, this is the closest one can get to creating a fully conjugated fullerene adduct.

The experimental data show, however, that the influence both π-systems have on each other is small. A maximal red-shift of 11 nm was observed for a benzylidene [5,6] fulleroid (**6.7a**). Calculations also show a small effect in bond lengths and atomic charges. The appearance of a shoulder at 664 nm in the UV-Vis spectrum of (**6.7a**) was observed.

The simultaneously synthesized [6,6]bridged benzylidene fullerenes do show quite a large interaction between the two π-systems, eventhough there is no alternating single-double bond pathway from the addend to the fullerene in this case. The large red shifts (18 and 21 nm) in UV-Vis spectroscopy that are observed are believed to be caused by a highly effective peri-conjugation. The results are furthermore supported by semi-emperical calculations. The difference between the benzylidene and the 4-nitro-benzylidene substituted fullerenes is marginal. For future research it would be very interesting to introduce an electron donating substituent on the phenyl ring like a dimethylamino group. This would create a push-pull fullerene molecule, which could have interesting properties. Furthermore, a larger π-system than the ones we have used, would be expected to show a more pronounced overlap because of better energy matching.

Overall we conclude that [6,6]bridged fullerenes offer the best possibilities of altering the electronic properties of fullerenes. They are rather easy to synthesize and show unmatched interaction between the two separate π-systems. A wide variety of fullerenes can be synthesized according to the presented methodology in this chapter, allowing for extensive tuning of the electronic properties of fullerenes. Thus providing new interesting fullerenes for different applications in molecular electronics.

6.6 Experimental

6.6.1 Materials

All reagents and solvents were used as received or purified using standard procedures. [60]-Fullerene (99.5 %) was purchased from MTR, Ltd (Cleveland, Ohio) and used without further purification. Flash chromatography was performed using silica gel (Kieselgel Merck Type 9385 (230-400 mesh)). ^{1}H NMR and ^{13}C NMR were performed on a Varian Unity Plus (400 MHz), on a Varian VXR-300 (300 MHz) or on a Varian VXR-200 (200 MHz) instrument as indicated, at 298 K using TMS as an internal standard. IR measurements were performed on a Nicolet Nexus FT-IR instrument. HPLC analyses were performed on a Hewlett Packard HP LC-Chemstation 3D (HP 1100 Series) using an analytical Cosmosil Buckyprep® column (4.6 x 250 mm). Elemental analysis was performed by the Microanalytical Department of this laboratory.

6.6.2 Synthesis

All precursors were synthesized by literature procedures as discussed in paragraph 6.2 The benzylidene fulleroids **6.7a,b** and fulleroid **6.13b** were not obtained in sufficient quantities for full characterization.

General Procedure for Diazirine addition: A flame-dried three-necked flask equipped with thermometer, condensor, N_2-inlet and stirring egg was charged with a solution of C_{60} in ODCB (20 mg/ml). This solution was thoroughly degassed by 3 N_2/vacuum purges. To this solution the diazirine (5 eq.) was added at once. The resulting reaction mixture was heated to 60 ^{0}C. The reaction is followed by HPLC and stopped at the following conversion: C_{60} : 50%, [6,6]adduct : 32 % and [5,6]adduct : 5%. The different products were then isolated by preparative HPLC using a Cosmosil® Buckyprep Waters packed column of 4.6 x 10 mm. and cyclohexane/toluene (1:1) as the eluens.

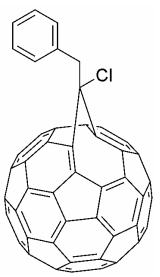

1-Benzyl-1-chloro [5,6] fulleroid C_{61} (6.13a): IR (KBr) = ν (cm^{-1}): 3425 (s), 3060 (m), 3028 (s), 2923 (s), 2851 (m), 1722 (m), 1601 (m), 1495 (s), 1454 (s), 1433 (s), 1380 (m), 1260 (w), 1174 (w), 1033 (m), 747 (s), 697 (s), 527 (s). ^{1}H NMR (D_2O/CS_2, 400 MHz); δ (ppm): 7.56 – 7.44 (m, 5H), 3.44 (s, 2H). UV/Vis (toluene/cyclohexane 1:1); λ (nm): 537, 602. Mass m/z calcd. for $C_{68}H_7Cl$: 858.02, Found: 858.8

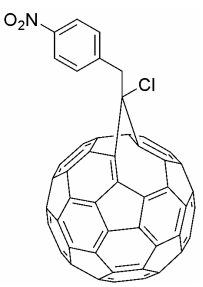

1-Chloro-1-(4-nitrobenzyl) [5,6] fulleroid C_{61} (6.13b): UV/Vis (toluene/cyclohexane 1:1); λ (nm): 540, 664. Mass m/z calcd. for $C_{68}H_6ClNO_2$: 903.01, Found: 903.8

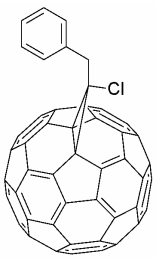

1-Benzyl-1-chloro [6,6] cyclopropafullerene C_{60} (6.14a): IR (KBr) = ν (cm^{-1}): 3426 (s), 3026 (w), 1602 (w), 1494 (m), 1465 (m), 1452 (m), 1429 (m), 1385 (w), 1186 (m), 698 (m), 577 (m), 526 (s). ^{1}H NMR (D_2O/CS_2, 300 MHz); δ (ppm): 7.78 (d, *J* = 6.9 Hz, 2H), 7.47–7.7.56 (m, 3H), 4.67 (s, 2H). ^{13}C NMR (D_2O/CS_2, 300 MHz); δ (ppm): 39.1, 57.3, 78.8, 127.3, 128.4, 129.7, 130.1, 135.2, 137.0, 138.7, 140.6, 140.9, 141.4, 141.7, 141.8, 141.9, 142.7, 142.9, 143.2, 144.0, 144.1, 144.2, 144.4, 144.5, 144.6, 144.7, 144.8, 145.3, 145.6. UV/Vis (toluene/cyclohexane 1:1); λ (nm): 431, 497, 692. Mass m/z calcd. for $C_{68}H_7Cl$: 858.02, Found: 858.6.

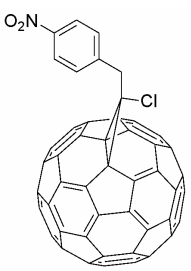

1-Chloro-1-(4-nitrobenzyl) [6,6] cyclopropafullerene C_{60} (6.14b): IR (KBr) = ν (cm^{-1}): 3424 (s), 1601 (m), 1517 (s), 1430 (m), 1340 (s), 854 (w), 578 (w), 526 (s). ^{1}H NMR (D_2O/CS_2, 400 MHz); δ (ppm): 8.45 (d, J = 8.8 Hz, 2H) , 8.06 (d, *J* = 8.8 Hz, 2H), 4.58 (s, 2H). UV/Vis (toluene/cyclohexane 1:1); λ (nm): 438, 490, 685. Mass m/z calcd. for $C_{68}H_6ClNO_2$: 903.01, Found: 903.3.

General Procedure for HCl elimination reaction: A flame dried flask was charged with a solution of fullerene in ODCB. This solution was heated to 50 °C and KOtBu (2 eq) was then added. The reaction was followed by HPLC. When a conversion of around 85% was reached, the reaction was stopped and the products were purified by the same preperative HPLC procedure as before.

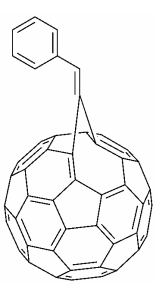

Benzylidene [5,6] fulleroid C_{61} (6.7a): UV/Vis (toluene/cyclohexane 1:1); λ (nm): 548, 603, 664. Mass m/z calcd. for $C_{68}H_6$: 822.04, Found: 822.7.

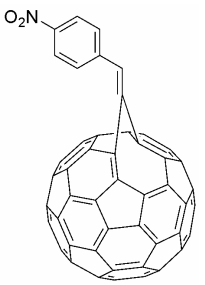

4-Nitrobenzylidene [5,6] fulleroid C_{61} (6.7b): UV/Vis (toluene/cyclohexane 1:1); λ (nm): 547. Mass m/z calcd. for $C_{68}H_5NO_2$: 867.03, Found: 867.8.

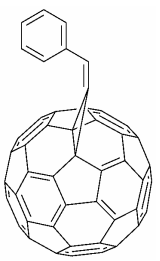

Benzylidene [6,6] cyclopropafullerene C_{60} (6.8a): IR (KBr) = v (cm^{-1}): 3026 (s), 1538 (w), 1496 (w), 1466 (m), 1452 (m), 1429 (s), 1259 (m), 1188 (s), 1076 (m), 915 (w), 879 (w), 752 (m), 743 (m), 688 (s), 525 (s), 518 (s). ^{1}H NMR (D_2O/CS_2, 300 MHz); δ (ppm): 8.1 (d, J = 7.7 Hz, 2H), 7.63 (t, *J* = 6.9 Hz, 2H), 7.54–7.58 (m, 1H). 7.47 (s, 1H). UV/Vis (toluene/cyclohexane 1:1); λ (nm): 427, 515, 690. Mass m/z calcd. for $C_{68}H_6$: 822.04, Found: 822.7.

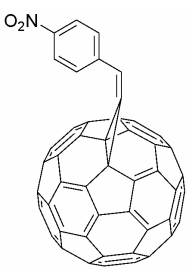

4-Nitrobenzylidene [6,6] cyclopropafullerene C_{60} (6.8b): IR (KBr) = v (cm^{-1}): 3446 (s), 1597 (m), 1516 (s), 1429 (m), 1340 (s), 1109 (m), 526 (s). ^{1}H NMR (D_2O/CS_2, 400 MHz); δ (ppm): 8.49 (d, *J* = 8.8 Hz, 2H), 8.30 (d, *J* = 8.8 Hz, 2H), 7.58 (s, 1H). UV/Vis (toluene/cyclohexane 1:1); λ (nm): 511. Mass m/z calcd. for $C_{68}H_5NO_2$: 867.03, Found: 867.7.

6.7 References

1. M. Prato and D. M. Guldi, *Acc.Chem.Res.*, 1998, **31**, 519.
2. M. Maggini, G. Scorrano, and M. Prato, *J.Amer.Chem.Soc.*, 1993, **115**, 9798.
3. C. Bingel, *Chem.Ber.*, 1993, **126**, 1957.
4. R. González, J. C. Hummelen, and F. Wudl, *J.Org.Chem.,* 1995, **60**, 2618.

5. A. Hirsch and M. Brettreich, *Fullerenes Chemistry and Reactions*, Wiley-VCH Verlag GmbH & Co. KgaA, Weinheim, 2005.
6. F. B. Kooistra, J. Knol, F. Kastenberg, L. M. Popescu, W. J. H. Verhees, J. M. Kroon, and J. C. Hummelen, *Org.Lett.*, 2007, **9**, 551.
7. M. Eiermann, R. C. Haddon, B. Knight, Q. C. Li, M. Maggini, N. Martin, T. Ohno, M. Prato, T. Suzuki, and F. Wudl, *Angew.Chem.Int.Ed.*, 1995, **34**, 1591.
8. H. Dürr and R. Gleiter, *Angew.Chem.Eng.Ed.*, 1978, **17**, 559.
9. R. Hoffmann, A. Imamura, and G. D. Zeiss, *J.Amer.Chem.Soc.*, 1967, **89**, 5215.
10. H. E. Simmons and T. Fukunaga, *J.Amer.Chem.Soc.,* 1967, **89**, 5208.
11. M. J. Goldstein and R. Hoffmann, *J.Amer.Chem.Soc.,* 1971, **93**, 6193.
12. P. Maslak, M. P. Augustine, and J. D. Burkey, *J.Amer.Chem.Soc.,* 1990, **112**, 5359.
13. a) C.-C. Wu, W.-G. Liu, W.-H. Hung, T.-L. Liu, K.-T. Wong, Y.-Y. Chien, R.-T. Chen, T.-H. Hung, T.-C. Chao, and Y.-M. Chen, *Appl.Phys.Lett.*, 2005, **87**, 052103. b) P. Sandín, A. Martínez-Grau, L. Sánchez, C. Seoane, R. Pou-Amérigo, E. Ortí, N. Martín, *Org.Lett*., 2005, **7**, 295.
14. F. Wudl, T. Sukuki, and M. Prato, *Synth.Met.*, 1993, **59**, 297.
15. W. Fu, J.-K. Feng, G.-B. Pan, and X. Zhang, *Theor.Chem.Acc.*, 2001, **106**, 241.
16. E. Vogel, F. Weyres, H. Lepper, and V. Rautenstrauch, *Angew.Chem.*, 1966, **78**, 754.
17. S. Itô, H. Ohtani, S. Narita, and H. Honma, *Tetrahedron Lett.,* 1972, **13**, 2223.
18. K. Yamamoto, J. Ojima, N. Morita, and T. Asao, *J.Chem.Soc.,Chem.Commun.*, 19871851.
19. K. Yamamoto, J. Ojima, N. Morita, and T. Asao, *Bull.Chem.Soc.Jpn.*, 1988, **61**, 1281.
20. H. R. Blattmann, W. A. Böll, E. Heilbronner, G. Hohlneicher, E. Vogel, and J. P. Weber, *Helv.Chim.Act.*, 1966, **7**, 2017.
21. H. Cerfontain, A. Koeberg-Telder, H. J. A. Lambrechts, W. Lindner, S.-Z. Zhang, and E. Vogel, *J.Org.Chem.,* 1987, **52**, 3373.
22. K. M. Creegan, J. L. Robbins, W. K. Robbins, J. M. Millar, R. D. Sherwood, P. J. Tindall, and D. M. Cox, *J.Amer.Chem.Soc.*, 1992, **114**, 1103.
23. D. Heymann, S. M. Bachilo, R. B. Weisman, F. Cataldo, R. H. Fokkens, N. M. M. Nibbering, and L. P. F. Chibante, *J.Amer.Chem.Soc.*, 2000, **122**, 11473.
24. M. Prato, Q. Chan Li, F. Wudl, and V. Lucchini, *J.Amer.Chem.Soc.*, 1993, **115**, 1148.
25. J. C. Hummelen, B. W. Knight, F. Lepeq, F. Wudl, J. Yao, and C. L. Wilkins, *J.Org.Chem.*, 1995, **60**, 532.
26. R. C. Haddon and K. Raghavachari, *Tetrahedron*, 1996, **52**, 5207.
27. R. C. Haddon, *J.Amer.Chem.Soc.*, 1986, **108**, 2837.
28. R. A. Moss, *Acc.Chem.Res.*, 2006, **39**, 267.

29. M. T. H. Liu, *Chem.Soc.Rev.*, 1982, **11**, 127.
30. I. D. R. Stevens, *J.Chem.Soc.,Perkin Trans.2.*, 1990661.
31. R. Bonneau and M. T. H. Liu, *J.Amer.Chem.Soc.*, 1996, **118**, 7229.
32. E. L. Tae and M. S. Platz, *Tetrahedron Lett.*, 1999, **40**, 2875.
33. X. Fu, R. A. Moss, P. Piotrowiak, M. Myahkostupov, and I. R. Gould, *Org.Lett.*, 2006, **8**, 4807.
34. J. Wang, G. Burdzinski, J. Kubicki, M. S. Platz, R. A. Moss, X. Fu, P. Piotrowiak, and M. Myahkostupov, *J.Amer.Chem.Soc.*, 2006, **128**, 16446.
35. T. Akasaka, M. T. H. Liu, Y. Niino, Y. Maeda, T. Wakahara, M. Okamura, K. Kobayashi, and S. Nagase, *J.Amer.Chem.Soc.*, 2000, **122**, 7134.
36. T. Wakahara, Y. Niino, T. Kato, Y. Maeda, T. Akasaka, M. T. H. Liu, K. Kobayashi, and S. Nagase, *J.Amer.Chem.Soc.*, 2002, **124**, 9465.
37. M. T. H. Liu, Y.-K. Choe, M. Kimura, K. Kobayashi, S. Nagase, T. Wakahara, Y. Niino, M. O. Ishitsuka, Y. Maeda, and T. Akasaka, *J.Org.Chem.*, 2003, **68**, 7471.
38. E. Schmitz and R. Ohme, *Chem.Ber.*, 1961, **94**, 2166.
39. E. Schmitz and R. Ohme, *Chem.Ber.*, 1962, **95**, 795.
40. W. H. Graham, *J.Amer.Chem.Soc.*, 1965, **87**, 4396.
41. M. T. H. Liu, N. H. Chishti, M. Tencer, H. Tomoka, and Y. Izawa, *Tetrahedron*, 1984, **40**, 887.
42. J. March, in *Advanced Organic Chemistry*, John Wiley & Sons, Inc., New York, 4 edn., 1992, ch.10, pp. 293-500.

Chapter 7

Giant Pearl-Necklace Fullerene Macrocycles

In this Chapter the synthesis of large fullerene macrocycles is described. The macrocycles were synthesized by transesterification reactions between bis-PCBM and diols, applying dibutyltinoxide (DBTO) as a catalyst. Cycles containing up to eighteen fullerenes were detected by MALDI-TOF techniques. These structures present the first example of true pearl-necklace macrocycles.

[*]Part of this work was published:

Floris B. Kooistra, Frank Brouwer, and Jan C. Hummelen, **2007**, *submitted for publication.*

7.1 Introduction

Three dimensional supramolecular structures containing buckminsterfullerene, C_{60}, have been studied widely ever since the discovery of C_{60} by Kroto, Smalley, and Curl.[1] These structures are usually based on the complexing ability of fullerenes with conjugated systems, which have either ball, bowl, or belt shapes.[2-4] (see figure 7.1).

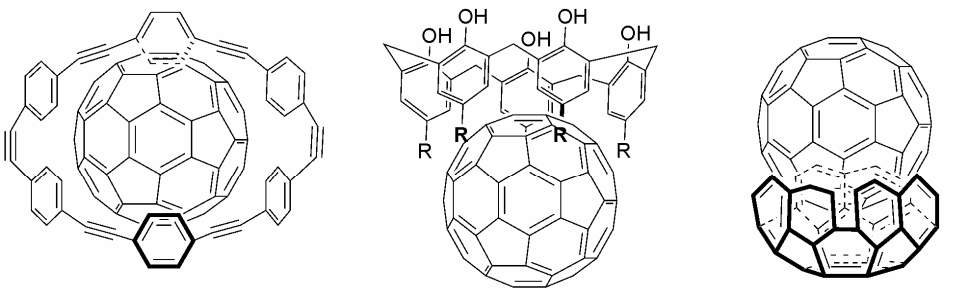

7.1 7.2 7.3

Fig. 7.1: Some examples of supramolecular fullerene complexes.[4]

Covalently bound, large molecular structures containing fullerene moieties are scarce. Four different types of structures can be imagined (see figure 7.2), charm-bracelet polymers (A) and macrocycles (B), and pearl-necklace polymers (C) and macrocycles (D). Charm-bracelet polymers consisting of a backbone with pendant fullerenes are well known.[5] Charm-bracelet macrocycles are much less known. The only good example of this type of structure, to our opinion, was made by Diederich et al.[6,7] These structures consist of a polyacetylene macrocycle with three or four pendant fullerenes (see figure 7.3). Furthermore, tethered fullerene adducts can be considered to be fullerene macrocyclic structures, but they contain only one fullerene unit and are therefore not considered to be true pearl-necklace macrocycles.[8,9] Pearl-necklace polymers of fullerenes are very rare. The only such structures are obtained by a [2+2] cycloaddition of fullerene units.[10] Pearl-necklace macrocycles on the contrast are unknown until now. It is worth mentioning here that some first 'monomers' of pearl-necklace and charm-bracelet structures were developed as early as 1992 by the group of Wudl (see figure 7.4).[11,12] However, polymeric, let alone macrocyclic structures were never realized.

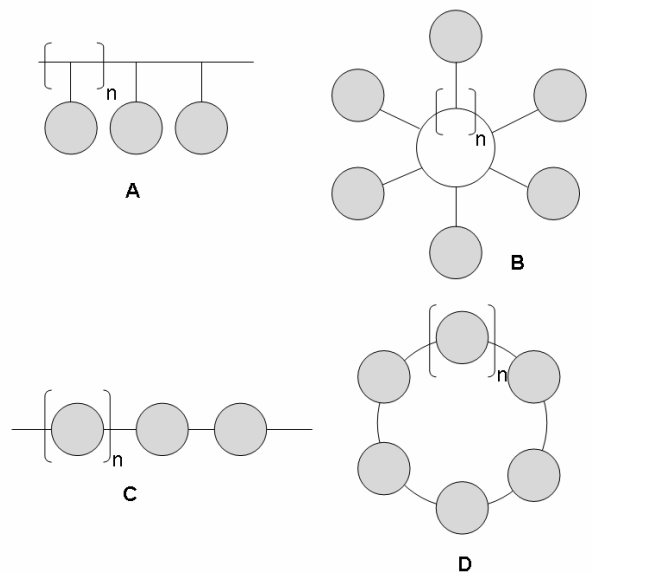

Fig. 7.2: Charm-bracelet structures (A and B) and, Pearl-necklace structures (C and D).

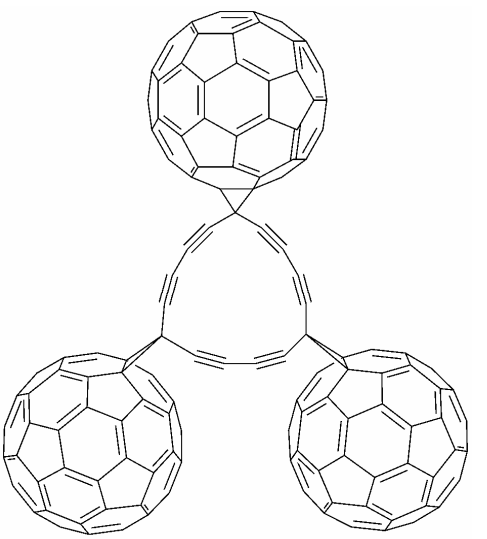

7.4

Fig. 7.3: Example of a charm-bracelet structure by Diederich et al.[7;9]

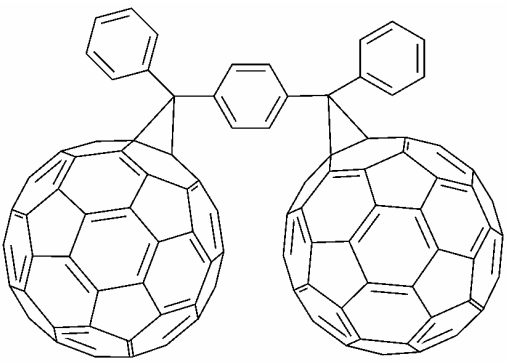

7.5

Fig. 7.4: Precursor for pearl-necklace structures synthesized by Wudl et al.

7.1.1 Macrocyles

The synthesis of macrocycles has attracted much attention recently and numerous examples are known: natural products containing macrocycles,[13] amino acid derived macrocycles,[14] porphyrine ring structures (**7.6**),[15] conjugated macrocycles (**7.7**),[16] cyclooligomerized macrocycles (**7.8**),[17] and pyrrole macrocycles (**7.9**).[18] Their applicability ranges from ion transport across membranes, and antibiotics to catalysis.[14] Some examples of electronically interesting macrocyclic structures are depicted in figure 7.5.

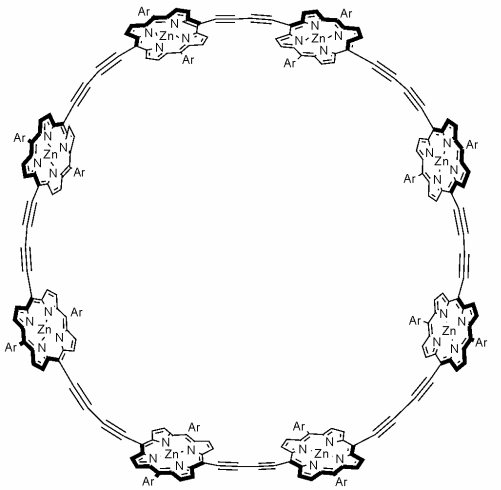

7.6: porphyrin macrocycle

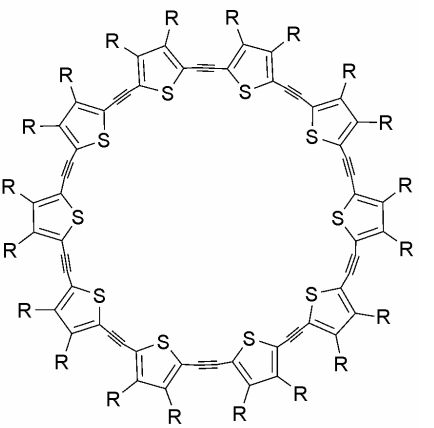

7.7: oligothiophene macrocycle

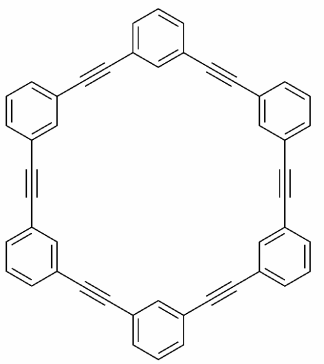

7.8: hexameric phenyleneethynylene macrocycle

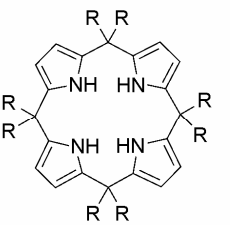

7.9: calix[4]pyrrole

Fig. 7.5: Some examples of electronically interesting macrocycles

7.1.2 Ring forming polycondensations

The formation of ring structures has been studied extensively for polycondensation reactions.[19-22] These reactions can either be thermodynamically controlled polycondensations (TCP) or kinetically controlled polycondensations (KCP), which are defined as: "*KCP means that equilibration reactions are absent, and the reaction mixtures do not represent the thermodynamic optimum of the system under investigation. TCP means that equilibration reactions including ring-chain and ring-ring equilibria are present throughout the polymerization process, so that*

reaction mixtures represent the thermodynamic optimum at any stage of polycondensation".[21]

Cyclization is favored under highly diluted conditions, and should be the sole product under ideal KCP conditions.[23-26] In the case of TCP, cyclic oligomers are formed due to so-called 'back-biting degradation'.[27] Furthermore, the formation of cycles will be favored under TCP conditions when temperatures are high and concentrations low. This directly results from an entropy gain when many small cycles are formed, instead of one large chain.[22]

7.1.3 Dialkyltinoxide catalyzed transesterification.

One of the most famous polycondensation reactions is polyesterification. Polyesterification reactions can be catalyzed very efficiently by dialkyltinoxides.[28,29] The origin of the catalytic efficiency of dialkyltinoxides has recently been reviewed by Llauro and Michel.[30] The catalytic species is a dimeric alkoxy distannoxane compound (**7.10**), which is formed *in situ* when the dialkyltinoxide reacts with the polymer ester functionalities. First the alkoxydistannoxane is formed, which coordinates to the ester. Subsequent alcoholysis yields the transesterified product (see scheme 7.1).

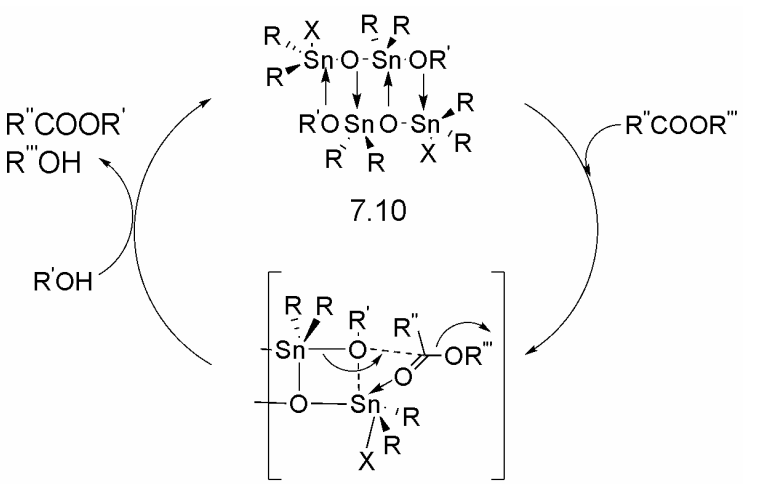

Scheme 7.1: Catalytic cycle of dialkyltinoxide catalyzed transesterification.[28]

Baumhof et al. found that this transesterification reaction is also applicable for 'regular' molecules, when applying dibutyltinoxide (DBTO) as the catalyst.[31] This methodology has been applied succesfully in our labs to perform transesterification reactions on phenyl–C_{61}–butyric acid methylester (PCBM).[32]

7.1.4 Research Goal

As was demonstrated in chapter 5, fullerenes can be applied in time-gated holographic imaging (TGHI) as the charge transporting matrix. However, low Tg materials are needed, which are processable and thermally stable. Polymeric structures, containing fullerenes, would be highly interesting materials for this application.

The structures resulting from transesterification reactions between bis-PCBM (**7.11**) and several diols, using DBTO as a catalyst (see scheme 7.2), were studied with MALDI-TOF techniques. We hypothesized that this reaction would lead to polymeric fullerene structures.

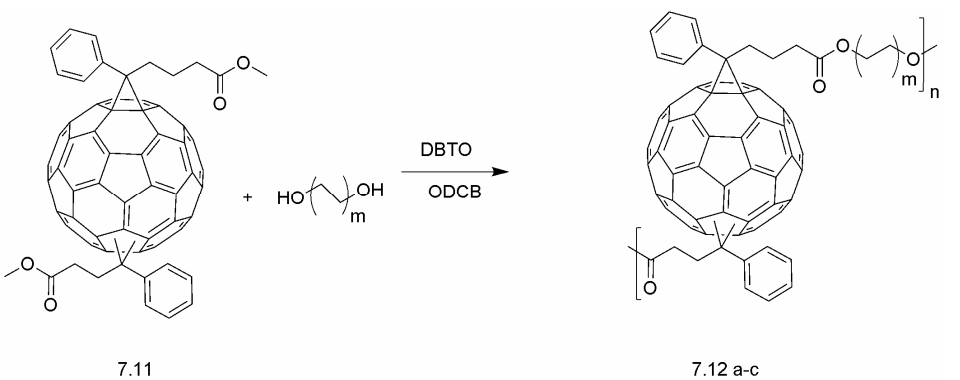

*Scheme 7.2: Proposed co-polymerization of bis-PCBM (**7.11**) with α,ω-diols (a: m=1,b: m=2, c: m=3) to yield linear (open) chain products.*

7.2 Synthesis

Pure bis-PCBM (**7.11**) was subjected to transesterification reactions with different diols (ethyleneglycol (m=1), 1,4-butanediol (m=2), and 1,6-hexanediol (m=3)), using DBTO as the catalyst (see scheme 7.2). No linear (open) chain polymeric structures, but formation of large ring structures was found (see scheme 7.3), for which proof will be presented in the next paragraphs. Apparently the low concentration, under which the reactions were performed (due to the low solubility of fullerenes), resulted in formation of ring structures. Since fullerenes are known to form aggregates in solution, we suggest that the possible formation of fullerene aggregates in solution could facilitate the formation of ring structures even more.

In order to be able to fully characterize a macrocycle, an attempt was made to selectively synthesize a cycle consisting of only two fullerenes (**7.14**). First, bis-PCBM (**7.11**) was transesterified by allowing it to react with a large excess of 1,6-hexanediol (40 eq.) and DBTO as the catalyst. The bis-esterified product (**7.14**) was successfully obtained. This product was then allowed to react with bis-PCBM (**7.11**) in a stoichiometric fashion, once again applying DBTO as the catalyst (see scheme 7.4). The reaction, however, yielded a mixture of rings of various sizes, as will be shown in the next paragraphs.

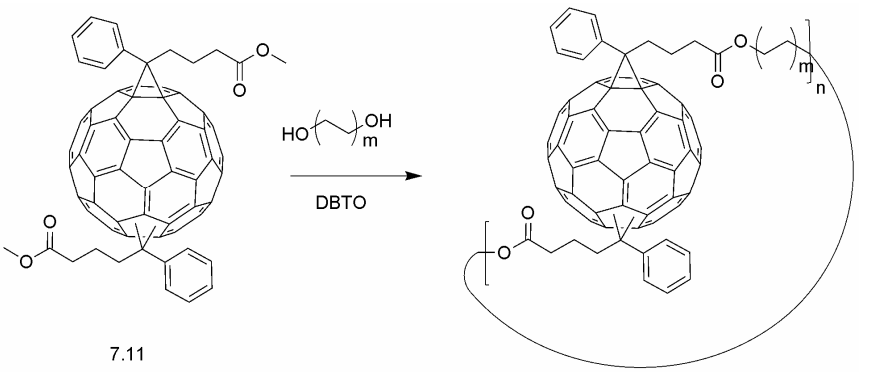

Scheme 7.3: Synthesis of fullerene macrocycles. m=1,2,3.

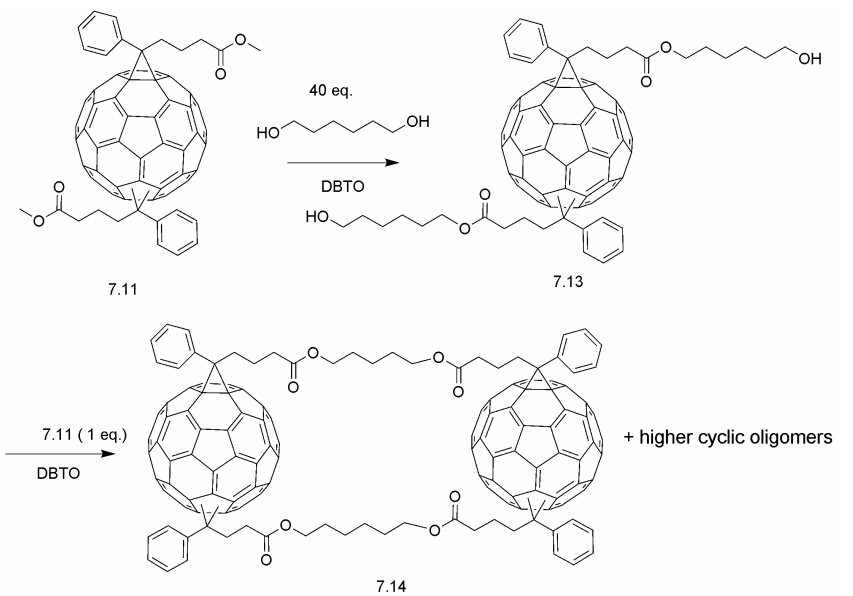

*Scheme 7.4: Attempted selective synthesis of a macrocycle consisting of two fullerenes (**7.14**).*

7.3 MALDI-TOF Spectroscopy

All products were analyzed by matrix-assisted laser desorption/ionization time of flight (MALDI-TOF) spectroscopy. A sample consisting of the object of study and a UV absorbing matrix is subjected to laser light. Most of the energy of the laser will be absorbed by the matrix, which prevents undesired fragmentation of the object of study. MALDI-TOF is therefore called a soft ionization technique. All ionized molecules are accelerated in an electric field and are separated based on their mass. The method is usually applied in the characterization of large molecules like peptides, proteins, oligosaccharides and oligonucleotides. Masses up to 350.000 Da can be detected. The method is therefore also very useful for the characterization of polymers and, in this case, fullerene structures.

In the structures studied here, various reaction intermediates were observed besides large cyclic structures. Tin complexes however, were never observed, which might be due to the applied washing and precipitation methods (see experimental section). As can be expected the largest ring structures are found when 1,6-hexanediol is used as the alcohol. The longer 'chain' might facilitate the intramolecular transesterification and, in principle, might induce solubility allowing for larger structures to form in solution.

MALDI-TOF spectra of all three types of macrocycles (i.e. n=1,2,3) are depicted in figure 7.6 (for full size spectra see Appendix I). In the insets of figure 7.6 the MALDI-TOF spectra show the highest mass regions. Eventhough it is not possible to assign structures with any certainty to these masses, it does illustrate that our method of cyclization/polymerization is highly effective, obtaining cyclic/polymeric structures with masses up to ~48.500 amu. containing at least 42 fullerene units.

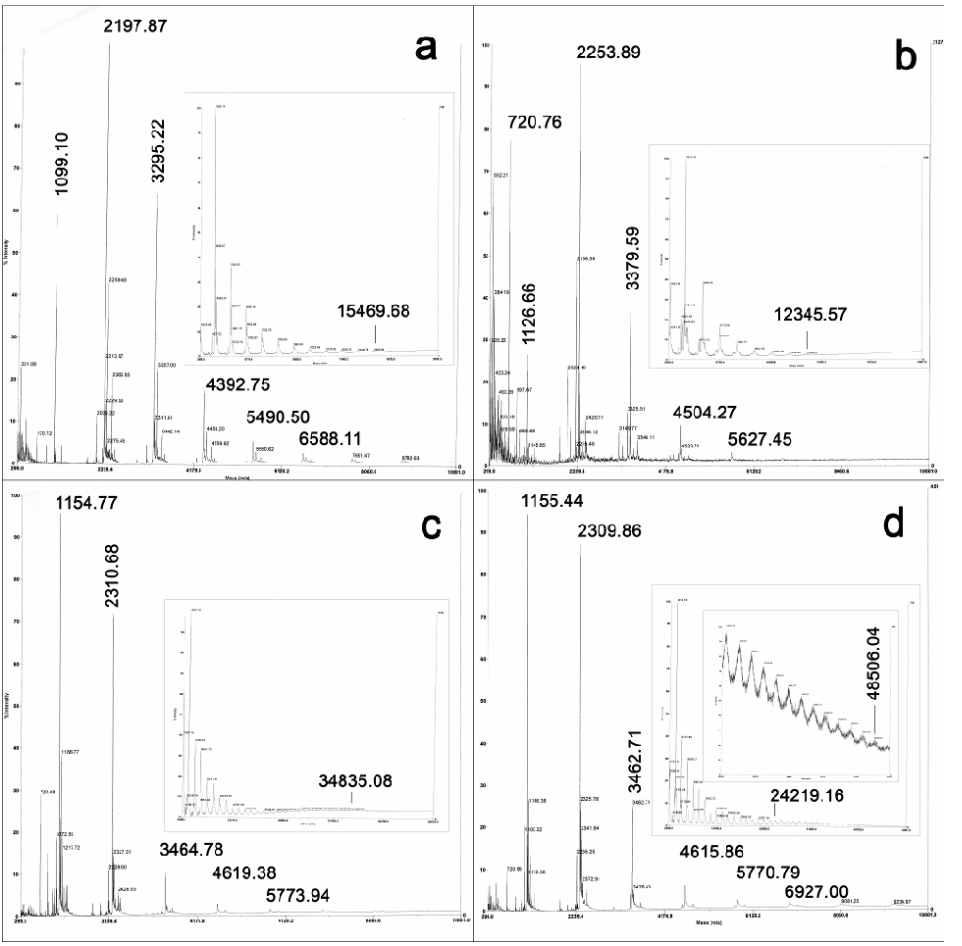

Fig. 7.6: MALDI-TOF spectra. A) n=1, B) n=2, C) n=3, D) n=3: obtained from the reaction depicted in scheme 7.4. The insets show the higher mass regions.

The structures and masses assigned to each macrocycle (up to a cycle containing five fullerenes) are shown in figure 7.7. The MALDI-TOF spectra clearly show the formation of macrocycles containing up to eighteen fullerenes. Masses of structures containing at least 42 fullerenes are visible in the case of n=3 (see figure 7.6d). These peaks, however, broaden significantly and it is therefore not possible to assing a definitive structure. Also, the experimental error becomes too large to

differenciate between ring-closed and ring-opened structures.[I] The mass difference between ring-closed and ring-opened (one side a methyl ester and on the other side an alcohol) is 32. Due to hydrolysis ring-opened structures can be formed as well with a mass of 18 higher. When masses exceed 30.000 it is impossible to distinguish ring-closed from ring-opened structures.

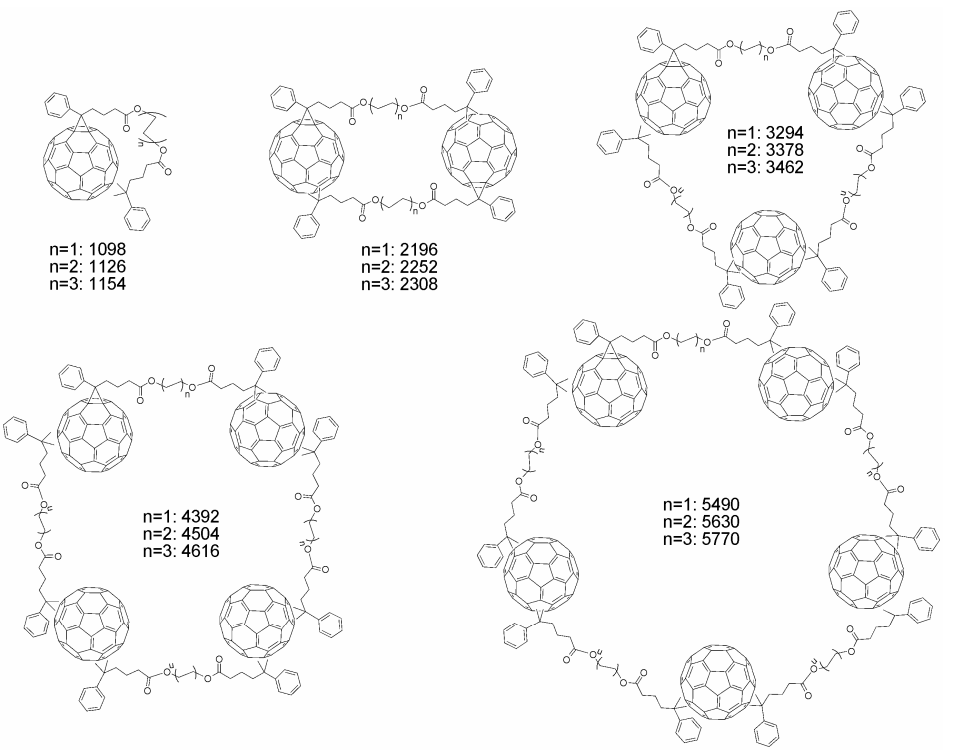

Fig. 7.7: Structures of the smallest pearl-necklace macrocycles including their calculated mass (isotope effects excluded).

Besides cyclic structures, minor amounts of structures of intermediate compounds are also observed. These intermediates consist of mono- and di-esterified bis-PCBM, as well as some ring opened structures (see figure 7.8).

[I] Experimental error for MALDI-TOF is ~ 0.1%.

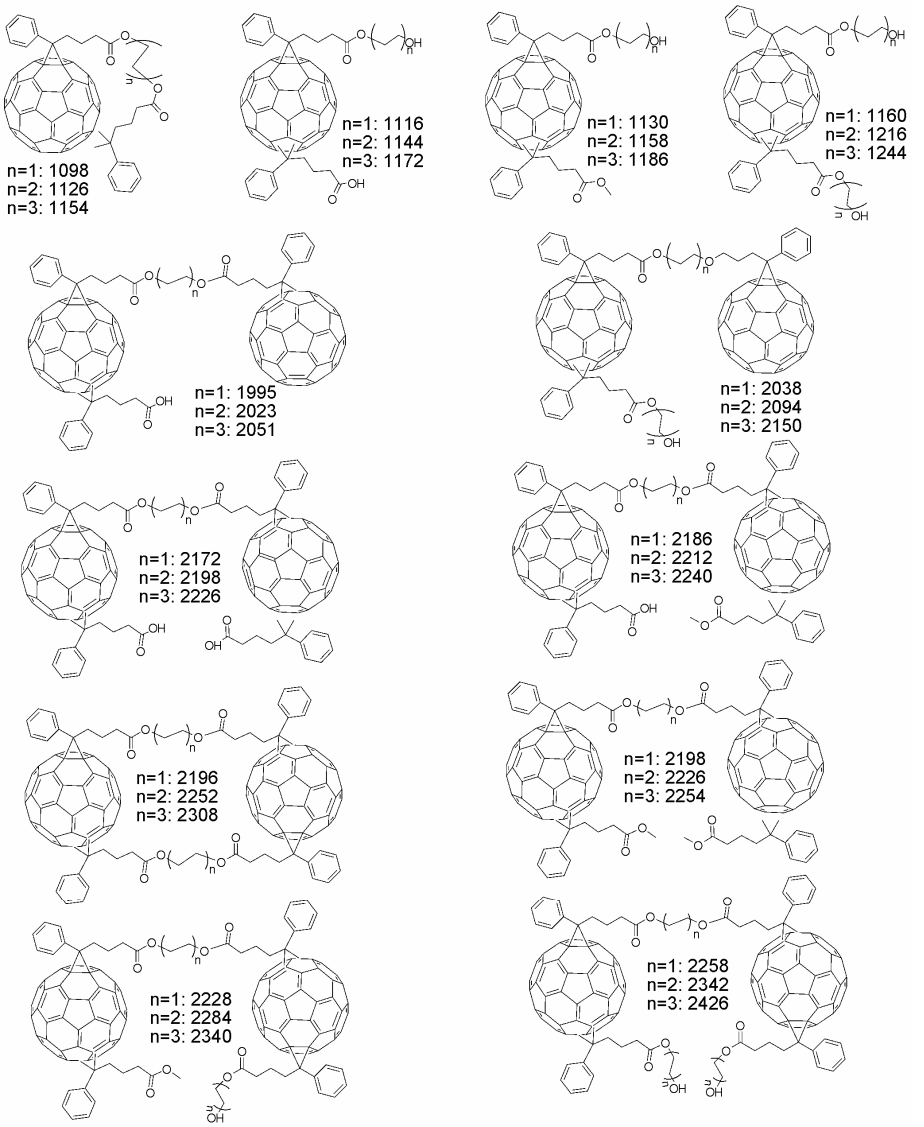

Fig. 7.8: Possible intermediates during cyclization reactions and their respective masses (isotope effects excluded).

The intermediates that are visible in the MALDI-TOF spectra differ for each reaction. All visible masses up to structures containing two fullerenes can be explained by the structures depicted in figure 7.8. Masses that show up in the MALDI-TOF, which are 16 higher than expected are attributed to oxidized fullerenes. Masses that are 17 higher than expected can be explained by

hydrolysis of cyclic esters. In negative mode MALDI-TOF the carboxylic acid will be deprotonated, hence a mass of 17 higher and not 18 higher, will be found.

The most intense signals, however, are clearly those of cyclic structures. We furthermore, deduct from the differences in spectrum 7.6c and 7.6d that for obtaining high mass structures it is favorable to first synthesize the transesterified bis-PCBM (**7.13**) and subsequently allow this to react with bis-PCBM (**7.11**) (see scheme 7.4). Interestingly, spectrum 7.6d does not show a mass of signal of compound **7.13** (1272 amu.), indicating full conversion. The mass signal of 1155, belonging to a cycle containing one fullerene, furthermore, proves that intramolecular esterification is taking place when DBTO is added to compound **7.13**.

7.4 Conclusions

True pearl-necklace fullerene giant macrocycles were synthesized by polyesterification reactions using DBTO as the catalyst. MALDI-TOF spectroscopy shows the presence of cycles containing up to eighteen fullerene units. Even higher masses are observed, but these can not be assigned with any certainty to ring-closed or ring-opened structures. Since these macrocyclic structures are quite soluble in fullerene solvents, they may play a future role in fullerene based molecular electronic applications.

7.5 Experimental

MALDI-TOF measurements were performed on a Voyager-DE Pro apparatus. S_8 was used as the matrix. The MALDI-TOF measurements were calibrated with a mixture of proteins (dimer of α-cyano-4-hydroxycinnamic acid, bradykinin, angiotensin, ACTH and insuline) until a mass of ~5500 amu. The calibrated measurements were done for a range of 300 to 10.000 amu. Higher masses were detected by applying a low mass gate of 3500, filtering out low mass macrocycles.[33]

All reagents and solvents were used as received or purified using standard procedures. Bis-PCBM (**7.11**) was obtained as a byproduct from regular PCBM synthesis.[34] Its spectral data were discussed in the experimental section of chapter 5.

Macrocycle formation from bis-PCBM (7.11) and ethyleneglycol: A 50 ml. flame dried three-necked flask was charged with bis-PCBM (**7.11**) (250 mg, 0.227 mmol) and *ortho*-dichlorobenzene (10 ml.) The resulting solution was degassed by three N_2/vacuum purges. Next, ethyleneglycol (24 mg, 0.387 mmol, 1.7 eq.) and DBTO (11.3 mg, 0.046 mmol, 0.2 eq.) were added.

The mixture was stirred at 120 ^{0}C for 5 days. The products in the resulting mixture were precipitated with methanol and centrifuged yielding a brown pellet. This pellet was washed repeatedly with toluene until the supernatant toluene layer became colorless. A small brown pellet remained which was dried *in vacuo* at 50 ^{0}C yielding 31 mg of polymer/cycles. IR (KBr); ν (cm^{-1}): 3429 (br) (H_2O in KBr), 2925 (s), 2855 (m), 1739 (s), 1601 (m), 1494 (m), 1446 (m), 1245 (m), 1150 (s), 1076 (m), 1034 (m), 967 (w), 884 (w), 801 (w), 753 (m), 701 (s), 677 (w), 660 (w), 641 (w), 605 (w), 586 (w), 571 (w), 562 (w), 553 (w), 542 (w), 526 (s), 500 (w), 488 (w). ^{1}H NMR (D_2O/CS_2, 300 MHz); δ (ppm): 8.28 – 7.42 (broad signals, phenyl ring), 7.38 – 7.18 (m, ODCB solvent), 4.40 – 4.18 (br., -OCOCH_2-), 3.80 (br., -CH_2OH and -OCH_3), 3.23 – 2.05 (broad signals, -C-CH_2-C-), 1.50 – 1.02 (m, pentane solvent).

Macrocycle formation from bis-PCBM (7.11) and 1,4-butanediol: A 50 ml. flame dried three-necked flask was charged with bis-PCBM (**7.11**) (247 mg, 0.22 mmol) and *ortho*-dichlorobenzene (15 ml.) The resulting solution was degassed by three N_2/vacuum purges. Next, 1,4-butanediol (90 mg, 0.98 mmol, 4 eq.) and DBTO (15 mg, 0.06 mmol, 0.35 eq.) were added. The mixture was stirred at 120 ^{0}C for one week. The products in the mixture were precipitated in methanol and centrifuged yielding a brown pellet. The brown pellet was then washed with toluene (2x) and pentane (1x). The resulting brown pellet was dried *in vacuo* at 50 ^{0}C, yielding 163 mg of polymer/cycles. IR (KBr); ν (cm^{-1}): 3448 (br) (H_2O in KBr), 3057 (w), 3025 (w), 2954 (s), 2867 (m), 1735 (s), 1601 (m), 1581 (w), 1514 (w), 1494 (m), 1446 (m), 1429 (m), 1393 (w), 1247 (m), 1155 (s), 1077 (m), 1026 (w), 1002 (w), 914 (w), 879 (w), 841 (w), 799 (w), 759 (m), 729 (w), 700 (m), 677 (w), 586 (w), 572 (w), 545 (w), 526 (s), 482 (w). ^{1}H NMR (D_2O/CS_2, 300 MHz); δ (ppm): 8.18 – 7.39 (broad signals, phenyl ring), 4.09 – 3.86 (br., -OCOCH_2-), 3.69 – 3.52 (br., -CH_2OH and -OCH_3), 2.81 – 1.02 (broad signals, -C-CH_2-C-).

Macrocycle formation from bis-PCBM (7.11) and 1,6-hexanediol: A 50 ml. flame dried three-necked flask was charged with bis-PCBM (**7.11**) (512 mg, 0.465 mmol) and *ortho*-dichlorobenzene (30 ml.) The resulting solution was degassed by three N_2/vacuum purges. Next, 1,6-hexanediol (55 mg, 0.465 mmol) and DBTO (46.3 mg, 0.186 mmol, 0.4 eq.) were added. The mixture was stirred at 120 ^{0}C for one week. The products in the resulting mixture were precipitated with methanol and centrifuged, yielding a brown pellet. The pellet was washed repeatedly with toluene until the supernatant was colorless. The supernatant (toluene) layers were combined and dried *in vacuo* yielding 354 mg of polymer/cycles. IR (KBr); ν (cm^{-1}): 3445 (br) (H_2O in KBr), 3057 (w), 3025 (w), 2952 (s), 2865 (m), 1734 (s), 1601 (m), 1566 (m), 1495 (m), 1459 (m), 1446 (m), 1429 (w), 1392 (w), 1250 (w), 1178 (m), 1156 (m), 1077 (w), 1026 (w), 1002 (w), 880 (w), 841 (w), 798 (w), 755 (m), 729 (w), 700 (s), 676 (w), 571 (w), 546 (m), 527 (s), 456 (w). ^{1}H NMR ($CDCl_3$, 300 MHz); δ (ppm): 8.18 – 7.35 (broad signals, phenyl ring), 4.2 – 3.9 (br., -OCOCH_2-), 3.55 – 3.63 (br., -CH_2OH and –OCH_3), 3.15 – 0.7 (broad signals, -C-CH_2-C-).

Macrocycle formation from bis-PCBM (7.11) and bis Phenyl C_{62} bis butyric acid bis 6-hydroxyhexyl ester (7.13). A 25 ml. flame dried three-necked flask was charged with transesterified bis-PCBM (**7.13**) (50 mg, 3.93 x 10^{-2} mmol), bis-PCBM (**7.11**) (43 mg, 3.93 x 10^{-2} mmol) and *ortho*-dichlorobenzene (8 ml.) The resulting

solution was degassed by three N_2/vacuum purges. Next, DBTO (1 mg, 8 x 10^{-3} mmol, 0.2 eq.) was added. The resulting mixture was stirred at 150 ^{0}C for 3 days. The products in the mixture were then precipitated with methanol and centrifuged yielding a brown pellet. The pellet was washed once with pentane and dried *in vacuo* at 50 ^{0}C. IR (KBr); ν (cm^{-1}): 3439 (br) (H_2O in KBr), 3058 (w), 3026 (w), 2933 (s), 2858 (m), 1734 (s), 1601 (w), 1495 (w), 1446 (m), 1392 (w), 1249 (m), 1156 (s), 1077 (w), 1026 (w), 755 (m), 700 (s), 675 (w), 571 (w), 545 (m), 527 (s), 504 (w), 478 (w). ^{1}H NMR (D_2O/CS_2, 300 MHz); δ (ppm): 8.16 – 7.29 (broad signals, phenyl ring), 4.05 (br., -$OCOCH_2$-), 3.63 (br., -CH_2OH and –OCH_3), 3.18 – 0.99 (broad signals, -C-CH_2-C-).

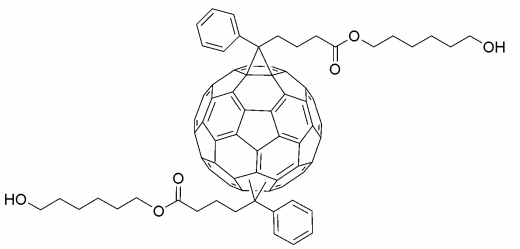

Bis–Phenyl–C_{62} bisbutyric acid bis 6-hydroxyhexyl ester (7.13): A 50 ml. flame dried three-necked flask was charged with bis-PCBM (**7.11**) (250 mg, 0.22 mmol), 1,6-hexanediol (1.07 g, 9.1 mmol, 40 eq.) and DBTO (13.3 mg, 5.34 x 10^{-2} mmol, 0.24 eq.) and dissolved in ODCB (15 ml). The resulting mixture was stirred at 140 ^{0}C for ~17 h. The reaction mixture was purified by column chromatography over silica gel (2 x 15 cm). The column was prepared with toluene, the mixture was deposited and eluted with a toluene/pyridine (95/5) mixture. The first fraction consists of singly esterified product and internally ring-closed product. The second fraction tailed hugely, but contained mainly product, polluted with some internally ring-closed product. This second fraction was purified by column chromatography once more, yielding a sticky brown solid. This sticky solid was dried on the vacuum line with a hotgun. The resulting dry solid was dissolved in CS_2 and precipitated in pentane yielding a brown pellet. The pellet was washed with pentane and dried *in vacuo* at 50 ^{0}C yielding 115 mg (9 x 10 $^{-2}$ mmol, 41%) of bis-transesterified product (**7.12**). IR (KBr); ν (cm^{-1}): 3430 (s), 2932 (s), 2858 (s), 1732 (s), 1495 (m), 1459 (m), 1466 (m), 1430 (m), 1394 (m), 1338 (m), 1252 (m), 1179 (m), 1155 (m), 1056 (m), 761 (w), 572 (w), 545 (w), 527 (s). ^{1}H NMR ($CDCl_3$, 300 MHz); δ(ppm): 7.94 – 7.39 (m, 10H), 4.09 – 4.00 (m, 4H), 3.64 – 3.62 (m, 4H), 3.10 – 2.34 (m, 10H), 2.15 – 2.10 (m, 10H), 1.56 – 1.35 (m, 10H). ^{13}C NMR ($CDCl_3$, 100 MHz); δ(ppm): 173.02, 172.96, 146.42, 146.23, 146.11, 146.02, 145.89, 145.68, 145.44, 145.34, 145.02, 144.54, 144.24, 144.01, 143.89, 143.65, 143.11, 143.04, 141.65, 136.92, 132.11, 131.86, 131.80, 131.76, 131.61, 131.55, 131.35, 128.34, 128.18, 128.06, 127.90, 127.84, 80.13, 79.72, 79.12, 78.66, 75.81, 64.36, 62.62, 50.71, 49.16, 33.94, 33.90, 33.57, 33.35, 32.98, 32.39, 28.42, 28.38, 25.56, 25.53, 25.21, 25.20, 22.33, 22.13. MALDI-TOF m/z: 1273.44.

7.6 References

1. H. W. Kroto, J. R. Heath, S. C. O'Brien, R. F. Curl, and R. E. Smalley, *Nature*, 1985, **318**, 162.
2. T. Kawase, K. Tanaka, Y. Seirai, N. Shiono, and M. Oda, *Angew.Chem.Int.Ed.,* 2003, **42**, 5597.
3. T. Kawase, K. Tanaka, N. Shiono, Y. Seirai, and M. Oda, *Angew.Chem.Int.Ed.*, 2004, **43**, 1722.
4. T. Kawase and H. Kurata, *Chem.Rev.,* 2006, **106**, 5250.
5. X. Zhang, A. B. Sieval, J. C. Hummelen, and B. Hessen, *Chem.Commun.,* 2005, 1616.
6. L. Isaacs, F. Diederich, and R. F. Haldimann, *Helv.Chim.Acta*, 1997, **80**, 317.
7. L. Isaacs, P. Seiler, and F. Diederich, *Angew.Chem.Int.Ed.*, 1995, **34**, 1466.
8. U. Reuther, T. Brandmüller, W. Donaubauer, F. Hampel, and A. Hirsch, *Chem.Eur.J.*, 2002, **8**, 2261.
9. F. Diederich and R. Kessinger, *Acc.Chem.Res.,* 1999, **32**, 537.
10. G. M. Bendele, P. W. Stephens, K. Prassides, K. Vavekis, K. Kordatos, and K. Tanigaki, *Phys.Rev.Lett.*, 1998, **80**, 736.
11. T. Suzuki, Q. Li, K. C. Khemani, and F. Wudl, *J.Amer.Chem.Soc.*, 1992, **114**, 7300.
12. F. Wudl, *Acc.Chem.Res.*, 1992, **25**, 157.
13. A. Gradillas and J. Pérez-Castells, *Angew.Chem.Int.Ed.*, 2006, **45**, 6086.
14. S. E. Gibson and C. Lecci, *Angew.Chem.Int.Ed.,* 2006, **45**, 1346.
15. P. Anzenbacher Jr, R. Nishiyabu, and M. A. Palacios, *Coord.Chem.Rev.*, 2006, **250**, 2929.
16. K. Nakao, M. Nishimura, T. Tamachi, Y. Kuwatani, H. Miyasaka, T. Nishinaga, and M. Iyoda, *J.Amer.Chem.Soc.*, 2006, **128**, 16740.
17. W. Zhang and J. S. Moore, *Angew.Chem.Int.Ed.*, 2006, **45**, 4416.
18. M. Hoffmann, C. J. Wilson, B. Odell, and H. L. Anderson, *Angew.Chem.Int.Ed.*, 2007, **46**, 3122.
19. M. Gordon and G. R. Scantlebury, *J.Chem.Soc.B.*, 19671.
20. X.-F. Yuan, A. J. Masters, C. V. Nicholas, and C. Booth, *Makromol.Chem.*, 1988, **189**, 823.
21. H. R. Kricheldorf and G. Schwarz, *Macromol.Rapid Commun.*, 2003, **24**, 359.
22. H. R. Kricheldorf, M. Rabenstein, D. Langanke, G. Schwarz, M. Schmidt, M. Maskos, and R.-P. Krüger, *High Perfor. Polym.*, 2001, **13**, S123.
23. R. F. T. Stepto and D. R. Waywell, *Makromol.Chem.*, 1972, **152**, 263.
24. J. L. Stanford and R. F. T. Stepto, *J.Chem.Soc. Faraday Trans.,* 1975, **71**, 1308.
25. M. Gordon and W. B. Temple, *Makromol.Chem.*, 1972, **152**, 277.
26. M. Gordon and W. B. Temple, *Makromol.Chem.,* 1972, **160**, 263.
27. H. Jacobsen and W. H. Stockmayer, *J.Chem.Phys.*, 1950, **18**, 1600.
28. J. Otera, *Chem.Rev.*, 1993, **93**, 1449.
29. R. C. Poller and S. P. Retout, *J.Organomet.Chem.*, 1979, **173**, C7.

30. M.-F. Llauro and A. Michel, *C.R. Chimie*, 2006, **9**, 1363.
31. P. Baumhof, R. Mazitschek, and A. Giannis, *Angew.Chem.Int.Ed.,* 2001, **40**, 3672.
32. D. F. Kronholm, J. C. Hummelen, and A. B. Sieval. USPatent: 2005245606, 2005.
33. W. E. Wallace, C. M. Guttman, and J. M. Antonucci, *Polymer*, 2000, **41**, 2219.
34. J. C. Hummelen, B. W. Knight, F. Lepeq, F. Wudl, J. Yao, and C. L. Wilkins, *J.Org.Chem.*, 1995, **60**, 532.

Appendix I

MALDI-TOF Spectra chapter 7

Full sized MALDI-TOF spectra corresponding to figure 7.4 can be found here.

Corresponding with figure 7.4a, masses from 300 until 10.000

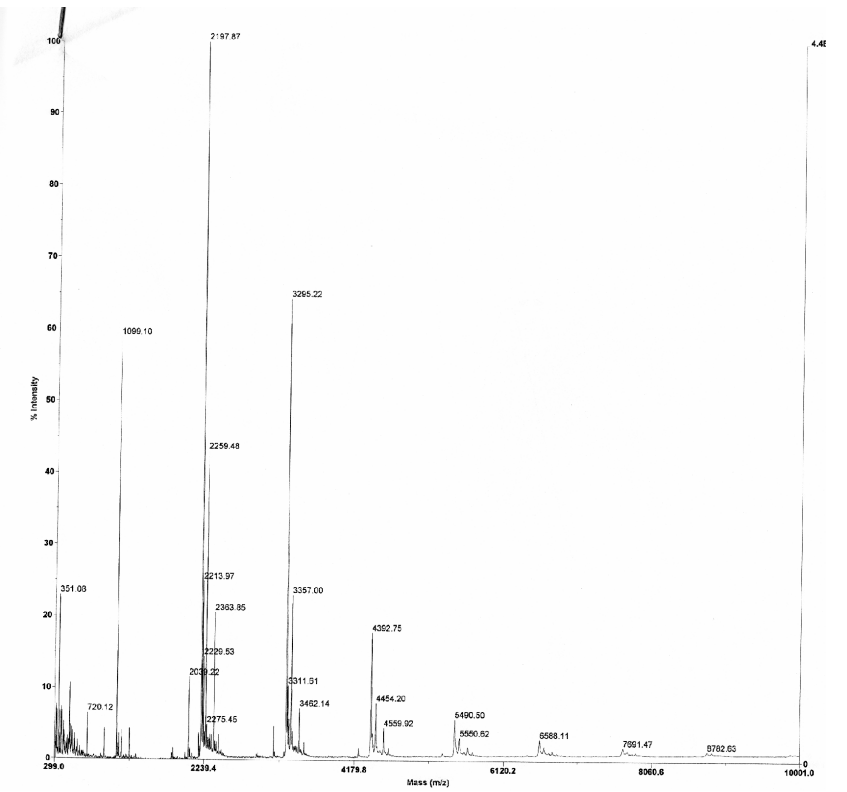

Corresponding to figure 7.4a, masses from 3.500 until 20.000

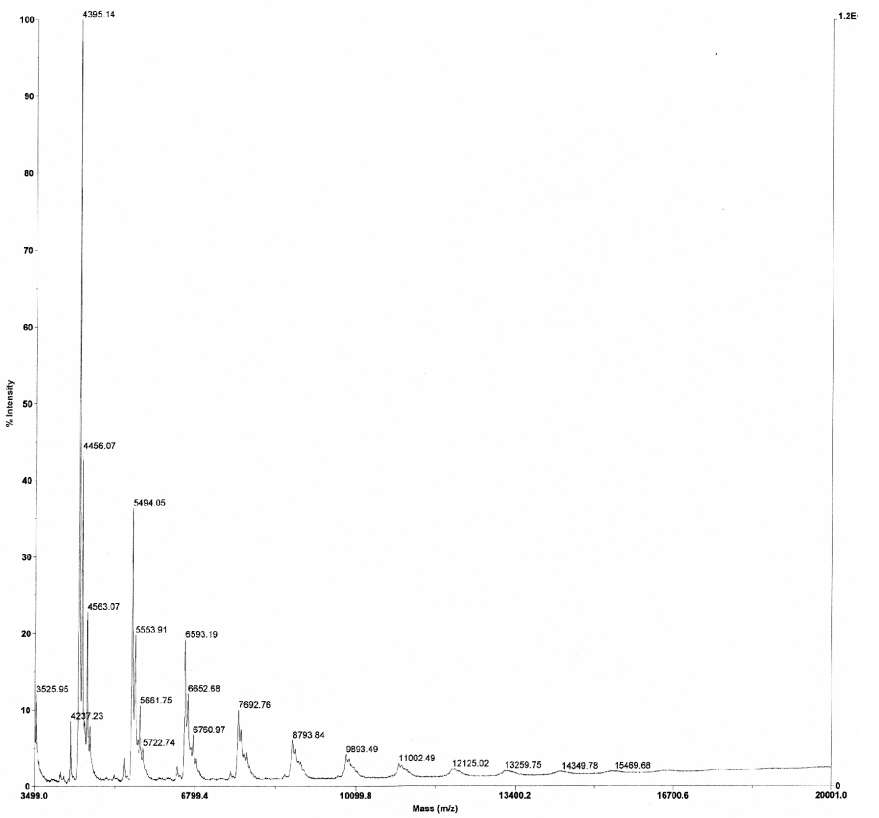

Corresponding to figure 7.4b, masses from 300 until 10.000

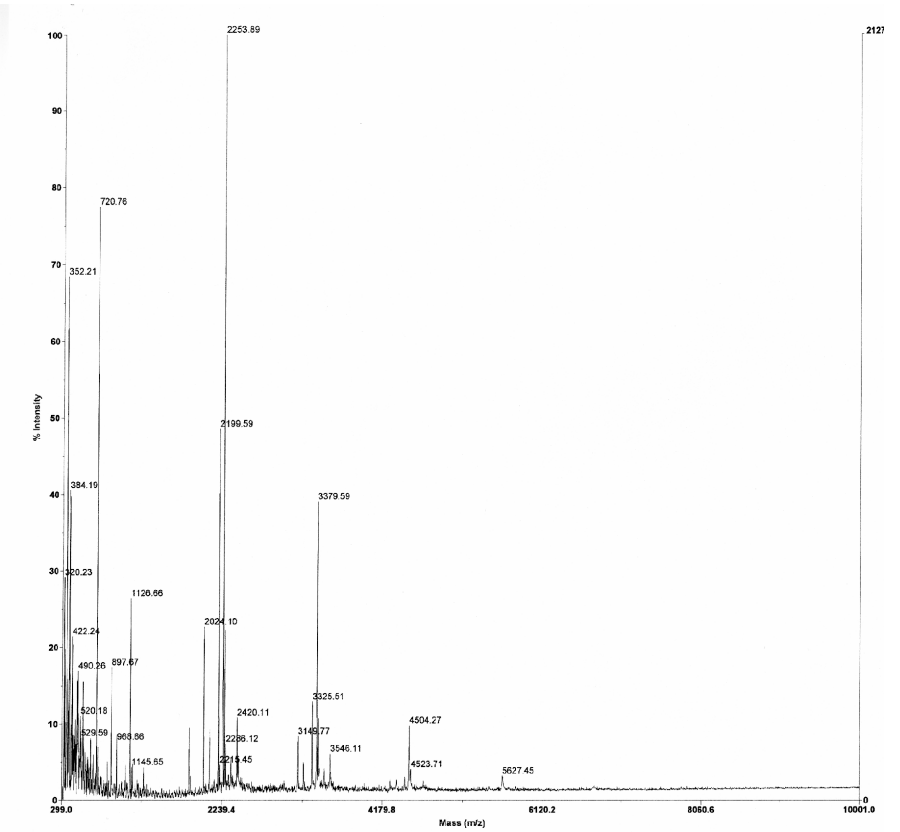

Corresponding to figure 7.4b, masses from 3.500 until 20.000

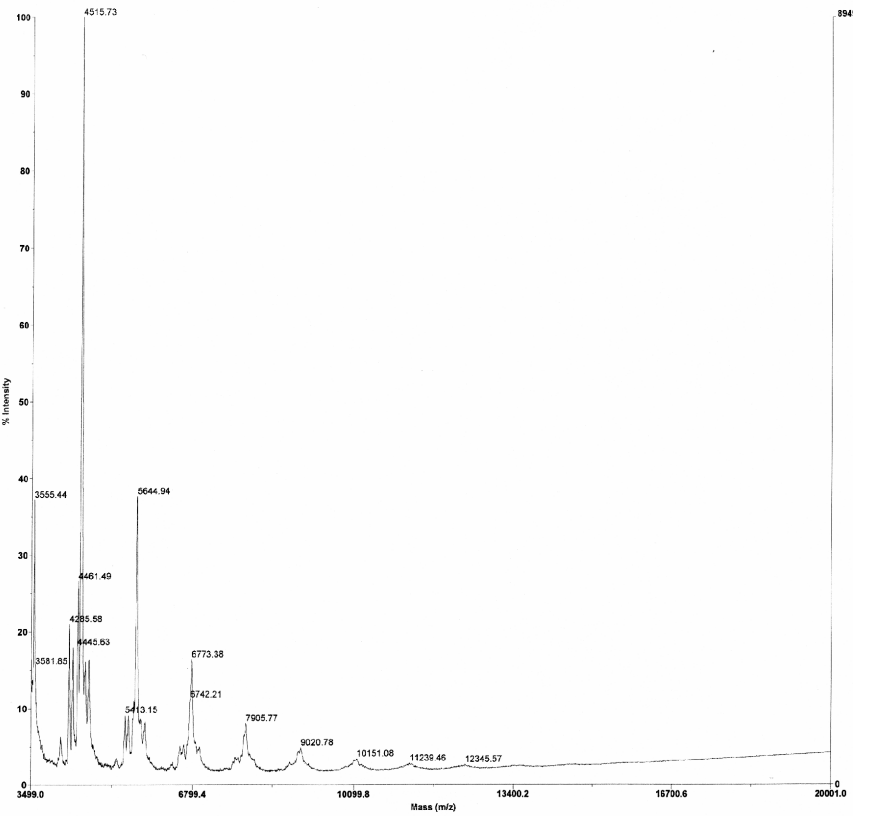

Corresponding to figure 7.4c, masses from 3.500 until 10.000

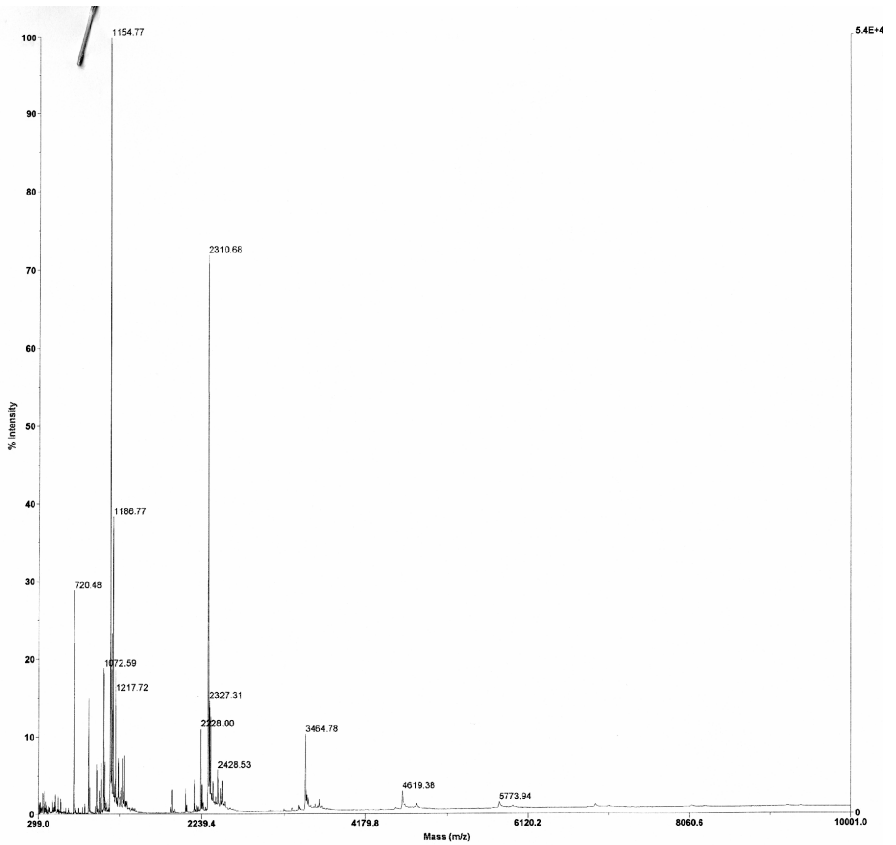

Corresponding to figure 7.4c, masses from 3.500 untill 50.000

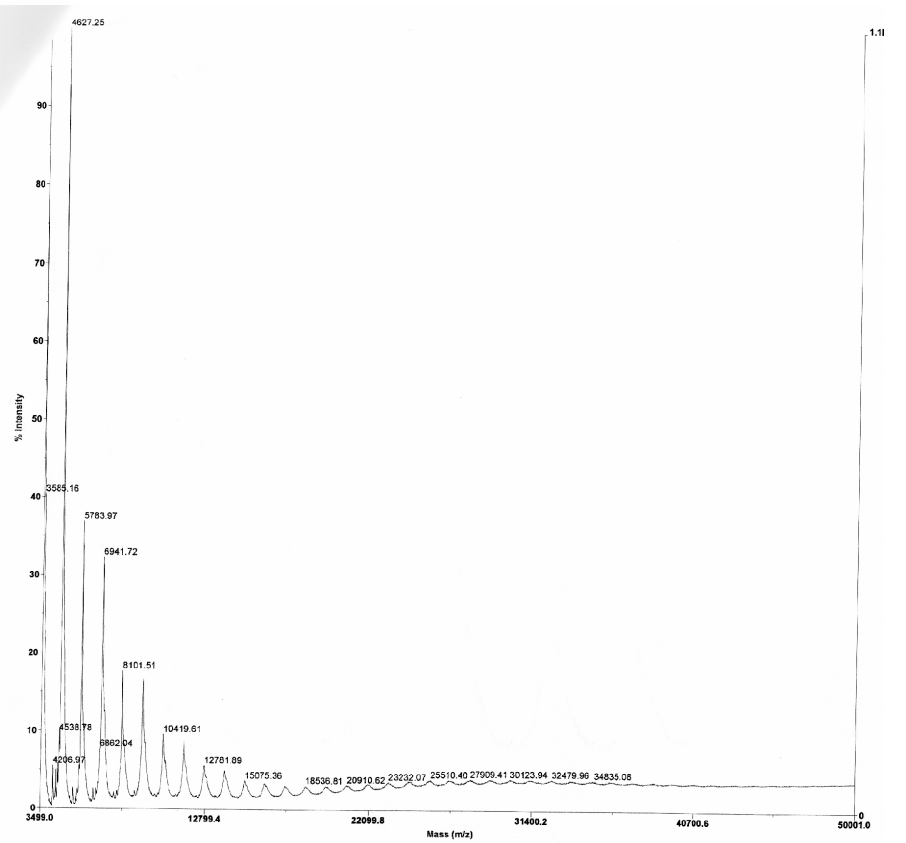

Corresponding to figure 7.4d, masses from 300 until 10.000

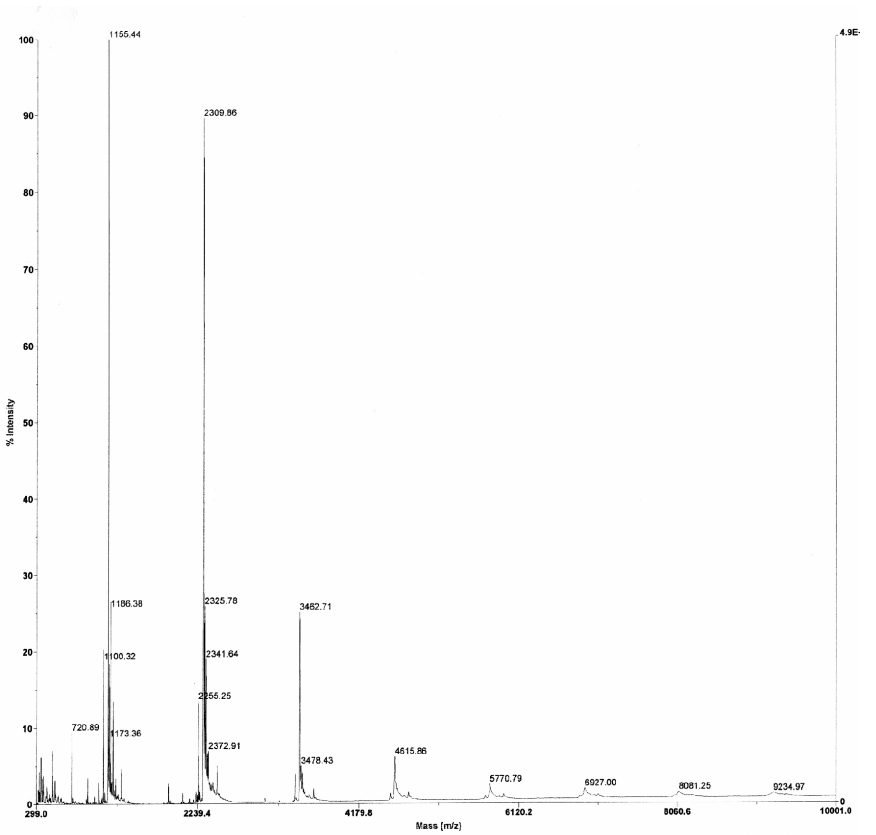

Corresponding to figure 7.4d, masses from 3.500 until 50.000

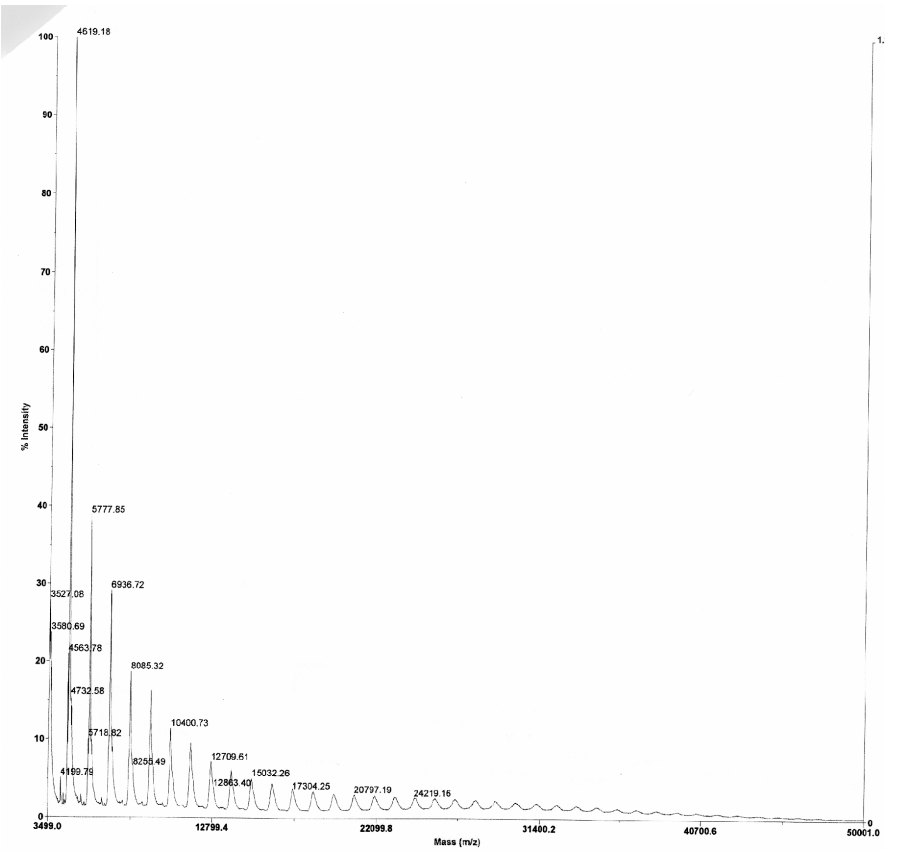

Corresponding to figure 7.4d, enlargement of masses from 34.000 until 50.000

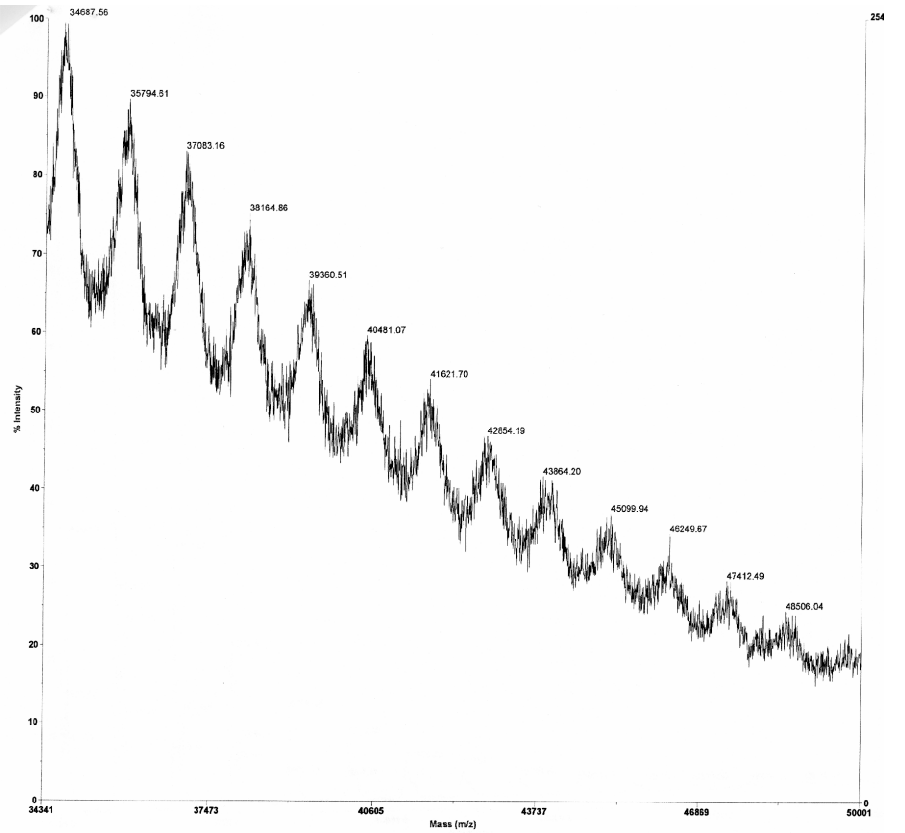

Samenvatting

Lange tijd werd gedacht dat pure koolstof slechts in twee allotropen (vormen) voor kon komen. De eerste allotroop is bekend als grafiet en bestaat uit 'losse' lagen koolstof. De tweede allotroop is diamant, dat uit een drie dimensionaal netwerk van koolstof atomen bestaat. In de jaren tachtig (1985) werd echter een derde allotroop ontdekt, de zogenaamde fullerenen (zie figuur 1). Fullerenen zijn moleculen die enkel en alleen uit koolstof bestaan en een gesloten bal vormen. Deze sferische structuur bestaat uit hexagons (zeshoeken) en pentagons (vijfhoeken). Elk fullereen bestaat per definitie uit 12 pentagons omdat een bal bestaande uit *n* hexagons anders niet gesloten kan worden (theorema van Euler). Bovendien moet elk pentagon vanwege energetische redenen omringd worden door hexagons (Isolated Pentagon Rule). De kleinste bal die aan deze condities voldoet is C_{60}. Dit molecuul, bestaande uit zestig koolstof atomen, vormt een perfecte voetbal structuur. C_{60} wordt ook wel Buckminster Fullereen genoemd naar de architect Richard Buckminster Fuller die geodetische koepels ontwierp. Naast C_{60} zijn ook grotere fullerenen mogelijk. Meest bekend en voorkomend zijn C_{70} en C_{84}. De eigenschappen van deze fullerenen verschillen onderling sterk waardoor hun toepassingsgebieden kunnen variëren.

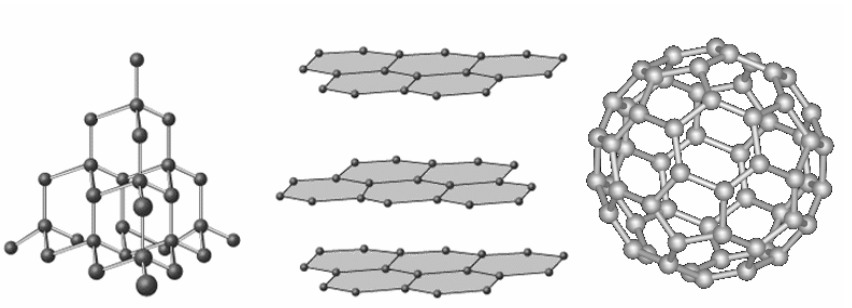

Fig. 1: Koolstof allotropen. Van links naar rechts: diamant, grafiet en fullereen.

Fullerenen hebben enkele unieke eigenschappen waardoor ze geschikt zijn voor vele toepassingen variërend van medicijnen tot organische elektronica. Fullerenen hebben de uitzonderlijke eigenschap dat ze erg goed elektronen kunnen accepteren en geleiden. Het zijn voornamelijk deze eigenschappen van fullerenen die de interesse van wetenschappers hebben getrokken. Fullerenen worden tegenwoordig vooral gebruikt in organische zonnecellen, transistoren en holografische materialen. Omdat fullerenen erg slecht oplosbaar zijn worden ze over het algemeen eerst gemodificeerd voor ze gebruikt kunnen worden.

Dit proefschrift beschrijft de toepassing van fullerenen in verschillende takken van organische elektronica. Door middel van chemische modificatie van het fullereen is geprobeerd de eigenschappen van het fullereen zodanig aan te passen dat het beter geschikt wordt voor een bepaalde applicatie.

In zowel hoofdstuk 2 als hoofdstuk 3 worden nieuwe fullerenen gepresenteerd voor gebruik in organische zonnecellen. Organische zonnecellen bestaan uit twee componenten: een lichtabsorberend polymeer dat tevens positieve lading kan geleiden en fullerenen die elektronen accepteren en vervolgens geleiden. Een organische zonnecel werkt als volgt: een polymeer absorbeert zonlicht. Door de energie van dit zonlicht wordt een elektron van het polymeer in een aangeslagen toestand (hogere energetische toestand) gebracht. Als er nu een goed elektronaccepterend materiaal (fullereen) in de buurt is kan dit elektron hiernaar overspringen. Er blijft nu een 'gat' of positieve lading over op het polymeer terwijl het elektronaccepterende materiaal nu een negatieve lading heeft. Beide ladingen zijn nu van elkaar gescheiden. Als er elektrodes op het materiaal zijn aangesloten kan de positieve lading naar de ene elektrode reizen terwijl de negatieve lading naar de andere elektrode kan reizen (zie figuur 2). We hebben nu stroom opgewekt! Grote voordelen van organische zonnecellen zijn bijvoorbeeld: goedkope productie, flexibiliteit van het materiaal en milieuvriendelijke productie.

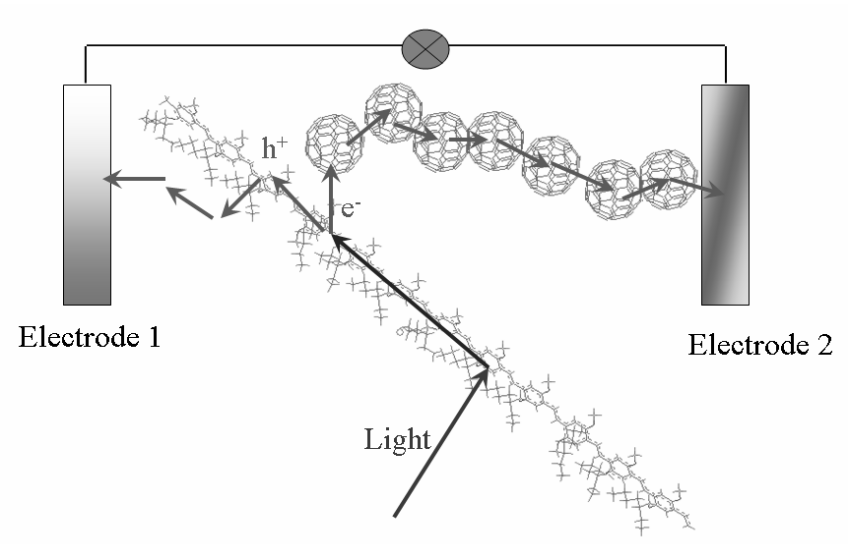

Fig. 2: Werking van een zonnecel. Licht wordt geabsorbeerd door het polymeer waardoor een exciton (gebonden + en – lading) gevormd wordt. Daar waar het fullereen en polymeer grenzen, vindt ladingscheiding plaats. De ladingen bewegen vervolgens naar de elektrodes en zo wordt stroom opgewekt.

De hoeveelheid licht dat geabsorbeerd wordt is van essentieel belang voor de efficiëntie van de zonnecel. Normaal gesproken absorberen de fullerenen niet veel zonlicht. In hoofdstuk 2 wordt beschreven hoe een chemisch gemodificeerd groter

fullereen C_{84} (zie figuur 3) gebruikt kan worden om meer licht te absorberen. Alhoewel er inderdaad meer licht geabsorbeerd wordt als het C_{84} derivaat gebruikt wordt in plaats van het vergelijkbare C_{60} derivaat, werkt de zonnecel toch een stuk minder. Dit komt omdat de spanning van de zonnecel dramatisch lager is geworden. Bovendien lijkt het erop dat de geleiding van positieve lading door het polymeer niet toeneemt als het gemengd wordt met het fullereen, waar dat wel het geval is als het vergelijkbare C_{60} derivaat gebruikt wordt.

In hoofdstuk drie wordt de synthese beschreven van een serie fullerenen gebaseerd op C_{60}, waarbij geprobeerd is de elektronen-accepterende eigenschappen van het fullereen te veranderen. Dit is gedaan door elektron-zuigende en -stuwende groepen op het fullereen te zetten (zie figuur 3). We zijn erin geslaagd kleine veranderingen te bewerkstelligen. Het effect van deze veranderingen op de werking van het fullereen in organische zonnecellen is bestudeerd. De resultaten van de zonnecellen gaven aan dat het voltage van de zonnecel afhankelijk is van het elektronen accepterend vermogen van de fullerenen. Hoe slechter het fullereen elektronen accepteert hoe hoger het voltage van de zonnecel.

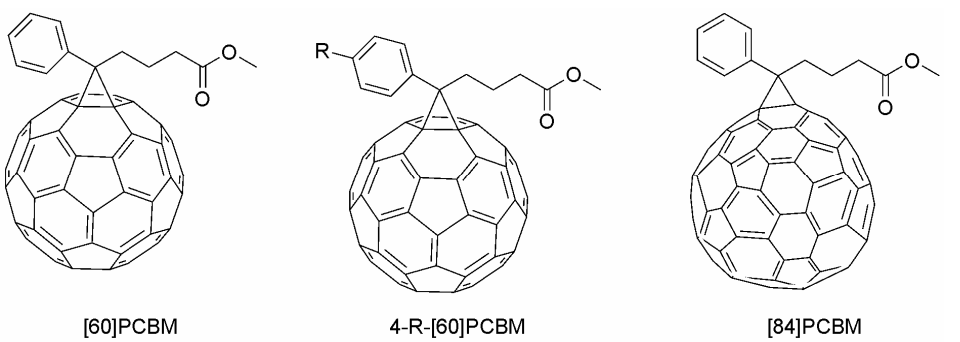

[60]PCBM 4-R-[60]PCBM [84]PCBM

Fig. 3: Links: standaard gefunctionaliseerd C_{60}, midden: C_{60} molecuul met elektronen zuigende of stuwende groep (R), rechts: gefunctionaliseerd C_{84} molecuul.

Een belangrijke andere toepassing van fullerenen is als halfgeleider in transistoren. Transistoren worden veelvuldig gebruikt in elektronica en zijn als het ware een soort schakelaars die onder bepaalde omstandigheden wel geleiden en onder andere omstandigheden niet. De voordelen van organische transistoren zijn, wederom, goedkope productiekosten en flexibiliteit van het materiaal. Normaal gesproken geleiden transistoren *of* alleen elektronen *of* alleen positieve ladingen. Fullerenen kunnen echter beide ladingen geleiden (ambipolair) en zijn daarom zeer interessant voor gebruik in transistoren. Het grootste probleem van bekende, uit fullerenen gemaakte, transistoren is dat ze niet stabiel zijn aan de lucht. In

hoofdstuk vier worden twee verschillende pogingen beschreven om, aan de lucht stabiele, transistoren te maken uit fullerenen. De eerste manier maakt gebruik van het in hoofdstuk 2 beschreven C_{84} derivaat. De geladen vorm van dit molecuul is dermate stabiel dat het geen redoxreacties aangaat met water en zuurstof. We laten hier de eerste 'ambipolaire' organische transistoren zien die lucht– en lichtstabiel zijn. De tweede manier om luchtstabiliteit te genereren is het introduceren van fluoratomen in het molecuul. Fluoratomen zijn namelijk water-afstotend. De synthese van een aantal fluor bevattende fullerenen wordt beschreven. De met deze fullerenen gefabriceerde transistoren bleken echter niet luchtstabiel te zijn.

De laatste toepassing van fullerenen die in dit proefschrift onderzocht is, is in hologrammen. Holografische technieken kunnen gebruikt worden voor medische diagnosen. De huid is namelijk transparant voor licht van bepaalde golflengtes (infrarood). Dit licht kan door deeltjes onder de huid teruggekaatst worden. Licht dat slechts een keer gereflecteerd wordt kan gebruikt worden om informatie over het weefsel te verkrijgen. Dit licht moet echter wel gedetecteerd worden. Dit is mogelijk met behulp van hologrammen (zie figuur 4). Het holografische film materiaal bestaat uit drie componenten: een polymeer (matrix) dat licht absorbeert en positieve lading geleidt, niet lineair optische chromoforen die zich oriënteren naar een elektrisch veld, en zogenaamde sensitizers (fullerenen) die negatieve ladingen vasthouden. Als een laserbundel samenkomt met het licht dat terugkomt van het weefsel wordt een interferentiepatroon gevormd, wat wil zeggen dat beide lichtbundels elkaar versterken of uitdoven. Daar waar versterking van het licht optreedt worden in het holografische materiaal ladingen gevormd in het polymeer. De sensiziters (fullerenen) nemen (net als in zonnecellen) de negatieve lading op. Omdat er heel weinig sensitizers zijn kunnen de negatieve ladingen niet verder bewegen. De positieve ladingen kunnen wel bewegen door het polymeer. Door deze 'scheiding' van positieve en negatieve lading wordt een elektrisch veld gevormd. De chromoforen richten zich naar dit veld. Zodra dit gebeurt, verandert de brekingsindex van het materiaal. Dit betekent dat licht dat op het materiaal valt anders weerkaatst wordt dan voorheen. Deze verandering kan gedetecteerd worden en levert zo een beeld op van het weefsel dat zich op een bepaalde diepte bevindt. Het maken, lezen en wissen van een dergelijk hologram kan zo snel dat ze met videosnelheid na elkaar uitgelezen kunnen worden! In hoofdstuk 5 wordt bestudeerd wat de invloed van het elektron accepterende vermogen van fullerenen is op de snelheid van de opbouw van het hologram. We laten hier zien dat hoe beter het fullereen elektronen opneemt hoe sneller (tot 4x) het hologram gevormd wordt. Daarnaast laten we een tweede manier om holografische materialen te maken zien. In plaats van een polymere matrix die positieve ladingen geleidt kunnen fullerenen gebruikt kunnen worden als matrix die negatieve ladingen geleidt. Zowel de synthese van speciale fullerenen voor dit doeleinde als de holografische testen worden beschreven in dit hoofdstuk.

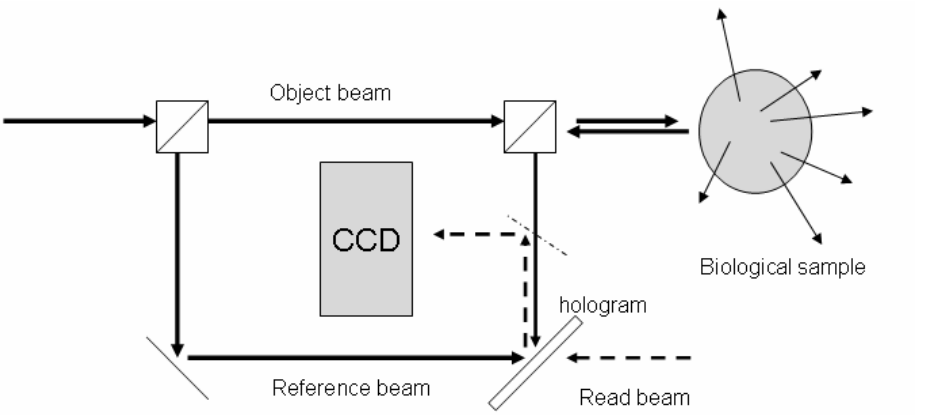

Fig. 4: Set-up holographic detection method. A laser beam is split in a 'reference' beam and an 'object' beam. Light, which is reflected by the sample, interacts with the 'reference' beam. A hologram is now 'written', which is read out by a 'read' beam and subsequently erased with another laser beam. A CCD camera provides video imaging of the repeating process.

The final two chapters of this thesis are of more fundamental nature, without looking at a direct application.

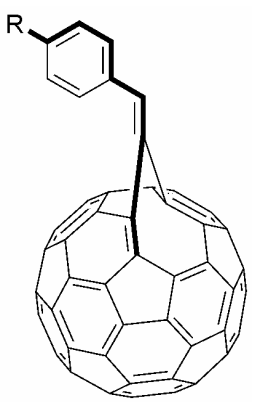

In chapter six, a method is described to place functional groups on a fullerene in a conjugated manner. In other words, a functional group is connected to the fullerene sphere by an alternating pathway of single and double bonds (see figure 5). This new method offers unique opportunities to influence the electronic properties of the fullerene in a more direct way than ever before.

In the concluding chapter seven, the synthesis of giant pearl-necklace structures is shown. By polymerizing fullerenes, containing two ester moieties, with α,ω-alcohols, giant ring structures are formed (see figure 6).

Fig. 5: Conjugated fullerene compound. In bold the pathway of alternating single and double bonds between the functional group and the fullerene is shown.

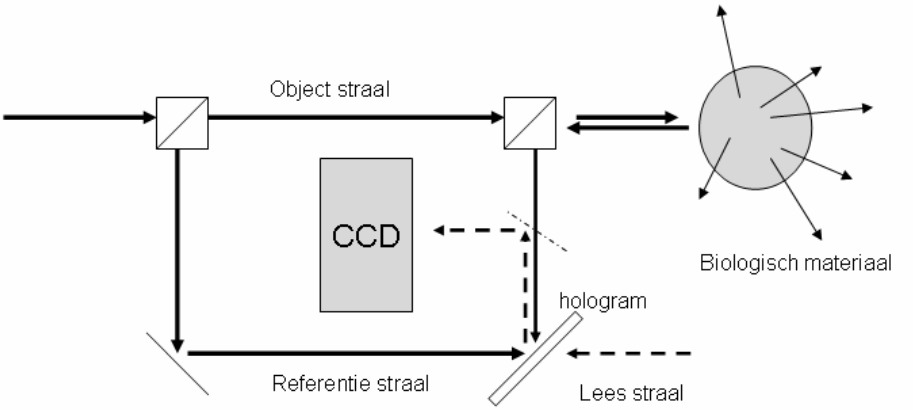

Fig. 4: Set-up holografische detectiemethode. Een laser straal wordt gesplitst in een 'referentie' straal en een 'object' straal. Het licht dat terug komt van het biologische materiaal komt samen met de 'referentiestraal'. Nu wordt het hologram 'geschreven', dat wordt uitgelezen door de 'leesstraal' en vervolgens gewist met weer een laserstraal. Een CCD camera zorgt voor videobeeld van het herhalend proces.

De laatste twee hoofdstukken van dit proefschrift zijn meer fundamenteel gericht zonder dat er een direct toepassing onderzocht is.

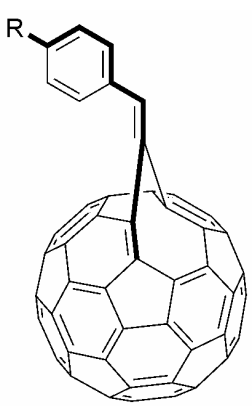

In hoofdstuk zes wordt de eerste methode beschreven om functionele groepen aan fullerenen te zetten op een geconjugeerde manier. Dit betekent dat een functionele groep via opeenvolgende enkele en dubbele bindingen aan het fullereen gebonden is (zie figuur 5). Deze nieuwe methode biedt de mogelijkheid om de elektronische eigenschappen van fullerenen nog directer te beïnvloeden dan voorheen mogelijk was.

Als laatste wordt in hoofdstuk zeven de synthese van grote parelkettingstructuren beschreven. Door fullerenen, gefunctionaliseerd met twee estergroepen, te polymeriseren met α,ω-alkoholen worden grote ringstructuren gevormd (zie figuur 6).

Fig. 5: Geconjugeerde fullereenverbinding. Dikgedrukt is aangegeven hoe de sfeer en de functionele groep via afwisselende dubbele en enkele bindingen verbonden zijn.

We laten met behulp van massaspectrometrie zien dat er ringstructuren gevormd worden bestaande uit wel 18 fullerenen. Deze structuren zijn de eerste echte voorbeelden van parelkettingstructuren.

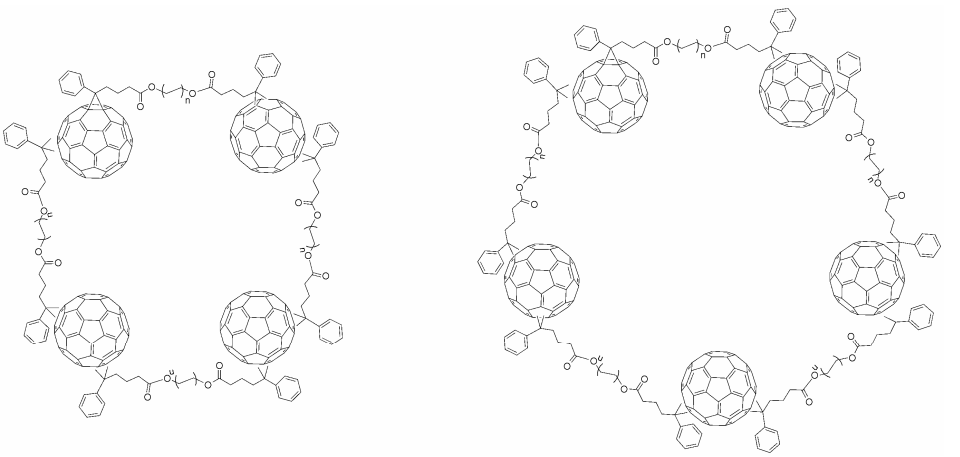

Fig. 6: Voorbeelden van parelkettingstructuren met n=1,2,3.

Summary

Readers who are interested in a more detailed summary of the discussed chapters are referred to the abstracts at the beginning of each chapter.

For a long time it was thought that pure carbon only existed in two allotropes (forms). The first allotrope is known as graphite and consists of 'loose' layers of carbon. The second allotrope is diamond, which is formed by a three dimensional network of carbon atoms. In the 1985 a third allotrope of carbon was discovered, the so called fullerenes (see figure 1). Fullerenes are molecules consisting of carbon, forming a closed sphere structure. These spherical structures are built up out of hexagons and pentagons. Each fullerene, per definition, consists out of 12 pentagons, since a sphere containing *n* hexagons can not be closed otherwise (Euler's theorem). Besides, for energetic reasons, every pentagon has to be surrounded by hexagons (Isolated Pentagon Rule). The smallest sphere fulfilling these conditions is C_{60}. This molecule, consisting of sixty carbon atoms, forms a perfect soccer ball structure. C_{60} is also known as Buckminster Fullerene, named after the architect Richard Buckminster Fuller, who designed geodetic domes. Next to C_{60}, larger fullerenes are also possible. Most known and common are C_{70} and C_{84}. Because the properties of these fullerenes differ strongly, their areas of application can vary.

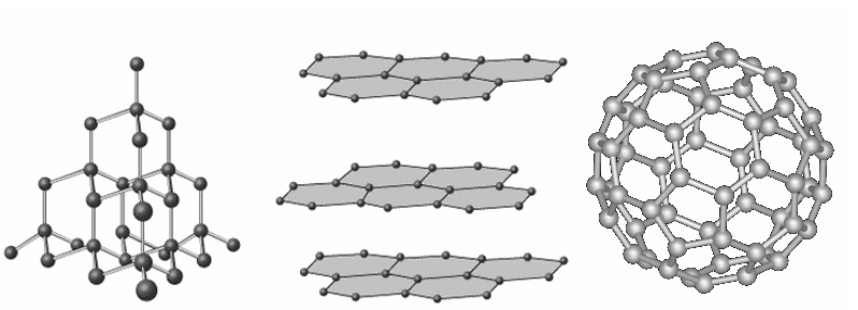

Fig. 1: Carbon allotropes. From left to right: diamond, graphite and fullerene.

Fullerenes posses some unique properties, rendering them suitable for many applications varying from medicine to organic electronics. Fullerenes have the exceptional capability of being very good electron acceptors and conductors. It is these properties that have drawn most attention of scientists. Fullerenes are nowadays mainly used in organic solar cells, transistors, and holographic materials. Since fullerenes are highly insoluble they need to be functionalized prior to being used for any application.

This thesis describes the application of fullerenes in different types of organic electronics. By means of chemical modification the fullerene properties were adapted to fit the desired application.

In chapter two as well as chapter three, new fullerenes are presented for use in solar cells. Organic solar cells consist of two components: a light absorbing polymer, which also conducts positive charges, and fullerenes which accept electrons and subsequently conduct electrons. The operating principle of an organic solar cell is as follows: A polymer absorbs sunlight. The energy of this light causes an electron of the polymer to be exited to a higher energetic state. If an electron accepting material (fullerene) is near, this electron can jump to this material. A hole, or positive charge, remains on the polymer, while the electron accepting material is negatively charged. Both charges are now separated. When electrodes are connected to the material, the positive charge can travel to one electrode and the negative charge to the other electrode (see figure 2). We have a current now! Major advantages of organic solar cells are, for example: cheap production, flexibility of the material and environmentally friendly construction.

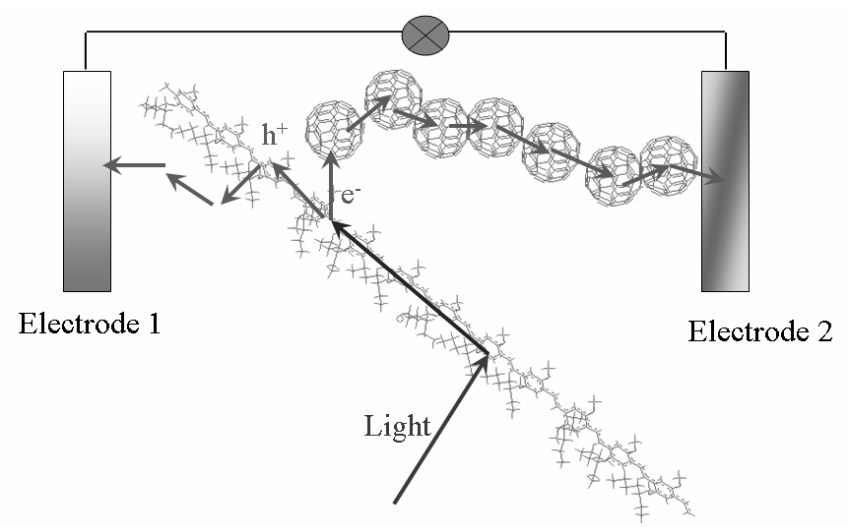

Fig. 2: Operating principle of a solar cell. Light is absorbed by the polymer forming an exciton (bound + and – charge). At the interface, of the polymer and the fullerene, charges are separated. The charges then move to the electrodes.

The amount of light that is absorbed, is essential for the efficiency of the solar cell. Normally, fullerenes do not absorb much sunlight. Chapter two describes how a modified, larger, C_{84} fullerene (see figure 3) can be used to absorb more light. Although more light is indeed absorbed when the synthesized C_{84} derivative is

used in stead of its C_{60} analogue, the solar cell is less efficient. The cause of this low efficiency is the dramatic drop in voltage. Besides, it seems that the conduction

of positive charges through the polymer does not increase when mixed with the fullerene, while this is the case when the C_{60} equivalent is used.

In chapter three, the synthesis of a series of fullerenes, based on C_{60}, is described. We attempted to alter the electron accepting properties of the fullerenes. This was accomplished by placing electron donating and electron pushing groups on the fullerene (see figure 3). We succeeded in inducing small changes. The effect of these changes on the application of these fullerenes in organic solar cells was studied. The results of the solar cells indicate that the voltage of the solar cell is directly related to the electron accepting capability of the fullerenes. The voltage of the solar cells increases when the electron accepting capability of the fullerene decreases.

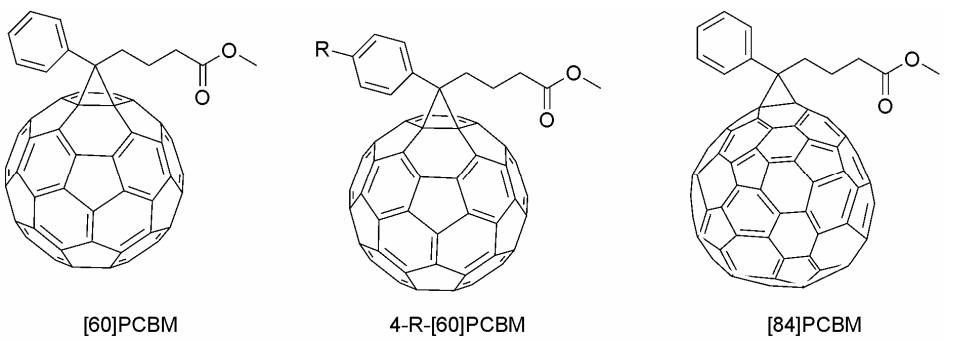

[60]PCBM 4-R-[60]PCBM [84]PCBM

Fig. 3: Left: standard functionalized C_{60}, middle: C_{60} molecule with electron donating or pushing group (R), right: functionalized C_{84} molecule.

An important different application of fullerenes is as a semiconductor in transistors. Transistors are often used in electronics and can be considered to be a type of switches, which conduct only under certain conditions. The advantages of organic transistors are once more, cheap production costs and flexibility of the material. Normally speaking, transistors conduct either electrons or positive charges. Fullerenes, however, can conduct both charges (ambipolar) and are therefore highly interesting as material for transistors. The biggest challenge is the instability of fullerenes in air. In chapter four, two different attempts are described to achieve air stable transistors with fullerenes. The first method uses the, in chapter two described, C_{84} derivate. The charged form of this molecule is so stable that it does not undergo redox reactions with water and oxygen. We show here, the first, air and light stable, 'ambipolar' organic transistors. The second way to generate air-stability is by introducing fluor atoms in the molecule. Fluor atoms are water repellent. The synthesis of a number of fluorine containing fullerenes is described. The transistors fabricated with these fullerenes however, were not stable in air.

The last application of fullerenes that is investigated in this thesis is holograms. Holographic techniques can be used for medical diagnostic purposes. Because skin is transparant for light of certain wavelengths (infrared), light can be reflected by particles underneath the skin. Light, which is only reflected once, can be used to obtain information about the tissue it was reflected from. This light has to be detected however. This is possible with holograms (see figure 4). The holographic film material consists of three components: a polymer (matrix) which absorbs light and conducts positive charges, non linear optical chromophores which orientate in an electric field, and 'so-called' sensitizers (fullerenes) which trap negative charges. When a laser beam combines with light reflected from the tissue, an interference pattern is formed. This means that both light beams either enhance or dim each other. Charges are formed, in the polymer of the holographic material, at the point where the beams enhance each other. The sensitizers (fullerenes) accept a negative charge (as in solar cells). Since there are very few sensitizers, the negative charge is trapped and can not move through the material. The positive charges, however, are able to move through the polymer matrix. This 'separation' of positive and negative charges creates an electric field in the material. The chromophores orientate according to this field. When this happens the diffractive index of the material as a whole is changed. This means that light, which falls on the material, is reflected in a different way. This change can be detected and will ultimately give an image of the tissue at a certain depth. Writing, reading and erasing of such a hologram can be achieved at such high speeds that video images can be produced! In chapter five the influence of the electron accepting capability of the fullerenes on the build up speed of the hologram is studied. We show here that the build up speed increases (up to 4x) with better electron accepting fullerenes. Next, we show a second way of making holographic materials. Instead of using a polymer matrix which conducts positive charges, fullerenes can be used as a matrix which conducts negative charges. Both the synthesis of specially designed fullerenes and the holographic tests are described in this chapter.

We show by means of mass spectrometry that giant ring structures are formed, containing up to 18 fullerenes. These structures are the first real examples of pearl-necklace structures.

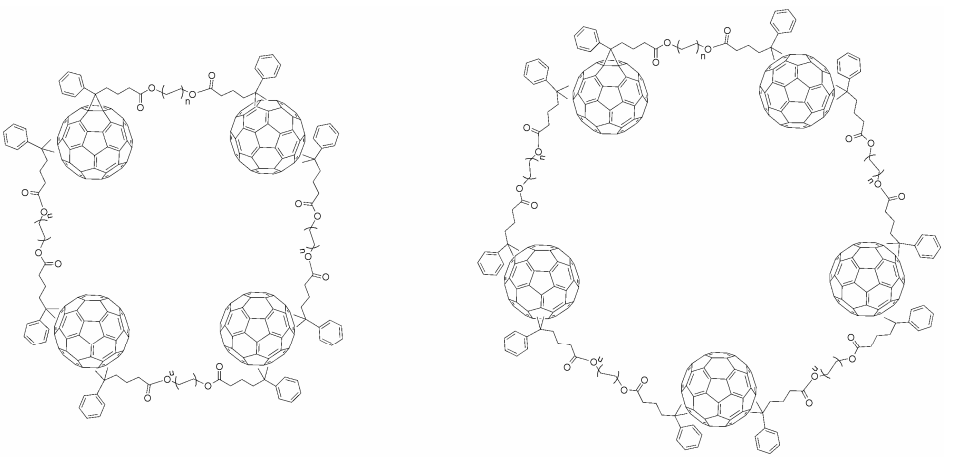

Fig. 6: Examples of pearl-necklace structures with n=1,2,3.

Dankwoord

Na negen jaar zit het er dan op in Groningen. Een rare gedachte om weg te gaan uit de stad waar ik zolang met plezier gewoond en gewerkt heb. Dat het zo'n leuke tijd is geweest heb ik aan veel mensen te danken.

Als eerste wil ik mijn promotor Kees Hummelen graag bedanken voor de meer dan enthousiaste en geïnteresseerde begeleiding gedurende de afgelopen jaren. Kees, ik was de eerste student die in je groep kwam afstuderen en toen je vroeg of ik interesse had om er nog vier jaar aan vast te knopen heb ik eigenlijk geen moment getwijfeld. Ik heb genoten van de vele discussies over de afwisselende projecten waar we de afgelopen jaren aan gewerkt hebben. Je hebt me alle vrijheid gegeven in mijn onderzoek en daar ben ik je erg dankbaar voor.

I owe a great deal of thanks to the members of the reading committee: Paul Blom, Klaus Meerholz and Nazario Martín. Your comments and suggestions have been very useful for improving the book. Paul, ik wil je hartelijk bedanken voor de fijne samenwerking die ik de afgelopen vier jaar met je groep heb gehad. Ik heb het altijd bijzonder leuk gevonden te zien wat jullie allemaal met mijn fullerenen kunnen doen. Klaus, I have thoroughly enjoyed our cooperation in the holographic imaging project over the years. Thanks for all the nice meetings and explanations of difficult physics. Nazario, he disfrutado mucho mi tiempo en su grupo en Madrid, por eso me allegra mucho que tu estarás presente durante la defensa de mi thesis.

Bijna alle hoofdstukken van dit boek maken onderdeel uit van samenwerkingsprojecten. Ik ben dan ook vele mensen dankbaar voor hun contributies. Het werk beschreven in hoofdstuk 2 was nooit tot stand gekomen zonder Valentin Mihailetchi die alle device preparatie en fysica voor zijn rekening heeft genomen. Valy, many thanks for all the work on the [84]PCBM solar cells. Hoofdstuk 3 was een samenwerkingsproject met ECN. Jan Kroon en Wiljan Verhees wil ik graag bedanken voor de vele zonnecellen die met mijn fullerenen gemaakt zijn. I would like to thank Thomas Anthopoulos for the nice cooperation of the past couple of years in the field of the FETs. I think we had quite some success, but most importantly I found it very pleasant to work together. It was great to have met you in Dublin. Sebastian Köber contributed greatly to the work presented in chapter 5. I have really enjoyed working with you. Thanks for explaining all the complicated physics of photorefractive materials to me. I also enjoyed the meetings we had, and will never forget how a German guy manages to get phonenumbers thrown at him within the first minute he walks into a Dutch pub!

Ik heb de afgelopen jaren het genoegen gehad veel studenten te mogen begeleiden. Johannes you were the first student entrusted to me. I had great fun with you, thanks for all the nice 'kuchen' and for all the fun we had drinking beers. Also of course, thanks for all the synthesis you did. Some of your molecules found their way into chapter 5. Athir, ik heb je met veel plezier 8 maanden begeleid. Ik heb er veel bewondering voor hoe je vanuit Irak naar Nederland bent gekomen en hier nu een nieuw leven begonnen bent. Veel succes bij Syncom! Erik, ik denk dat jij van alle studenten het langst bent blijven hangen. Gelukkig was het een erg

plezierige periode. Je werk is opgenomen in hoofdstuk 3 en er is ook een mooie publicatie uit voort gekomen. Ik wens je heel veel plezier met je leraren opleiding en hoop nog regelmatig een biertje met je te kunnen drinken. Enrique, veniste de Madrid para aprender mas del quimica de los fullerenos. Espero que hayas disfrutado tu tiempo aqui en Groningen. Muchas gracias por el trabajo que hiciste. Tus compuestos están presentados en el capitulo 6 y espero que podamos publicar nuestros resultados pronto. Tessa, je was de vijfde en laatste studente die ik heb mogen begeleiden. Ik vond het erg leuk om met je samen te werken en natuurlijk op vrijdagmiddag een biertje te drinken. Je werk maakt deel uit van hoofdstuk 6 en hopelijk komt er nog een mooie publicatie uit. Veel succes met het verdere verloop van je studie, maar ik twijfel er niet aan dat dat wel goed gaat komen.

Een prettige werkomgeving is voor mij ontzettend belangrijk. Ik ben altijd met veel plezier naar het lab gekomen. Voor de leuke sfeer wil ik iedereen bedanken die deel uitmaakt of heeft uitgemaakt van de vakgroep: Renate, Renate, Harry, Lacra thanks for all the measurements, Mihai, Reinder, Marleen, Minze, Joop, Tineke, Ben, Ricardo, Daniel, Hang, Hennie, Jan tot de volgende bbq van Maaike!, Alfred, Frank bedankt voor alle gezelligheid ook buiten het lab en natuurlijk de mooie MALDI-TOF spectra van hoofdstuk 7. De Solenners: Patrick, Alex bedankt voor de vele discussies en raad, Dave thanks for the C84! en Renske. De groep van Paul Blom, in het bijzonder Afshin, Martijn, Bert en Magda bedankt voor de leuke samenwerking. Onze buren van anorganische chemie wil ik ook bedanken voor de leuke sfeer op de gang.

Ik heb tijdens mijn tijd hier een Groningen een ontzettend leuke groep vrienden gehad. Velen van jullie zijn inmiddels helaas vertrokken uit Groningen maar gelukkig zien we elkaar nog regelmatig op allerlei feestjes. Mirjam, Thomas, Jet, Willem en Irna: ik verhuis richting het westen dus hopelijk zien we binnenkort meer van elkaar! Arjan, er zijn weinig mensen met wie ik zo enorm kan lachen, ik kijk uit naar onze toekomstige email chats! Danny, gelukkig toch nog iemand die op het lab bleef. Ik heb altijd ontzettend veel plezier gehad met je tijdens alle koffie en lunchpauzes en niet te vergeten alle voetbalwedstrijden zowel live in het stadion als voor de buis! Sven, ik hoop nog vaak een lekker glas whisky met je te delen tijdens wat voor gelegenheid dan ook. Maaike, bedankt voor alle etentjes en bbq's.

Ik ben enorm veel dank verschuldigd aan mijn familie. Ik ging altijd met veel plezier op bezoek bij mijn opa en oma in Groningen. Helaas is opa er niet meer om dit moment mee te maken. Ik wil jullie allebei enorm bedanken voor alle gezelligheid. Pa en Ma ontzettend bedankt voor alle steun en liefde. Het is dankzij jullie altijd fijn om thuis te komen. Roelf en Petra bedankt voor alle lol die we altijd samen hebben. Ik vind het ontzettend leuk dat jullie mijn paranimfen willen zijn!

Als laatste wil ik Diana bedanken. Woorden kunnen niet beschrijven wat je voor mij betekent. Je bent naar Nederland gekomen zodat we samen konden zijn en daar ben ik je ontzettend dankbaar voor. Gracias por compartir tu vida con mí.